Mobile Information Systems

Emerging Trends in Mobile Collaborative Systems

Guest Editors: Sergio F. Ochoa, Weiming Shen, Giancarlo Fortino, and Wenfeng Li

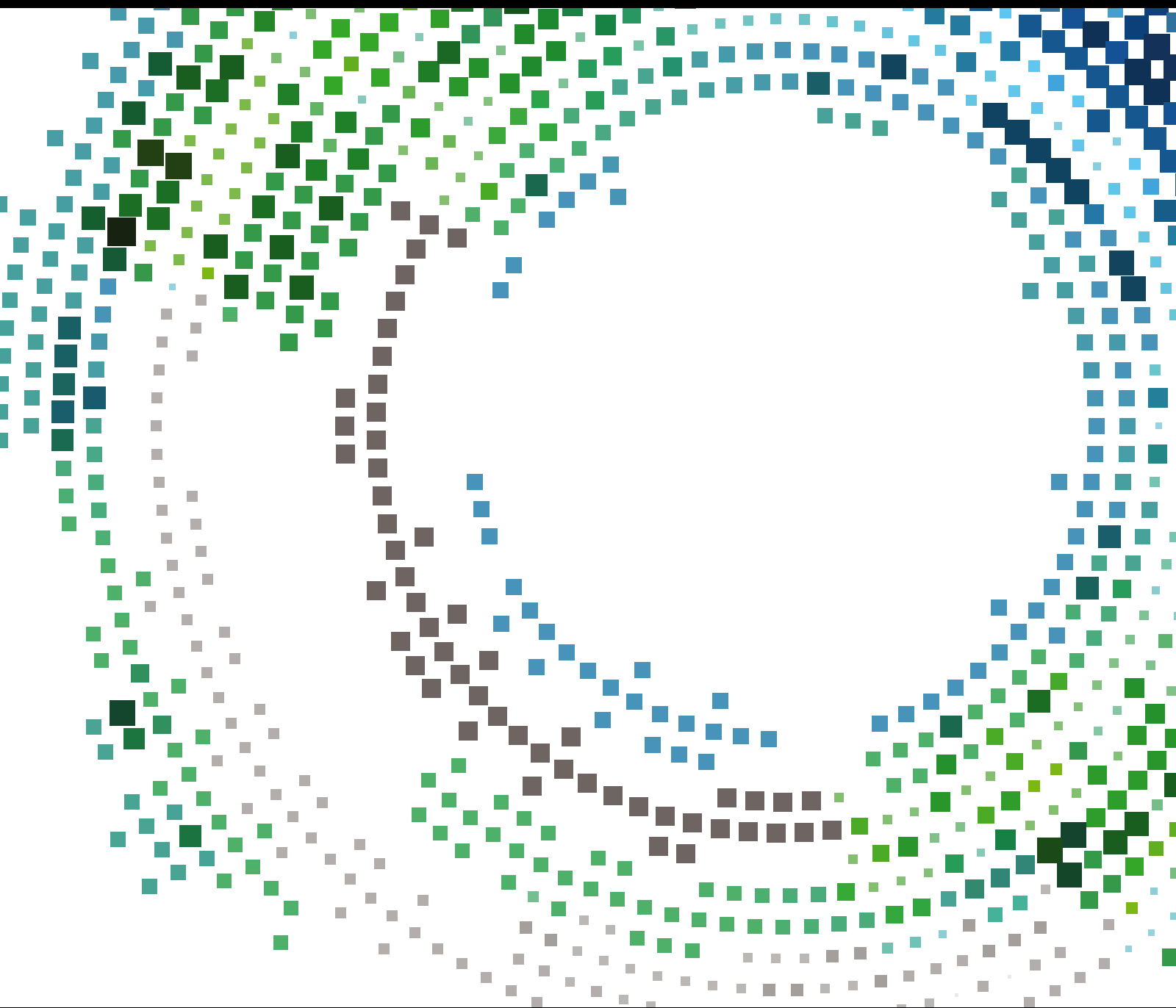

Emerging Trends in Mobile Collaborative Systems

Mobile Information Systems

Emerging Trends in Mobile Collaborative Systems

Guest Editors: Sergio F. Ochoa, Weiming Shen, Giancarlo Fortino, and Wenfeng Li

Contents

Hindawi Publishing Corporation
Mobile Information Systems
Volume 2016, Article ID 3421901, 2 pages
http://dx.doi.org/10.1155/2016/3421901

Editorial

Emerging Trends in Mobile Collaborative Systems

Sergio F. Ochoa,[1] Weiming Shen,[2] Giancarlo Fortino,[3] and Wenfeng Li[4]

[1]*Department of Computer Science, University of Chile, 837-0456 Santiago, Chile*
[2]*National Research Council of Canada, Ottawa, ON, Canada K1A 0R6*
[3]*Department of Informatics, Modeling, Electronics and Systems, University of Calabria, 87036 Rende, Italy*
[4]*School of Logistics Engineering, Wuhan University of Technology, Wuhan 430070, China*

Correspondence should be addressed to Sergio F. Ochoa; sochoa@dcc.uchile.cl

Received 18 July 2016; Accepted 19 July 2016

During the last decades mobile collaborative systems have become transversal applications that provide services not only to end-users, but also to other systems like mobile social applications, context-aware recommender systems, monitoring systems, and crowd sourcing and participatory sensing applications. Providing support services in mobile collaboration scenarios is complex, because the work context of each participant could be different, and also such a context is dynamic. Moreover, these solutions involve a wide range of devices that should interoperate to provide particular services in heterogeneous scenarios, like in Internet of Things based working contexts.

Regardless the advantages that these systems bring to the mobile collaboration research and application domains, they also raise several challenges to system developers, particularly in terms of design, implementation, use, and evaluation of these solutions. This special issue covers some of the new trends and challenges of these systems, by presenting interesting articles that were accepted after a rigorous peer-reviewing process.

One of the key issues in this computing scenario is the positioning of the nodes, since their mobility usually makes them change their work context and therefore the services that they can consume and provide to other nodes. Position accuracy (particularly in indoor environments), energy consumption, and deployment effort of these solutions are aspects highly researched by the community. In this sense, the paper by W. Kim et al. proposes a localization method named FreeLoc that deals with major technical issues in the crowdsourcing-based systems that involve indoor positioning. This method uses existing Wi-Fi infrastructure for performing the positioning and it does not require calibration (fingerprinting). This approach also considers the heterogeneity of devices that are usually available in a crowdsourcing scenario, which represents an important advance towards easy-to-deploy indoor positioning systems.

The paper by S.-H. Lee et al. also helps improve the positioning capability of these systems. It focuses on the positioning accuracy. The article proposes a beacon-based indoor positioning method, using an extended Kalman filter that recursively processes positioning information that also includes noise. This method improves the accuracy of indoor positioning techniques by fusing the information about the resources location with the data obtained from existing wireless indoor positioning technology. Thus, this method allows reaching average positioning errors that are between 26 and 28 centimeters.

The systems mentioned above usually have high power consumption since they exchange an important number of messages, not only to perform the positioning but also to support the mobile collaboration process. Many researches have already been done to reduce the energy consumption of mobile collaborative applications. In this sense, the paper by J. E. Luzuriaga et al. proposes an extension to the well-known publish/subscribe scheme of the MQTT protocol, by introducing an intermediate buffer that takes care of message transfer. The experimental evaluation in a real environment shows that the nodes movement has a marginal impact in the message transfer. Particularly, this proposal guarantees that no information loss appears in the presence of variable length handoffs.

The paper by M. Chincoli et al. also explores the energy consumption from a different perspective. It analyzes the conditions under which coordinated power reduction in

wireless sensor networks may lead to increasing its efficiency, mitigating interference, and thus improving the network performance. Using simulations the authors analyze the relationship between transmission power and communication efficiency, in order to determine how appropriate power reduction can improve both energy and spectrum efficiency.

The paper by L. Li et al. also addresses the energy consumption, but analyzing the network efficiency in terms of information dissemination. This work presents a novel and efficient model for studying the effect of nodes on information diffusion over mobile social networks. The proposal is based on the universal generating function method and the discrete stress-strength interference theory. In this model, the effect of the users on information diffusion is quantified as node susceptibility, and, based on that, the proposed model helps various decision-makers identify the most susceptible nodes to the corresponding information at different time periods.

The paper by T. Shin J. Byun presents a social-enabler (S-Enabler) middleware architecture for supporting the development of social IoT-based smart systems. This middleware helps convert the existing objects into social objects, and it was used for supporting the activities of vehicle social networks focusing on its energy saving. By using sharing and competition strategies the energy saving service can reduce energy consumption by up to 31.7% per node.

The mobile collaborative systems can impact several applications domains; particularly, the papers by D. E. Arias et al. and A. Neyem et al. present two systems focused on healthcare. The first paper introduces a mobile sensing device for supporting mobility of people using wheelchair. These chairs are instrumented with various sensors to get information from the user pressure relief habits, activity levels, vital signs, and ambient conditions. The results of a case study performed during two weeks, involving six full-time wheelchair users, indicate the system is able to capture pressure relief patterns and tilt-in-space usage, a mechanism required to avoid pressure ulcers. With a different goal, the paper of A. Neyem et al. presents a cloud-based mobile system for supporting team collaboration, risk evaluation, and decision-making while patients in critical health condition are transported between health centers. This system helps local and remote medical personnel to stay aware of the patients' status in real time and take preventive actions and early response activities when required. Thus, the system intends to increase the safety of the interhospital transfers.

Collectively, this corpus of knowledge advances the state of the art in the mobile collaborative systems domain, and it provides insights for new researches and applications in this area.

Sergio F. Ochoa
Weiming Shen
Giancarlo Fortino
Wenfeng Li

Hindawi Publishing Corporation
Mobile Information Systems
Volume 2016, Article ID 4961014, 19 pages
http://dx.doi.org/10.1155/2016/4961014

Research Article

Modeling Random Forwarding Actions for Information Diffusion over Mobile Social Networks

Ling Li,[1,2] Min Liu,[1] Weiming Shen,[1,3] and Guoqing Cheng[2]

[1]*School of Electronic and Information Engineering, Tongji University, Shanghai 201804, China*
[2]*School of Information Engineering, Jingdezhen Ceramic Institute, Jingdezhen 333403, China*
[3]*The Key Laboratory of Embedded System and Service Computing, Ministry of Education, Tongji University, Shanghai 200092, China*

Correspondence should be addressed to Min Liu; lmin@tongji.edu.cn

Received 4 February 2016; Revised 23 May 2016; Accepted 30 May 2016

Academic Editor: Hua Lu

Modeling information diffusion over social networks has attracted a lot of attention from both academia and industry. Based on universal generating function method and discrete stress-strength interference theory, a novel method is proposed to model the users' random forwarding actions, and the most susceptible users are extracted. The effect of a user on information diffusion is quantified as node susceptibility (NS), and NS is defined as the probability that quantity of information (message) the user forwards is larger than that he receives. The model can address three questions: which users are most susceptible, which types of information they are most susceptible to, and when they are most susceptible. The solutions of these questions are very helpful for the practitioners. A case study is used to illustrate the feasibility and practicality of the proposed model.

1. Introduction

With the development of Internet and mobile information technologies, social networks have incrementally become the most popular applications [1, 2]. A mobile social network connects organizations or individuals using smartphones with sharing of information through social networking applications such as MySpace, Facebook, and scientific collaboration networks [3, 4]. Mobile social networks are present in virtual communities and work with web-based social networks to spread content, increase accessibility, and connect users from wherever they are [5]. One of the distinguishing factors of social networks is the ability to enable people to simultaneously share information with large number of peers [6]. Due to its diverse implication, research on social networking from various perspectives has received remarkable attention. In the area of social networks, modeling and analyzing their networking structures [7], dynamic evolution [8], and the characteristics of information diffusion [9] are hot topics.

More recently, the smartphones have increased rapidly, and social networks are experiencing explosive growth, not only in the number of communities but also in the overall population [10]. For example, Facebook has over 1.18 billion monthly active users as of August 2015 [11]. Everyday users are sharing and exchanging the information by means of "word-of-mouth" communications in such large-scale social networks. Under such circumstances, in-depth analyzing and quantifying random actions (to forward the information or not) of users for information diffusion over social networks have become more and more important [12]. For each user (a human in a social network or a website on the Internet), whether to forward the information depends on several uncertain factors, including the interestingness of the information, the reliability of the information, egoistic motivation, and altruistic motivation [13]. Whatever the motivation, forwarding actions indicate that the user is susceptible to the information, and the higher the frequency, the more susceptible the user. In this sense, the study of random forwarding actions can help the politicians/enterprises to identify the susceptible users and then to achieve the most effective advocation/advertisement. On the other hand, the global diffusion of detrimental information (e.g., computer viruses, rumors) causes great damage to society. It is of great importance to identify the susceptible users and timely quarantine them [14]. Therefore, from the point of view of the

security, the study of random forwarding actions can help to prevent the diffusion of detrimental information.

The rapid developments of communication and information technologies enable us to access, collect, and store the real-world big data on information diffusion, making the related research meaningful and versatile and, meanwhile, more challenging. Back to 2001, Pastor-Satorras and Vespignani [15] studied epidemic/computer virus spreading over network, indicating that the study on information diffusion originates from the study on epidemic/computer virus diffusion. One of the earliest and prominent studies on information diffusion is [16], which studied and analyzed the dynamics of information dissemination through blogspace from two points of view: macroscopic and microscopic. Subsequently, there are numerous related works addressing information diffusion over social networks. Here, we summarize the most representative works that are relevant to our study. The existing related works can be broadly classified into two categories. The first one focuses on analyzing the effect of network structure on information diffusion [17–21]. In [17], the authors studied the scaling law of a few large networks and showed that the vertex connectivity obeys a scale-free distribution of power law. Donetti et al. [18] reported that scale-free structures may be generated by optimal designing for network mechanisms. The work [19] reported that the scale-free network can optimize the network performance. Recently, how the network structure of microblog influences information diffusion was studied in [20]. By studying followers' topology, the authors presented an invariant characteristic that the users' followers count obeys a distribution of power law with exponent near 2. In [21], the authors comparatively explored the network structure, geographic distribution of users, and interaction pattern in social networks. Based on the study, the authors suggested that information can be organized by a few central users bridging small communities.

The second category focuses on analyzing the effect of network nodes (users) on information diffusion using different mathematical models [22–28]. Kimura et al. [22] considered the optimization problem of extracting the most influential nodes over a social network. Later, Yu et al. [23] proposed a community-based greedy algorithm to mine top-k influential nodes over mobile social networks. By identifying the important information nodes, Ilyas et al. [24] studied how to restrain the private information diffusion. As social networks (e.g., Twitter and Facebook) become ubiquitous, the global effect of a node on diffusion rate on Twitter was studied in [25, 26]. More recently, Saito et al. [27] proposed an efficient method to find a new kind of influential nodes (supermediators) over a social network and characterized the properties of supermediators. From another perspective, Belák et al. [28] studied the effect of hidden nodes on information diffusion and characterized information cascades.

The study presented in this paper focuses on modeling nodes' random forwarding actions and analyzing the effect of these actions on information diffusion; that is, our study falls into the second category. Although the above-cited literatures provide systematic approaches and useful tools for analyzing the effect of network nodes on information diffusion, the majority of them neglect the dynamic and random characteristics of this problem. Given the complexity and uncertainty of social network, it is difficult for nodes to maintain the same effect on information diffusion during different periods. In addition, most of them mainly focus on extracting the most influential nodes, while mining the most susceptible nodes has not been well investigated. In fact, quantifying nodes' random forwarding actions and finding the most susceptible nodes also play an important role for information diffusion. On the one hand, from the academic research point of view, for information to diffuse, it in essence relies on nodes to forward the information that they receive. However, whether to forward the information is uncertain and depends on many factors. Therefore, quantifying nodes' random forwarding actions can help to objectively and rationally analyze which nodes are susceptible to the information and when they are most susceptible. On the other hand, from the practical significance point of view, for politicians/enterprises, it is easier to obtain advocation/purchasing from the susceptible nodes, rather than the influential nodes. Therefore, identifying the most susceptible nodes can help politicians/enterprises to achieve the most effective advocation/advertisement.

This work is motivated by the challenges of quantifying nodes' random forwarding actions and finding the most susceptible nodes, at the same time emphasizing the dynamics characteristics of this problem. The study aims to address three key questions: (1) which nodes are most susceptible. (2) which types of information they are most susceptible to. and (3) when they are most susceptible. To this end, a novel and efficient model for analyzing the effect of nodes on information diffusion is proposed based on universal generating function (UGF) method and discrete stress-strength interference (DSSI) theory. Stress-strength interference models have been widely used in component reliability analysis, but to the best of our knowledge, it is the first time that stress-strength interference model is applied to information diffusion analysis. In our model, the effect of node is quantified as node susceptibility (NS), which is relevant to two random variables: quantity of information (message) that the node receives and quantity of information (message) that the node forwards, and NS is defined as the probability that the latter (strength) is larger than the former (stress). Based on NS, the proposed model can help decision-makers to dynamically identify which nodes are most susceptible to the corresponding information at different periods of time. The innovations and practical significance of this paper are as follows.

(i) Approach Innovations. To model random forwarding actions over mobile social networks, DSSI model is applied to information diffusion analysis for the first time. Unlike the continuous stress-strength interference (CSSI) model, DSSI model can calculate system reliability (NS in this paper) based on observations of stress and strength when the distributions of stress and strength are unavailable. Moreover, since the stress and strength in the paper are discrete random variables, UGF method is utilized to represent their probability mass functions for the calculation of NS. In this sense,

the calculation of NS is based on actual observation data, rather than being dependent on decision-makers' subjective judgments; therefore, the decision results are objective and will be updated with the updated observation data.

(ii) Practical Significance. For the decision-makers (practitioners), modeling and decision process are easy to implement, since the calculation of NS is based on the observations of random variables which can be obtained directly from the database. In conventional approaches, decision-makers need to know specialized knowledge of filtering appropriate criteria from a lot of criteria and specifying the weights of criteria for optimization decisions, but, here, they only need to record the observations of the relevant variables, which can simplify the process of decision.

The rest of this paper is organized as follows. Section 2 describes the theoretical background of the proposed model. Model formulation is presented in Section 3. In Section 4, a case study is presented to illustrate the feasibility and efficiency of the proposed model. The paper ends with conclusions in Section 5.

2. Theoretical Background

Before describing the mathematical model, we introduce some definitions and notations related to universal generating function (UGF) method and discrete stress-strength interference (DSSI) model. They will be used in Section 3.

2.1. Brief Description of UGF Method. We put emphasis on the basic concept but not the fundamental mathematics of UGF method. Ushakov [29] first introduced the concept of UGF. Then, Lisnianski and Levitin [30] and Levitin [31] applied UGF method to reliability analysis and optimization of multistate system.

Suppose that a discrete random variable (r.v.) X has a probability mass function (p.m.f.) characterized by the vector x consisting of the possible values of X and the vector p consisting of the corresponding probabilities, which can be formulated by the following expressions: $x = (x_1, x_2, \ldots, x_k)$ and $p = (p_1, p_2, \ldots, p_k)$, where $p_i = \Pr(X = x_i)$, $i = 1, 2, \ldots, k$.

Definition 1 (UGF of discrete random variable). The UGF of X is defined as a polynomial function of variable z, $u_X(z)$, and

$$u_X(z) = p_1 z^{x_1} + p_2 z^{x_2} + \cdots + p_k z^{x_k} = \sum_{i=1}^{k} p_i z^{x_i}. \quad (1)$$

It should be mentioned that there exists a one-to-one correspondence between the p.m.f. and UGF of a discrete r.v. This means that, for an arbitrary discrete r.v., its UGF is uniquely determined by its p.m.f..

Definition 2 (UGF of discrete random variables). Consider n independent discrete r.v. $X_1, X_2, \ldots, X_n$. Let the UGF of each r.v. be $u_{X_1}(z), u_{X_2}(z), \ldots, u_{X_n}(z)$, respectively, and $f(X_1, X_2, \ldots, X_n)$ an arbitrary function of variables $X_1, X_2, \ldots, X_n$. Then, by employing composition operator $\bigotimes$, the UGF of $f(X_1, X_2, \ldots, X_n)$, $u_f(z)$ can be obtained as follows:

$$u_f(z) = \bigotimes \left(u_{X_1}(z), u_{X_2}(z), \ldots, u_{X_n}(z)\right). \quad (2)$$

Definition 3 (composition operator $\bigotimes$). According to Definition 1, $u_{X_i}(z) = \sum_{j_i=1}^{k_i} p_{ij_i} z^{x_{ij_i}}$, $i = 1, 2, \ldots, n$, where $k_1, k_2, \ldots, k_n$ are, respectively, the number of possible values of each r.v. To obtain the UGF of $f(X_1, X_2, \ldots, X_n)$, composition operator $\bigotimes$ is defined as follows:

$$\begin{aligned} &\bigotimes \left(\sum_{j_1=1}^{k_1} p_{1j_1} z^{x_{1j_1}}, \sum_{j_2=1}^{k_2} p_{2j_2} z^{x_{2j_2}}, \ldots, \sum_{j_n=1}^{k_n} p_{nj_n} z^{x_{nj_n}} \right) \\ &= \sum_{j_1=1}^{k_1} \sum_{j_2=1}^{k_2} \cdots \sum_{j_n=1}^{k_n} \left(\prod_{i=1}^{n} p_{ij_i} z^{f(x_{1j_1}, x_{2j_2}, \ldots, x_{nj_n})} \right). \end{aligned} \quad (3)$$

Property 1. In the operation of UGF, commutative law and associative law are applicable:

$$\begin{aligned} u_f(z) &= \bigotimes \left(u_{X_1}(z), u_{X_2}(z), \ldots, u_{X_i}(z), u_{X_{i+1}}(z), \ldots, u_{X_n}(z)\right) \\ &= \bigotimes \left(u_{X_1}(z), u_{X_2}(z), \ldots, u_{X_{i+1}}(z), u_{X_i}(z), \ldots, u_{X_n}(z)\right), \\ u_f(z) &= \bigotimes \left(u_{X_1}(z), u_{X_2}(z), \ldots, u_{X_i}(z), u_{X_{i+1}}(z), \ldots, u_{X_n}(z)\right) \\ &= \bigotimes \left(\bigotimes \left(u_{X_1}(z), u_{X_2}(z), \ldots, u_{X_{i+1}}(z)\right), \right. \\ &\quad \left. \bigotimes \left(u_{X_i}(z), \ldots, u_{X_n}(z)\right)\right). \end{aligned} \quad (4)$$

2.2. Discrete Stress-Strength Interference (DSSI) Model. Stress-strength interference model [32] has been widely used for reliability analysis of component, where "component" is not necessarily the raw goods or parts but can be an entire system. Stress-strength analysis is an efficient tool used in reliability engineering.

Definition 4 (component reliability). Let S_1 and S_2 denote stress on a component and strength of a component, respectively; then, the component reliability denoted by R is defined as

$$R = \Pr\left(S_2 > S_1\right). \quad (5)$$

Equation (5) is the most basic expression of the stress-strength interference model, which indicates that the component reliability is defined as the probability that the strength is larger than the stress.

If S_1 and S_2 are treated as continuous r.v. and their probability density functions are denoted by $f_1(S_1)$ and $f_2(S_2)$, respectively, (5) can be rewritten as

$$R = \int_{-\infty}^{+\infty} f_1(S_1) \cdot \left[\int_{S_1}^{+\infty} f_2(S_2)\, dS_2 \right] dS_1 \quad (6a)$$

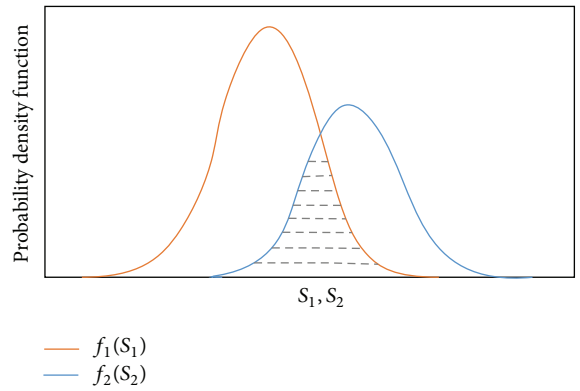

Figure 1: Component reliability as overlap of stress and strength.

or

$$R = \int_{-\infty}^{+\infty} f_2(S_2) \cdot \left[\int_{-\infty}^{S_2} f_1(S_1)\, dS_1 \right] dS_2. \tag{6b}$$

Figure 1 exhibits visually the component reliability which is defined by the area where both tail curves interfere or overlap with each other. For the sake of clarity, (6a) and (6b) can be called the continuous stress-strength interference (CSSI) model.

If S_1 and S_2 are two discrete r.v. with the p.m.f. as follows,

$$\begin{aligned} S_1 &= \left(S_{11}, S_{12}, \ldots, S_{1k_1}\right), \\ p_1 &= \left(p_{11}, p_{12}, \ldots, p_{1k_1}\right), \\ S_2 &= \left(S_{21}, S_{22}, \ldots, S_{2k_2}\right), \\ p_2 &= \left(p_{21}, p_{22}, \ldots, p_{2k_2}\right), \end{aligned} \tag{7}$$

where k_1 and k_2 are, respectively, numbers of possible values that S_1 and S_2 can take on, then, according to Definition 1, the UGF of S_1 and S_2 can be obtained as follows:

$$\begin{aligned} u_{S_1}(z) &= \sum_{j_1=1}^{k_1} p_{1j_1} z^{S_{1j_1}}, \\ u_{S_2}(z) &= \sum_{j_2=1}^{k_2} p_{2j_2} z^{S_{2j_2}}. \end{aligned} \tag{8}$$

If $f(S_1, S_2)$ is a function of S_1 and S_2, based on the UGF method introduced above, we can obtain the UGF of $f(S_1, S_2)$ as follows:

$$\begin{aligned} u_f(z) &= \bigotimes \left(u_{S_1}(z), u_{S_2}(z)\right) \\ &= \sum_{j_1=1}^{k_1} \sum_{j_2=1}^{k_2} \left(\prod_{i=1}^{2} p_{ij_i} z^{f(S_{1j_1}, S_{2j_2})} \right) = \sum_{j=1}^{K} P_j z^{f_j}, \end{aligned} \tag{9}$$

where f_j and P_j $(j = 1, 2, \ldots, K)$ are possible values of function $f(S_1, S_2)$ and corresponding probabilities, respectively, and $K \le k_1 \times k_2$.

Definition 5 (discrete stress-strength interference (DSSI) model). If $f(S_1, S_2) = S_2 - S_1$, the component reliability can be calculated as

$$R = \Pr\left(f(S_1, S_2) > 0\right) = \sum_{j=1}^{K} P_j \sigma\left(f_j\right). \tag{10}$$

Equation (10) is called the DSSI model, where $\sigma(f_j)$ is a binary-valued function with domain on the set of possible values of function $f(S_1, S_2)$ as

$$\sigma\left(f_j\right) = \begin{cases} 1, & f_j > 0, \\ 0, & f_j \le 0. \end{cases} \tag{11}$$

3. Model Formulation

In this section, a mathematical model is formulated for random forwarding actions for information diffusion over social networks. First, model description and notations used to develop the model are presented. Then, based on DSSI model introduced above, the effect (forwarding actions) of node is quantified as node susceptibility (NS). Finally, the most susceptible node is identified.

3.1. Model Description and Notations. In the model, one social network and N nodes (users) of the social network are considered. User n can receive different types of information (message) at different periods. Here, suppose that the unit of information is the piece. Let M denote the number of types of information and T the number of periods. Each period includes multiple time nodes, which divide the period into multiple equal time intervals. As shown in Figure 2, period P_t includes L_t time nodes Q_{tj}, $j = 1, 2, \ldots, L_t$, which divide the period into L_t equal time intervals $[Q_{t,j-1}, Q_{tj}]$, $j = 2, 3, \ldots, L_t$ and $[Q_{tL_t}, Q_{t+1,1}]$. In time interval $[Q_{t,j-1}, Q_{tj}]$ at period P_t, for a piece of information, the user randomly forwards it or not. Whether to forward the information depends on several uncertain factors, including the interestingness of the information, the reliability of the information, egoistic motivation, and altruistic motivation. Whatever the motivation, forwarding actions indicate that the user is susceptible to the information, and the higher the frequency, the more susceptible the user. The decision problems addressed in this paper are as follows: (1) which users are most susceptible, (2) which types of information they are most susceptible to, and (3) when they are most susceptible.

For the sake of clarity of model description and development, we give the notations used to develop the model in Notation.

3.2. Quantifying Forwarding Actions Based on DSSI Model. In this subsection, definition of node (user) susceptibility (NS) is first given. Then, calculation steps of NS are presented.

3.2.1. Definition of Node Susceptibility (NS). As previously analyzed, forwarding actions indicate that the user is susceptible to the information, and the higher the frequency,

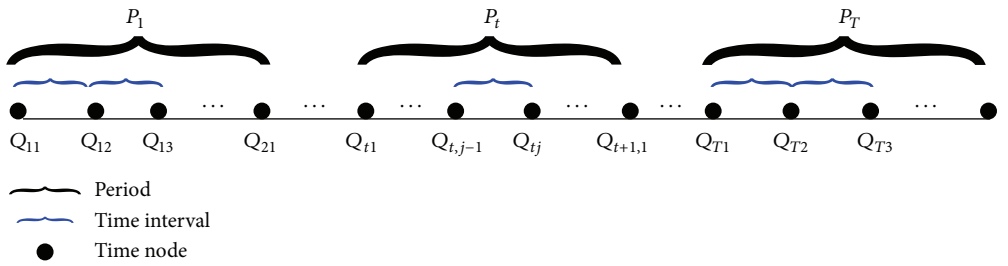

Figure 2: Modeling period and time node.

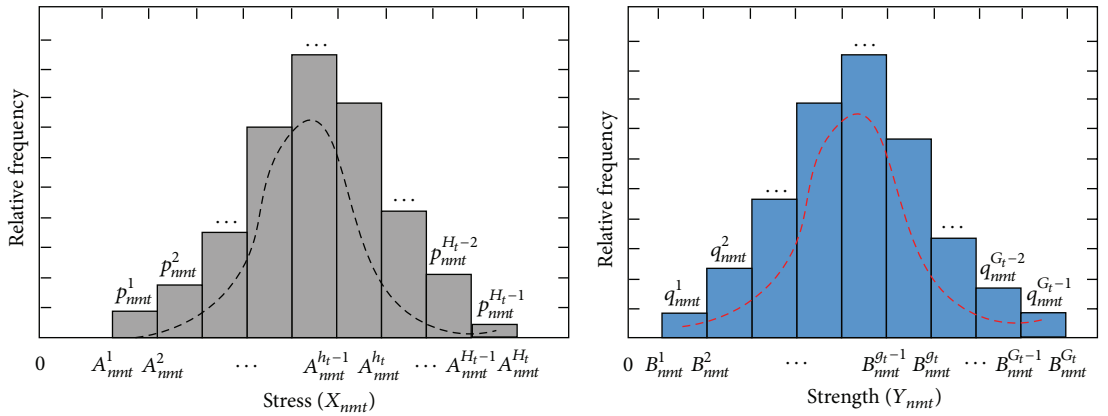

Figure 3: Histograms of stress and strength observations.

the more susceptible the user. To model the forwarding actions, a novel and universal criterion for the effect of user on information diffusion will be introduced, namely, node susceptibility (NS). NS is based on DSSI model and UGF method introduced in Section 2.

DSSI model considers two main random variables (r.v.): a stress which is any load applied on a component and a strength which is the maximum tolerance that the component can withstand without failing. To develop the model, this paper recognizes U_n as equivalent to component, random quantity of I_m that U_n received at P_t, X_{nmt} as equivalent to stress, and random quantity of I_m that U_n forwarded at P_t, Y_{nmt}, as equivalent to strength. For the sake of clarity, we give the following definition of NS.

Definition 6 (node susceptibility (NS)). Suppose that quantity of I_m that U_n received at P_t, X_{nmt} and quantity of I_m that U_n forwarded at P_t, Y_{nmt} are r.v. NS of U_n in regard to I_m at P_t denoted by NS_{nmt} is the probability that Y_{nmt} is larger than X_{nmt}. As a result, NS_{nmt} is given by

$$\mathrm{NS}_{nmt} = \Pr\left(Y_{nmt} > X_{nmt}\right). \tag{12}$$

The following should be noted about the definition of NS:

(1) The statistic character of X_{nmt} is based on a group of observations, that is, the observation parameters A_{nmtj}. Similarly, the statistic character of Y_{nmt} is also based on a group of observations, that is, the observation parameters B_{nmtj}. This means that X_{nmt}'s p.m.f. and Y_{nmt}'s p.m.f. can be obtained from their observations, respectively.

(2) Since the observations are objective, NS_{nmt} is not dependent on the subjective judgments of the decision-makers. In addition, the more the observations are, the more accurate the evaluation is going to be.

(3) According to the definition of NS, random forwarding actions are quantified as a probability, which shows the degree of user's susceptibility to the corresponding information at the corresponding period. Therefore, based on NS, decision-maker can identify which users are most susceptible to the corresponding information at different periods.

3.2.2. Calculation Steps of NS. According to UGF method and DSSI model introduced previously, calculation steps of NS are given as follows.

Step 1 (deriving X_{nmt}'s p.m.f. and Y_{nmt}'s p.m.f.). Suppose that the observations of X_{nmt} are $A_{nmt1}, A_{nmt2}, \ldots, A_{nmtL_t}$ and the observations of Y_{nmt} are $B_{nmt1}, B_{nmt2}, \ldots, B_{nmtL_t}$. Two groups of observations can be described by histograms, as shown in Figure 3, and the class intervals of observations and their corresponding relative frequencies are obtained.

To obtain X_{nmt}'s p.m.f., the midpoint values of each class interval $[A^{h_t-1}_{nmt}, A^{h_t}_{nmt}]$, $h_t = 2, 3, \ldots, H_t$, are treated as possible values of X_{nmt}, and relative frequencies of each

class interval $[A_{nmt}^{h_t-1}, A_{nmt}^{h_t}]$, $h_t = 2, 3, \ldots, H_t$, are treated as corresponding probabilities. Thus, X_{nmt}'s p.m.f. is obtained as follows:

$$\begin{aligned} & X_{nmt} \\ & = \left(\frac{A_{nmt}^2 - A_{nmt}^1}{2}, \frac{A_{nmt}^3 - A_{nmt}^2}{2}, \ldots, \frac{A_{nmt}^{H_t} - A_{nmt}^{H_t-1}}{2} \right) \\ & \triangleq \left(X_{nmt}^1, X_{nmt}^2, \ldots, X_{nmt}^{H_t} \right), \\ & p_{nmt} = \left(p_{nmt}^1, p_{nmt}^2, \ldots, p_{nmt}^{H_t} \right), \end{aligned} \tag{13}$$

where $X_{nmt}^{h_t} = (A_{nmt}^{h_t} - A_{nmt}^{h_t-1})/2$, $h_t = 1, 2, \ldots, H_t$.

Similarly, the midpoint values of each class interval $[B_{nmt}^{g_t-1}, B_{nmt}^{g_t}]$, $g_t = 2, 3, \ldots, G_t$, are treated as possible values of Y_{nmt}, and relative frequencies of each class interval $[B_{nmt}^{g_t-1}, B_{nmt}^{g_t}]$, $g_t = 2, 3, \ldots, G_t$, are treated as corresponding probabilities. Thus, Y_{nmt}'s p.m.f. is obtained as follows:

$$\begin{aligned} & Y_{nmt} \\ & = \left(\frac{B_{nmt}^2 - B_{nmt}^1}{2}, \frac{B_{nmt}^3 - B_{nmt}^2}{2}, \ldots, \frac{B_{nmt}^{G_t} - B_{nmt}^{G_t-1}}{2} \right) \\ & \triangleq \left(Y_{nmt}^1, Y_{nmt}^2, \ldots, Y_{nmt}^{G_t} \right), \\ & q_{nmt} = \left(q_{nmt}^1, q_{nmt}^2, \ldots, q_{nmt}^{G_t} \right), \end{aligned} \tag{14}$$

where $Y_{nmt}^{g_t} = (B_{nmt}^{g_t} - B_{nmt}^{g_t-1})/2$, $g_t = 1, 2, \ldots, G_t$.

Step 2 (deriving X_{nmt}'s UGF, Y_{nmt}'s UGF, and $f(X_{nmt}, Y_{nmt})$'s UGF). According to Definition 1, the UGFs of X_{nmt} and Y_{nmt} can be given as follows:

$$\begin{aligned} u_{X_{nmt}}(z) &= p_{nmt}^1 z^{X_{nmt}^1} + p_{nmt}^2 z^{X_{nmt}^2} + \cdots + p_{nmt}^{H_t} z^{X_{nmt}^{H_t}} \\ &= \sum_{h_t=1}^{H_t} p_{nmt}^{h_t} z^{X_{nmt}^{h_t}}, \\ u_{Y_{nmt}}(z) &= q_{nmt}^1 z^{Y_{nmt}^1} + q_{nmt}^2 z^{Y_{nmt}^2} + \cdots + q_{nmt}^{G_t} z^{Y_{nmt}^{G_t}} \\ &= \sum_{g_t=1}^{G_t} q_{nmt}^{g_t} z^{Y_{nmt}^{g_t}}. \end{aligned} \tag{15}$$

Because $f(X_{nmt}, Y_{nmt})$ is a function of X_{nmt} and Y_{nmt}, based on Definitions 2 and 3, the UGF of $f(X_{nmt}, Y_{nmt})$ can be obtained as follows:

$$\begin{aligned} u_f(z) &= \bigotimes \left(u_{X_{nmt}}(z), u_{Y_{nmt}}(z) \right) \\ &= \bigotimes \left(\sum_{h_t=1}^{H_t} p_{nmt}^{h_t} z^{X_{nmt}^{h_t}}, \sum_{g_t=1}^{G_t} q_{nmt}^{g_t} z^{Y_{nmt}^{g_t}} \right) \\ &= \sum_{h_t=1}^{H_t} \sum_{g_t=1}^{G_t} \left(p_{nmt}^{h_t} z^{f(X_{nmt}^{h_t}, Y_{nmt}^{g_t})} q_{nmt}^{g_t} z^{f(X_{nmt}^{h_t}, Y_{nmt}^{G_t})} \right) \\ &= \sum_{r=1}^{R} \lambda_r z^{f_r}, \end{aligned} \tag{16}$$

where f_r and λ_r ($r = 1, 2, \ldots, R$) are possible values of function $f(X_{nmt}, Y_{nmt})$ and corresponding probabilities, respectively, and $R \le H_t \times G_t$.

Step 3 (calculating NS_{nmt} based on DSSI model). Suppose that $f(X_{nmt}, Y_{nmt}) = Y_{nmt} - X_{nmt}$, according to Definition 5, NS_{nmt} can be calculated as

$$\mathrm{NS}_{nmt} = \Pr\left(f\left(X_{nmt}, Y_{nmt} \right) > 0 \right) = \sum_{r=1}^{R} \lambda_r \sigma\left(f_r \right), \tag{17}$$

where $\sigma(f_r)$ is a binary-valued function with domain on the set of possible values of function $(Y_{nmt} - X_{nmt})$ as

$$\sigma\left(f_r \right) = \begin{cases} 1, & f_r > 0 \\ 0, & f_r \le 0. \end{cases} \tag{18}$$

3.3. Identifying the Most Susceptible User at Different Periods. Without loss of generality, we give the process of identifying the most susceptible user in regard to information I_m. Based on the above calculation of NS, we can obtain each user's NS in regard to I_m at different periods, as shown in the following:

$$\begin{gathered} \mathrm{NS}_{1m1}, \mathrm{NS}_{2m1}, \ldots, \mathrm{NS}_{Nm1}, \\ \mathrm{NS}_{1m2}, \mathrm{NS}_{2m2}, \ldots, \mathrm{NS}_{Nm2}, \\ \vdots \\ \mathrm{NS}_{1mT}, \mathrm{NS}_{2mT}, \ldots, \mathrm{NS}_{NmT}, \end{gathered} \tag{19}$$

$$\mathrm{NS}_{n_1 m1} = \max_{1 \le n \le N} \left\{ \mathrm{NS}_{nm1} \right\}, \quad 1 \le n_1 \le N, \tag{19a1}$$

$$\mathrm{NS}_{n_2 m2} = \max_{1 \le n \le N} \left\{ \mathrm{NS}_{nm2} \right\}, \quad 1 \le n_2 \le N, \tag{19a2}$$

$$\vdots$$

$$\mathrm{NS}_{n_T mT} = \max_{1 \le n \le N} \left\{ \mathrm{NS}_{nmT} \right\}, \quad 1 \le n_T \le N. \tag{19aN}$$

Equations (19a1), (19a2), and (19aN) shows that at corresponding period, which user is most susceptible to information I_m. For example, at period P_1, user U_{n_1} is most susceptible to information I_m, and at period P_T, user U_{n_T} is most susceptible to information I_m. Therefore, based on each user's NS, three main questions are solved: (1) which user is most susceptible. (2) which type of information he is most susceptible to, and (3) when he is most susceptible. In real-life decision, more susceptible users can be extracted as needed. To this end, decision-makers (politicians

or enterprises) only need to rank NS_{nmt}, $t = 1, 2, \ldots, T$; and $n = 1, 2, \ldots, N$, and set thresholds to mine the top ranked ones and then extract the corresponding users. To achieve the most effective advocation/advertisement, at the corresponding period, politicians/enterprises can post the corresponding information to these users.

4. Case Study

This section aims to illustrate the feasibility and practicality of the proposed model through its application to a test case.

4.1. Case Description. The case study was motivated by the problem of extracting appropriate users for advertisement over a social network—Meituan. Meituan is a Chinese group-buying website for locally found consumer products and retail services, and it sells vouchers from merchants for deals, subject to minimum number of buyers who demand a discount. Meituan generates most of its revenue from mobile application services, and it has partnering agreement with 400 thousand Chinese local businesses. In 2014, Meituan accounts for 60% of the market share of deal-of-the-day group-buying websites in China, and in 2015 it has 200 million users [36]. One of the goals of Meituan is to find the most appropriate consumers for merchants and to provide the most efficient Internet promotion [37]. To this end, the proposed model in this paper will be applied to address the problem. Based on the model, decision-maker can extract appropriate consumers for different advertisements (e.g., cate, entertainment, and shopping) at different periods and then develop the most efficient Internet promotion strategy.

Without loss of generality, in this case study, six candidate users (i.e., $N = 6$) are under consideration, and three types of advertisement information (i.e., $M = 3$) will be posted to them. The observation of random forwarding actions contains four periods (i.e., $T = 4$), and each period contains thirty time nodes (i.e., $L_t = 30$, $t = 1, 2, 3, 4$). The objective is to determine which two users should be extracted and which type of advertisement information should be posted to these users at the corresponding period. It should be noted that the dimension of candidate set of users in case study is much less than the actual number of the users. The setting of this parameter is mainly based on the following two considerations. On the one hand, the main purpose of conducting case study is demonstrating the application of the proposed model, and low-dimensional parameter setting helps to clearly demonstrate calculation process. On the other hand, in the proposed model, although the dimensions of parameter settings have effect on computational complexity, the effect is little, because there are many data processing tools for mass data under the environment of big data. In essence, the key step of calculation of NS is Step 1: deriving X_{nmt}'s p.m.f. and Y_{nmt}'s p.m.f., where the class intervals of observations and their corresponding relative frequencies can be obtained from the histograms of observations. In real life, when the amount of observations is massive, the histograms can be directly obtained by using Statistic Package for Social Science (SPSS, a widely used program for statistical analysis in social science) (see the Appendix). In this sense, the model implementation in practice is feasible.

For the sake of clarity, the observation parameters A_{nmtj} and B_{nmtj} are, respectively, listed in Tables 1 and 2.

4.2. Results and Analysis. Based on the calculation steps of NS introduced in Section 3, we can obtain each user's NS in regard to corresponding advertisement information at corresponding period. As an example of calculation steps, we give the calculation of NS_{123} as follows.

According to the observation parameters in Tables 1 and 2, we describe two groups of data (data in bold font) by histograms as shown in Figure 4.

Therefore, X_{123}'s p.m.f. and Y_{123}'s p.m.f. are obtained as follows:

$$\begin{aligned} X_{123} &= (22.5, 27.5, 32.5, 37.5, 42.5, 47.5, 52.5), \\ p_{123} &= (0.03, 0.07, 0.20, 0.30, 0.27, 0.10, 0.03), \\ Y_{123} &= (24.5, 29.5, 34.5, 39.5, 44.5, 49.5, 54.5), \\ q_{123} &= (0.07, 0.10, 0.17, 0.30, 0.20, 0.13, 0.03). \end{aligned} \tag{20}$$

Thus, we have

$$\begin{aligned} \mathrm{NS}_{123} &= \Pr\left(f\left(X_{123}, Y_{123}\right) > 0\right) = \sum_{r=1}^{R} \lambda_r \sigma\left(f_r\right) \\ &= 0.07 \times 0.03 + 0.10 \times (0.03 + 0.07) + 0.17 \\ &\quad \times (0.03 + 0.07 + 0.20) + 0.30 \\ &\quad \times (0.03 + 0.07 + 0.20 + 0.30) + 0.20 \\ &\quad \times (0.03 + 0.07 + 0.20 + 0.30 + 0.27) + 0.13 \\ &\quad \times (0.03 + 0.07 + 0.20 + 0.30 + 0.27 + 0.10) + 0.03 \\ &\quad \times (0.03 + 0.07 + 0.20 + 0.30 + 0.27 + 0.10 + 0.03) \\ &= 0.5778. \end{aligned} \tag{21}$$

All NS_{nmt} ($n = 1, 2, 3, 4, 5, 6$; $m = 1, 2, 3$; $t = 1, 2, 3, 4$) can be obtained, as shown in Table 3, where the values in bold font are the maximum two values of each row. Figure 5 visually shows each user's NS in regard to corresponding advertisement information at different periods.

Table 3 and Figure 5 show which two users should be extracted and which type of advertisement information should be posted to them at the corresponding period. For example, at the first period, users U_3 and U_4 are most susceptible to information I_1, while users U_2 and U_6 are most susceptible to information I_2. At the second and third periods, users U_2 and U_4 are most susceptible to information I_1. Users U_3 and U_4 are most susceptible to information I_2 at the third and fourth periods. These indicate that on the one hand different users are susceptible to different types of information at the same period, and on the other hand the same user is susceptible to different types of information at different periods. On the whole, users U_2, U_3, U_4, and U_6 are more susceptible, and information I_1 and information I_2 are

Table 1: Observation parameters A_{nmtj}.

	$t = 1$			$t = 2$		
	I_1	I_2	I_3	I_1	I_2	I_3
U_1	39, 37, 37, 39, 43, 49, 44, 39, 36, 29, 34, 29, 33, 39, 37, 29, 24, 34, 34, 49, 53, 43, 37, 39, 31, 44, 44, 47, 43, 42	34, 49, 45, 47, 38, 40, 35, 39, 37, 29, 24, 34, 38, 38, 37, 40, 45, 43, 53, 45, 38, 29, 34, 34, 32, 35, 43, 47, 44, 45	41, 39, 38, 40, 41, 39, 36, 44, 35, 25, 44, 41, 26, 35, 26, 31, 35, 40, 40, 55, 51, 50, 40, 30, 39, 45, 41, 43, 45, 51	37, 36, 38, 37, 33, 48, 41, 37, 39, 27, 33, 28, 34, 37, 39, 29, 23, 33, 33, 47, 54, 43, 36, 38, 33, 41, 43, 47, 41, 44	54, 49, 33, 44, 36, 37, 39, 39, 39, 36, 42, 41, 33, 36, 37, 29, 23, 34, 53, 38, 38, 28, 34, 29, 31, 43, 42, 47, 44, 44	44, 47, 35, 48, 39, 40, 34, 38, 39, 27, 25, 33, 37, 39, 36, 40, 43, 44, 51, 37, 39, 29, 35, 32, 33, 34, 44, 47, 45, 44
U_2	39, 36, 39, 29, 31, 28, 38, 37, 44, 39, 35, 49, 33, 38, 38, 27, 22, 32, 34, 46, 52, 45, 37, 38, 34, 47, 43, 49, 44, 43	33, 49, 54, 44, 36, 37, 39, 39, 39, 36, 42, 41, 33, 36, 37, 29, 23, 34, 53, 38, 38, 28, 34, 29, 31, 43, 42, 47, 44, 44	34, 48, 44, 43, 38, 39, 38, 36, 36, 37, 42, 44, 32, 39, 39, 27, 23, 33, 54, 39, 37, 29, 34, 28, 33, 43, 41, 49, 44, 42	39, 32, 45, 25, 29, 35, 38, 38, 38, 37, 44, 42, 33, 49, 45, 48, 38, 53, 48, 40, 37, 25, 35, 35, 38, 35, 45, 50, 30, 43	41, 40, 34, 29, 27, 34, 49, 40, 37, 24, 32, 34, 34, 49, 39, 50, 39, 55, 37, 38, 38, 42, 44, 45, 44, 31, 42, 50, 45, 40	39, 40, 37, 37, 43, 45, 50, 41, 41, 24, 32, 34, 32, 44, 43, 50, 39, 52, 31, 39, 41, 27, 27, 35, 36, 34, 41, 37, 40, 40
U_3	36, 34, 44, 31, 32, 28, 39, 41, 46, 38, 53, 46, 31, 37, 35, 27, 21, 32, 34, 45, 50, 38, 36, 39, 43, 49, 39, 45, 40, 41	37, 37, 44, 27, 35, 29, 38, 39, 39, 36, 34, 46, 31, 37, 37, 28, 25, 33, 31, 47, 51, 44, 37, 39, 43, 48, 45, 46, 44, 44	38, 37, 41, 30, 32, 27, 39, 37, 45, 36, 33, 46, 34, 37, 36, 29, 25, 33, 35, 37, 52, 43, 37, 39, 43, 49, 41, 47, 38, 41	37, 39, 42, 24, 33, 28, 39, 37, 43, 38, 34, 49, 34, 38, 40, 29, 24, 33, 33, 48, 53, 44, 37, 39, 44, 47, 42, 49, 44, 44	38, 37, 44, 28, 33, 29, 36, 38, 42, 38, 32, 48, 31, 39, 39, 26, 24, 34, 31, 49, 55, 44, 39, 39, 31, 46, 41, 47, 41, 42	36, 36, 37, 27, 33, 29, 36, 36, 41, 37, 34, 48, 31, 39, 39, 29, 24, 33, 34, 46, 51, 43, 36, 39, 31, 41, 42, 47, 44, 41
U_4	37, 40, 38, 37, 33, 49, 39, 37, 43, 30, 34, 28, 33, 37, 39, 28, 24, 34, 35, 47, 53, 45, 38, 39, 44, 50, 51, 47, 43, 44	38, 39, 43, 26, 35, 27, 39, 37, 37, 37, 33, 46, 33, 36, 36, 29, 25, 33, 32, 46, 53, 44, 37, 39, 44, 49, 41, 47, 36, 45	37, 39, 37, 28, 35, 27, 39, 39, 45, 38, 33, 49, 31, 37, 36, 29, 24, 33, 32, 47, 53, 44, 37, 37, 44, 49, 42, 52, 43, 44	35, 48, 51, 42, 39, 38, 38, 39, 37, 37, 42, 48, 31, 37, 37, 27, 24, 33, 54, 38, 36, 26, 34, 28, 32, 43, 44, 49, 44, 41	31, 38, 37, 29, 24, 34, 33, 49, 42, 44, 38, 38, 39, 38, 37, 38, 43, 43, 52, 38, 36, 29, 34, 30, 30, 33, 42, 49, 45, 41	31, 50, 44, 49, 36, 39, 31, 37, 40, 29, 26, 35, 37, 39, 37, 39, 44, 41, 54, 43, 37, 24, 34, 35, 35, 35, 45, 49, 41, 41
U_5	44, 50, 39, 21, 31, 35, 35, 47, 41, 48, 38, 53, 35, 39, 41, 30, 29, 31, 36, 38, 37, 40, 45, 44, 37, 35, 41, 49, 45, 45	41, 46, 36, 25, 35, 31, 35, 44, 45, 49, 37, 53, 35, 40, 41, 29, 29, 34, 39, 38, 40, 40, 43, 44, 38, 32, 44, 36, 45, 41	44, 35, 43, 49, 40, 55, 39, 40, 36, 39, 44, 34, 39, 43, 42, 23, 32, 33, 35, 38, 41, 29, 27, 35, 40, 32, 41, 36, 41, 46	39, 37, 38, 37, 33, 49, 39, 37, 43, 30, 34, 28, 33, 37, 39, 28, 24, 34, 35, 47, 53, 45, 38, 39, 44, 50, 51, 47, 43, 44	38, 38, 43, 26, 35, 27, 39, 37, 37, 37, 33, 46, 33, 36, 36, 29, 25, 33, 32, 46, 53, 44, 37, 39, 44, 49, 41, 47, 36, 45	38, 37, 39, 28, 35, 27, 39, 39, 45, 38, 33, 49, 31, 37, 36, 29, 24, 33, 32, 47, 53, 44, 37, 37, 44, 49, 42, 52, 43, 44
U_6	38, 44, 38, 27, 32, 29, 37, 36, 41, 39, 31, 49, 34, 38, 36, 29, 24, 34, 31, 49, 52, 43, 39, 39, 41, 53, 41, 49, 42, 44	39, 39, 36, 29, 31, 28, 38, 37, 44, 39, 35, 49, 33, 38, 38, 27, 22, 32, 34, 46, 52, 45, 37, 38, 34, 47, 43, 49, 44, 43	39, 37, 37, 29, 34, 27, 39, 36, 41, 39, 31, 46, 33, 38, 38, 24, 24, 31, 32, 46, 53, 41, 39, 39, 33, 41, 44, 49, 44, 44	33, 47, 55, 43, 36, 40, 37, 39, 45, 27, 35, 28, 38, 37, 39, 37, 34, 47, 35, 37, 39, 30, 24, 34, 41, 48, 41, 41, 38, 42	39, 38, 41, 37, 33, 50, 36, 38, 36, 28, 34, 26, 32, 37, 37, 26, 25, 31, 34, 48, 52, 43, 38, 36, 45, 49, 45, 54, 45, 34	36, 37, 38, 24, 45, 27, 34, 42, 36, 24, 28, 35, 37, 38, 45, 36, 43, 51, 32, 49, 46, 44, 39, 39, 32, 37, 41, 34, 42, 31
	$t = 3$			$t = 4$		
	I_1	I_2	I_3	I_1	I_2	I_3
U_1	36, 51, 53, 43, 37, 39, 38, 37, 36, 39, 43, 49, 43, 39, 36, 31, 34, 29, 35, 39, 37, 29, 24, 34, 30, 44, 43, 47, 43, 42	**33, 47, 42, 47, 39, 41, 38, 38, 37, 40, 45, 43, 36, 39, 37, 29, 24, 34, 51, 45, 38, 29, 34, 34, 33, 35, 43, 47, 44, 45**	43, 38, 38, 43, 41, 40, 26, 35, 25, 31, 35, 40, 36, 44, 35, 45, 44, 41, 39, 55, 51, 50, 40, 30, 39, 44, 40, 40, 45, 50	40, 36, 39, 27, 33, 28, 35, 36, 38, 37, 33, 48, 34, 37, 38, 29, 23, 33, 32, 47, 54, 44, 36, 38, 35, 41, 42, 47, 41, 43	38, 39, 37, 36, 42, 41, 32, 36, 37, 29, 23, 34, 55, 49, 35, 44, 36, 37, 51, 38, 38, 28, 34, 29, 32, 43, 42, 47, 44, 41	33, 38, 39, 28, 25, 33, 46, 47, 35, 48, 39, 40, 38, 39, 37, 40, 43, 44, 52, 37, 39, 29, 35, 32, 35, 34, 43, 47, 45, 36

Table 1: Continued.

U_2	35, 37, 44, 38, 35, 49, 39, 36, 39, 29, 31, 28, 32, 38, 38, 27, 22, 32, 31, 46, 52, 45, 37, 38, 35, 47, 44, 49, 44, 43	38, 39, 36, 29, 31, 28, 36, 37, 44, 39, 35, 49, 33, 38, 38, 27, 22, 32, 34, 46, 52, 45, 37, 38, 34, 47, 43, 49, 44, 43	34, 37, 38, 37, 33, 49, 39, 37, 43, 30, 34, 28, 33, 37, 39, 28, 24, 34, 35, 47, 53, 45, 38, 39, 44, 50, 51, 49, 43, 44	U_2	37, 38, 39, 37, 44, 41, 37, 32, 45, 26, 29, 35, 32, 49, 40, 48, 38, 53, 47, 44, 38, 25, 35, 35, 39, 35, 45, 50, 45, 42	50, 40, 38, 24, 32, 34, 40, 41, 34, 29, 27, 34, 35, 49, 39, 50, 38, 55, 38, 38, 38, 42, 43, 40, 45, 31, 42, 50, 45, 40	51, 40, 41, 24, 32, 34, 33, 45, 43, 50, 39, 52, 37, 40, 37, 37, 43, 45, 32, 39, 41, 27, 27, 35, 38, 34, 41, 37, 46, 42
U_3	38, 32, 45, 25, 29, 35, 36, 38, 38, 37, 44, 42, 33, 49, 45, 48, 38, 53, 48, 44, 37, 26, 35, 35, 38, 35, 45, 50, 45, 40	42, 35, 43, 49, 40, 55, 39, 40, 36, 39, 44, 34, 37, 43, 42, 23, 32, 33, 35, 38, 41, 29, 27, 35, 46, 32, 41, 36, 41, 45	55, 49, 33, 44, 36, 37, 35, 39, 39, 36, 42, 41, 31, 36, 37, 29, 23, 34, 52, 38, 38, 28, 34, 29, 30, 43, 42, 47, 44, 40	U_3	38, 37, 43, 38, 34, 48, 36, 39, 42, 24, 33, 28, 35, 38, 40, 29, 24, 33, 32, 48, 53, 44, 37, 39, 42, 47, 42, 49, 44, 45	37, 38, 42, 39, 32, 48, 32, 39, 39, 26, 24, 34, 37, 36, 44, 28, 33, 29, 31, 49, 55, 44, 39, 39, 29, 46, 41, 47, 41, 40	31, 38, 39, 29, 24, 33, 37, 36, 37, 27, 33, 29, 35, 36, 41, 37, 34, 48, 36, 46, 51, 43, 36, 39, 30, 41, 42, 47, 45, 41
U_4	38, 37, 42, 30, 34, 29, 39, 40, 38, 37, 33, 49, 35, 37, 39, 28, 24, 34, 35, 47, 53, 45, 38, 39, 43, 50, 54, 47, 43, 44	38, 36, 37, 36, 33, 46, 32, 36, 36, 29, 25, 33, 38, 37, 43, 26, 35, 27, 32, 45, 53, 44, 37, 39, 43, 49, 41, 47, 36, 45	40, 39, 45, 38, 33, 49, 36, 39, 37, 28, 35, 27, 30, 37, 36, 29, 24, 33, 31, 47, 53, 44, 37, 37, 45, 49, 42, 52, 43, 44	U_4	36, 37, 38, 27, 24, 35, 32, 48, 51, 42, 39, 39, 36, 39, 37, 38, 42, 48, 53, 38, 37, 26, 34, 28, 33, 43, 44, 49, 46, 41	38, 39, 37, 38, 43, 44, 30, 39, 37, 29, 24, 34, 35, 49, 42, 44, 38, 39, 51, 38, 36, 29, 34, 30, 35, 33, 44, 49, 45, 40	30, 54, 44, 49, 36, 39, 36, 39, 37, 39, 44, 41, 30, 37, 41, 29, 23, 35, 52, 43, 37, 24, 34, 36, 36, 35, 45, 48, 31, 39
U_5	36, 47, 41, 48, 38, 53, 44, 50, 39, 21, 31, 35, 36, 39, 41, 30, 29, 31, 36, 38, 37, 40, 45, 44, 38, 35, 41, 49, 45, 45	36, 44, 45, 49, 37, 53, 40, 46, 36, 25, 35, 31, 34, 40, 41, 29, 29, 34, 37, 38, 40, 40, 43, 44, 39, 32, 44, 36, 45, 41	37, 40, 36, 39, 44, 34, 45, 35, 43, 49, 40, 55, 38, 43, 42, 23, 32, 33, 35, 38, 41, 29, 27, 35, 41, 32, 41, 36, 40, 40	U_5	38, 37, 36, 37, 33, 48, 32, 37, 39, 28, 24, 34, 38, 37, 43, 30, 34, 28, 36, 47, 53, 45, 39, 39, 45, 50, 51, 47, 43, 45	38, 37, 36, 37, 33, 46, 35, 36, 36, 29, 25, 33, 37, 38, 43, 26, 35, 27, 35, 46, 53, 44, 37, 39, 44, 48, 41, 47, 36, 44	38, 39, 45, 38, 33, 48, 29, 37, 36, 29, 24, 33, 39, 37, 39, 29, 35, 27, 35, 47, 53, 44, 37, 37, 47, 49, 42, 52, 43, 39
U_6	36, 37, 41, 39, 31, 49, 39, 44, 38, 27, 32, 29, 35, 38, 36, 29, 24, 34, 30, 49, 52, 43, 39, 39, 40, 53, 41, 49, 42, 44	39, 37, 44, 39, 35, 49, 37, 38, 36, 29, 31, 29, 34, 38, 38, 27, 22, 32, 33, 46, 52, 45, 37, 38, 32, 47, 44, 49, 44, 43	40, 36, 41, 37, 31, 46, 34, 38, 39, 24, 24, 31, 38, 37, 37, 29, 34, 27, 33, 46, 53, 41, 39, 39, 32, 41, 44, 49, 44, 45	U_6	38, 39, 45, 25, 35, 28, 35, 37, 39, 37, 34, 47, 34, 47, 55, 43, 36, 40, 36, 37, 39, 30, 27, 34, 44, 48, 41, 41, 38, 40	32, 38, 37, 26, 25, 31, 38, 39, 41, 37, 33, 50, 37, 38, 36, 29, 34, 26, 35, 48, 52, 43, 38, 37, 47, 45, 45, 54, 45, 35	35, 42, 36, 24, 28, 35, 37, 38, 44, 36, 43, 51, 37, 37, 38, 24, 45, 27, 34, 49, 46, 44, 39, 39, 31, 37, 41, 34, 42, 38

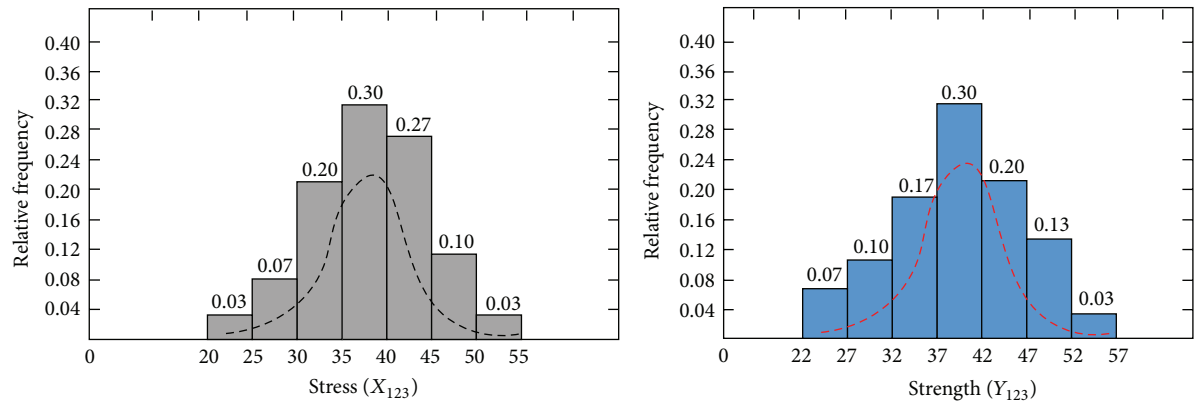

Figure 4: Histograms of X_{123} and Y_{123}.

Table 2: Observation parameters B_{nmtj}.

	$t = 1$			$t = 2$		
	I_1	I_2	I_3	I_1	I_2	I_3
U_1	39, 53, 50, 51, 39, 29, 36, 45, 34, 41, 34, 39, 27, 36, 25, 30, 30, 39, 38, 40, 41, 39, 49, 50, 42, 45, 39, 44, 45, 53	37, 46, 35, 39, 34, 38, 27, 36, 25, 31, 36, 40, 42, 53, 51, 50, 39, 33, 44, 39, 41, 41, 50, 51, 45, 45, 42, 45, 46, 52	42, 40, 41, 39, 48, 49, 30, 36, 25, 30, 37, 40, 37, 53, 48, 52, 40, 32, 34, 45, 35, 46, 35, 41, 42, 45, 39, 46, 44, 54	34, 45, 51, 44, 37, 38, 36, 35, 40, 28, 35, 24, 38, 44, 43, 35, 34, 57, 33, 34, 37, 29, 42, 30, 43, 49, 43, 46, 40, 41	37, 39, 39, 41, 46, 51, 23, 36, 25, 29, 31, 40, 40, 56, 54, 48, 40, 30, 34, 47, 36, 39, 34, 41, 44, 43, 39, 46, 44, 52	40, 41, 40, 39, 51, 49, 25, 35, 27, 31, 34, 41, 42, 56, 51, 50, 41, 31, 37, 46, 36, 44, 36, 38, 43, 46, 39, 45, 46, 52
U_2	31, 33, 26, 31, 35, 38, 37, 45, 35, 45, 35, 42, 41, 55, 49, 50, 40, 29, 41, 43, 40, 40, 46, 45, 39, 45, 38, 43, 46, 51	45, 38, 38, 39, 41, 45, 38, 54, 51, 50, 42, 31, 36, 46, 35, 46, 44, 41, 27, 36, 26, 29, 35, 38, 42, 45, 40, 43, 46, 51	42, 57, 52, 50, 44, 35, 35, 47, 35, 47, 46, 41, 48, 40, 39, 44, 37, 44, 27, 36, 26, 31, 37, 40, 43, 46, 38, 44, 45, 47	41, 40, 41, 45, 39, 45, 24, 36, 26, 31, 30, 39, 42, 51, 55, 48, 36, 39, 33, 42, 32, 33, 37, 38, 43, 47, 41, 48, 46, 55	40, 38, 39, 41, 47, 46, 35, 46, 36, 44, 44, 40, 31, 36, 25, 30, 36, 41, 41, 54, 50, 50, 41, 31, 37, 46, 41, 45, 46, 50	32, 43, 43, 50, 39, 52, 39, 41, 37, 37, 43, 45, 51, 41, 41, 24, 32, 34, 32, 39, 41, 55, 27, 35, 37, 34, 41, 37, 43, 42
U_3	37, 45, 34, 40, 35, 40, 39, 55, 51, 48, 37, 32, 25, 37, 41, 29, 31, 40, 41, 39, 39, 41, 49, 41, 45, 43, 41, 44, 46, 53	26, 35, 41, 32, 29, 38, 41, 39, 39, 40, 48, 39, 39, 54, 52, 49, 38, 31, 33, 45, 35, 39, 36, 41, 43, 44, 26, 45, 45, 43	39, 54, 51, 49, 38, 31, 41, 38, 39, 41, 48, 38, 34, 45, 36, 39, 37, 38, 35, 36, 42, 28, 31, 38, 44, 45, 27, 44, 45, 47	32, 44, 35, 46, 34, 41, 28, 36, 25, 30, 36, 40, 37, 53, 48, 51, 40, 30, 42, 40, 41, 39, 48, 48, 42, 45, 38, 46, 44, 53	40, 39, 38, 40, 41, 45, 35, 44, 35, 45, 44, 41, 27, 35, 26, 31, 35, 40, 41, 55, 51, 50, 40, 30, 38, 45, 41, 43, 45, 50	57, 36, 38, 27, 33, 28, 35, 39, 41, 37, 34, 48, 30, 39, 39, 29, 24, 33, 35, 46, 51, 43, 36, 38, 30, 41, 42, 47, 46, 41
U_4	42, 44, 42, 45, 54, 47, 38, 57, 49, 51, 41, 40, 35, 46, 35, 45, 46, 47, 29, 36, 30, 31, 41, 35, 48, 41, 38, 47, 37, 27	47, 54, 52, 48, 46, 39, 37, 46, 42, 42, 25, 45, 53, 42, 39, 45, 35, 46, 36, 46, 34, 47, 38, 42, 28, 35, 32, 31, 41, 37	48, 41, 38, 46, 41, 43, 36, 45, 36, 47, 46, 27, 42, 46, 39, 44, 54, 42, 50, 46, 52, 49, 45, 39, 31, 34, 32, 32, 40, 37	40, 38, 41, 39, 49, 48, 33, 45, 35, 46, 36, 41, 30, 36, 25, 32, 36, 40, 41, 55, 49, 51, 40, 31, 40, 45, 38, 46, 44, 54	47, 38, 39, 39, 40, 45, 38, 54, 51, 50, 41, 32, 34, 46, 35, 46, 44, 40, 27, 36, 26, 29, 35, 38, 42, 45, 40, 43, 46, 51	30, 50, 44, 49, 37, 39, 38, 39, 37, 39, 44, 41, 33, 37, 40, 29, 23, 35, 53, 43, 37, 24, 34, 35, 36, 35, 45, 49, 41, 39
U_5	42, 39, 40, 40, 48, 52, 39, 56, 52, 49, 39, 31, 26, 36, 42, 31, 30, 41, 37, 46, 34, 38, 36, 41, 45, 45, 39, 45, 47, 53	32, 48, 36, 39, 36, 38, 38, 40, 38, 42, 45, 41, 37, 53, 51, 47, 38, 33, 27, 37, 41, 32, 31, 41, 42, 43, 41, 48, 46, 53	38, 53, 50, 48, 39, 31, 36, 45, 35, 40, 37, 38, 40, 39, 38, 40, 49, 41, 36, 35, 40, 29, 31, 39, 45, 43, 26, 46, 56, 46	38, 39, 43, 30, 34, 28, 34, 37, 39, 28, 24, 34, 39, 39, 38, 37, 33, 49, 34, 47, 53, 45, 38, 39, 43, 50, 51, 47, 43, 45	37, 39, 37, 39, 33, 46, 33, 36, 36, 29, 25, 33, 39, 38, 43, 26, 35, 29, 31, 46, 53, 44, 38, 39, 45, 49, 41, 47, 39, 45	39, 37, 39, 28, 35, 27, 32, 37, 36, 29, 24, 33, 31, 47, 53, 44, 38, 38, 37, 39, 45, 38, 33, 49, 42, 49, 42, 52, 43, 44
U_6	39, 54, 51, 49, 38, 28, 23, 35, 27, 31, 29, 41, 33, 44, 34, 38, 37, 38, 38, 41, 40, 41, 48, 50, 42, 46, 41, 45, 46, 53	41, 38, 42, 43, 49, 52, 24, 36, 27, 31, 28, 44, 36, 55, 50, 48, 38, 29, 32, 46, 36, 40, 37, 39, 43, 45, 42, 44, 48, 53	39, 42, 39, 42, 47, 51, 25, 35, 27, 33, 30, 39, 42, 53, 50, 48, 39, 29, 33, 45, 32, 39, 36, 37, 43, 45, 39, 44, 47, 54	40, 37, 39, 37, 34, 47, 34, 47, 56, 43, 36, 40, 38, 39, 45, 27, 35, 28, 36, 37, 39, 30, 24, 34, 40, 48, 41, 41, 38, 42	37, 38, 36, 28, 34, 26, 31, 39, 39, 26, 25, 31, 40, 38, 41, 39, 33, 50, 35, 48, 52, 43, 38, 36, 44, 39, 45, 54, 45, 35	38, 38, 45, 36, 43, 49, 39, 37, 38, 24, 45, 57, 34, 42, 36, 24, 28, 35, 31, 49, 46, 44, 39, 39, 33, 39, 41, 34, 42, 31
	$t = 3$			$t = 4$		
	I_1	I_2	I_3	I_1	I_2	I_3
U_1	32, 37, 40, 29, 23, 35, 38, 39, 38, 39, 44, 41, 33, 50, 44, 49, 36, 39, 53, 43, 38, 24, 34, 35, 36, 35, 45, 49, 41, 42	**39, 45, 42, 45, 55, 27, 48, 25, 51, 49, 32, 41, 37, 46, 34, 44, 38, 45, 49, 42, 39, 45, 39, 39, 33, 34, 31, 30, 41, 35**	38, 47, 34, 46, 46, 46, 41, 56, 50, 51, 42, 38, 42, 45, 42, 42, 45, 44, 28, 35, 28, 32, 41, 36, 51, 42, 39, 45, 37, 26	37, 46, 35, 46, 40, 46, 39, 44, 42, 41, 52, 43, 42, 53, 52, 48, 44, 38, 27, 34, 32, 30, 40, 35, 53, 41, 38, 41, 35, 47	26, 36, 28, 30, 42, 37, 43, 47, 39, 42, 44, 45, 42, 56, 51, 51, 43, 36, 33, 46, 35, 41, 47, 42, 51, 41, 38, 42, 36, 42	41, 39, 39, 41, 49, 41, 39, 55, 51, 48, 38, 32, 27, 37, 41, 30, 31, 40, 36, 45, 34, 39, 35, 40, 45, 43, 41, 44, 46, 53

Table 2: Continued.

U_2	33, 47, 53, 44, 38, 39, 39, 37, 39, 28, 35, 27, 39, 39, 45, 38, 33, 49, 32, 38, 36, 29, 24, 33, 43, 49, 42, 52, 43, 45	48, 41, 38, 46, 41, 44, 34, 45, 36, 47, 46, 42, 42, 46, 39, 44, 54, 42, 53, 46, 52, 49, 45, 39, 27, 34, 32, 32, 40, 37	40, 44, 42, 45, 54, 47, 38, 57, 49, 51, 41, 40, 35, 42, 35, 45, 46, 47, 29, 36, 30, 31, 41, 35, 48, 41, 38, 47, 37, 26	U_2	36, 46, 34, 47, 44, 42, 42, 54, 52, 49, 46, 39, 38, 46, 42, 47, 52, 40, 53, 42, 39, 41, 35, 46, 27, 35, 32, 31, 41, 36	27, 35, 26, 31, 35, 40, 40, 39, 38, 40, 41, 45, 35, 44, 35, 45, 44, 41, 40, 54, 51, 50, 40, 30, 38, 45, 41, 43, 45, 51	38, 55, 50, 49, 39, 31, 42, 38, 39, 40, 48, 42, 26, 36, 40, 31, 30, 41, 36, 46, 35, 38, 36, 41, 44, 45, 40, 45, 47, 55
U_3	33, 49, 46, 44, 39, 38, 35, 38, 38, 28, 45, 27, 34, 53, 36, 24, 28, 35, 39, 38, 45, 38, 43, 49, 34, 38, 41, 34, 42, 33	47, 43, 51, 48, 44, 40, 38, 48, 35, 46, 45, 44, 37, 44, 40, 45, 56, 41, 49, 42, 39, 42, 40, 45, 33, 37, 30, 29, 41, 35	37, 43, 41, 46, 54, 45, 44, 56, 50, 49, 42, 39, 36, 45, 35, 47, 42, 42, 28, 35, 31, 29, 40, 34, 51, 42, 39, 44, 34, 26	U_3	48, 45, 49, 51, 45, 42, 39, 42, 37, 43, 43, 45, 48, 39, 39, 36, 38, 45, 42, 45, 42, 46, 55, 38, 25, 36, 30, 29, 39, 35	36, 46, 35, 46, 44, 40, 38, 54, 51, 50, 41, 31, 47, 38, 38, 39, 40, 45, 27, 36, 26, 29, 35, 38, 42, 45, 40, 43, 46, 51	34, 47, 36, 39, 35, 39, 38, 40, 38, 41, 49, 40, 39, 53, 51, 48, 38, 32, 25, 36, 41, 32, 31, 42, 42, 43, 41, 47, 46, 54
U_4	41, 39, 41, 42, 48, 51, 27, 35, 41, 32, 29, 40, 39, 55, 51, 48, 38, 29, 35, 45, 33, 39, 37, 39, 45, 46, 40, 46, 45, 54	40, 39, 38, 41, 49, 40, 37, 55, 51, 48, 38, 32, 27, 37, 41, 30, 31, 40, 35, 45, 34, 39, 35, 40, 43, 43, 41, 45, 46, 53	36, 45, 35, 39, 36, 41, 41, 38, 39, 40, 48, 39, 38, 54, 52, 49, 38, 31, 26, 35, 41, 30, 29, 39, 46, 44, 26, 45, 45, 43	U_4	41, 39, 41, 42, 48, 51, 26, 35, 41, 32, 29, 40, 38, 55, 51, 47, 38, 29, 33, 45, 33, 39, 37, 39, 44, 46, 40, 46, 45, 55	41, 39, 39, 41, 49, 41, 37, 55, 51, 48, 38, 32, 26, 37, 41, 30, 31, 40, 37, 45, 34, 39, 35, 40, 43, 43, 41, 44, 46, 53	33, 45, 35, 39, 36, 41, 42, 39, 38, 40, 48, 39, 39, 53, 52, 37, 38, 31, 26, 35, 41, 30, 29, 39, 43, 44, 26, 45, 45, 43
U_5	35, 46, 35, 38, 36, 41, 42, 38, 39, 40, 48, 42, 38, 55, 50, 49, 39, 31, 27, 36, 40, 31, 30, 41, 44, 44, 40, 45, 47, 55	39, 53, 51, 49, 39, 32, 35, 46, 34, 38, 37, 40, 41, 38, 40, 41, 48, 38, 27, 36, 41, 31, 29, 38, 45, 44, 25, 46, 46, 43	36, 37, 40, 29, 25, 42, 39, 40, 38, 40, 49, 39, 34, 46, 37, 38, 37, 54, 38, 53, 50, 49, 39, 32, 42, 43, 26, 43, 46, 45	U_5	52, 42, 39, 45, 35, 46, 45, 54, 52, 49, 46, 39, 38, 46, 42, 42, 55, 45, 34, 41, 34, 40, 42, 47, 27, 35, 32, 31, 41, 37	48, 41, 38, 46, 41, 42, 34, 45, 36, 47, 46, 27, 42, 46, 39, 44, 54, 42, 52, 46, 52, 49, 45, 39, 31, 34, 32, 32, 40, 36	42, 45, 42, 36, 55, 38, 42, 39, 38, 46, 38, 45, 39, 34, 37, 43, 43, 45, 48, 45, 49, 51, 45, 42, 26, 36, 30, 29, 39, 33
U_6	32, 34, 38, 29, 23, 30, 39, 35, 40, 28, 35, 25, 38, 44, 43, 35, 35, 47, 35, 45, 50, 48, 38, 39, 41, 49, 43, 56, 40, 42	37, 39, 39, 40, 46, 51, 25, 36, 25, 29, 31, 40, 42, 56, 54, 48, 40, 30, 36, 47, 36, 39, 34, 41, 45, 42, 39, 46, 44, 52	42, 41, 40, 41, 51, 48, 25, 34, 26, 31, 34, 41, 42, 56, 51, 50, 41, 31, 37, 46, 36, 45, 36, 38, 43, 46, 38, 45, 46, 53	U_6	39, 43, 41, 42, 54, 45, 44, 56, 50, 49, 42, 39, 34, 45, 35, 47, 45, 42, 29, 35, 31, 29, 40, 34, 51, 42, 39, 44, 34, 27	37, 44, 41, 27, 56, 46, 50, 41, 38, 46, 38, 42, 48, 41, 50, 48, 43, 41, 37, 45, 33, 40, 43, 44, 32, 36, 32, 32, 42, 34	38, 44, 40, 45, 56, 41, 49, 42, 39, 47, 40, 45, 37, 47, 35, 46, 45, 41, 48, 42, 51, 48, 44, 40, 32, 37, 30, 27, 41, 34

Table 3: NS_{nmt} ($n = 1, 2, 3, 4, 5, 6$; $m = 1, 2, 3$; $t = 1, 2, 3, 4$).

			$t = 1$							$t = 2$			
NS	U_1	U_2	U_3	U_4	U_5	U_6	NS	U_1	U_2	U_3	U_4	U_5	U_6
I_1	0.5989	0.5344	**0.6211**	**0.6178**	0.5933	0.5778	I_1	0.5911	**0.5922**	0.5844	**0.6267**	0.5667	0.5267
I_2	0.5667	**0.6200**	0.5844	0.6089	0.5800	**0.6289**	I_2	0.5889	0.5900	**0.6122**	**0.6656**	0.5422	0.5322
I_3	0.5789	**0.6533**	0.5111	**0.6311**	0.6122	0.6100	I_3	**0.6322**	0.5589	0.5222	0.5444	0.5244	**0.5689**
			$t = 3$							$t = 4$			
NS	U_1	U_2	U_3	U_4	U_5	U_6	NS	U_1	U_2	U_3	U_4	U_5	U_6
I_1	0.5356	**0.5856**	0.5067	**0.6111**	0.5711	0.5400	I_1	**0.6700**	0.6156	0.6356	0.6022	0.6122	**0.6400**
I_2	0.5778	**0.6511**	**0.6456**	0.6167	0.5900	0.5956	I_2	0.5822	0.6056	**0.6322**	**0.6433**	0.6211	0.6222
I_3	0.5889	0.6067	0.6244	0.5844	**0.6278**	**0.6378**	I_3	**0.6378**	0.5956	0.6300	0.5844	0.6200	**0.6756**

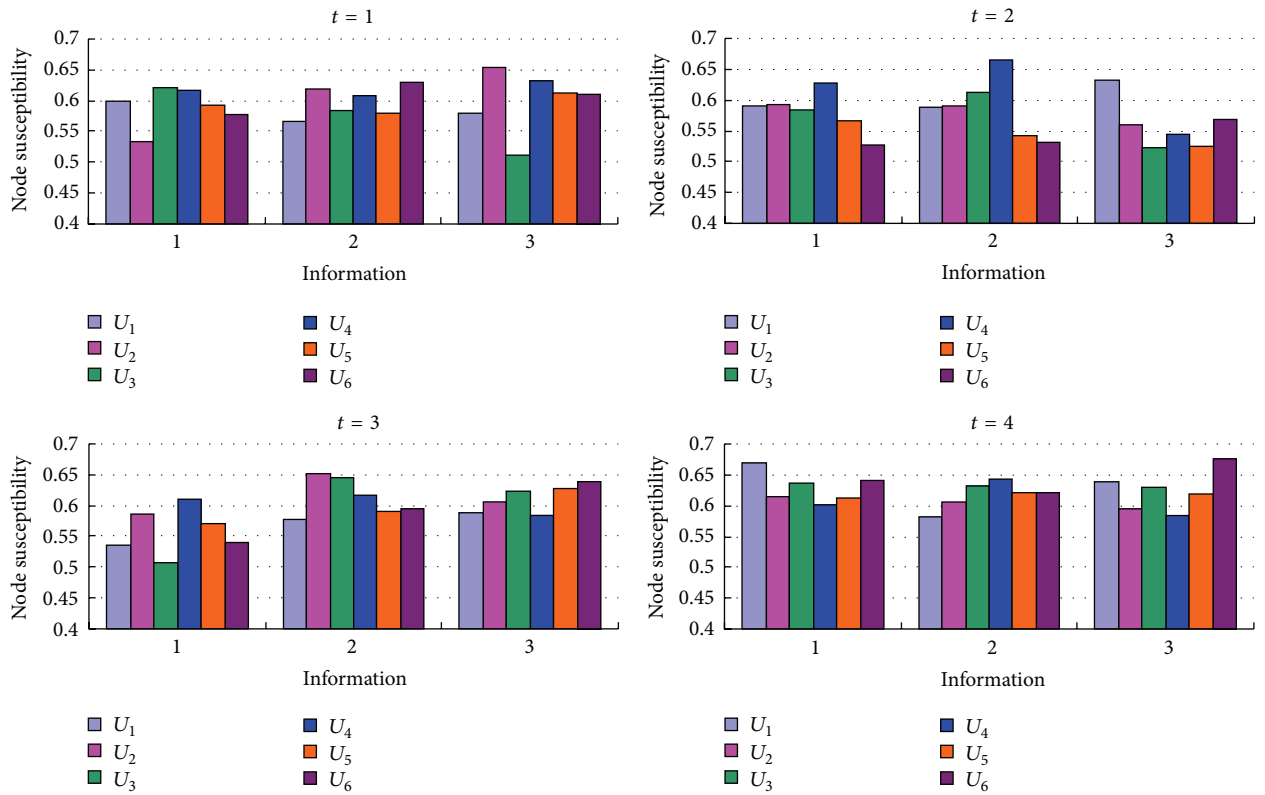

Figure 5: User's NS in regard to the corresponding information at different periods.

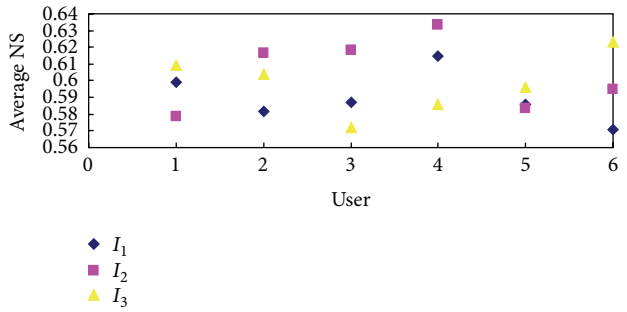

Figure 6: User's average NS.

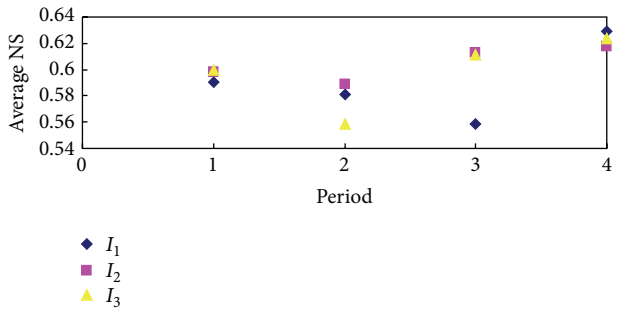

Figure 7: Information's average NS.

more attractive. To quantitatively perform further analysis on the conclusion mentioned above, we calculate user's average NS and information's average NS, respectively, shown in Figures 6 and 7.

It can be seen from Figure 6 that, in regard to information I_1, U_4 is the most susceptible user, followed by U_1. In regard to information I_2, U_4 is also the most susceptible user, followed by U_3. In regard to information I_3, U_6 is the most susceptible user, followed by U_1. Compared with other users, U_5 is the least susceptible user, and he seems to be susceptible to none of these types of information. Indeed, information I_2 and information I_1 are more attractive, which can also be shown in Figure 7. Moreover, Figure 7 shows that values of average NS of three types of information at the fourth period are the highest, which means that advertisement at this period will be most effective.

4.3. Comparison with Other Methods of Measuring User Susceptibility in the Existing Literature. To comprehensively analyze the proposed method for measuring user susceptibility, in this subsection, we will give the comparison with other methods in the existing literature [33–35]. The comparison includes quantified items, quantitative measures, mathematical model, key input parameters for decisions, implementation process in practice, and decision objectives. For the sake of clarity, the results of the comparison are displayed in Table 4.

Table 4: Comparison with other methods in the existing literature.

	Literature [33]	Literature [34]	Literature [35]	This paper
Quantified items	User susceptibility in the product adoption decisions in a social network	User susceptibility that contributes to sentiment-charged content diffusion in a social network	User susceptibility to online brand-related information while making a brand purchase decision	Node susceptibility (NS) to different types of information diffused in a social network
Quantitative measures	Modeling time to peer adoption as a function of the peer's treatment status	Defining user susceptibility to be how easy the user adopts the same sentiments diffused by other users	Using 7-point Likert scales (1: strongly disagree to 7: strongly agree)	Defining NS as the probability that quantity of information the user forwards is larger than quantity of information the user receives
Mathematical model	A continuous-time single-failure proportional hazards model: $\lambda_j(t, X_i, X_j, N_j) = \lambda_0(t) \exp\left[N_j(t)\beta_N + X_i\beta^i_{\text{spont}} + X_j\beta^j_{\text{spont}} + N_j(t)X_i\beta_{\text{infl}} + N_j(t)X_j\beta_{\text{susc}}\right]$	An influence-susceptibility cynical (ISC) model: $S(v) = W_2(v)/\lvert X_{\overleftarrow{i}}(v)\rvert \sum_{x \in X_{\overleftarrow{ds}}(v)} \text{Avg}_{u \in F_{\overleftarrow{ds}}(v,x)} (\Delta x(u, v)(1 - I(u)))$	None	A discrete stress-strength interference (DSSI) model based on universal generating function (UGF): $\text{NS}_{nmt} = \Pr(f(X_{nmt}, Y_{nmt}) > 0) = \sum_{r=1}^{R} \lambda_r \sigma(f_r)$
Key input parameters for decisions	(1) A set of individual attributes of an application user; (2) baseline hazard; (3) the number of notifications received by peer	(1) Item sentiment adopted by user before diffusion; (2) item sentiment adopted by user after diffusion; (3) number of followees of user; (4) number of times sentiment is diffused to user by his followees; (5) set of item sentiments diffused to user and he adopts the same item; (6) set of followees who diffuse item sentiment to user and the user adopts the same item sentiment	(1) Gender; (2) education; (3) personal status; (4) occupation; (5) age; (6) income (per month)	(1) Observation parameter: cumulative quantity of information user received in corresponding time interval; (2) observation parameter: cumulative quantity of information user forwarded in corresponding time interval

Table 4: Continued.

	Literature [33]	Literature [34]	Literature [35]	This paper
Implementation process in practice	Conducting a randomized experiment to estimate β_N, β^i_{spont}, β^j_{spont}, β_{infl}, and β_{susc}	Employing an iterative computation method. The algorithm first initializes susceptibility for all users with 0.5, and the computation process repeats until the values converge	Conducting an online survey on a survey website using a consulting firm panel from Shanghai and Nanjing	Recording the abovementioned observation parameters on corresponding time node and inputting observation parameters to calculate NS
Decision objectives	Identifying which individuals are more susceptible to adopt the product offered	Determining how a user is susceptible to sentiment-charged tweets diffused by others	Determining the extent to which online brand-related information impacted users' brand attitudes and purchase intentions	Determining three questions: (1) which users are most susceptible, (2) which types of information they are most susceptible to, and (3) when they are most susceptible

It can be seen from Table 4 that, on the one hand, mathematical models are common tools of quantifying user susceptibility for information diffusion and, on the other hand, given the difference in decision objectives and quantitative measures, the expression of the model is different, making the input parameters for decisions different in different methods. Generally, in the case that the complexities of the models are equivalent, the model with fewer input parameters is easier for decision-makers (practitioners) to implement in practice. Solving the model with more input parameters requires decision-makers to know specialized knowledge and make subjective judgments, which can enhance difficulty and subjectivity of decision-making. In this sense, the models in literature [33] and this paper may be superior to those in literature [34].

With respect to the models in literature [33] and this paper, it is difficult to say which one is better, since different models serve different decision objectives. By conducting a randomized experiment, the decision results in literature [33] are that younger users are more susceptible than older users, and married individuals are the least susceptible in the decision to adopt the product offered. These decision results give some suggestions in the spread of the product in social networks from a macroscopic perspective. In comparison, the decision results (answers to the three questions) in this paper can provide the practitioners with specific reference to make rational decisions on effective information diffusion. In addition, the decision results in literature [33] are static to some extent. Our decision results are dynamic and can be updated with the updated observation data, which can help the practitioners to make information diffusion strategy dynamically.

5. Conclusion

In this work, a novel and efficient model for analyzing the effect of nodes on information diffusion is proposed based on universal generating function (UGF) method and discrete stress-strength interference (DSSI) theory. In this model, the effect of user on information diffusion is quantified as node susceptibility (NS), and based on NS the proposed model can help decision-makers to identify which users are most susceptible to the corresponding information at different periods. The contributions of the research can be summarized as follows.

(1) To take into account the influence of randomness and uncertainty, the model introduces a novel and universal evaluation criterion—node susceptibility (NS), based on discrete stress-strength interference (DSSI) theory. Since the calculation of NS is based on the realistic observations of the corresponding random variables, the decision results are rational and objective.

(2) By modeling random forwarding actions, the effect of network nodes on information diffusion is analyzed quantitatively and dynamically. In proposed model, three main questions are solved: (i) which nodes are most susceptible, (ii) which types of information they are most susceptible to, and (iii) when they are most susceptible. The solutions of these questions are very helpful for the practitioners to make rational decisions on effective information diffusion.

(3) Different from the existing related works that mainly focus on extracting the most influential nodes, this work focuses on extracting the most susceptible nodes, which exploits a new idea for studying information diffusion over social networks.

Despite the contributions, this study has several limitations. Although the proposed model can provide objective and dynamic decisions based on NS, it cannot provide the cause of the fluctuation of NS. In other words, decision-makers may not know why some users are not susceptible and why some types of information are not attractive. In addition, users' forwarding actions may be influenced by network structure or topology relationship of users, which are not considered in the model.

Based on these considerations, this research suggests two avenues for future research. (i) To make the factors that influence the fluctuation of NS more obvious, future researchers can introduce information evaluation mechanism in the model. (ii) When modeling random forwarding actions, network structure or topology relationship of users can be considered as one of the factors influencing information diffusion. It is envisioned to be possible to apply the point-set topology theory and graph theory to address this new issue.

Appendix

Steps of Calculation of NS by Using SPSS

The steps of calculation of NS by using SPSS will be given in detail as follows.

*Step 1** (deriving X_{nmt}'s p.m.f. and Y_{nmt}'s p.m.f. by using SPSS)

(a) Creating the Data Files of X_{nmt}'s Observations and Y_{nmt}'s Observations. In "Variable View," "X_{nmt}" is set as the variable name (Figure 8). Then, W (the number of X_{nmt}'s observations) values of data are imported in "Data View" (Figure 9), and a data file with W rows and one column is created.

Similarly, "Y_{nmt}" is set as another variable name in "Variable View." Z (the number of Y_{nmt}'s observations) values of data are imported in "Data View," and another data file with Z rows and one column is created.

(b) Plotting Histograms with Relative Frequency as Ordinate. We choose the options of "Graphs," "Legacy Dialogs," "Interactive," and "Histogram" in sequence (Figure 10), and then a "Create Histogram" dialog box will appear. In "Assign Variables" list box, we select "X_{nmt}" and drag it into "Create Histogram" dialog box. To set relative frequency as ordinate, we need to select "Percent" in "Assign Variables" list box, and drag it into "Count" dialog box (Figure 11).

In "Histogram" option, we choose "Normal curve" check box, which means that normal curve will appear in the output. Meanwhile, we set "Number of interval" as 7 (decision-maker can set it as other values as needed), which means that

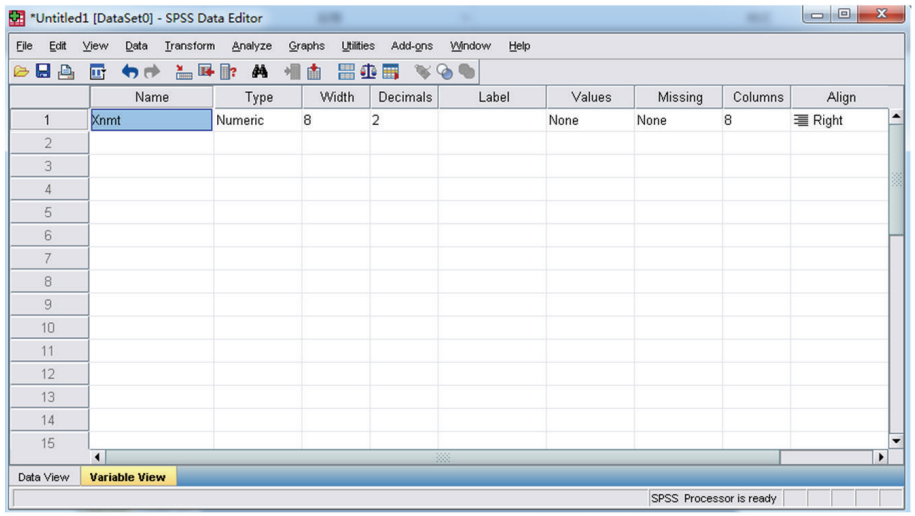

Figure 8: Set X_{nmt} as the variable name in "Variable View."

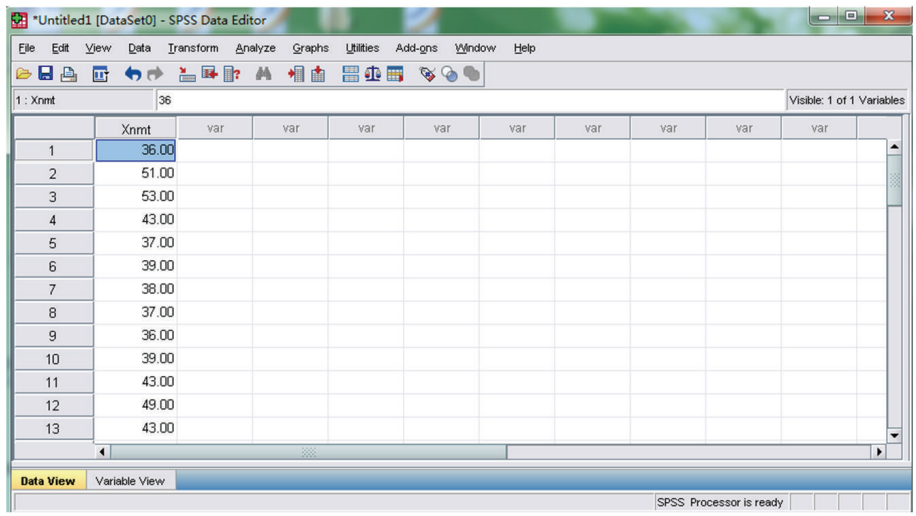

Figure 9: Import values of data in "Data View."

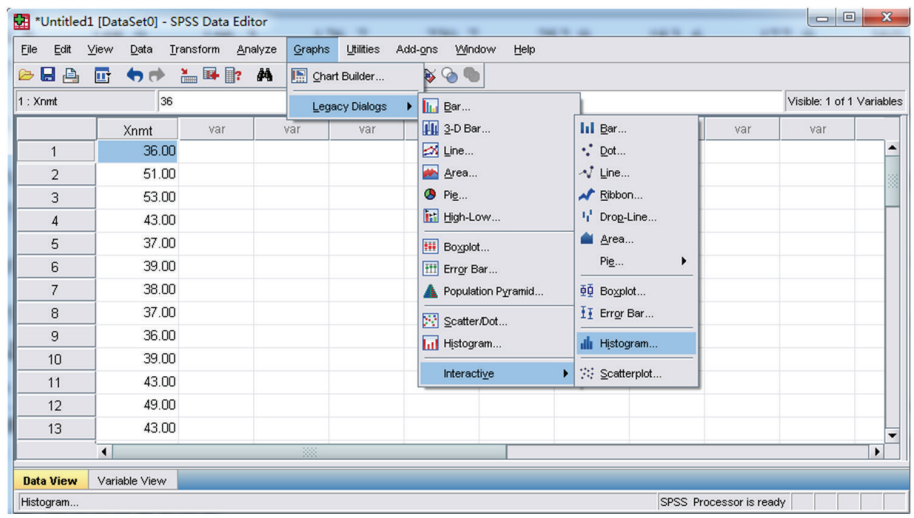

Figure 10: "Data Editor" dialog box.

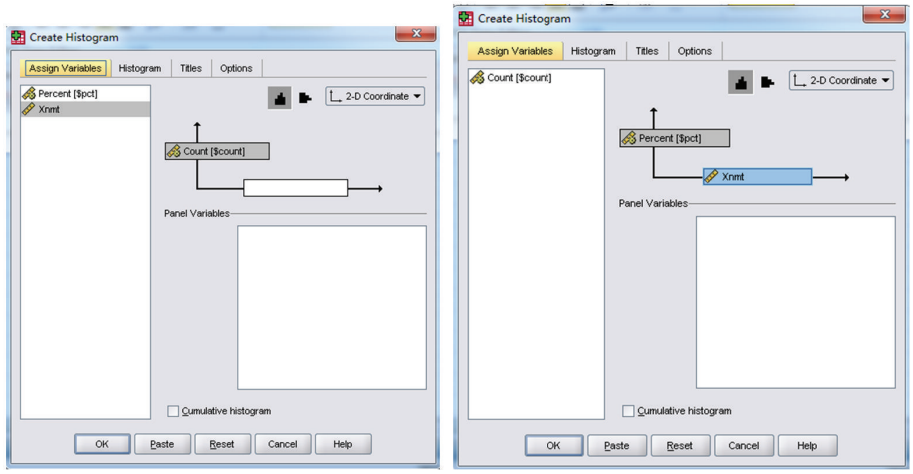

Figure 11: "Create Histogram" dialog box.

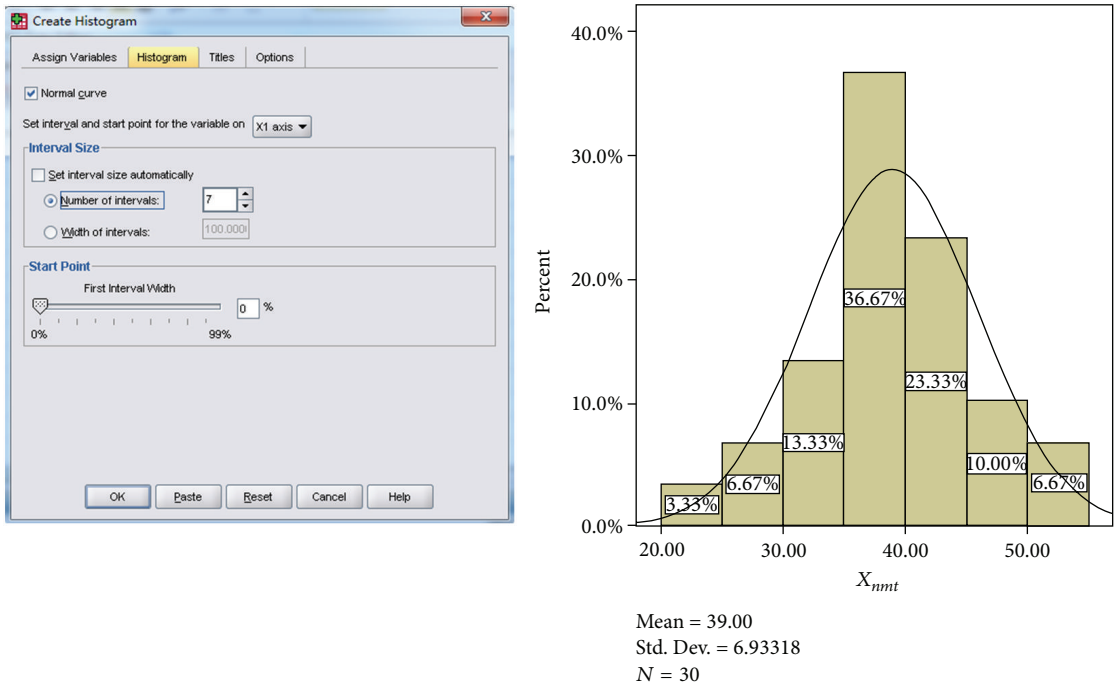

Figure 12: Creating histogram with relative frequency as ordinate.

the number of interval of output is 7. Finally, click OK, and the histogram of X_{nmt}'s observations is obtained (Figure 12). Similarly, the histogram of Y_{nmt}'s observations can also be obtained based on the steps above. The general forms of two histograms are shown in Figure 3.

(c) Obtaining X_{nmt}'s p.m.f. and Y_{nmt}'s p.m.f. Based on the Histograms in (b). The midpoint values of each class interval of two histograms are, respectively, treated as possible values of X_{nmt} and Y_{nmt}, and relative frequencies of each class interval are treated as corresponding probabilities. Thus, X_{nmt}'s p.m.f. and Y_{nmt}'s p.m.f. can, respectively, be obtained according to (13)–(14) in Section 3.2.2.

Steps 2* and 3* are the same as Steps 2 and 3 we presented in Section 3.2.2, so we will not repeat here for reasons of brevity.

Notations

n: Index of users
m: Index of types of information
t: Index of periods
tj: Index of time nodes of the tth period
U_n: The nth user
I_m: The mth type of information
P_t: The tth period

Q_{tj}: The jth time node of P_t
$[Q_{t,j-1}, Q_{tj}]$: The $(j-1)$th, $j = 2, 3, \ldots, L_t$, time interval of P_t
A_{nmtj}: Cumulative quantity of I_m that U_n received in time interval $[Q_{t,j-1}, Q_{tj}]$, and it is an observation parameter on time node Q_{ij}
B_{nmtj}: Cumulative quantity of I_m that U_n forwarded in time interval $[Q_{t,j-1}, Q_{tj}]$, and it is an observation parameter on time node Q_{ij}
X_{nmt}: Quantity of I_m that U_n received at P_t, and it is a discrete random variable
Y_{nmt}: Quantity of I_m that U_n forwarded at P_t, and it is a discrete random variable
NS_{nmt}: Susceptibility of U_n in regard to I_m at P_t
N: Number of users
M: Number of types of information
T: Number of periods
L_t: Number of time nodes of P_t.

Competing Interests

The authors declare that they have no competing interests.

Acknowledgments

This work was supported by the National Natural Science Foundation of China under Grant no. 61173015, no. 61573257, no. 61273046, and no. 11401273. The authors should show their great thanks to all of their hard working fellows in the projects above.

References

[1] E. Bakshy, I. Rosenn, C. Marlow, and L. Adamic, "The role of social networks in information diffusion," in *Proceedings of the 21st Annual Conference on World Wide Web (WWW '12)*, pp. 519–528, Lyon, France, April 2012.

[2] J. Xu, J. X. Xiang, X. Chen, F. B. Liu, and J. J. Yu, "ODMBP: behavior forwarding for multiple property destinations in mobile social networks," *Mobile Information Systems*, vol. 2016, Article ID 7908328, 11 pages, 2016.

[3] M. Kimura and K. Saito, "Tractable models for information diffusion in social networks," in *Knowledge Discovery in Databases: PKDD 2006*, vol. 4213 of *Lecture Notes in Computer Science*, pp. 259–271, Springer, Berlin, Germany, 2006.

[4] Y. Wang, C. Zhao, Q. Xu, Z. Zheng, Z. Chen, and Z. Liu, "Fair secure computation with reputation assumptions in the mobile social networks," *Mobile Information Systems*, vol. 2015, Article ID 637458, 8 pages, 2015.

[5] Wikipedia, Mobile Social Network, https://en.wikipedia.org/wiki/Mobile_social_network.

[6] A. L. Traud, P. J. Mucha, and M. A. Porter, "Social structure of facebook networks," *Physica A: Statistical Mechanics and Its Applications*, vol. 391, no. 16, pp. 4165–4180, 2012.

[7] R. Xiang, J. Neville, and M. Rogati, "Modeling relationship strength in online social networks," in *Proceedings of the 19th International Conference on World Wide Web*, pp. 981–990, ACM, April 2010.

[8] C. Jiang, Y. Chen, and K. J. R. Liu, "Evolutionary dynamics of information diffusion over social networks," *IEEE Transactions on Signal Processing*, vol. 62, no. 17, pp. 4573–4586, 2014.

[9] O. Yağan, D. Qian, J. Zhang, and D. Cochran, "Conjoining speeds up information diffusion in overlaying social-physical networks," *IEEE Journal on Selected Areas in Communications*, vol. 31, no. 6, pp. 1038–1048, 2013.

[10] E. K. Lua, R. Chen, and Z. Cai, "Social trust and reputation in online social networks," in *Proceedings of IEEE 17th International Conference on Parallel and Distributed Systems*, pp. 811–816, Tainan, Taiwan, December 2011.

[11] Wikipedia, Facebook, https://en.wikipedia.org/wiki/Facebook.

[12] G. Miritello, E. Moro, and R. Lara, "Dynamical strength of social ties in information spreading," *Physical Review E*, vol. 83, no. 4, Article ID 045102, 2011.

[13] C. Jiang, Y. Chen, and K. J. R. Liu, "Graphical evolutionary game for information diffusion over social networks," *IEEE Journal on Selected Topics in Signal Processing*, vol. 8, no. 4, pp. 524–536, 2014.

[14] J. Jiang, S. Wen, S. Yu, Y. Xiang, and W. Zhou, "K-center: an approach on the multi-source identification of information diffusion," *IEEE Transactions on Information Forensics and Security*, vol. 10, no. 12, pp. 2616–2626, 2015.

[15] R. Pastor-Satorras and A. Vespignani, "Epidemic spreading in scale-free networks," *Physical Review Letters*, vol. 86, no. 14, pp. 3200–3203, 2001.

[16] D. Gruhl, R. Guha, D. Liben-Nowell, and A. Tomkins, "Information diffusion through blogspace," in *Proceedings of the 13th International World Wide Web Conference (WWW '04)*, pp. 491–501, New York, NY, USA, May 2004.

[17] A.-L. Barabási and R. Albert, "Emergence of scaling in random networks," *Science*, vol. 286, no. 5439, pp. 509–512, 1999.

[18] L. Donetti, P. I. Hurtado, and M. A. Mũoz, "Network synchronization: optimal and pessimal scale-free topologies," *Journal of Physics A: Mathematical and Theoretical*, vol. 41, no. 22, Article ID 224008, 2008.

[19] M. Lin and N. Li, "Scale-free network provides an optimal pattern for knowledge transfer," *Physica A: Statistical Mechanics and Its Applications*, vol. 389, no. 3, pp. 473–480, 2010.

[20] Y. Li, M. Qian, D. Jin, P. Hui, and A. V. Vasilakos, "Revealing the efficiency of information diffusion in online social networks of microblog," *Information Sciences*, vol. 293, pp. 383–389, 2015.

[21] S. J. Park, Y. S. Lim, and H. W. Park, "Comparing Twitter and YouTube networks in information diffusion: the case of the 'Occupy Wall Street' movement," *Technological Forecasting and Social Change*, vol. 95, pp. 208–217, 2015.

[22] M. Kimura, K. Saito, R. Nakano, and H. Motoda, "Extracting influential nodes on a social network for information diffusion," *Data Mining and Knowledge Discovery*, vol. 20, no. 1, pp. 70–97, 2010.

[23] W. Yu, G. Cong, G. Song, and K. Xie, "Community-based Greedy algorithm for mining top-K influential nodes in mobile social networks," in *Proceedings of the 16th ACM SIGKDD International Conference on Knowledge Discovery and Data Mining (KDD '10)*, pp. 1039–1048, July 2010.

[24] M. U. Ilyas, M. Z. Shafiq, A. X. Liu, and H. Radha, "A distributed and privacy preserving algorithm for identifying information hubs in social networks," in *Proceedings of the IEEE International Conference on Computer Communications (IEEE INFOCOM '11)*, pp. 561–565, Shanghai, China, April 2011.

[25] J. Yang and S. Counts, "Predicting the speed, scale, range of information diffusion in twitter," in *Proceedings of the 4th International AAAI Conference on Weblogs and Social Media*, pp. 355–358, 2010.

[26] J. Yang and J. Leskovec, "Modeling information diffusion in implicit networks," in *Proceedings of the IEEE International Conference on Data Mining*, pp. 599–608, IEEE, Sydney, Australia, December 2010.

[27] K. Saito, M. Kimura, K. Ohara, and H. Motoda, "Super mediator—a new centrality measure of node importance for information diffusion over social network," *Information Sciences*, vol. 329, pp. 985–1000, 2016.

[28] V. Belák, A. Mashhadi, A. Sala, and D. Morrison, "Phantom cascades: the effect of hidden nodes on information diffusion," *Computer Communications*, vol. 73, pp. 12–21, 2016.

[29] I. A. Ushakov, "A universal generating function," *Soviet Journal of Computer and Systems Sciences*, vol. 24, no. 5, pp. 118–129, 1986.

[30] A. Lisnianski and G. Levitin, *Multi-State System Reliability: Assessment, Optimization and Applications*, World Scientific, Singapore, 2003.

[31] G. Levitin, *The Universal Generating Function in Reliability Analysis and Optimization*, Springer, London, UK, 2005.

[32] C. Ebeling, *An Introduction to Reliability and Maintainability Engineering*, Waveland Press, Long Grove, Ill, USA, 2005.

[33] S. Aral and D. Walker, "Identifying influential and susceptible members of social networks," *Science*, vol. 337, no. 6092, pp. 337–341, 2012.

[34] R. K. Lee and E. Lim, "Measuring user influence, susceptibility and cynicalness in sentiment diffusion," in *Advances in Information Retrieval: 37th European Conference on IR Research, ECIR 2015, Vienna, Austria, March 29–April 2, 2015. Proceedings*, vol. 9022 of *Lecture Notes in Computer Science*, pp. 411–422, Springer, Berlin, Germany, 2015.

[35] J. Chen, L. Teng, Y. Yu, and X. Yu, "The effect of online information sources on purchase intentions between consumers with high and low susceptibility to informational influence," *Journal of Business Research*, vol. 69, pp. 467–475, 2016.

[36] Wikipedia, Meituan, https://en.wikipedia.org/wiki/Meituan.com.

[37] baike.baidu, Meituan, http://baike.baidu.com/view/3318024.htm.

Hindawi Publishing Corporation
Mobile Information Systems
Volume 2016, Article ID 4916563, 18 pages
http://dx.doi.org/10.1155/2016/4916563

Research Article

Crowdsource Based Indoor Localization by Uncalibrated Heterogeneous Wi-Fi Devices

Wooseong Kim,[1] Sungwon Yang,[2] Mario Gerla,[2] and Eun-Kyu Lee[3]

[1]*Department of Computer Engineering, Gachon University, 1342 Seongnam-ro, Gyeonggi 461701, Republic of Korea*
[2]*Department of Computer Science, University of California, Los Angeles, Los Angeles, CA 90095, USA*
[3]*Department of Information and Telecommunication Engineering, Incheon National University, 119 Academy-ro, Yeonsu-gu, Incheon 406772, Republic of Korea*

Correspondence should be addressed to Eun-Kyu Lee; eklee@cs.ucla.edu

Received 15 March 2016; Accepted 4 May 2016

Academic Editor: Sergio F. Ochoa

Many indoor localization techniques that rely on received signals from Wi-Fi access points have been explored in the last decade. Recently, crowdsourced Wi-Fi fingerprint attracts much attention, which leads to a self-organized localization system avoiding painful survey efforts. However, this participatory approach introduces new challenges with no previously proposed techniques such as heterogeneous devices, short measurement time, and multiple values for a single position. This paper proposes an efficient localization method combating the three major technical issues in the crowdsourcing based systems. We evaluate our indoor positioning method using 5 places with different radio environment and 8 different mobile phones. The experimental results show that the proposed approach provides consistent localization accuracy and outperforms existing localization algorithms.

1. Introduction

Navigation ability of smart phones and tablets at indoor environment becomes a challenge as recent mobile Location Based Services (LBSs) [1–3] require more accurate and seamless positioning at both indoor and outdoor environment. Outdoor localization had been provided reasonably by global satellite positioning systems using Global Positioning System (GPS), GLObal NAvigation Satellite System (GLONASS), Galileo, and so forth. On contrary, the indoor localization still continues to a challenge even though it has been exploited during last several years. Several techniques for the indoor localization have been proposed [4–6]. In a survey of indoor localization techniques [7], many techniques are compared such as GPS, RFID, WLAN, and Bluetooth in terms of accuracy, complexity, and scalability. Some of previous works uses a specially designed hardware like a beacon installed on walls or ceilings such as RFID, ultrasound, and infrared technologies [8–10]. Other systems use a combination of different sensors to increase accuracy [11, 12]. Those which use the hardware of short range communication technologies are costly to deploy on a large area, even though those systems provide fine-grained accuracy in indoor localization.

In contrast, Wi-Fi based positioning systems are very common and easily achieved as shown that Internet map services of Google, Apple, Microsoft, and so forth already use received signals from many deployed access points (APs) for localization. Recently, Wi-Fi is becoming more popular and ubiquitous with countless Wi-Fi-enabled smart devices. Accordingly, indoor localization using the Wi-Fi APs receives much attention from mobile computing research area, which has the advantage of avoiding the cost of specialized hardware deployment.

Typically, Wi-Fi based localization estimates the location based on observed and stored "fingerprints" which are composed of a MAC address and corresponding Received Signal Strength (RSS) value from a Wi-Fi AP [10, 13]. While previous researches mainly dealt with localization algorithms to improve accuracy based on the fingerprint database, recent studies focus on building the database with less effort. "Crowdsource" Based Indoor Localization (CIL) [14–19] by autonomous users is one of cost efficient approaches, which

reduces the map building and maintenance expense compared to an expert surveyor based approach. The CIL is driven by normal mobile users who participate in the Wi-Fi AP survey as a contributor, a user, or both. Also, this multiple-surveyor-multiple-user model has the advantages of fast radio map building and quick update.

Figure 1 shows an example of the CIL, which consists of two phases: "training phase" (or "offline phase") and "localization phase" (or "online phase"). In the training phase, fingerprint data of locations have been captured to establish a radio map. After then, mobile phones inquire their location with measured fingerprint data to a remote server that holds the radio map in the localization phase. In the figure, the five users (i.e., A, B, C, D, and E) are untrained normal people who are carrying different types of mobile phones. Users A, D, and E are surveyors for Room 101, Room 102, and Room 103 who measure RSS of Wi-Fi APs and upload the measured data with corresponding AP information to a local DB server. The uploaded data is processed on the server and converted to fingerprint data. When user B inquires the current location information, the server returns to Room 101 if user B's RSS measurement matches one from the user A.

However, the CIL also introduces a new set of challenges. First, the CIL has to extract accurate fingerprint values from short measurement time for Received Signal Strength (RSS) because the mobile users as voluntary surveyors probably provide short-term RSS measurements. Second, the CIL has to support calibration-free indoor localization across different devices. Typically, users as surveyors carry various types of devices in terms of hardware and software, for example, Wi-Fi chipsets, antenna pattern, and operating systems. The RSS measurement results in different values across the heterogeneous devices even at exactly the same positions.

This crowdsourcing approach has been considered in many recent researches [14–19]. However, many of them address those challenges in the CIL. In [20] about survey-free localization, several researches [21–23] dealt with heterogeneous devices for CIL using difference of RSS samples from APs instead of absolute RSS values to combat measurement variance from heterogeneous devices. Previously, we proposed "Freeloc" [24] that uses a list of APs ordered by RSS for the fingerprint instead of the RSS itself. Thus, the Freeloc consistently results in robust and reliable outcomes resolving those challenges. In this paper, we compare the Freeloc with existing practical indoor localization algorithms for the CIL in terms of accuracy. In addition, we investigate how to decide a gap between sample RSSs for difference localization environment and conduct measurement study for the Freeloc in variance of wireless channel because of interference from dense Wi-Fi APs, deep fading from many pedestrians, and path loss from short distance.

The remainder of this paper is organized as follows: we introduce background knowledge with related works on indoor localization schemes in Section 2. Section 3 introduces existing localization algorithms for CIL. Section 4 describes our system and algorithm together with the three major challenges covered in the CIL. We show the performance evaluation and comparison with existing localization algorithms from Sections 5 to 7. In Section 5, Freeloc performance is compared according to various localization environment. We compare Freeloc with other CIL algorithms in Section 6. In Section 7, Freeloc performance is investigated with varying delta values. We conclude the paper in Section 8.

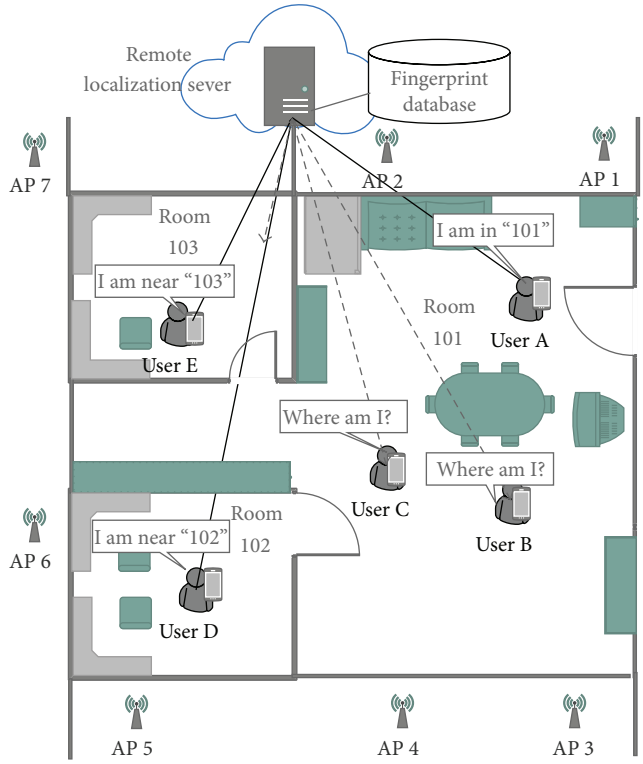

Figure 1: Crowdsource Based Indoor Localization (CIL) approach which collects RSS values of Wi-Fi APs measured by multiple users, users A–E at different positions of Rooms 101, 102, and 103, together with corresponding AP information, which is finally converted to fingerprint data of each location.

2. Background

2.1. Indoor Localization Techniques. Many indoor localization techniques have been proposed over the past decade. Some indoor localization techniques require special hardware to determine the devices location like active badge [9] and active bat [25] that are attached on ceilings and walls of buildings and transmits out infrared and ultrasound pulses for proximity estimation. The cricket and cricket compass [8, 26] used a combination of RF and ultrasound technologies. Techniques using active RFID were also proposed [27, 28].

Recently, Wi-Fi based indoor localization receives much attention as Wi-Fi APs become used for outdoor localization. Like the outdoor localization in cellular networks, triangulation using time difference of signal arrival from neighbour APs can be considered [13, 29]. This time of arrival (TOA) based approach could suffer from timely varying signal path at complex indoor environment. Instead, Received Signal Strength (RSS) can be used. RADAR [10] adopts this RF signal intensity first for the purpose of indoor localization. Now, many researchers concentrate on techniques that use Wi-Fi

RSS data. Studies like [30] analyzed the properties of Received Signal Strength values reported by wireless network interface cards. References [5, 31] show that the Wi-Fi fingerprint (i.e., a basic service set identification (BSSID) and its RSS value) methods can fulfil accuracy required for many indoor LBS applications.

2.2. Crowdsourced Indoor Localization. Survey-free localization [16–19] or Crowdsource Based Indoor Localization (CIL) [14, 15] has rigorously been explored in order to reduce effort and cost involved in expert surveyor based system as smart hand-held devices are deployed widely. The CIL is a self-organized participatory system where normal mobile users contribute measurement of Wi-Fi fingerprints at various locations for localization. Reference [15] carried out experiments in indoor environments and have discussed encouraging results. Teller et al. in [16] have designed and deployed an organic location system and achieved position accuracy that is comparable to the accuracy achieved by a survey driven system. A crowdsourcing based approach by Ledlie et al. models the world as a tree of hierarchical namespaces and provides an algorithm that explicitly accounts for temporal variations in signal space [19]. Recently, accelerator assisted dead-reckoning techniques are adopted for enhancing accuracy of crowdsourced indoor localization [11, 12].

A main issue with the CIL is the heterogeneity of hardware devices, usually a variety of mobile phones, to collect Wi-Fi fingerprints during the training phase. This leads to variation in the values of observed signal strength measurements due to the different chipsets present on different devices. Park et al. explore this issue in [17] and compare various methods used to mitigate this problem. The main parameters that are used are signal strength values and access point detection. The Kernel function based estimation, which predicts user location using a naive Bayes classifier, has been proposed to obtain better results than linear transformation based approaches [32]. Tsui et al. proposed an unsupervised learning method that automatically tries to solve hardware variance problem in Wi-Fi localization [33]. Wu et al. proposed site survey-free indoor localization with off-the-shelf devices, which needs complex conversion from virtual to physical space based on measurement [21]. References [22–24] show that robust fingerprints can be derived using signal strength difference (SSD), instead of absolute RSS values in the heterogeneous mobile devices for measurement.

3. Localization Algorithm for CIL

Although several localization algorithms were proposed for CIL, most of them use log-distance or similarity of RSSs [20]. We introduce several practical approaches that are less complicated and easy to apply for the fingerprint based indoor localization to compare performance with Freeloc.

First, Euclidean distance of RSSs of k-nearest neighbours (k-NN) is calculated to find a location with minimum value of summation of the distance values. Here we consider unweighted k-NN in which distance values are equally added at the summation. Second, similarity based on the Tanimoto coefficient is considered. Third, we evaluate the N-gram that compares BSSID subsequences between two fingerprints to calculate probability of appearance of the same contiguous subsequence. With these four algorithms, we apply the same experiment environment that is used for "Freeloc" evaluation for the comparison:

(i) k-nearest-neighbour (k-NN) is a popular localization method to analyze RSS pattern from k neighbour APs using some recognition techniques. For instance, it can simply calculate Euclidean distance of two fingerprints' RSS values that are measured and stored in a remote server. Like this, k-NN estimates a location with the distance values of most frequently appeared k neighbour APs:

$$\arg\min_{f_{L_i} \in F} \sqrt{\sum_{i=1}^{k} \left\| f_i - f_{L_i} \right\|}, \tag{1}$$

where L_i is locations $\{L_0, L_1, \ldots, L_n\}$ and f_i is a measured fingerprint and f_{L_i} is a stored fingerprint of location i. That is to say, k-NN selects a location that has minimum sum of distance of most strong k fingerprints between the measured and stored values.

(ii) Two fingerprint similarities can be evaluated by *Tanimoto* coefficient, which is widely used for estimating similarity of Wi-Fi fingerprints. Reference [34] shows that place detection can be achieved by similarity of radio environment using Tanimoto coefficient. As in below equation, location L_i with maximum *Tanimoto* coefficient can be chosen:

$$\arg\max_{f_{L_i} \in F} T\left(f_i, f_{L_i}\right) = \frac{f_i \cdot f_{L_i}}{\left\| f_i \right\|^2 + \left\| f_{L_i} \right\|^2 - f_i \cdot f_{L_i}}. \tag{2}$$

(iii) N-gram algorithm is a different approach compared to above two approaches, which calculates likelihood of two subsequences of the measured and stored fingerprints [35]. N-gram only concerns strength order of the fingerprints while k-NN and Tanimoto considers signal strength itself. The order of fingerprint strength does not change probably even if the signal strength of the fingerprints changes dynamically. For this, N-gram sorts the fingerprints in descending order of the RSS and compares subsequences of the fingerprints. For instance, subsequence N-gram $(f_s) = \{f_s, f_{s+1}, \ldots, f_{s+n-1}\}$ is a fingerprint sequence from a sth fingerprint to a $i + (n - 1)$th fingerprint with size of n. Here we can find a location, L_i that maximizes a following equation:

$$\arg\max_{f_{L_i} \in F} \prod_{s} P\left(N\text{-gram}\left(f_s\right) \mid L_i\right) P\left(L_i\right). \tag{3}$$

That is to say, the algorithm selects a location with maximum probability that a set of the subsequences f_s appears in the location L_i. N-gram motivates us to improve it for crowdsourced localization in which measured fingerprints are varying with locations and devices as described in a following subsection.

4. Freeloc: Calibration-Free Indoor Localization

In this section, we briefly describe our localization algorithm, Freeloc, with a usage scenario in Figure 1. Freeloc solves following three critical challenges in fingerprint derivation based on the RSSs captured by untrained mobile users:

(i) RSS measurement for short duration: it is well known that multipath fading in an indoor environment causes RSS to fluctuate over time even if the receiver is absolutely fixed [36]. One simple method to reduce RSS variance is to record the RSS data for a long time. As the number of RSS samples increases it is easier to identify one single fingerprint value which ensures construction of a more robust and accurate radio map. However, it is almost impossible to have normal users collect RSS data for such a long time in the crowdsourcing based model. We believe that the RSS survey time at each location will not exceed one minute assuming all the surveyors are usual mobile users. Therefore, a technique that extracts accurate fingerprint data from short-time measurement is necessary.

(ii) Device heterogeneity in CIL system: it is inevitable that diverse devices get involved in establishing the radio map database. Since there is no expert surveyor who uses specially designed hardware, it is highly likely that the RSS data gathered from each user varies even though it is collected at the exact same position. Different chipsets and antenna designs of the Wi-Fi devices cause varying RSS records per each device and make it difficult to calibrate them. This device heterogeneity is another key problem for crowdsourced localization.

(iii) Multiple measurements for one location: another problem is that more than one user can upload one's own fingerprint data with the same location label, but it is obtained at different measurement points. This results in multiple fingerprint data sets for one location, which leads to inefficient memory usage and more time to estimate the current location. None of the previous studies take this into account even though this is also a principal cause of localization accuracy degradation.

4.1. Fingerprint Value Extraction. This section presents how a RSS value of each fingerprint can be extracted at a particular location with variation in response rate and RSS values. In contrast RSS can be measured for a long time (e.g., from more than one hour to a month) to get average value in the expert surveyor system [37]; CIL has short measurement duration to extract robust fingerprint. We propose a practical and resilient RSS abstraction method for the fingerprint based on the experimental results we conducted:

(i) AP response rate: in our experiments, we observed strong correlation between AP response rate and RSS. Ledlie et al. [19] thought that the correlation between the response rate and RSS is rather weak, which led to using the response rate as fingerprint information with RSS. However, our results show that APs with RSS values of greater than −70 dBm provide over 90% of response rate and APs with RSS between −70 dBm and −85 dBm provide over 50% of response rate. APs with RSS of less than −90 dBm present very poor response rate. Therefore, we decide to give lower weights to weak RSS values, which reflects the lower AP response rate naturally for fingerprint.

(ii) RSS variance: RSS of a particular AP is varying over time due to shadowing and multipath fading, and RSS fluctuation could be higher in indoor environment rather than outdoor, which degrades the localization accuracy. For CIL that requires short measurement duration, probabilistic methods based on Gaussian distribution were proposed in several studies proposed [16, 19, 32] to obtain the average value, which are however feasible only in ideal environment.

Instead, we propose a simple yet effective method based on our experiment results that show the most frequently captured RSS in short duration is very close to the most RSS in the long-duration measurement case. In other words, most frequent RSSs can be obtained regardless of the duration of measurement time. The proposed method extracts fingerprint RSS values by ignoring RSS records that are far away from the most frequent RSS and giving the maximum weight to the RSSs with peak value as shown in (4), which provides tolerance to the RSS variation over time. V_{fp} is the fingerprint value for an AP and RSS_{peak} is the RSS value of highest frequency during the measurement. The width of the range is set by ω_{LT} and ω_{RT}:

$$V_{\text{fp}} = \frac{\sum_{n=1}^{\omega_{LT}} \left(\text{RSS}_{\text{peak}} - n\right) + \text{RSS}_{\text{peak}} + \sum_{m=1}^{\omega_{RT}} \left(\text{RSS}_{\text{peak}} + m\right)}{\omega_{LT} + \omega_{RT} + 1}. \quad (4)$$

4.2. Online Localization Algorithm

4.2.1. Relative RSS Comparison. Most of previous localization techniques estimate a location with an absolute RSS value based on the radio map built during the offline phase. However, CIL where surveyors carry heterogeneous hardware devices can have different fingerprint data sets even for the same location because RSS values measured by those devices are different from each other.

In this section, we explain a novel localization technique, Freeloc, instead of modifying existing techniques for the heterogeneous device environment that is aligned with our target indoor usage scenarios. Thanks to the proliferation of Wi-Fi technology, some office or university buildings have more than 50 APs installed for personal purpose or for offloading of wireless cellular networks. RSS values of those APs are widely distributed (e.g., −40 dBm to −100 dBm), which is good to abstract relative RSS strength among APs.

Input: fingerprint data $\text{Fp}_{\text{unknown}}$
Output: estimated location Loc
(1) score ← 0, $\text{score}_{\text{MAX}}$ ← 0
(2) $\text{bssid}_{\text{MAP}}$ ← {}
(3)
(4) **for each** possible Fp_{Loc_x} in the radio map **do**
(5) **for each** AP_i in $\text{Fp}_{\text{unknown}}$ **do**
(6) **if** AP_i is found in Fp_{Loc_x} at mth AP **then**
(7) $\text{bssid}_{\text{MAP}} \leftarrow L(\text{AP}_{j,\delta(m)})$ vector where $\text{AP}_i = \text{AP}_m$
(8) **for each** BSSID in $\text{AP}_{j,\delta(i)}$ **do**
(9) **if** BSSID is found in $\text{bssid}_{\text{MAP}}$ **then**
(10) score ← score + 1
(11) **end if**
(12) **end for**
(13) **end if**
(14) **end for**
(15) **if** score > $\text{score}_{\text{MAX}}$ **then**
(16) $\text{score}_{\text{MAX}}$ ← score
(17) Loc ← Loc_x
(18) **end if**
(19) **end for**
(20) **return** Loc

Algorithm 1: Estimate the location.

Table 1: RSS measurement results from each user.

AP	User A	User B	User C	User D
AP1	−50	−65	−65	−92
AP2	−55	−68	−51	−80
AP3	−67	−74	−53	−67
AP4	−72	−52	−66	−75
AP5	−88	−91	−82	−58
AP6	−90	−87	−85	−54

In contrast to several approaches using RSS difference of APs for fingerprints, Freeloc generates fingerprints using an AP order instead of RSS value itself as shown in

$$\text{Fp}\left(\text{Loc}_x\right) = \left\{\text{Loc}_x, \left[\text{AP}_i, L\left(\text{AP}_{j,\delta(i)}\right)\right]\right\}$$
$$i, j \in \text{APs of } \text{Loc}_x,\ i \neq j \quad (5)$$
$$\text{RSS}\left(\text{AP}_i\right) - \text{RSS}\left(\text{AP}_j\right) \geq \delta.$$

Each fingerprint data element Fp of location Loc_x has a location label Loc_x (e.g., room number) where measurement is taken, and a detected AP's BSSID (AP_i) that has the ith strongest V_{fp}. $L(\text{AP}_{j,\delta})$ is an order of other detected APs' BSSIDs of which RSS is weaker than RSS of the AP_i by more than δ value. Our proposed method adopts the delta (δ) as a marginal value for varying RSS which is different from N-gram [35] that considers only similarity between two continuous subsequences of the ordered fingerprint even though both schemes focus on relationship between detected APs in terms of RSS, rather than RSS value itself. The delta value keeps the relationship consistent under wireless channel fading and enables our method to deal with heterogeneous devices without calibration efforts and also multiple Fp elements for the same location from many different devices.

Table 2: Fingerprint data of each location.

(a)

Room 101	
AP_i	$\text{AP}_{j,\delta(i)}$
AP1*	{AP3, AP4, AP5, AP6}
AP2*	{AP3, AP4, AP5, AP6}
AP3	{AP5, AP6}
AP4	{AP5, AP6}
AP5	{}
AP6	{}

(b)

Room 102	
AP_i	$\text{AP}_{j,\delta(i)}$
AP6*	{AP1, AP2, AP3, AP4}
AP5*	{AP1, AP2, AP4}
AP3	{AP1, AP2}
AP4	{AP1}
AP2	{AP1}
AP1	{}

For example, suppose that users A and D are the surveyors and users B and C want to know their positions in Figure 1, and the measurement of user A–D is presented in Table 1; the fingerprints of Rooms 101 and 102 can be defined in Table 2. For instance, AP1 with −50 dBm RSS value has 4

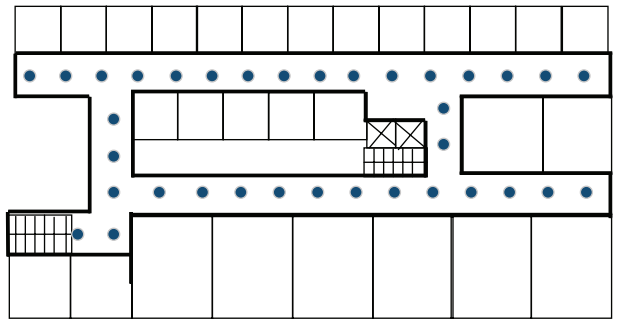

(a) 5th floor of Gachon IT building

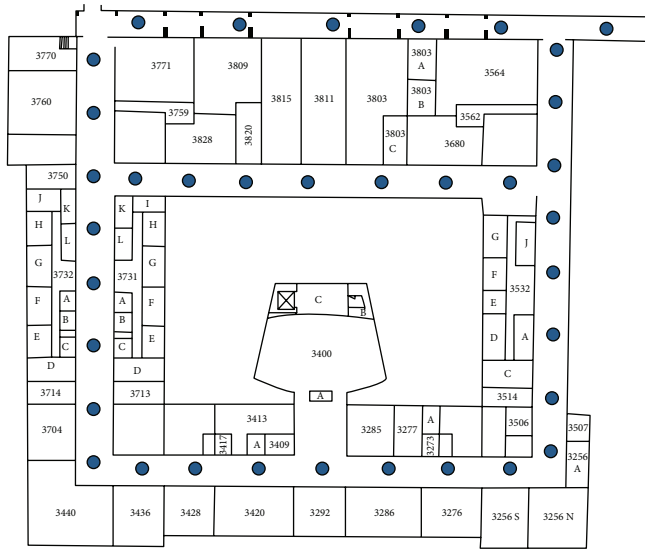

(b) 3rd floor of UCLA engineering building

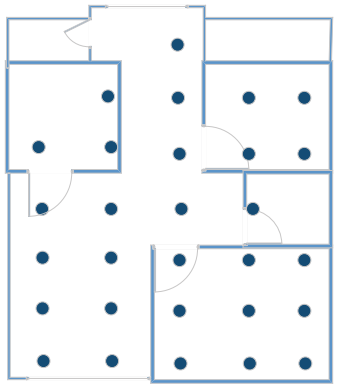

(c) Resident house

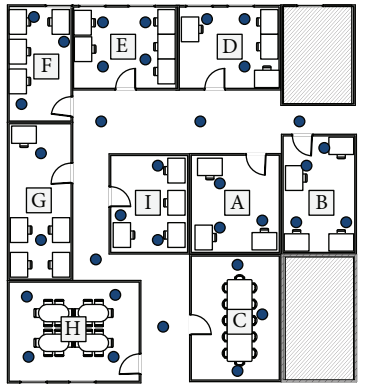

(d) UCLA NRL laboratory

(e) Indoor Coex shopping mall in Seoul

Figure 2: Floorplans for evaluation.

other detected APs nearby (AP3–AP6 dBm) that show lower signal strength by more than 10 dBm (i.e., the δ value).

From now on, we describe details of Freeloc localization algorithm in Algorithm 1. In the aforementioned scenario, users B and C request their positions to a localization server with own fingerprint values in Table 2, and then the fingerprint values are compared with the stored fingerprint map that is created by users A and D. First, AP4 as the strongest AP of user B is searched in Room 101 map. AP4 in the map has other APs, AP5, and AP6 that are weaker by the delta. Since AP5 and AP6 are commonly found in both the user B's fingerprint and the location map, Room 101 earns two points. Like this, our algorithm finally acquires 8 points for Room 101 but only 1 for the 102. For the user C, the scores are 9 and

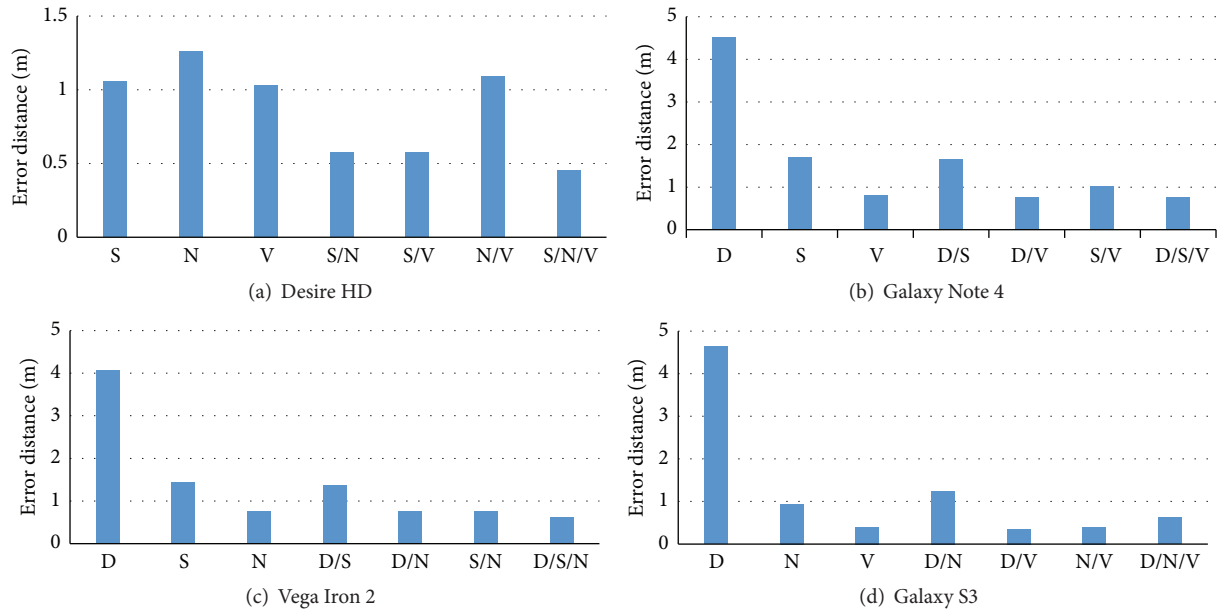

Figure 3: Impact of device heterogeneity experiment at 5th floor of Gachon IT building.

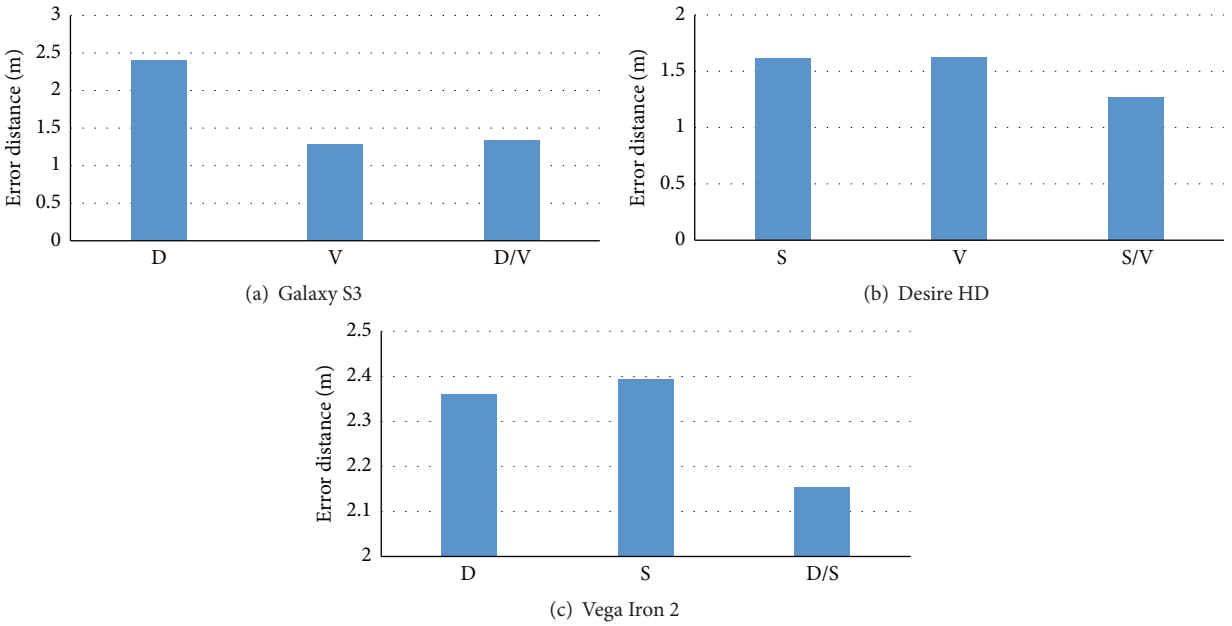

Figure 4: Distance errors of localization at a resident house.

2 for Room 101 and 102, respectively. Therefore we conclude that both users B and C are in Room 101.

In order to achieve fast retrieval (line 4 in Algorithm 1), we utilize an "importance flag," a one-bit flag in fingerprint data, Table 2. The flag is set if the AP_i ranks high with strong RSS. When the localization server receives such location request, it selects fingerprint data with flagged AP_i in the map which matches the flagged AP_i in the request data.

For example, in the same aforementioned scenario, the flagged AP_is are {AP1 and AP2} for Room 101 and {AP6 and AP5} for Room 102 if we set the criterion for the flag as the top two APs. The flagged AP_is are marked with asterisk in Table 2. When users B and C request their positions, at least one flagged AP_i^* in their fingerprint data is found in the fingerprint data of Room 101 (i.e., AP1 for user B and AP2 for user C) while no matching flagged AP is found in the fingerprint data of Room 102. Therefore, only Room 101 is considered for the possible location in this example. However, we can be bothered from high rank AP_i^*s if adjacent locations have high probability of receiving strong RSS from the same APs. If no matches are found, we regard the position where the measurement is taken as an unlabeled location.

Table 3: Measured fingerprint data for localization.

(a)

User B	
AP_i	$AP_{j,\delta(i)}$
AP4*	{AP1, AP2, AP3, AP5, AP6}
AP1*	{AP5, AP6}
AP2	{AP5, AP6}
AP3	{AP5, AP6}
AP6	{}
AP5	{}

(b)

User C	
AP_i	$AP_{j,\delta(i)}$
AP2*	{AP1, AP4, AP5, AP6}
AP3*	{AP1, AP4, AP5, AP6}
AP1	{AP5, AP6}
AP4	{AP5, AP6}
AP5	{}
AP6	{}

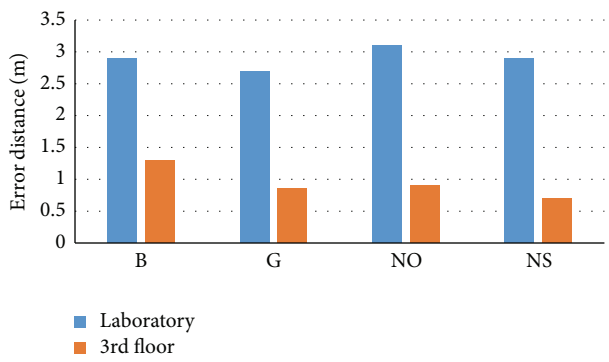

Figure 5: Localization accuracy comparison between laboratory and third floor in UCLA building [24].

4.2.2. Fingerprint Update. In CIL, mobile users as surveyors upload continuously different fingerprints for the same location with their heterogeneous devices, which increases the number of RSS data sets for the same location label in the map database and time to compare all sets for localization.

Freeloc can provide a simple update procedure that builds a unique fingerprint without any calibration, which just merges multiple fingerprints into a single fingerprint. For example, the new fingerprint data will be established as in Table 4 if B uploads its RSS measurements with the same location label as shown in Table 3 and they merge with an existing Room 101 fingerprint in Table 2 created by user A. The proposed $\{AP_i, L(AP_{j,\delta(i)})\}$ fingerprint data structure and the δ value increase the similarity among multiple fingerprint data although they are measured at slightly different locations with different devices.

Table 4: Merged fingerprint data for Room 101.

Room 101: user A + B	
AP_i	$AP_{j,\delta(i)}$
AP1	{AP3, AP4, AP5, AP6}
AP2	{AP3, AP4, AP5, AP6}
AP3	{AP5, AP6}
AP4	{AP1, AP2, AP3, AP5, AP6}
AP5	{}
AP6	{}

Table 5: Devices used for data collection.

Device	MFR	Wi-Fi chipset	Android
Bionic (B)	Motorola	TI WL1285C	2.3.4
Galaxy S2 (G)	Samsung	BCM4330	2.3.4
Galaxy S3 (S)	Samsung	M2322007	4.3
Galaxy Note 4 (N)	Samsung	BCM4358	5.1
Desire HD (D)	HTC	BCM4329	4.1.2
Vega Iron 2 (V)	Pantech		4.4.2
Nexus One (NO)	HTC	BCM4329EKUBG	2.3.3
Nexus S (NS)	Samsung	BCM4329GKUBG	2.3.6

5. Performance Comparison at Different Environment

From this section, we evaluate the Freeloc with 8 multivendor smart phones in Table 5 which have different Wi-Fi hardware chipsets and mobile OSs. For evaluation, we varied the number and type of devices which participate in the fingerprint map for each user device. The same device was never used for both generating fingerprinting map and localization.

5.1. Building Floor. First, 5th floor of the IT building at Gachon University and 3rd floor of the UCLA engineering building as office/school building environment where long corridors and surrounded meeting rooms and laboratories exist as shown in Figures 2(a) and 2(b). The width of the corridor is approximately 2 m, and some APs are visible with line-of-sight. Their floor plan is similar to each other, but Wi-Fi AP density is different; Gachon IT building has more than 300 detected APs while the UCLA building captures about 50 APs. We measured RSSs at 36 different positions at the third floor of the engineering buildings in UCLA campus and 35 positions at the IT building of Gachon University. Small dots in figure indicate the locations where RSS measurements were taken. The data collected at these points were used for experiments. The adjacent points are approximately 6 m apart.

In the experiment, Freeloc localization algorithm is demonstrated for feasibility of CIL with heterogeneous multiple devices at corridor based office buildings. Localization results from the heterogeneous devices at the Gachon University are shown in Figure 3. First three bars are the cases when only one device was used for the fingerprinting. The next three bars are the cases when the fingerprint maps were generated from two different devices and these fingerprint

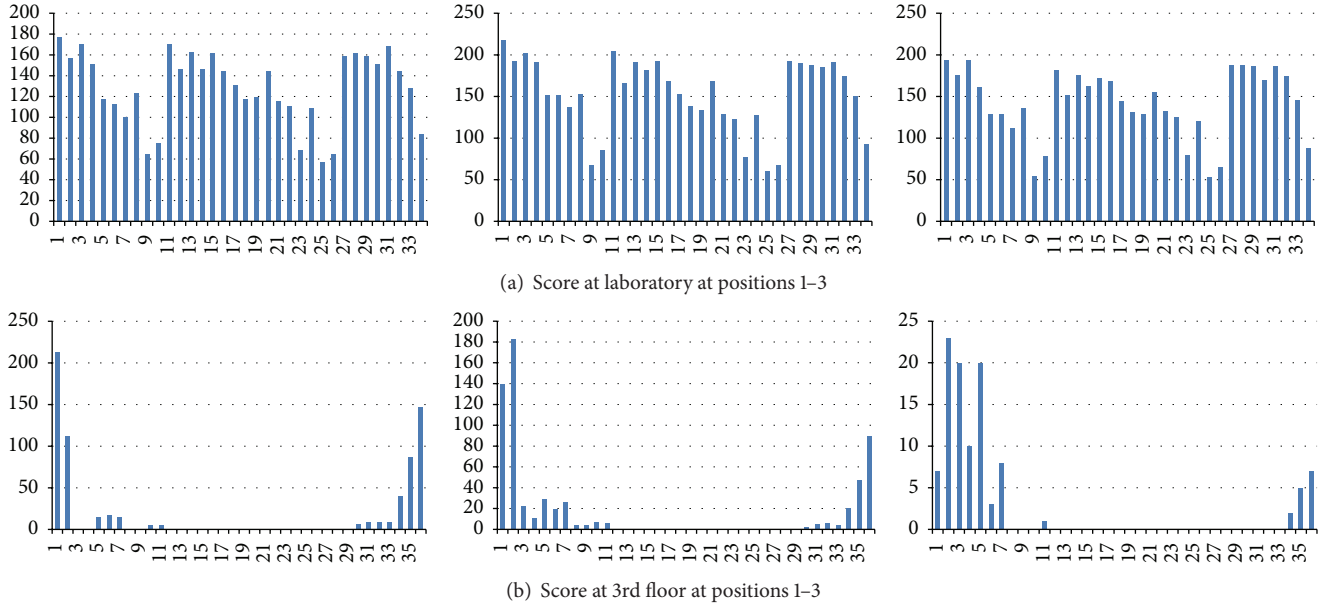

(a) Score at laboratory at positions 1–3

(b) Score at 3rd floor at positions 1–3

Figure 6: Localization scores at measurement locations of UCLA laboratory and 3rd floor.

maps were merged to form one fingerprint map. The last bar denotes the case when fingerprint maps have been generated from three different devices and merged.

Figure 3 shows that the accuracy did not degrade mostly when more than one fingerprint data from different devices are merged. Particularly, HTC Desire HD (D) results in higher distance error to any fingerprint created by other phones. The distance error has been observed exceeding 4 m with the Desire HD. But the distance error decreases with additional fingerprints combined by other heterogeneous devices to less than 1 m. Herein we can conjecture that more additional measurements from other heterogeneous devices contribute to reduce the distance error. Furthermore, the distance error will decrease considerably as the homogeneity of devices increase in the crowdsourced system.

Experiment results in Gachon and UCLA buildings [24] show that Freeloc can provide consistent performance among heterogeneous devices. According to our observation in Figure 5 [24], error distance in Gachon IT building is less than UCLA engineering building, about 1 versus 3 m, which implies that the number of APs and degree of their distribution can affect localization performance in the Freeloc.

5.2. Residential Area. Next localization experiment for small residential area had been conducted at UCLA laboratory and a residential house, which have many different types of furniture and only a few residential people stay. However, the UCLA laboratory is partitioned by thin plywood for rooms and the partitions do not reach to ceiling while the residential house has rooms separated by thick concrete walls, for example, a living room, a kitchen, and a restroom. In the residential house and UCLA laboratory, 29 and 34 positions are measured, respectively. Each of the measurement points is approximately 1.5 m apart.

Figure 4 depicts distance errors of a resident house with three heterogeneous devices (D, S, and V). Cross-device error exceeds 1.5 m that is a distance between measurement positions in case of localization with a single fingerprint. However, the distance error becomes less than the 1.5 m with two fingerprints given by heterogeneous devices. In all cases of the figure, the accuracy did not degrade when more than one fingerprint data from different devices are merged. This reaffirms that the Freeloc can be a feasible solution for the CIL.

The localization performance at the resident house shows better than UCLA laboratory in Figure 5 even though their sizes are similar. We can conclude that the residential house can obtain unique and stable fingerprints rather than the UCLA laboratory since the rooms of the resident house are separated by the concrete walls and channel variation caused by residential people is smaller (e.g., more than 10 students in the UCLA laboratory and 2 residents in the house).

Figure 5 shows that the average distance error at the UCLA laboratory compared to the third floor of UCLA engineering building. The distance error at the UCLA laboratory is higher the third floor where the measurement point interval is longer than the laboratory (1.5 versus 6 m).

The reason for this observation of degraded accuracy in the laboratory can be difficulty to have a unique fingerprint compared to the third floor that has more unique fingerprints formed with thick concrete walls of the building due to path loss while the laboratory is made of thin plywood material for rooms inside.

Figure 6 shows score distribution derived from Algorithm 1 at the measurement position from 1 to 3, where localization error occurs at positions 2 and 3 of the laboratory and position 3 of the third floor. As can be seen in the figure, the scores of the laboratory are very similar to

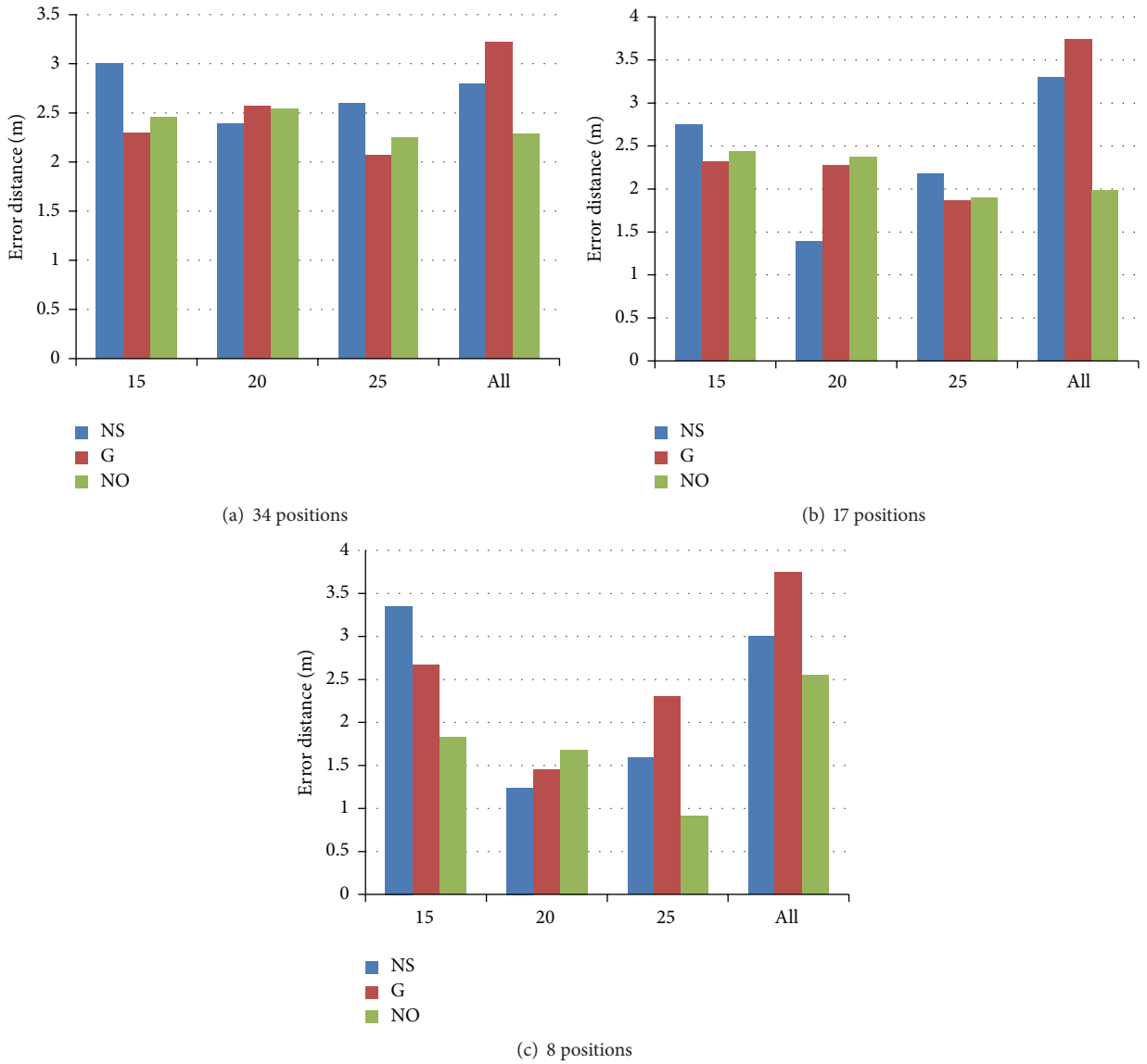

Figure 7: Analysis of localization performance at small region. Distance errors of Bionic user device with a reduced number of APs and measurement positions.

each other among measurement locations compared to the third floor, which leads to wrong prediction with higher probability than the third-floor case.

According to our analysis on the laboratory fingerprints, we observed that the similarity of the fingerprints is caused by similar order of the fingerprints. That is to say, fingerprints in the laboratory have almost the same sequence of AP BSSIDs due to plywood walls except several of the strongest APs that should be highlighted. To see impact of measurement distance and number of APs for a fingerprint, twofold is revisited as inputs for fingerprints as shown in Figure 7.

Since the short measurement distance at the small area like a laboratory may increase localization error probability compared to the corridor based office buildings, we experimented our localization algorithm with smaller number of measurement spots. With many APs in similar order, a long list of measured APs increases the score value and make the fingerprint undistinguishable. Thus, we tested with a reduced number of APs, for example, the strongest 15, 20, and 25 APs from more than 40 captured APs in the laboratory.

In Figure 7(a), 20 APs are most preferable for the fingerprint of the laboratory. The distance error decreases to 2.4 and 2.5 m from 2.8 and 3.2 m in NexusS (NS) and Galaxy (G), respectively. This error decreases more if the number of measured sites decreases by a half. The distance error of the NexusS and Galaxy decreases to 1.39 and 2.28 m as shown in Figure 7(b). The distance error decreases more with smaller measurement sites in Figure 7(c). Table 6 shows average distance error with a number of APs for the fingerprints. Without resizing a list of captured APs, the average distance error was not decreased only by reducing the number of measurement sites (little bit increase in case of *All*). On

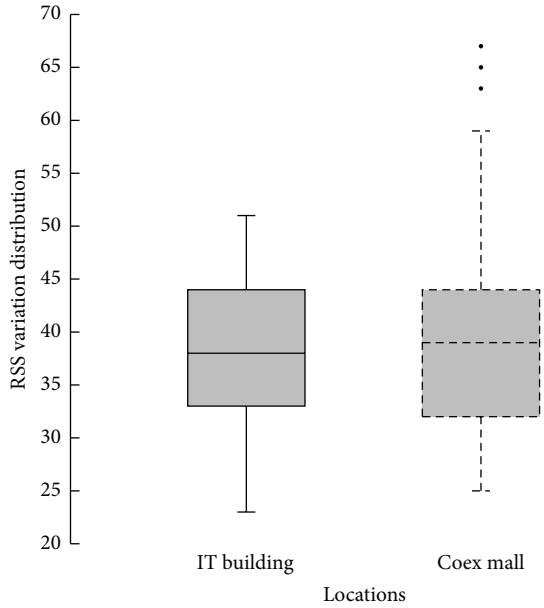

Figure 8: RSS variation at Gachon IT building and Coex. • represents the exceptional cases that are out of 95% confidence interval.

Table 6: Average distance error with a reduced number of APs.

APs	34 sites	17 sites	8 sites
15	2.58	2.5	2.61
20	2.5	2.01	1.45
25	2.31	1.98	1.6
All	2.77	3.01	3.08

contrary, the average distance error decreases from 2.5 to 1.45 m with 20 APs if the measurement sites are reduced from 34 to 8 sites. Such reduction of AP sequence can also decrease location estimation time that is proportional to the number of fingerprint data to be compared, in addition to give a highlight to the strong APs for a fingerprint.

Localization with fine granularity is still challenge especially in small open space where similar fingerprints are captured. Accordingly, measurement position distance or a number of APs used for fingerprints should be adjusted according to the localization environment, especially for the small area. However, we argue that Freeloc is still feasible for home localization as one of key technologies for Internet of Things (IoT).

5.3. Indoor Shopping Center. Wi-Fi channels at indoor environment are varying with moving objects, especially, people, which leads to variance in measured fingerprints. We can conjecture that the fingerprint abstraction based on (4) can deal with this problem. However, largely distributed RSSs can still mislead the localization with inconsistent fingerprints.

In order to demonstrate this problem, we experimented our localization method at the crowd indoor shopping mall, the Coex, one of the biggest indoor shopping centers in south Korea, which holds large convention rooms for exhibitions and conferences, many restaurants, and stores (Figure 2(e)). The Wi-Fi fingerprint data were collected at 40 positions for different Wi-Fi channel environment and each position is about 6 m apart the same as in the school buildings. We measured RSSs from more than 200 APs installed by Coex, stores, and Internet service providers.

We used four smart phones, Desire HD (D), Vega Iron (V), Galaxy S3 (S), and Note 4 (N) and measured RSSs with each phone at different time to experience different channels. To investigate degree of fading effect from pedestrians, RSS variation of two different places, Gachon IT building and Coex mall, is compared in Figure 8. The RSS variation in the Coex mall is higher than the IT building probably due to more pedestrians; RSS difference is almost about 10 dB in some of APs. However, the RSS distribution of strong APs is very similar in both locations.

Figure 9 shows error distance of pairwise experiments of those heterogeneous devices at the Coex mall. The distance error is bigger than the Gachon IT and UCLA building due to varying channel status even though more APs were captured for fingerprints. Also, measurement by Desire HD leads to increase distance error. However, the error distance decreases with fingerprints gathered by other three heterogeneous devices up to less than measurement distance, 6 m. According to this experiment results, localization performance for CIL is affected more by device characteristics, that is, heterogeneity rather than fading channel status because RSS value abstraction based on multiple measurement samples (e.g., more or less 10 samples) reduces the fading effect. Thus, Freeloc can be robust even in the crowd indoor environment that suffers from severe channel fading due to pedestrians.

6. Performance Comparison of Localization Algorithms

First, localization performance is compared when using a Bionic device and three fingerprints built by others. Figure 10 shows CDF of error distance at the laboratory for each different fingerprint. Error distance is slightly different from the fingerprints but comparable except k-NN. Maximum error distance is however very different from the localization techniques. Tanimoto approach shows biggest error, about 12 meters, among the four localization schemes since similarity between RSS fingerprints is undistinguishable to each other at the narrow laboratory environment. Figure 11 shows CDF of error distance at the third floor. k-NN and Tanimoto approaches show considerable error compared to the N-gram and Freeloc. N-gram and Freeloc show only about 5-meter error at more than 80% fingerprints error distance while k-NN and Tanimoto have more than 30-meter distance error. Accordingly, algorithms using relative information for the fingerprint outperform ones using the absolute vale of the RSS, especially for third-floor environment. Comparing the Freeloc and N-gram, the Freeloc shows better accuracy since Freeloc can detect unique BSSID subsequence effectively even under varying radio condition.

Figure 12 shows total average error distance of four localization schemes using 4 user devices used in above experiment at the laboratory and third floor. "Single" indicates an average distance error of single pairwise evaluations.

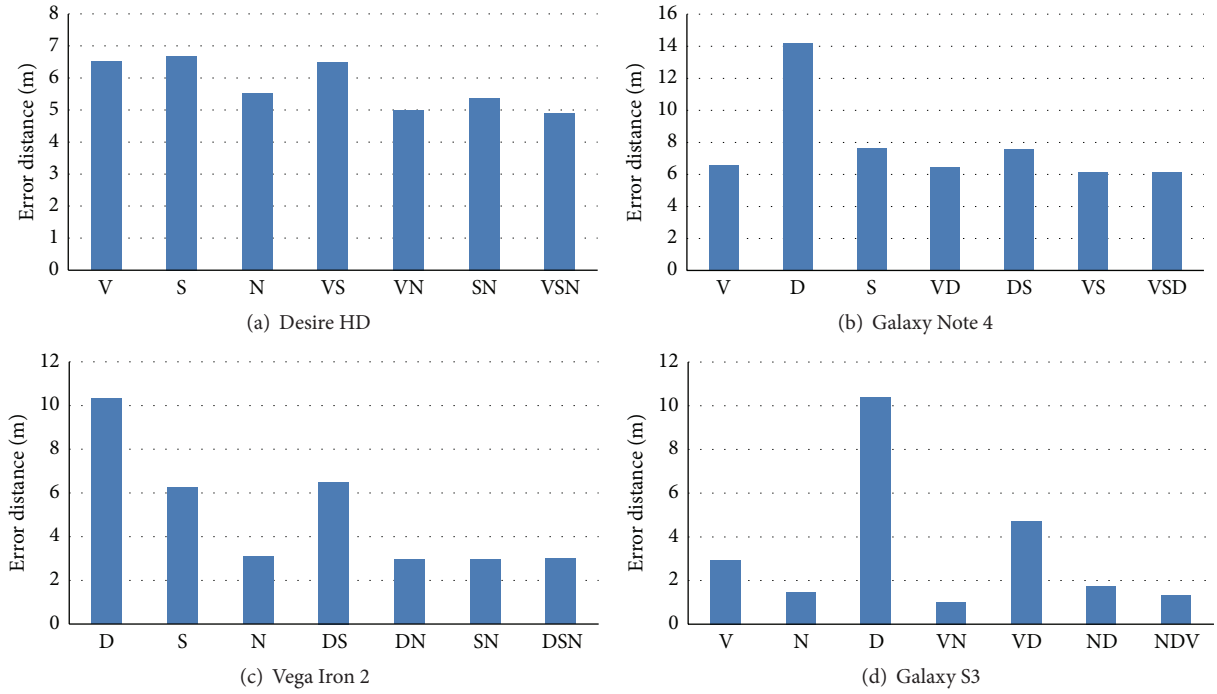

Figure 9: Localization error at a crowd indoor place with many pedestrians.

At the laboratory, most algorithms show competitive results that error distance is below 5 meters. However, signal strength based localization techniques result in serious outcomes at the third floor. At the laboratory, RSSs of many fingerprints can help in elaborating localization accuracy but can mislead in wide area like third floor. Considering typical room size, it could be challenge in localization performance. Freeloc achieves competitive localization performance in both areas. Average error distance of localization based on heterogeneous multiple devices (i.e., 2 or 3 devices) indicates bars with the label "multiple" in Figure 12. When using multiple heterogeneous devices for building a radio map, N-gram and Freeloc that use relative information obtain notable gain compared to the single device surveying. On the contrary, distance error of k-NN and Tanimoto gets even worse than single device case. In N-gram and Freeloc, merged fingerprint data do not affect localization results because they only concern relative information of them. As some omitted fingerprints from a single device are filled by others appropriately, the accuracy is improved. However, in k-NN and Tanimoto, the same fingerprint is not merged properly and newly added values from other devices can mislead outcomes because heterogeneous surveying devices without calibration can get different RSS values for the same location. Error ratio that is a success rate of localization against trials at all measurement points is shown in Figure 12(c). Error ratio at the laboratory is higher than at 3rd floor because distance between measurement points is too small to detect exact location.

Figures 13 and 14 illustrate distribution of error distance at the laboratory and third floor, respectively. Error distribution indicates stability of the localization algorithms. Although k-NN shows lower error ratio at the laboratory in Figure 12(c), distance error is widely spread (max error distance is almost 11 meters) compared to the Freeloc. At the third floor, distance error of the Freeloc is also distributed within very short range than others including the N-gram of which error ratio is similar in Figure 12(c). Consequently, Freeloc can estimate a location with relatively low error variance rather than other localization schemes. In case of using multiple devices for fingerprint surveying, improvement compared to the single device case is not very notable. The heterogeneous device made fingerprints contribute to reducing error ratio in Figure 12(c), but not to reducing distribution of error distance much.

7. Performance with Varying Delta Value

In this section, we describe how to derive the delta value for Freeloc fingerprints, which was not handled in our previous work [24]. Practically, two delta value acquisition methods can be considered for Freeloc implementation; one is an instant derivation that occurs occasionally with several stored fingerprints and the other is an accumulated evaluation that occurs every time a new measurement is received.

7.1. Delta Derivation with Instant Fingerprints. To find out the optimal δ value for subsequent localization, the distance error of pairwise devices is calculated with δ values varied from 1 to 15 for all devices. From this, we can find the optimal empirical δ value which minimizes average distance error. Here, the error distance of the pairwise devices is calculated for the

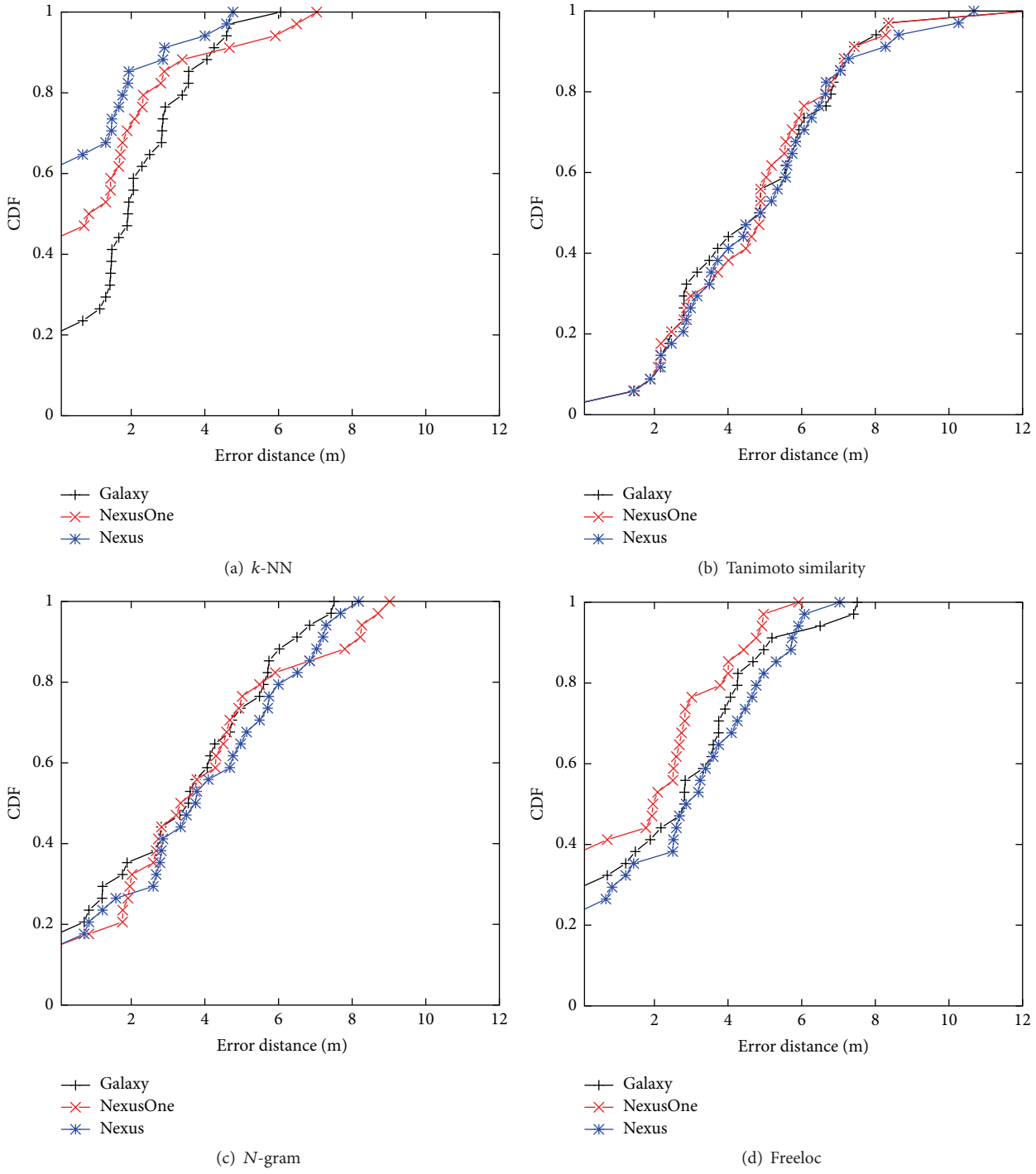

FIGURE 10: Localization of a Bionic device at laboratory.

cases where the predicted location of the user was different from the real location. For instance, if fingerprints measured at point 1 in Figure 2(b) are regarded as fingerprints of point 2 by our localization algorithm, then error distance is an actual distance between those two measurement points.

For example, the instant average of each distance error from pairwise evaluation of four phones at the UCLA laboratory decreases until $\delta = 12$ as shown in Figure 15(a). Accordingly, optimal delta value can be set around 12 dBm as noted in the average line in Figure 15. Practically, the localization server holds RSSs reported by several surveyors for the δ evaluation time and derives the optimal δ internally. This instant derivation can be performed periodically or occasionally to adapt to changed environment such as newly installed Wi-Fi APs and new type mobile devices.

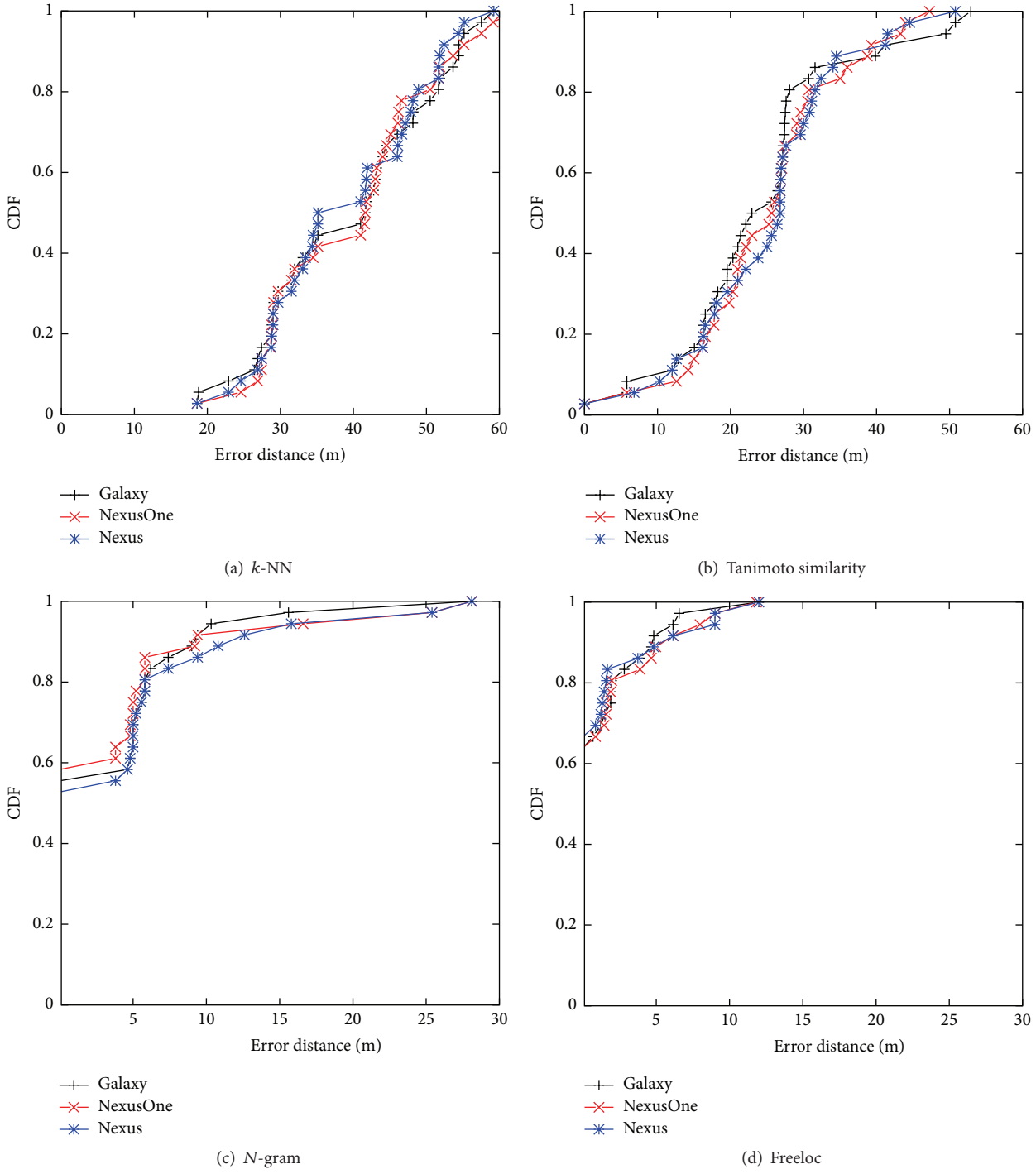

Figure 11: Localization of a Bionic device at 3rd floor.

7.2. Delta Derivation with Accumulated Fingerprints. With accumulated fingerprints, the localization server derives a new optimal δ with a newly reported RSS from a phone based on the current fingerprint. For example, an initial fingerprint from the Bionic (B) is compared by the Galaxy (G) RSS that is reported later. With two, a first δ value is derived. After then, NexusS (NS) and NexusOne (NO) can update δ, sequentially. Whenever the fingerprint is reported, it is used to derive δ combined to a single fingerprint per each location. Here, the localization server does not need to maintain raw RSS values of the reported fingerprints to derive δ. The server only updates the current δ value based on fingerprints newly reported by surveyors. In Figure 15(b), for example, first the B/G pair has an optimal δ in 14 dBm, and δ is updated to 12 dBm by the NS. Finally, δ is set as 13 dBm by the NO.

Figure 16 shows localization errors of the HTC Desire HD (D) with varying δ values at Gachon IT building. A merged fingerprint of two different devices does not show

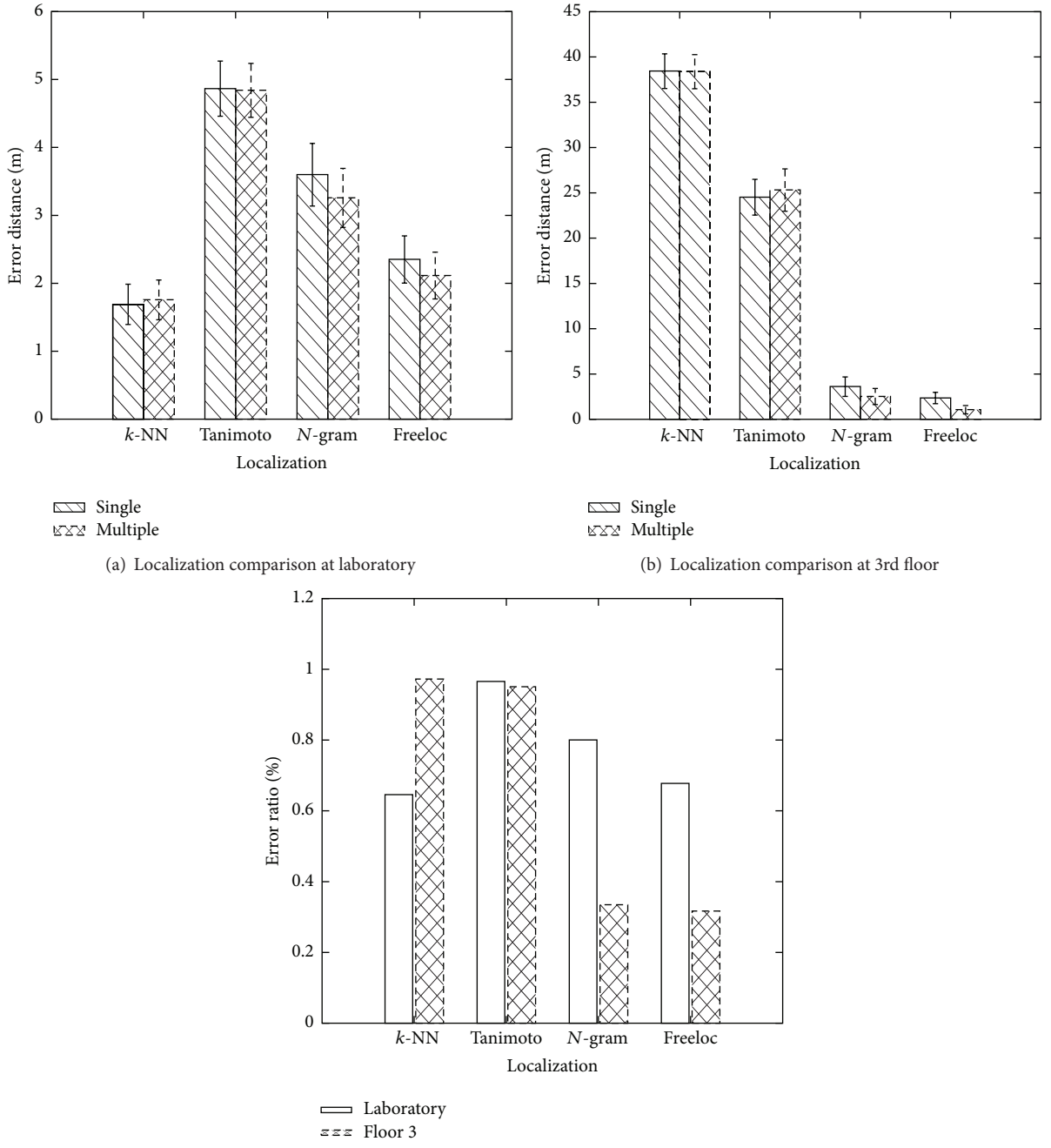

(a) Localization comparison at laboratory

(b) Localization comparison at 3rd floor

(c) Location detection error ratio

Figure 12: Comparison of different localization schemes.

better performance than a single device fingerprint in some of δ values. However, the most robust fingerprint has been formed from three different devices even though distance error is varying according to the δ value. This experiment justifies that our method can achieve impressive performance among heterogeneous devices in crowdsourced environment. We believe that error will decrease considerably as the homogeneity of devices increase in the crowdsourced system.

In this study, considering general performance in terms of total distance error, 10 dBm δ value is used for the UCLA engineering building and the Coex mall, and 2 dBm is used for the Gachon IT building and the resident house in the rest of the evaluations.

8. Conclusion

FreeLoc is a novel, calibration-free indoor localization scheme that uses existing Wi-Fi infrastructure. The proposed radio map building and localization techniques are based on the overall relationship among RSS by APs. Our techniques provide robust localization accuracy in a crowdsourced environment in which device heterogeneity and multiple

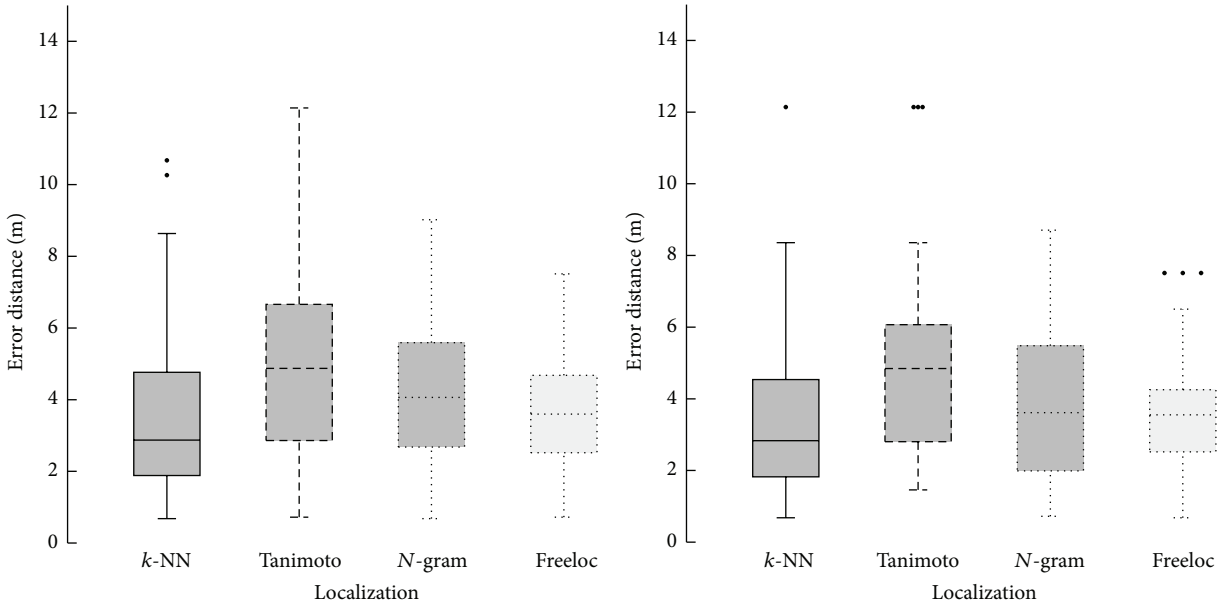

(a) Fingerprint of a single device

(b) Fingerprint of multiple devices

Figure 13: Error distributions at laboratory.

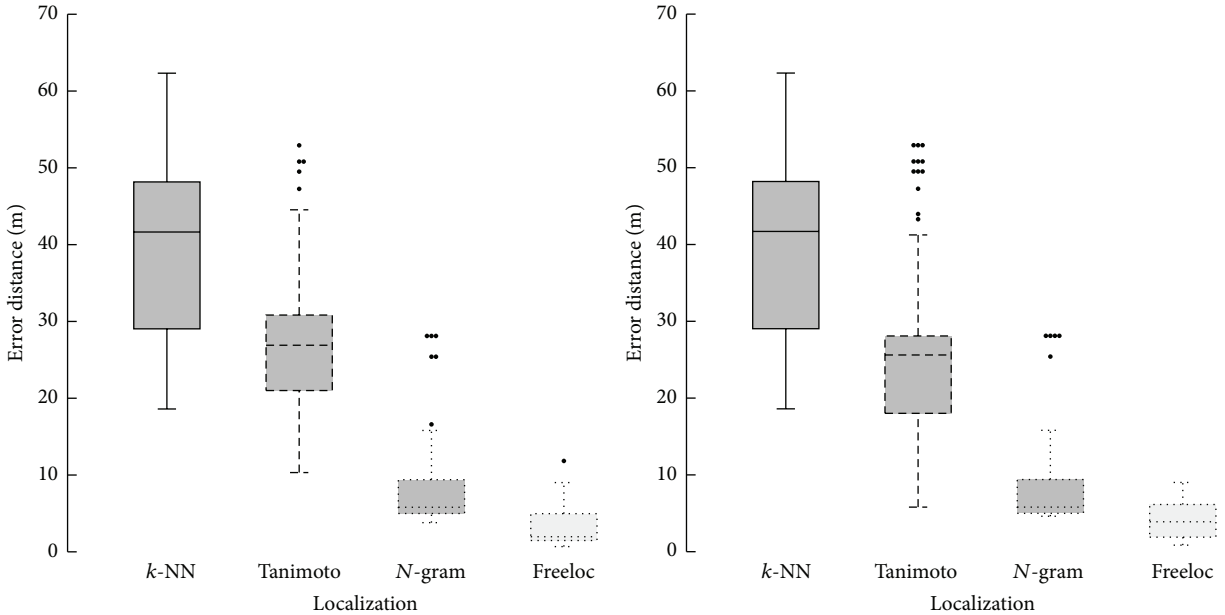

(a) Fingerprint of a single device

(b) Fingerprint of multiple devices

Figure 14: Error distributions at 3rd floor.

untrained surveyors mainly cause performance degradation. The main contribution of our work is a novel approach to fingerprint data management and a localization algorithm that are capable of handling diverse users and their devices without complicated calibrations or transformations. Experiments using heterogeneous devices in two sites that have different environments have confirmed that our novel scheme is reliable and feasible and achieve better performance than localization algorithms using RSS absolute values. We will then expand the scale of our experiments to cover the entire university and perform long-term usability testing.

Competing Interests

The authors declare that there are no competing interests regarding the publication of this paper.

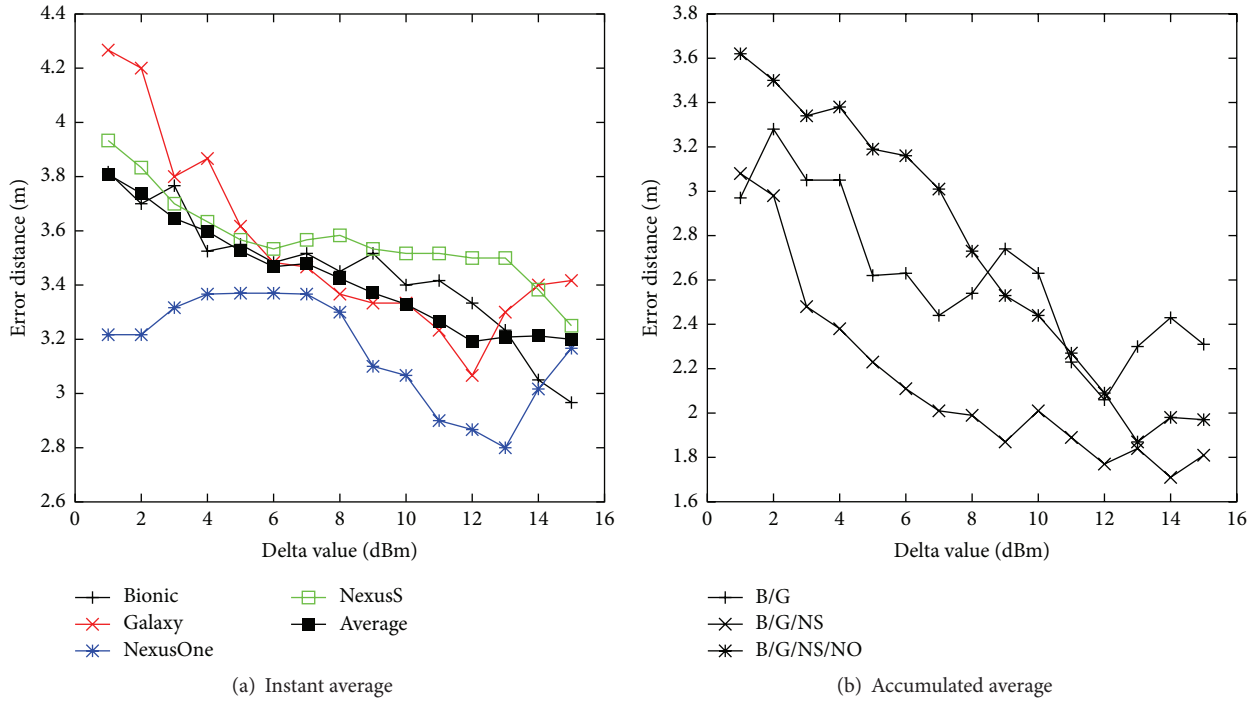

(a) Instant average

(b) Accumulated average

FIGURE 15: δ derivation using instant or accumulated fingerprints at UCLA laboratory.

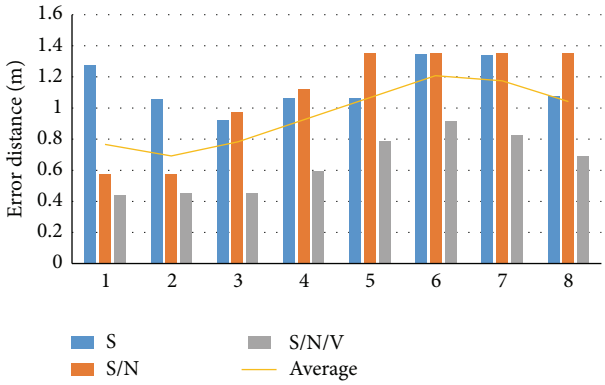

FIGURE 16: Localization performance of a Desire HD fingerprint at 5th floor of the Gachon IT building with varying delta value.

Acknowledgments

This research was supported by the Gachon University Research Fund GCU-2015-0044 of 2015.

References

[1] S. Wang, J. Min, and B. K. Yi, "Location based services for mobiles: technologies and standards," *Electronics*, pp. 78–92, 2008.

[2] D. Mohapatra and S. B. Suma, "Survey of location based wireless services," in *Proceedings of the 7th IEEE International Conference on Personal Wireless Communications (ICPWC '05)*, pp. 358–362, January 2005.

[3] M. Mohammadi, E. Molaei, and A. Naserasadi, "A survey on location based services and positioning techniques," *International Journal of Computer Applications*, vol. 24, no. 5, pp. 1–5, 2011.

[4] Y. Gu, A. Lo, and I. Niemegeers, "A survey of indoor positioning systems for wireless personal networks," *IEEE Communications Surveys and Tutorials*, vol. 11, no. 1, pp. 13–32, 2009.

[5] V. Honkavirta, T. Perälä, S. Ali-Löytty, and R. Piché, "A comparative survey of WLAN location fingerprinting methods," in *Proceedings of the 6th Workshop on Positioning, Navigation and Communication, (WPNC '09)*, pp. 243–251, Hannover, Germany, March 2009.

[6] D. Zhang, F. Xia, Z. Yang, L. Yao, and W. Zhao, "Localization technologies for indoor human tracking," in *Proceedings of the 5th International Conference on Future Information Technology (FutureTech '10)*, May 2010.

[7] H. Liu, H. Darabi, P. Banerjee, and J. Liu, "Survey of wireless indoor positioning techniques and systems," *IEEE Transactions on Systems, Man and Cybernetics Part C: Applications and Reviews*, vol. 37, no. 6, pp. 1067–1080, 2007.

[8] N. B. Priyantha, A. Chakraborty, and H. Balakrishnan, "Cricket location-support system," in *Proceedings of the 6th Annual International Conference on Mobile Computing and Networking (MOBICOM '00)*, pp. 32–43, August 2000.

[9] R. Want, A. Hopper, V. Falcão, and J. Gibbons, "The active badge location system," *ACM Transactions on Information Systems*, vol. 10, no. 1, pp. 91–102, 1992.

[10] P. Bahl and V. N. Padmanabhan, "RADAR: an in-building RF-based user location and tracking system," in *Proceedings of the 19th Annual Joint Conference of the IEEE Computer and Communications Societies (INFOCOM '00)*, pp. 775–784, March 2000.

[11] H. Wang, S. Sen, A. Elgohary, M. Farid, M. Youssef, and R. R. Choudhury, "No need to war-drive: unsupervised indoor localization," in *Proceedings of the ACM 10th International Conference on Mobile Systems, Applications (MobiSys '12)*, pp. 197–210, Ambleside, UK, June 2012.

[12] G. Shen, Z. Chen, P. Zhang, T. Moscibroda, and Y. Zhang, "Walkiemarkie: indoor pathway mapping made easy," in *Proceedings of the 10th USENIX Conference on Networked Systems Design and Implementation*, pp. 85–98, USENIX Association, 2013.

[13] A. LaMarca, Y. Chawathe, S. Consolvo et al., "Place Lab: device positioning using radio beacons in the wild," in *Pervasive Computing: Third International Conference, PERVASIVE 2005, Munich, Germany, May 8–13, 2005. Proceedings*, vol. 3468 of *Lecture Notes in Computer Science*, pp. 116–133, Springer Berlin Heidelberg, Berlin, Heidelberg, 2005.

[14] P. Bolliger, "Redpin-adaptive, zero-configuration indoor localization through user collaboration," in *Proceedings of the 1st ACM International Workshop on Mobile Entity Localization and Tracking in GPS-Less Environments (MELT '08)*, pp. 55–60, ACM, San Francisco, Calif, USA, 2008.

[15] M. Lee, H. Yang, D. Han, and C. Yu, "Crowdsourced radiomap for roomlevel place recognition in urban environment," in *Proceedings of the 8th IEEE International Conference on Pervasive Computing and Communications Workshops (PERCOM Workshops '10)*, pp. 648–653, IEEE, Mannheim, Germany, April 2010.

[16] S. Teller, J. Battat, B. Charrow et al., "Organic indoor location discovery," Tech. Rep., MIT, 2008.

[17] J.-G. Park, D. Curtis, S. Teller, and J. Ledlie, "Implications of device diversity for organic localization," in *Proceedings of the 30th IEEE International Conference on Computer Communications (INFOCOM '11)*, pp. 3182–3190, Shanghai, China, April 2011.

[18] J.-G. Park, B. Charrow, D. Curtis et al., "Growing an organic indoor location system," in *Proceedings of the 8th International Conference on Mobile Systems, Applications, and Services (MobiSys '10)*, San Francisco, Calif, USA, June 2010.

[19] J. Ledlie, J. geun Park, D. Curtis, A. Cavalcante, and L. Camara, "Mole: a scalable, user-generated wifi positioning engin," in *Proceedings of the International Conference on Indoor Positioning and Indoor Navigation (IPIN '11)*, pp. 1–10, IEEE, Guimaraes, Portugal, 2011.

[20] A. K. M. Hossain and W.-S. Soh, "A survey of calibration-free indoor positioning systems," *Computer Communications*, vol. 66, pp. 1–13, 2015.

[21] C. Wu, Z. Yang, Y. Liu, and W. Xi, "WILL: wireless indoor localization without site survey," *IEEE Transactions on Parallel and Distributed Systems*, vol. 24, no. 4, pp. 839–848, 2013.

[22] A. K. M. M. Hossain, Y. Jin, W.-S. Soh, and H. N. Van, "SSD: a robust RF location fingerprint addressing mobile devices' heterogeneity," *IEEE Transactions on Mobile Computing*, vol. 12, no. 1, pp. 65–77, 2013.

[23] F. Dong, Y. Chen, J. Liu, Q. Ning, and S. Piao, "A calibrationfree localization solution for handling signal strength variance," in *Mobile Entity Localization and Tracking in GPS-Less Environments: Second International Workshop, MELT 2009, Orlando, FL, USA, September 30, 2009. Proceedings*, pp. 79–90, Springer, Berlin, Germany, 2009.

[24] S. Yang, P. Dessai, M. Verma, and M. Gerla, "FreeLoc: calibration-free crowdsourced indoor localization," in *Proceedings of the 32nd IEEE Conference on Computer Communications (INFOCOM '13)*, pp. 2481–2489, Turin, Italy, April 2013.

[25] A. Harter, A. Hopper, P. Steggles, A. Ward, and P. Webster, "The anatomy of a context-aware application," in *Proceedings of the 5th Annual ACM/IEEE International Conference on Mobile Computing and Networking (MobiCom '99)*, pp. 59–68, ACM, 1999.

[26] N. B. Priyantha, A. K. Miu, H. Balakrishnan, and S. Teller, "The cricket compass for context-aware mobile applications," in *Proceedings of the International Conference on Mobile Computing and Networking (MobiCom '01)*, Rome, Italy, July 2001.

[27] L. Ni, Y. Liu, Y. C. Lau, and A. Patil, "Landmarc: indoor location sensing using active rfid," in *Proceedings of the 1st IEEE International Conference on Pervasive Computing and Communications (PerCom '03)*, 10.1109/PERCOM.2003.1192765, pp. 407–415, Fort Worth, Tex, USA, March 2003.

[28] G.-Y. Jin, X.-Y. Lu, and M.-S. Park, "An indoor localization mechanism using active RFID tag," in *Proceedings of the IEEE International Conference on Sensor Networks, Ubiquitous, and Trustworthy Computing*, vol. 1, pp. 40–43, IEEE, Taichung, Taiwan, June 2006.

[29] M. Kanaan and K. Pahlavan, "A comparison of wireless geolocation algorithms in the indoor environment," in *Proceedings of the in Wireless Communications and Networking Conference (WCNC '04)*, vol. 1, pp. 177–182, IEEE, 2004.

[30] K. Kaemarungsi and P. Krishnamurthy, "Properties of indoor received signal strength for WLAN location fingerprinting," in *Proceedings of the 1st Annual International Conference on Mobile and Ubiquitous Systems: Networking and Services (MOBIQUITOUS '04)*, pp. 14–23, August 2004.

[31] S.-H. Fang, T.-N. Lin, and K.-C. Lee, "A novel algorithm for multipath fingerprinting in indoor WLAN environments," *IEEE Transactions on Wireless Communications*, vol. 7, no. 9, pp. 3579–3588, 2008.

[32] A. Haeberlen, E. Flannery, A. M. Ladd, A. Rudys, D. S. Wallach, and L. E. Kavraki, "Practical robust localization over large-scale 802.11 wireless networks," in *Proceedings of the 10th Annual International Conference on Mobile Computing and Networking (MobiCom '04)*, pp. 70–84, Philadelphia, Pa, USA, October 2004.

[33] A. W. Tsui, Y.-H. Chuang, and H.-H. Chu, "Unsupervised learning for solving RSS hardware variance problem in WiFi localization," *Mobile Networks and Applications*, vol. 14, no. 5, pp. 677–691, 2009.

[34] D. H. Kim, Y. Kim, D. Estrin, and M. B. Srivastava, "SensLoc: sensing everyday places and paths using less energy," in *Proceedings of the 8th ACM International Conference on Embedded Networked Sensor Systems (SenSys '10)*, pp. 43–56, ACM, Zurich, Switzerland, November 2010.

[35] Y. Jiang, X. Pan, K. Li et al., "ARIEL: automatic Wi-Fi based room fingerprinting for indoor localization," in *Proceedings of the 14th International Conference on Ubiquitous Computing (UbiComp '12)*, pp. 441–450, ACM, Pittsburgh, Pa, USA, September 2012.

[36] K. Pahlavan and P. Krishnamurthy, *Principles of Wireless Networks: A Unified Approach*, Prentice Hall, New York, NY, USA, 1st edition, 2001.

[37] A. Smailagic, J. Small, and D. P. Siewiorek, "Determining user location for context aware computing through the use of a wireless LAN infrastructure," *ACM Mobile Networks and Applications*, vol. 6, pp. 1–8, 2000.

Hindawi Publishing Corporation
Mobile Information Systems
Volume 2016, Article ID 4015625, 11 pages
http://dx.doi.org/10.1155/2016/4015625

Research Article

Improving MQTT Data Delivery in Mobile Scenarios: Results from a Realistic Testbed

Jorge E. Luzuriaga,[1] Miguel Perez,[2] Pablo Boronat,[2] Juan Carlos Cano,[1] Carlos Calafate,[1] and Pietro Manzoni[1]

[1]*Department of Computer Engineering, Universitat Politècnica de València, Camí de Vera, s/n, 46022 València, Spain*
[2]*Universitat Jaume I, Castelló de la Plana, Avenida de Vicent Sos Baynat, s/n, 12071 Castelló, Spain*

Correspondence should be addressed to Jorge E. Luzuriaga; jorlu@upv.es

Received 5 February 2016; Accepted 11 July 2016

Academic Editor: Wenfeng Li

MQTT is being widely used for data delivery in IoT applications but its architecture does not properly handle mobility when disconnection periods tend to be large. In this paper we describe an experimental evaluation, made in a real environment, of a solution that guarantees that there is no information loss when variable length hand-offs appear due to the movement of a node. Our proposal modifies the classical publish/subscribe scheme by introducing an intermediate buffer that takes care of message transfer. Finally, we study the impact related to the connectivity of mobile devices of the use of the standard Linux *Network Manager*. We propose a cross-layer solution that improves the device connectivity in conjunction with the data layer management. We show that our solution improves the data delivery guaranteeing that no information is lost.

1. Introduction

The Internet revolutionised how people communicate and work together. It led the way to a new era of free information for everyone, transforming life in ways that were hard to imagine in its early phases. But the next wave is not about people, it is about intelligent, connected devices. To interact successfully with the real world, these devices must work together with speeds, scales, and capabilities far beyond what individual users may need. The Internet of Things (IoT) will change the world, perhaps more profoundly than today's human-centric Internet.

MQTT was developed in 1999 for the monitoring of an oil pipeline through the desert. The goals were to have a bandwidth-efficient protocol that used little battery power, because the devices were connected via satellite link and this was extremely expensive at that time [1, 2]. The protocol uses publish/subscribe architecture in contrast to HTTP with its request/response paradigm. Publish/Subscribe architecture is event driven and enables messages to be pushed to clients. The central communication point is the MQTT broker. It is in charge of dispatching all messages between the senders and the rightful receivers. This architecture enables highly scalable solutions without dependencies between the data producers and the data consumers.

But MQTT was designed for fixed architectures and nowadays mobile devices are really the clear choice for our interactions with sensors and devices [3]. Smartphones diffusion rates in emerging and developing nations are rising at an extraordinary rate. Thus integrating mobile devices in a MQTT publish/subscribe architecture is a critical task and the one that we cover in this paper.

In this work we analyse, using a real scenario, the behaviour of a mobile smart device that is continuously sending information to servers while travelling through the coverage area of different access points. The solution we evaluate is capable of handling problems such as the expiration of TCP connections, the variable quality of network conditions, and applications misbehaviour due to changes of the assigned IP address. The proposed framework supports disconnected operation and tolerates spontaneous communications without data loss by caching messages to be sent and delivering them as soon as a path to the broker becomes available. The results show that our framework can support intermittent

connectivity using an asynchronous communication scheme very common in IoT networks.

The rest of the paper is organised as follows: a review of related work is offered in Section 2. We briefly describe the proposal in Section 3 and the methodology used to evaluate it in Section 4. In Section 5 we present the performance evaluation and result analysis. Eventually, some concluding remarks are available in Section 6.

2. Related Work

Acquiring data through remote sensing especially in the context of smart environment has been an important topic of research and development referred to and discussed concisely in [4–8].

Focussing on network layer provided mobility, a seamless handover for a hotspot network using a buffering technique is proposed in [9]. In this work the authors make a packet forwarding of the messages that during the handover of the mobile terminal are stored in the buffer placed on each access point. Thus, when a mobile terminal has moved from one access point to another the messages that were sent by the server to it are buffered in the first access point. After the handover the mobile terminal sends a movement notification packet to the new access point and it is resent to the rest of the access points where its tables are updated with the new address of the terminal. Then, all the packets that use the buffering technique are forwarding to the new access point and finally to the mobile terminal. From our point of view this approach has different drawbacks. In the first place it shows a problem of scalability since, with a high number of terminals moving around, the memory of each access point would be overload. Our approach alleviates this problem thanks to the buffer that is located on each mobile terminal. Secondly, the implementation of this proposal requires a modification of the drivers of the Linux bridge interface; in our proposal there is no need for such modifications.

In [10] the authors propose a link-layer packet forwarding scheme that can recover almost all packet loss during a hand-off. They implement "store and forwarding" and "hand-off detection" units in the device-driver of each access point, since all access points NICs have internal queues built in to hold many packets that have to be forwarded for each hand-off terminal after the reassociation. The store and forwarding unit is made to maintain an image queue in the driver to mirror the queue in the card. Thus every packet sent to the card has a copy in the driver and after a hand-off of a terminal the old AP will forward all packets including the packets of the driver buffer and the packets held in the image queue. The hand-off detection unit detects the hand-off process by a consecutive packet transmission failure and starts to buffer unsuccessfully transmitted packets for the hand-off terminal. Upon the reassociation of a hand-off terminal, the new AP sends out a broadcast update frame with the address of the terminal; thus all the devices update their routing table. The hand-off detection of the old AP unit also detects the hand-off completion when it checks the source address of the update frame and identifies if the terminal was once in its BSS. When the hand-off detection is complete the buffered packets are forwarded to the new destination of the terminal through the new AP.

In a lab testing environment [11] the performance of the protocols COAP, MQTT, and OPC UA is evaluated, measuring the transmission time of several messages with different length between two devices acting as a data-source and data-sink, respectively. Both devices are connected to the cellular and wired interfaces of the network simulator. This simulator supports the emulation of several radio technologies such as EDGE, UMTS, and LTE cellular network. They have found the following. [a] OPC UA has the lowest transmission time. [b] The protocols MQTT and OPC UA based on TCP achieve a better performance. [c] Reliable data exchange is not suitable for the transmission of large payloads over cellular networks. [d] In LTE the IP packets are concatenate in the same transport block until the transport block size is reached and then are sent as TCP frames.

Finally, the authors of [12, 13] consider similar issues also with smart objects-based IoT cyber-physical systems.

However, few studies propose an overall framework that increases the mobility support guaranteeing message delivery also improving the wireless connections quality, enabling the development of IoT applications where the mobility of the device is an issue without requiring network support through protocols like MobileIP or LISP [14] allowing that developers do not have to explicitly consider the changes in the point of attachment to the network.

3. Our Evaluated Proposal

Our proposal [15] maintains the *publish/subscribe* approach but decouples the pure data generation process by the data sending process by means of a technique called *intermediate buffering*. This decoupling allows for recovery when the communication channel presents disruption periods, even if they are very frequent and with length of various seconds, that is, in situations where TCP fails to recover.

We suppose having a message producer that continuously generates messages with a given frequency. A MQTT publisher takes the produced messages [16] and turns them it into MQTT messages, to be published with the same given periodicity to a predefined MQTT broker that will forward the incoming messages directly to the subscribers. A subscription is initially created by a client application on a predefined topic (simple subscription name). A basic diagram of the proposal can be seen in Figure 1.

When the connection between the publisher node and the message-broker suffers an interruption, the node enters in *roam mode*. The in-flight published messages (messages that have not received the acknowledgement from the message-broker) are stored in the MQTT internal buffer that is constrained with a very limited space available. These messages are delivered making a push diffusion [17] only when the node recovers the connection with the last access point (that means recover the last IP address); otherwise these messages are lost.

When longer disruption appears, our intermediate buffer takes charge of storing all the published messages that have not received the acknowledgement. Meanwhile, the MQTT network control mechanism manages the creation of the new

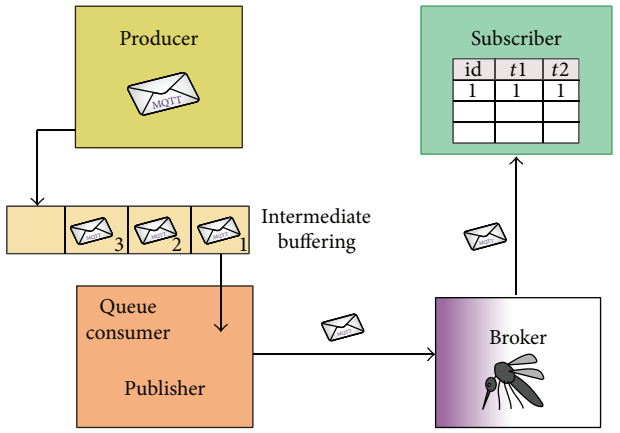

Figure 1: Diagram of the intermediate buffering proposal based on the publish/subscribe pattern of MQTT protocol.

connection and the correct closing of the aborted session. With the new connection, independently from the IP address that the node obtains, once the connection with the MQTT broker is reestablished, we can guarantee the delivery of all these messages in the same order that was published, followed by the messages which continue to be generated.

We evaluated our proposal using two software tools to manage the network connections. The first was the standard *Network Manager* version 1.0 [18] which is included in most of the Linux distributions and the second was our own tool called *signalBased Manager* (sBM) which we developed to allow faster handovers.

3.1. Network Manager. The Network Manager (NM) is an open source software project that enables the automatic configuration of the network interfaces of a Linux-based device as well as their network connections via the D-Bus interface. The NM consists of a system daemon that receives network settings from a pair of setting services by placing Connection-Objects on the system bus and a client application known as "nm-applet" that sends commands to the services to activate these connections. For the establishment of a connection with a wireless network, NM does an initial scan of available wireless networks if there is previously used network on the list connecting the device to it; otherwise it makes a selection based on an opportunistic approach attempting to use the best one.

When a device is moving around, the establishment of a connection using the wireless network is an issue to NM which causes that, most of the time during the displacements, the device remains in a disconnected state. If the device is moving in a network with several access points configured to offer a connectivity with the same service set identifier (ESSID), NM works fine connecting the device to the network because it tries to connect to the ESSID of the previous AP for three times and resumes the network connection successfully in a few seconds. But when the device is moving in a network with several access points configured with several ESSID NM does not work well. It attempts to reestablish the connection up to three times with a nonavailable access point; after this it tries to get a connection with a new detected network. This process takes around 5 minutes to get the device again online using a different service set identifier. Thus, we can say that the default behaviour of NM is not designed to support a device mobility between networks with different ESSID.

3.2. The signalBased Manager. We have developed this network which manages to improve the establishment of the wireless network connection of mobile users in highly dynamic scenarios. We observed that the standard Network Manager is not suitable for these environments since it decides to stay on a network even if the signal strength is very poor [19]. Moreover, when it gets to a total disconnection it keeps trying to reestablish the previous connection, even if it is not available in the current location.

We propose a mechanism that chooses in real time the best available radio based on signal strength measurements. This mechanism is included in the framework as a Network Manager tool called "*signalBased Manager*" (sBM) that support both handovers and hand-offs of a node moving around the coverage of different wireless networks especially to mesh or collaborative networks.

The mechanism is based on three phases: detection, discovery, and execution [20]. It starts the handover process on the client when its connection quality degrades to a predefined threshold (detection). It decides handover to a different AP based on the information of all the available access points in order to choose the best candidate (discovery); finally, the handover is completed with the client establishing a connection with the new access point (execution).

4. Methodology of the Experiments

This section presents the setup of the empirical evaluation we made. The indoor tests have been performed to study the behaviour of the MQTT protocol against an intermittent connectivity and the outdoor tests evaluated the behaviour of our proposal in a walking itinerary in Jaume I University Campus [21]. The walk imitated a common journey took by UJI students to reach the "*Espaitec center*" from the bus stop; these walks are hereafter referred to as AB and BA journeys. They are represented in Figure 2. All the outdoor experiments were performed while the *Guifi.net* nodes [22] were uniquely dedicated to be used with our generated traffic. In order to obtain a representative data set we have performed 32 tests with a duration of about 5 minutes each, generating four repetitions for each configuration and with each of the two Network Managers.

In general the traffic parameters used are a constant generation rate of messages fixed to 1 mps; a fixed publication periodicity of 1 second between each publication; two fixed messages size used of 512 Bytes and 6 Kbytes.

Our measurements were oriented to show different performance metrics calculated using the reception time-stamp of each message [23], that is, the maximum and mean disconnection times, the maximum amount of messages stored in the buffer, the amount of messages losses (packet loss rate), and the interdelivery regularity (jitter analysis).

Table 1: Summary of equipment used.

Device	Role	Radio	Protocols	OS
CS-UJInuvolguifi1	Mesh node	AR9582	802.11b/g/n	qMp 3.1 Clearance
	Access point	AR9341	802.11a/n	
CS-UJInuvolguifi2	Mesh node	Nanostation M5	802.11a/n	qMp 3.1 Clearance
	Access point	AR9341	802.11b/g/n	
CS-UJInuvolguifi3	Mesh node	AR9582	802.11a/n	qMp 3.1 Clearance
	Access point	Nanostation M2	802.11b/g/n	Airos (xs2.ar2316)
CS-UJInuvolguifi4	Mesh node	Nanostation M5	802.11a/n	qMp 3.1 Clearance
	Access point	Nanostation M2	802.11b/g/n	Airos (xs2.ar2316)
CS-UJInuvolguifi5	Mesh node	Nanostation M5	802.11a/n	qMp 3.1 Clearance
	Access point	Nanostation M2	802.11b/g/n	Airos (xs2.ar2316)
Samsung NC10	Client	Qualcomm Atheros	802.11b/g	Ubuntu 14.04
Desktop computer	Server	100 Base ethernet	802.3	Ubuntu 14.04

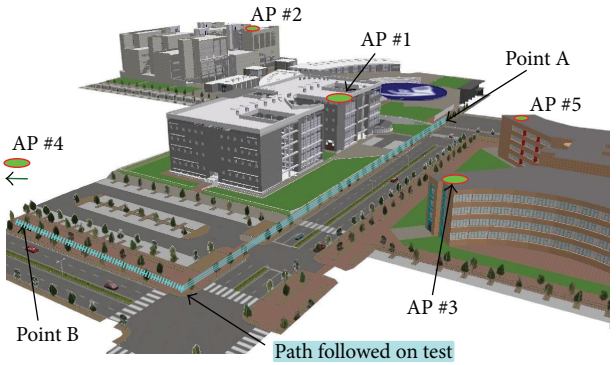

Figure 2: Testing scenario inside Jaume I University.

4.1. Experimental Scenario. Inside University Jaume I there is deployed a part of the wireless infrastructure of *Guifi.net* Community Network [22]. To ensure that the clients (students and staff) can roam smoothly, multiple nodes have been installed outdoors on the terraces of the principal buildings for a full coverage throughout the entire University Campus. In Figure 2 we can appreciate a scenario representation; more specifically we used the nodes *CS-UJInuvolguifi* (from 1 up to 5) [24]. The clients use IEEE802.11n links at 2.4 GHz, while fixed nodes are interconnected as a mesh at 5 GHz. A list of equipment types used is in Table 1.

These nodes are based on antennas and integrated routers such as Ubiquiti or tp-link running an open source community distribution based on the OpenWRT Linux distribution [25].

In these scenarios, we have travelled on a bidirectional pedestrian walkway that is around 500 m long, carrying a laptop trying to keep a constant pace of about 6 kph. The forward and return paths walkway are coincident but as we will see in the coming sections the connection establishment order with the access points and the behaviour related to the message delivery were quite different.

The duration of each test was 5 minutes, that is, the time necessary to move between these points.

Table 2: Summary of test setup parameters.

Parameter	Value(s)
Generation rate	1 mps
Publication rate	1 mps
Net manager	GNU Network Manager (NM), *signalBased Manager* (sBM)
Message size	512 Bytes, 6 Kbytes
Trips	from A to B, from B to A
Walkway length	~500 m
Velocity	~6 kph

During this period of time our mobile device generates several MQTT messages with different payload sizes. These messages were sent to the broker and then were delivered to the subscribers. Table 2 shows the parameters setup for MQTT measurements on the proposed system.

5. Evaluation and Results

This section includes the performance evaluation of the proposed framework and shows results obtained through different experiments on the field followed by a statistical analysis. The measured results are presented for the MQTT protocol with and without the proposed prebuffering technique and with and without the Network Manager improvement.

5.1. Using the MQTT Protocol without Prebuffering. To obtain some reference value about the behaviour of MQTT, in this section we evaluate its performance both in an outdoor environment without moving the devices ("static case") and over intermittent connections ("with disconnections case") to illustrate the weaknesses of the MQTT protocol. We simulated an unstable environment with disconnections using an indoor testbed where the mobility of a device was obtained turning off and on the wireless radio at intervals that were varied between 1, 5, and 30 seconds.

Table 3: Static case, without mobility.

Size (Bytes)	Mean (ms)	St dev	Min (ms)	Max (ms)
512	0.926	30.454	−250	240
6144	1.416	46.456	−344	301

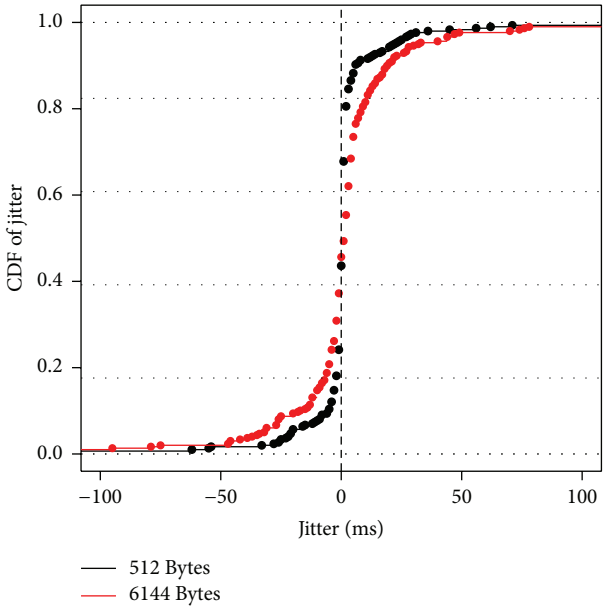

Figure 3: Static case.

5.1.1. Static Case. A set of tests were executed without any movement of the mobile devices. Specifically, we have executed the test ensuring a direct line-of-sight (LOS) link between the access point AP #5 and the mobile devices placed on a fixed spot of the central boulevard of the UJI, while the mobile device is publishing our testing messages.

Figure 3 shows the CDF of the jitter for each of the two message sizes. The jitter is basically very reduced and similar independently from the size of the messages. In Table 3, we can see that the mean values of the jitter with both message sizes are around 1 ms.

5.1.2. With Disconnections Case. To control disconnection periods we built a testbed in the laboratory that allowed us to control most of the factors that may influence an experiment. We have tested several parameter combinations, for instance, other message sizes, higher publishing frequencies (100 and 500 ms), and different on-off periods using the values of 1, 5, and 30 seconds.

With an off period of 30 s, Figure 4, we can see that slightly less than 50% of the cases have a negative values and less than 95% of the cases have values smaller than 100 ms. The same behaviour is observed with both message sizes used and even with messages of a smaller size (120 Bytes) as we can see from Table 4. We notice that lower standard deviation values are obtained with a higher messages sending frequency (100 ms).

We also evaluated the message loss values considering a message loss when a message sent by a publisher was not delivered to a subscriber or not even received by the broker. We used the MQTT quality of service set to "at least once" where the protocol ensures that a message arrives at the server at least once. When a message is published, a copy is stored in the publisher internal buffer until the reception of the ACK packet. When the acknowledgement is received it indicates a successful delivery and the copy of the message is discarded from the buffer. By default this internal buffer has been defined as the maximum number of in-flight messages to 10. Once this value is reached the buffer will overflow and all the outstanding MQTT messages sent to the broker will be lost. The reduced space available on the buffer allows that only a few messages can be stored. This is a problem in high data traffic environments where this value can be reached easily and quickly. In addition, the content of the buffer is delivered only if the MQTT session is active and only if the client maintains the same id, a problem that appears when reestablishing broken TCP/IP connections. Table 5 shows statistical information about the number of lost messages with different disconnection periods.

Table 4: Jitters obtained with a wireless radio off time of 30 seconds.

Size (B)	Period (ms)	Mean (ms)	St dev	Min (ms)	Max (ms)
1024	100	307.17	4,293.83	−100	62,353
1024	500	1,318.85	8,218.52	−465	51,930
1024	1000	2,691.85	11,871.21	−561	56,385
512	100	287.62	4,206.89	−100	63,636
512	500	988.59	7,568.70	−500	56,204
512	1000	1,542.55	9,953.38	−1,000	56,437
120	100	276.80	4,054.28	−100	62,601

Table 5: Number of message losses.

Radio turnoff time (sec.)	Median	Mean	St dev	Min	Max
1	125.5	116.35	24.68	60	154
5	125.0	125.82	3.98	121	134
30	521.0	530.40	19.38	511	560

As can be seen, even with not so high disconnection time (30 sec) the number of messages lost increases in a clear manner, thus reinforcing the need of an improvement of the architecture.

5.2. Using the MQTT Protocol with Buffering. In this subsection we present the results with our buffering proposal. First, we show the results using the default connection manager (i.e., Network Manager) which is integrated in most of the Linux distributions. Secondly, the results with our own connection manager are shown where we can observe an improvement in the overall results.

We focus our attention on the situations where the devices get disconnection, where we have identified the percentage of time among several reasons like (a) loss of coverage situations [26], (b) association to an access point without an IP address, or (c) keeping an old IP address assigned by the previous

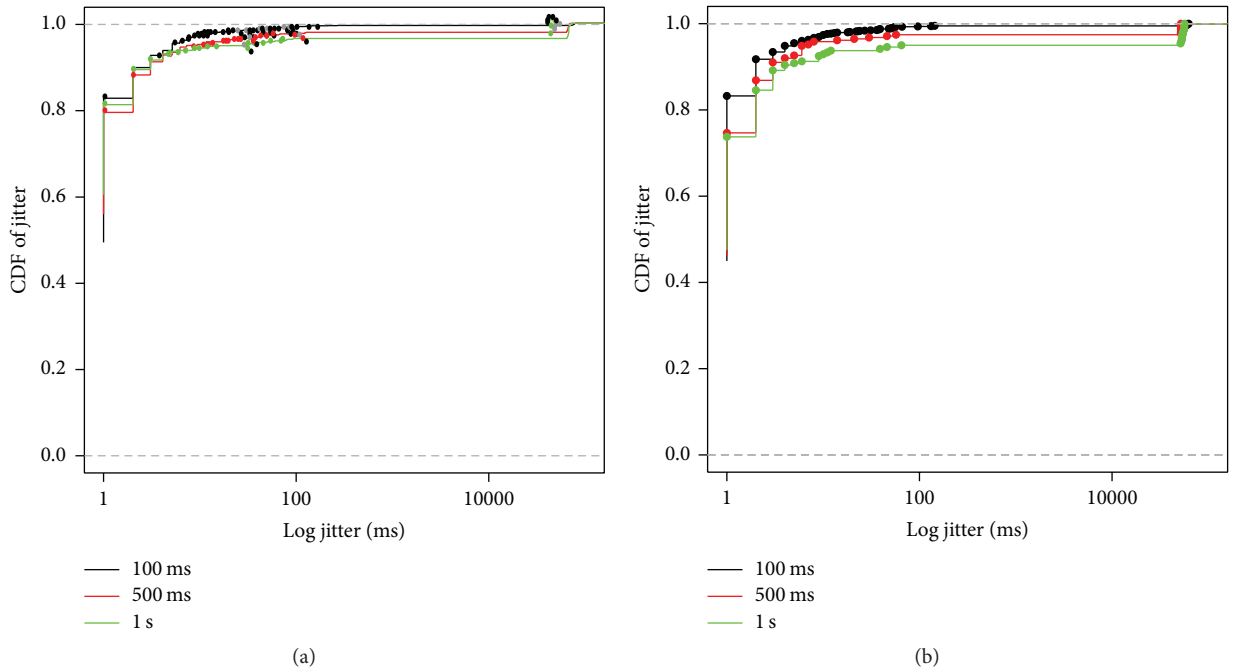

Figure 4: The CDF of jitter with a wireless radio off time of 30 sec. and message size of 512 Bytes (a) and 1024 Bytes (b).

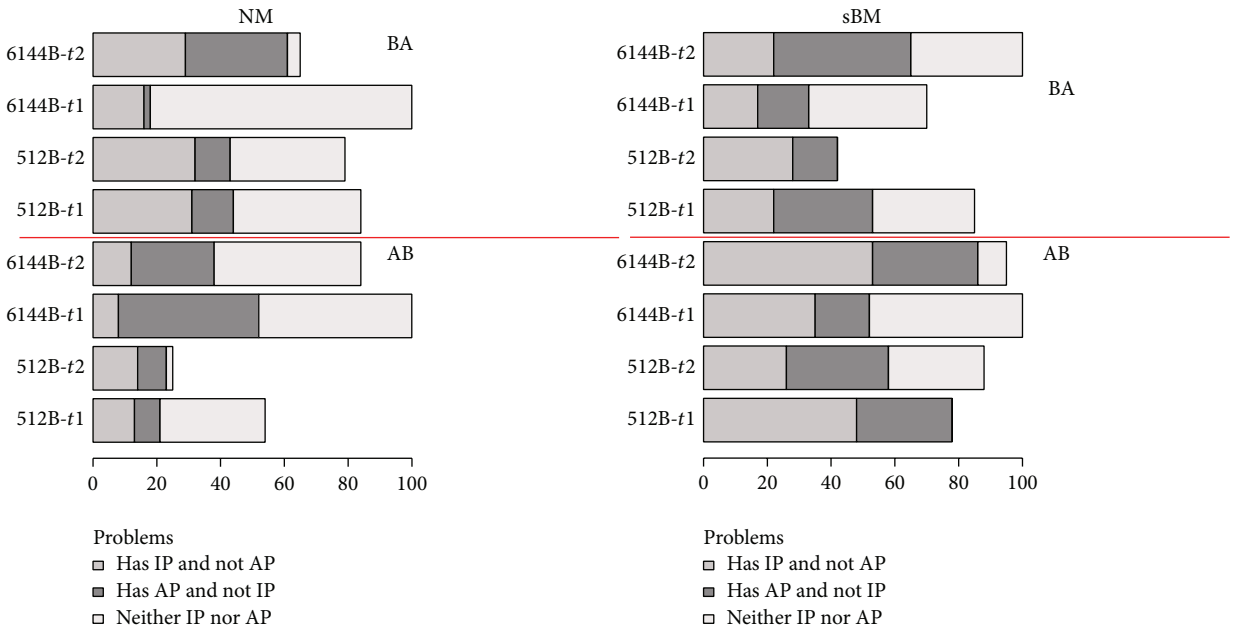

Figure 5: Connection problems with NM and sBM.

access point without getting a successful association with the new access point.

Figure 5 shows the percentage of time that the device had problems transmitting MQTT messages due to the connection breakdown during the execution of the test.

The size of each bar is proportional to the disconnection time presented by the device in each test. When NM is used the principal problem is the total isolation of the device, because the device most of the time was trying to connect to an unexcited network. While sBM is used the principal problem is related with the DHCP time out to the IP assignation.

We can say that the behaviour of the connection is very variable even when the same trajectory is repeated in another time, due an innumerable number of reasons making the results very dependent on a particular test.

Table 6: Jitter values using our buffering proposal with the standard Linux Network Manager.

Journey	Size (Bytes)	Median (ms)	Mean (ms)	St dev	Max (ms)
AB	512	201	1,063.82	6,320.82	102,413
AB	6 K	338.5	1,552.02	14,216.05	290,851
BA	512	865	1,511.91	17,252.24	481,502
BA	6 K	865	1,401.62	11,609.68	285,475

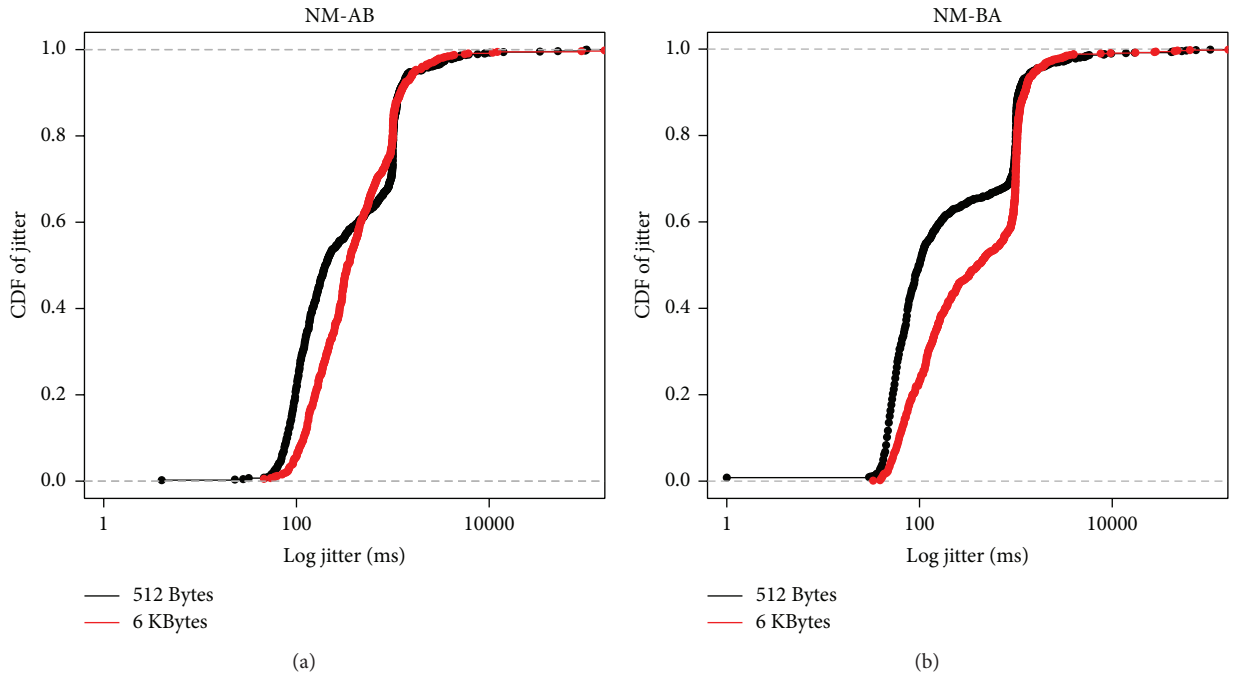

Figure 6: CDF of jitter in logarithmic scale using our buffering proposal, sending messages of two sizes 512 Bytes and 6 Kbytes on two journeys (a) AB and (b) BA trip, respectively.

5.2.1. Using the Standard Network Manager. In these tests we used the standard Linux Network Manager (NM) service. As we said before, the NM has a problem when the devices are moving around and getting out of a coverage area, since, for example, it tries to recover the connection with the old access point, making up to three repetitions to reestablish the previous connection. While this could be reasonable for a static user, it leads to bad performance for a mobile user.

As we can see from Figure 6, in both plots the small messages have a smaller jitter value. The 80% of probability of the values is around 1 second that basically corresponds to the sending rate. Then the biggest values in the graph are the disconnection times of each test.

In Table 6, we can see that in the AB journey with the biggest message size values of 290 seconds are reached. That means that almost all of the trip the client was disconnected. In the BA journey, we observe a chaotic situation in the network establishment during the walking test independently of the message size used; that is, there are cases where the client was disconnected along all the journey, and all the messages were stored in the buffer and transmitted uniquely at the arrival end point.

5.2.2. Using Our signalBased Manager. In the following tests we have used our proposal of Network Manager that tries to get the best available connection with an access point with a client moving through different coverage areas during data transmission.

Table 7 summarizes the obtained results, where we can see that standard deviation values are lower than the obtained ones with the standard Network Manager; indeed the maximum disconnection values are between 103 and 133 seconds and in the worst case a value of 256 seconds was obtained; that means that during the walking test 34 up to 44% of the time the device was disconnected, and in the worst case up to 85% was reached but never a total isolation as occurs with the standard manager.

Figure 7 shows that the biggest message has more regular jitter values than the smallest one, especially from 60 to 80%, that is, the median values. It is also evident that from 74 up to 86% of the jitter, values are close to 1 second.

To a better comparison between two managers, we have joined the results obtained of the two message sizes and then subtracted the generation periodicity for each message. By comparing these results in Figure 8, we can see that slightly

Table 7: Jitter values using the protocol with the buffer using *signalBased* Manager.

Journey	Size (Bytes)	Median (ms)	Mean (ms)	St dev	Max (ms)
AB	512	386.5	1,027.88	5,061.39	102,730
AB	6 K	249	1,016.23	6,592.85	122,835
BA	512	1,154	1,105.68	9,158.91	255,958
BA	6 K	576	1,189.65	8,472.11	133,159

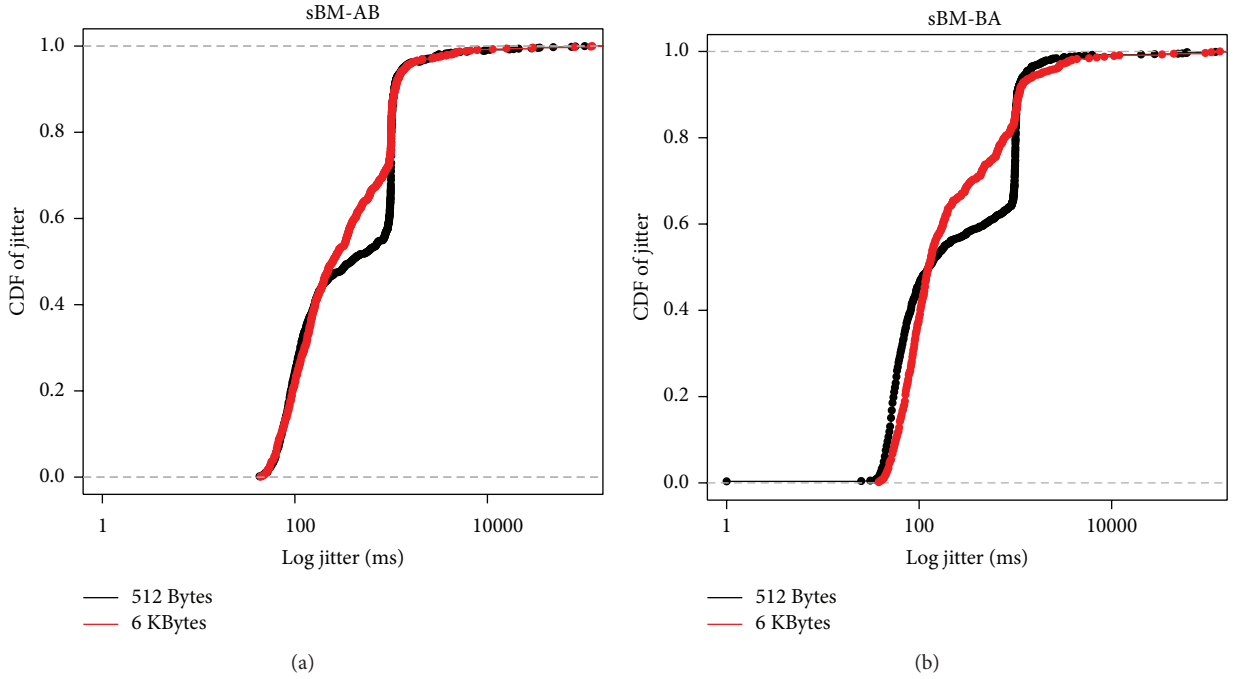

Figure 7: CDF of jitter in logarithmic scale using the buffer proposal sending messages of two sizes 512 Bytes and 6 Kbytes on two journeys (a) AB and (b) BA trip, respectively.

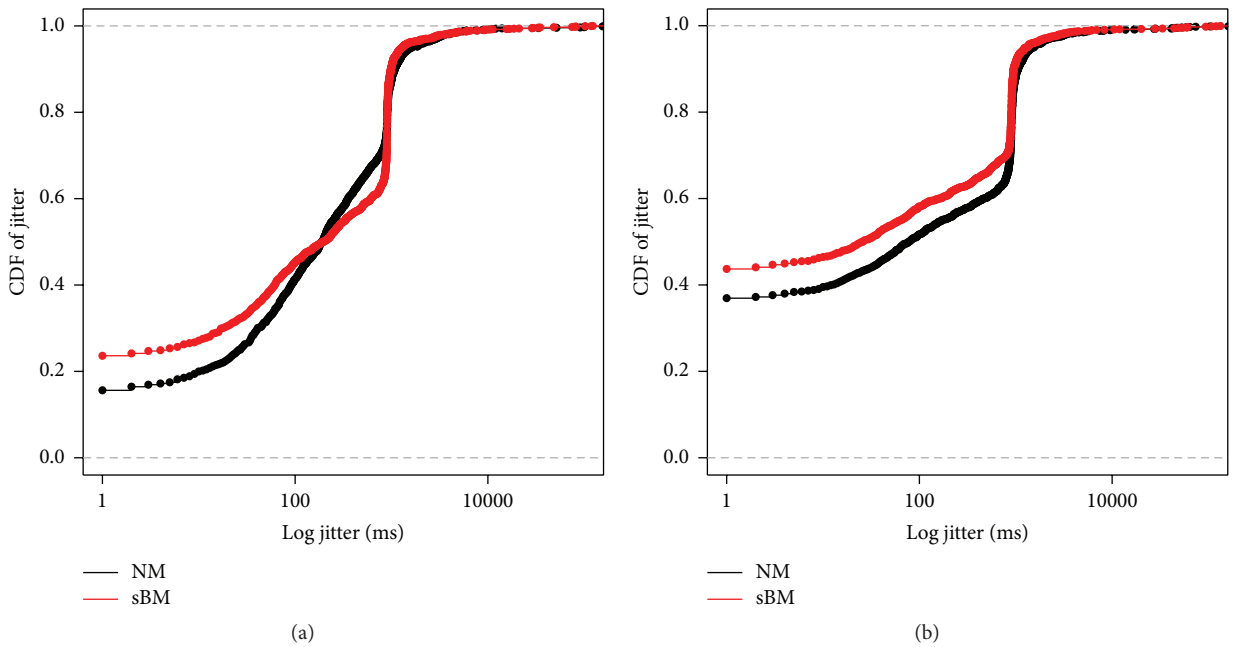

Figure 8: CDF of jitter in logarithmic scale using the buffer in (a) AB trip and (b) BA trip.

Table 8: Network manager comparative.

Journey	Manager	Median (ms)	Mean (ms)	St dev	Max (ms)
AB	NM	192	1,158.96	10,233.62	290,751
AB	sBM	197	922.89	5,765.98	122,735
BA	NM	79	1,356.77	14,700.01	481,402
BA	sBM	26.50	1,033.64	8,933.74	255,858

Table 9: Disconnection times in seconds.

Journey	Manager	Median (s)	Mean (s)	Min (s)	Max (s)
AB	NM	113.5	97.0	35.0	126.0
AB	sBM	60.50	64.00	49.00	86.00
BA	NM	49.00	56.25	32.00	95.00
BA	sBM	65.50	58.25	35.00	67.00

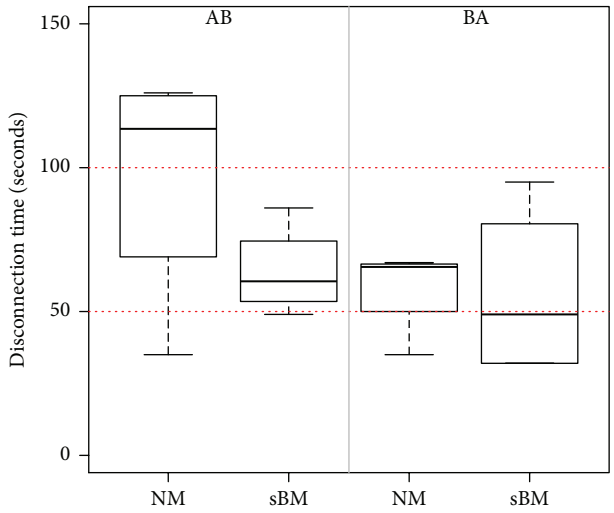

Figure 9: Disconnection times.

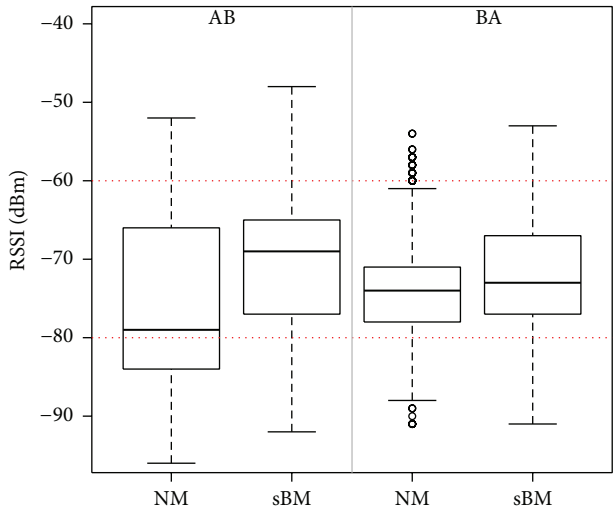

Figure 10: RSSI by journey and manager.

less than 20 and 40% in AB and BA journeys, respectively, have jitter values around zero, while more probability to get a less jitter is obtained using the *signalBased Manager*.

From this test, we know that the buffer proposal to the MQTT protocol in the client is working successfully with a high production rate in regard to IoT applications with the target devices in the real networking environments. Table 8 provides a comparison of both Network Managers. With these results we see that the maximum jitter value obtained in both journeys is lower with sBM than with NM.

Finally, we present how long the disconnection periods were during the execution of each testbed and the variation of their RSSI values in each one.

Regarding the maximum value of the network disconnection time of a device in a mobility case, we observed that it is highly correlated with the jitter measurements. As we can see in Table 9 the disconnection times are from the 32 seconds up to a maximum of 126 seconds. Figure 9 illustrates the disconnection times in the test with each manager where we confirm that the minimum disconnection values are obtained using *signalBased Manager*.

Regarding the RSSI observed with a user moving with a mobile device in outdoor environment during the tests, we observe that the received radio signals in general terms are weak due to various factors such as distance, mobility, and obstacles. We can see in Figure 10 that most of the values of the measurements of the power of the received radio signal are between −84 and −66 dBm. Specifically in Table 10 the mean values obtained are close to −70 and −75 dBm, with values of 35 dBm for really good connections and in the worst case a connection with a value of 126 dBm.

6. Conclusions

The Internet of Things (IoT) is already connecting computing devices, appliances, humans, and other living beings through the Internet. Accumulating data and knowledge through these things would improve a vast array of items and experiences throughout the world. The IoT is made of events and signals of many different kinds and require a standardised mode of communication. MQTT is IoT connectivity protocol so lightweight that it can be supported by some of the smallest

Table 10: RSSI values in decibel-milliwatts (dBm).

Journey	Manager	Median	Mean	St dev	Min	Max
AB	NM	−79	−75.75	10.06	−96	−52
AB	sBM	−69	−70.36	8.04	−92	−48
BA	NM	−74	−74.14	6.02	−91	−54
BA	sBM	−73	−71.94	7.21	−91	−53

measuring and monitoring devices, and it can transmit data over far reaching sometimes intermittent networks. Its architecture anyway does not properly handle mobility when disconnection periods tend to be large.

In this paper we described an experimental evaluation, made in a real environment, of a solution that guarantees that no information loss appears in the presence of variable length hand-offs due to the nodes movement. Our proposal modifies the classical publish/subscribe scheme by introducing an intermediate buffer that takes care of message transfer.

We showed that our solution allows the development of IoT applications where the mobility of the device is no more an issue. Developers do not have to explicitly consider the changes in the point of attachment to the network and no network support is required through protocols like MobileIP or LISP.

Moreover, we studied the impact related to the connectivity of mobile devices of the use of the standard Linux Network Manager. We proposed a cross-layer solution that improves the device connectivity in conjunction with the data layer management. From the experimental results related to the connection managers, the *signalBased Manager* is verified to show a slightly better performance compared to the standard Linux Network Manager, due to the fact that improves the RSSI and extends the connections' duration.

Competing Interests

The authors declare that they have no competing interests.

Acknowledgments

This work was partially supported by *Ministerio de Economía y Competitividad, Programa Estatal de Investigación, Desarrollo e Innovación Orientada a los Retos de la Sociedad, Proyectos I+D+I 2014*, Spain, under Grant TEC2014-52690-R.

References

[1] W. Chen, R. Gupta, V. Lampkin, D. Robertson, and N. Subrahmanyam, *Responsive Mobile User Experience Using MQTT and IBM MessageSight*, IBM Corp, 2014.

[2] G. Owojaiye and Y. Sun, "Focal design issues affecting the deployment of wireless sensor networks for pipeline monitoring," *Ad Hoc Networks*, vol. 11, no. 3, pp. 1237–1253, 2013.

[3] Network Working Group, *DNS Name Auto-Configuration for Internet of Things Devices*, 2016, https://tools.ietf.org/html/draft-jeong-homenet-device-name-autoconf-03.

[4] J.-A. Jiang, C.-L. Tseng, F.-M. Lu et al., "A GSM-based remote wireless automatic monitoring system for field information: a case study for ecological monitoring of the oriental fruit fly, *Bactrocera dorsalis* (Hendel)," *Computers and Electronics in Agriculture*, vol. 62, no. 2, pp. 243–259, 2008.

[5] M. Di Francesco, S. K. Das, and G. Anastasi, "Data collection in wireless sensor networks with mobile elements: a survey," *ACM Transactions on Sensor Networks*, vol. 8, no. 1, article 7, 2011.

[6] E. Fasolo, M. Rossi, J. Widmer, and M. Zorzi, "In-network aggregation techniques for wireless sensor networks: a survey," *IEEE Wireless Communications*, vol. 14, no. 2, pp. 70–87, 2007.

[7] Q. Gao, J. Zhang, X. Shen, and B. Larish, "A cross-layer optimization approach for energy efficient wireless sensor networks: coalition-aided data aggregation, cooperative communication, and energy balancing," *Advances in Multimedia*, vol. 2007, Article ID 56592, 12 pages, 2007.

[8] C. Perera, A. Zaslavsky, P. Christen, and D. Georgakopoulos, "Context aware computing for the internet of things: a survey," *IEEE Communications Surveys and Tutorials*, vol. 16, no. 1, pp. 414–454, 2014.

[9] F. Yamagata, D. Komaba, H. Oguma et al., "Seamless handover for hotspot network using buffered packet forwarding method," in *Proceedings of the 10th IEEE Singapore International Conference on Communications Systems (ICCS '06)*, pp. 1–5, Singapore, November 2006.

[10] M. Portolés, Z. Zhong, S. Choi, and C.-T. Chou, "IEEE 802.11 link-layer forwarding for smooth handoff," in *Proceedings of the 14th IEEE International Symposium on Personal, Indoor and Mobile Radio Communications (PIMRC '03)*, vol. 2, pp. 1420–1424, Beijing, China, September 2003.

[11] L. Dürkop, B. Czybik, and J. Jasperneite, "Performance evaluation of M2M protocols over cellular networks in a lab environment," in *Proceedings of the 2015 18th International Conference on Intelligence in Next Generation Networks (ICIN '15)*, pp. 70–75, IEEE, Paris, France, February 2015.

[12] G. Fortino, A. Guerrieri, W. Russo, and C. Savaglio, "Middlewares for smart objects and smart environments: overview and comparison," in *Internet of Things Based on Smart Objects: Technology, Middleware and Applications*, pp. 1–27, Springer, Berlin, Germany, 2014.

[13] G. Fortino, A. Guerrieri, M. Lacopo, M. Lucia, and W. Russo, "An agent-based mid-dleware for cooperating smart objects," in *Highlights on Practical Applications of Agents and Multi-Agent Systems: International Workshops of PAAMS 2013, Salamanca, Spain, May 22–24, 2013. Proceedings*, pp. 387–398, Springer, Berlin, Germany, 2013.

[14] T. Taleb and A. Ksentini, "Follow Me cloud: interworking federated clouds and distributed mobile networks," *IEEE Network*, vol. 27, no. 5, pp. 12–19, 2013.

[15] J. Luzuriaga, J. C. Cano, C. Calafate, P. Manzoni, M. Perez, and P. Boronat, "Handling mobility in IoT applications using the MQTT protocol," in *Proceedings of the Internet Technologies and*

Applications (ITA '15), pp. 245–250, Wrexham, UK, September 2015.

[16] Y. Gu, F. Ren, Y. Ji, and J. Li, "The evolution of sink mobility management in wireless sensor networks: a survey," *IEEE Communications Surveys & Tutorials*, vol. 18, no. 1, pp. 507–524, 2016.

[17] R. Rajagopalan and P. K. Varshney, "Data-aggregation techniques in sensor networks: a survey," *IEEE Communications Surveys and Tutorials*, vol. 8, no. 4, pp. 48–63, 2006.

[18] The GNOMEProject, NetworkManager, 2016, https://wiki.gnome.org/Projects/NetworkManager.

[19] P. Fazio, M. Tropea, C. Sottile, and A. Lupia, "Vehicular networking and channel modeling: a new Markovian approach," in *Proceedings of the 2015 12th Annual IEEE Consumer Communications and Networking Conference (CCNC '15)*, pp. 702–707, IEEE, Las Vegas, Nev, USA, January 2015.

[20] H. Velayos and G. Karlsson, "Techniques to reduce the IEEE 802.11b handoff time," in *Proceedings of the 2004 IEEE International Conference on Communications*, vol. 7, pp. 3844–3848, June 2004.

[21] UJI International, Universitat Jaume I of Castello, http://ujiapps.uji.es/perfils/internacional/.

[22] Guifi.net, "Telecommunications Networks as a Commons," http://guifi.net/en/what_is_guifinet.

[23] J. Luzuriaga, M. Perez, P. Boronat, J. C. Cano, C. Calafate, and P. Manzoni, "Testing AMQP protocol on unstable and mobile networks," in *Proceedings of the 7th International Conference on Internet and Distributed Computing Systems (IDCS '14), Calabria, Italy, September 2014*, Lecture Notes in Computer Science, pp. 250–260, Springer, 2014.

[24] Guifi.net, CastelloUJISolicom, http://guifi.net/en/uji-biblioteca.

[25] D. Vega, L. Cerdà-Alabern, L. Navarro, and R. Meseguer, "Topology patterns of a community network: Guifi.net," in *Proceedings of the IEEE 8th International Conference on Wireless and Mobile Computing, Networking and Communications (WiMob '12)*, pp. 612–619, IEEE, Barcelona, Spain, October 2012.

[26] B. Wang, "Coverage problems in sensor networks: a survey," *ACM Computing Surveys*, vol. 43, no. 4, article 32, pp. 1–53, 2011.

Hindawi Publishing Corporation
Mobile Information Systems
Volume 2016, Article ID 4568241, 14 pages
http://dx.doi.org/10.1155/2016/4568241

Research Article

Unobtrusive Support System for Prevention of Dangerous Health Conditions in Wheelchair Users

Diego E. Arias,[1] Esteban J. Pino,[1] Pablo Aqueveque,[1] and Dorothy W. Curtis[2]

[1] *Universidad de Concepción, 4070409 Concepción, Chile*
[2] *Massachusetts Institute of Technology, Cambridge, MA 02139, USA*

Correspondence should be addressed to Esteban J. Pino; epino@ieee.org

Received 5 February 2016; Revised 24 May 2016; Accepted 1 June 2016

Academic Editor: Giancarlo Fortino

This paper presents an assistive device for wheelchair users with severe disability. It consists of several sensors deployed on a wheelchair, able to sense pressure relief habits, activity level, vital signs, and ambient conditions. A pilot study was conducted to evaluate the potential capabilities of the system and the feasibility of implementing alarms. During a period of two weeks, six full-time wheelchair users were monitored. Results show that the system is able to capture pressure relief patterns and tilt-in-space usage, a mechanism required to avoid pressure ulcers. Data analysis shows that none of the volunteers fully complied with the tilting recommendations. It also shows varied activity levels, both within and between patients, indicating their engagement in daily activities. The system is also able to estimate heart and respiration rate during passive activities (e.g., watching TV and/or resting). Also, high temperatures in summer were monitored while patients were outside, to prevent heatstroke events. All the monitored variables are acquired with unobtrusive sensors, producing no discomfort to the patient and providing valuable information for better care. The final recommendation and alarm system is implemented in a single board computer, to be embedded in the wheelchair.

1. Introduction

Wheelchairs users are estimated at about 10% of disabled people worldwide [1]. The main causes of wheelchair usage are injuries and/or medical conditions that affect the central nervous system (CNS). Depending on how the CNS is damaged, the disability varies. Among the most severe cases are patients going through an advanced stage of a neurodegenerative disease such as Multiple Sclerosis (MS) and patients with tetraplegia or paraplegia who have been affected by a severe injury in the spinal cord.

Besides physical impairment, these patients can be affected by a variety of symptoms such as thermoregulatory problems and cardiorespiratory dysfunction. In sum, they cannot perform daily activity without assistance, and they require continuous nursing care and supervision usually provided by families or specialized caregivers. However, in some cases, the supervision fails and the patients can be exposed to dangerous conditions.

First of all, wheelchair users are prone to develop pressure ulcers (PU) because they spend long hours sitting. PU are injuries on the skin produced by prolonged pressure, usually over parts of the body in contact with the wheelchair. Excessive pressure reduces the blood flow producing tissue ischemia and death, resulting in an ulcer. To avoid PU, patients should relieve pressure frequently. To do that, caregivers should be aware of reminding patients when to relieve pressure and assist them if needed. However, high workload in nursing homes can lead caregivers to forget when the patient should relieve pressure. The same can happen when a family member is responsible for the patient's care. Both situations increase the probability of PU. Secondly, another dangerous situation occurs with disabled patients who suffer thermoregulatory problems. Long periods of time exposed to heat without caregiver's monitoring can produce sunburns, dehydration, heatstroke, and even death. There are reports of deaths produced by heat exposure in assisted living facilities as well as in patient's homes due to impaired self-awareness and failure in supervision [2–4]. Lastly, under severe mobility impairment, people can also develop comorbidities related to respiratory and cardiovascular function which should be constantly supervised by caregivers. For example, people

with MS can suffer respiratory muscle weakness and bulbar dysfunction which produce difficulty in breathing [5]. Also, the worst cases of spinal cord injury (SCI) are unable to breathe due to paralysis of respiratory muscles requiring ventilation support. Furthermore, this population presents autonomic dysfunction increasing the probability of suffering from heart diseases [6].

The examples described show how wheelchair users with severe disability are constantly at risk. Problems such as low mobility can produce PU, heat sensitivity can produce exacerbation of symptoms and/or heat stress during outdoor activities, and abnormal cardiorespiratory function can affect their health status. In those cases, supervision is very important to prevent dangerous conditions. To this end, a system to monitor variables related to these problems can help caregivers and medical staff to increase patient's quality of life.

2. Related Work

Advances in sensors, wireless communication systems, and information technologies make it possible to develop new assistive devices to monitor patients during daily life. Regarding wheelchair bound patients, several research groups have developed monitoring systems to alert patients and caregivers to dangerous situations like those previously described. For example, some groups have focused on developing systems to prevent PU. To this end, authors have deployed several sensors between the patient and the pressure relief cushion, to capture pressure changes. To acquire this information, they use commercial pressure mapping devices [7] and custom sensor arrays based on different technologies such as rigid copper electrodes [8], piezoresistive sensors [9], and force sensitive resistors (FSR) [10, 11]. Then, data are processed to generate alarms to warn patients and/or caregivers when a change in position is necessary. If any of the sensors detects a dangerous level of pressure during a long period of time, an alarm is generated. Another approach has been used to avoid PU when the patients use powered wheelchairs equipped with a tilt-in-space system. The tilt-in-space system allows modifying the seat angle orientation in relation to the ground while maintaining the seat to back angle [12]. This mechanism allows patients to redistribute the seat pressure, transferring it from the seat to the back. Authors have monitored how often wheelchair users perform a tilt to relieve pressure [13–17]. To this end, the proposed systems are composed of accelerometers able to detect when patients perform a tilt. Based on this information, it is possible to implement alarms to remind patients and caregivers when patients should tilt their chair.

Vital signs such as heart rate (HR) and respiratory rate (RR) are also monitored in wheelchair users. The main difference between the proposed systems lies in the types of sensors used, some of them being more obtrusive than others. For instance, some projects have used conventional sensors such as skin electrodes for ECG and respiration belts which can be difficult to wear, producing discomfort to impaired patients [18]. On the other hand, authors have measured Ballistocardiogram (BCG), defined as the mechanical activity of the heart which is an unobtrusive way to acquire cardiorespiratory activity [19]. To acquire BCG signals, an electromechanical film (EMFi) is deployed on the wheelchair seat and backrest. Using advanced signal processing, it is possible to acquire respiration and heart activity to calculate HR and RR to assess patient's health.

Regarding heat exposure, although there is no report of applications designed for wheelchair users, it is possible to find devices developed to provide an alert to dangerous heat exposure in situations such as workers [20, 21] and car drivers [22] exposed to hot environments. The implemented systems measure ambient temperature (T_{AMB}) and relative humidity (RH) to calculate indexes able to estimate thermal discomfort such as heat index (HI) and Wet Bulb Globe Temperature. Also, HR and RR are measured to obtain a more reliable estimation of the subject thermal state. Based on this information, alarms are implemented to decide whether people should stop working or whether car drivers are in good conditions to keep driving.

We propose that combining monitoring pressure relief patterns, physiological data, and thermal indexes provides sufficient and timely information about the patient's health while using the wheelchair. To this end, several noninvasive sensors are deployed on a patient's wheelchair to capture vital signs, ambient conditions, pressure relief habits, and patient activity providing useful context-aware information for patients, caregivers, and clinical staff without producing discomfort. Our previous work [23–27] presented different stages of the project, from design to preliminary findings. In this paper, we present the final setup, detailed algorithms, and the use of our assistive device to monitor these important variables during daily life. We also present the final hardware implemented to generate alarms and recommendations to caregivers and to the user. The system is designed to improve the care of wheelchair users who suffer severe mobility impairment by monitoring key parameters known to be relevant during daily activities.

3. Methods

3.1. Instrumentation. The system consists of several unobtrusive sensors deployed on a powered wheelchair, able to sense pressure relief habits, patient activity, vital signs, and ambient conditions. The selected sensors are able to capture seat and back pressure changes, tilt angle produced by the tilt-in-space system, respiration and heart activity from BCG signals, T_{AMB}, and RH. To capture pressure relieving habits, nine small FSR (model FSR 406 manufactured by Interlink Electronics) are deployed on the wheelchair to detect prolonged pressure over the buttock and back area. The sensors are distributed as follows: 4 sensors are put on the seat (FSR_S), under the pressure relief cushion, and 5 on the backrest (FSR_B), inside a piece of foam. To detect the wheelchair tilt and to capture information related to subject activity, an accelerometer (ADXL335 chip) is fixed to the wheelchair. The ADXL335 has analog output and resolution of ±3 g. Based on pressure and accelerometer data, it is possible to detect pressure redistribution produced by tilt-in-space system. To acquire heart and respiratory activity, BCG was measured using EMFi sensors (model L-3030 manufactured by EMFIT Ltd.), a highly sensitive electromechanical film

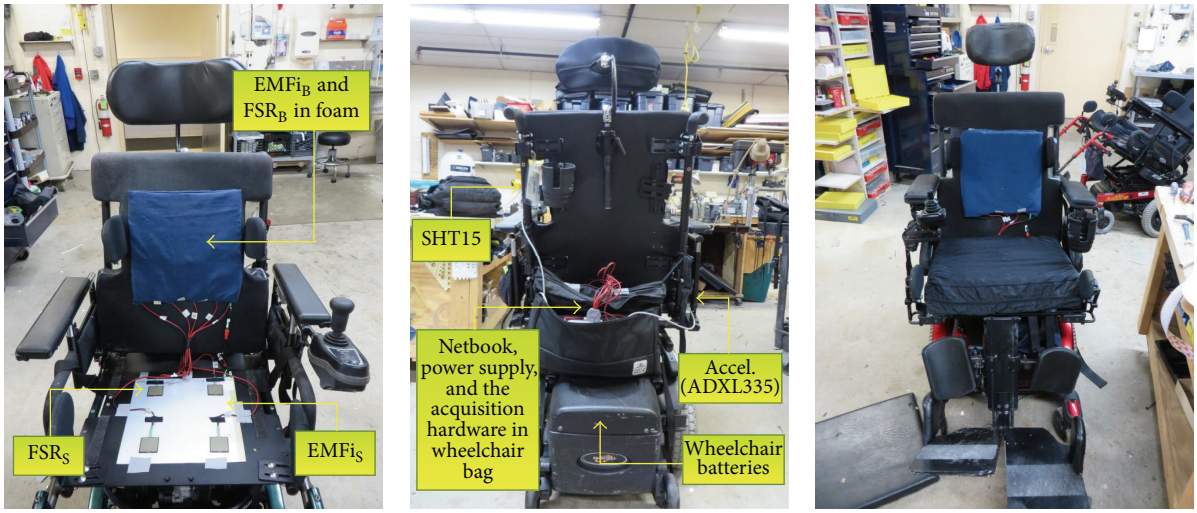

(a) (b) (c)

Figure 1: Pictures of the implemented system: (a) front, (b) back, and (c) system ready to use. Unobtrusive sensors are installed on the wheelchair, under backrest foam and pressure relief cushion on the seat. Ambient sensor and accelerometer are attached to wheelchair structure, away from the user. The system is powered by the wheelchair batteries.

sensor able to measure small pressure variations. One sensor was placed on the seat (EMFi$_S$), under the pressure relief cushion, and another was placed on the backrest (EMFi$_B$), inside a piece of foam. Also, an ambient sensor (SHT15 chip manufactured by Sensirion) allows measuring T_{AMB} and RH to avoid heat exposure during outdoor activities. This sensor integrates both variables in one chip. Its digital output data are sent to a microcontroller unit (MCU) using a proprietary communication protocol. This setup allows us to capture the information in a noninvasive way without discomfort to the user, because none of the sensors touch the patient directly. All information acquired by the sensors is sent to MCU which samples the data at 100 Hz with 11 bits of resolution. Then, the data are transmitted through the serial port to a small laptop mounted on the wheelchair. Finally, the data are stored in a PostgreSQL [28] database for further analysis. The whole system is powered by the wheelchair batteries. The power consumed by the system is minimal and does not affect the wheelchair performance. Figure 1 shows the implemented system mounted on the wheelchair.

3.2. PRT Detection Algorithm. An algorithm to detect pressure relief by tilting (PRT) was implemented. PRT is a wheelchair tilt due to the operation of the tilt-in-space system which produces relief of pressure over the buttocks area. This is achieved if the skin is unloaded for at least 3 min and 30 sec according to the study presented in [29], so the tissues are oxygenated. To ensure this phenomenon, a threshold of 5 min was used.

The algorithm uses the accelerometer data and the FSR sensors deployed on the seat. First of all, accelerometer data is filtered using a low-pass filter to extract the static component of acceleration and transform it into a tilt angle. The pressure sensors are also filtered to remove high frequency noise due to wheelchair vibration. The angle is averaged using a 10 sec sliding window to detect angle changes. When the tilt angle is reduced by at least 5 degrees, which means that the wheelchair is tilted back, and the pressure sensors reduce their level sharply, the tilt is marked as possible PRT. To consider the tilt as PRT, the subject should maintain this position or increase the tilt angle for at least 5 minutes. Otherwise, the algorithm is restarted. When the subject returns to the initial position, the tilt is finished. Figure 2 shows an example of PRT detection. This full record shows 4 PRT detection instances. Vertical lines marked with "X" indicate the start of a tilt. Lines marked with "O" indicate the end of a tilt. It is possible to observe how pressure over the buttocks area is transferred to the back during PRT. Also, analyzing the pressure sensors, it is possible to calculate the wheelchair occupancy time. In the example in Figure 2, the volunteer is on the wheelchair for 6 : 41 hours.

3.3. Activity Level Estimation. For wheelchair users with severe disability, a good indication of activity is when they are driving the wheelchair. Therefore, to estimate patient's activity, the dynamic component of the accelerometer was used because it reflects the subject's movement and the wheelchair vibration during driving. To extract this component, the standard deviation of the accelerometer is calculated using a sliding window. High standard deviation values reflect periods of time where the subject shows a high level of activity. Based on tests performed on lab settings, a fixed threshold of 0.5 was used to distinguish between high and low levels of activity as can be observed in Figure 3. Periods of time classified as high activity are used to calculate an activity index (AI) defined as the percentage of the wheelchair occupancy where patients show high activity.

3.4. Ballistocardiogram Processing. Raw EMFi signals are processed to extract respiration and BCG signals. To this end, a filter bank is implemented based on the Discrete Wavelet

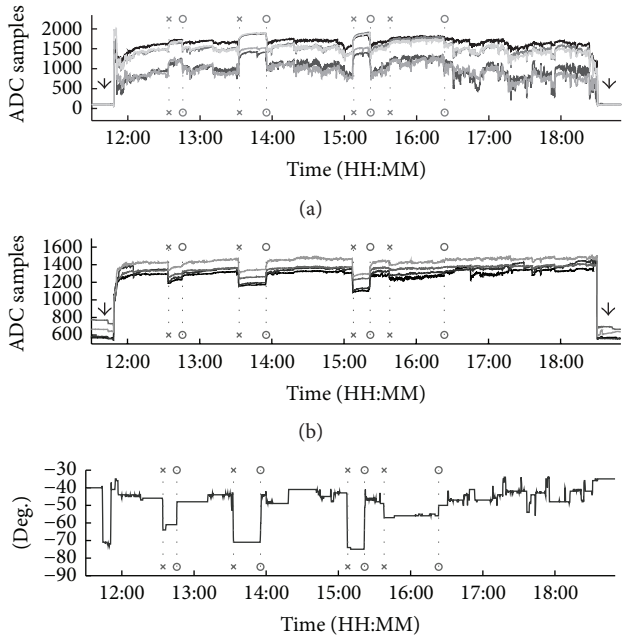

Figure 2: PRT detection algorithm. FSR_B (a), FSR_S (b), and tilt angle obtained with the accelerometer (c) allow capturing daily pressure relieving patterns. Vertical lines marked with "X" and "O" indicate the PRT detected. Arrows on the FSR sensors mark the beginning and end of the wheelchair occupancy.

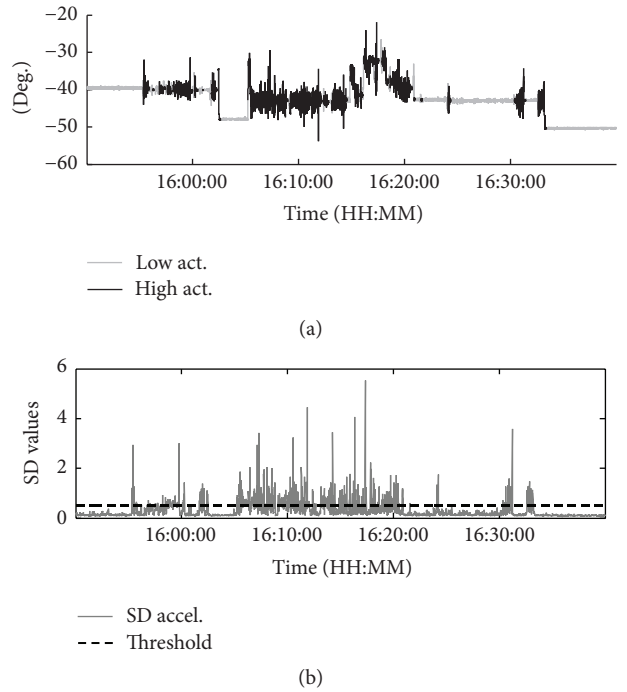

Figure 3: Processing the accelerometer data (a) allows estimating the activity level of each subject. Segments in bold show when the subject presents high activity (e.g., driving, tilting, and moving) as opposed to segments with low activity (e.g., resting, wheelchair stopped). The activity detection is based on the standard deviation of the accelerometer data (b) and a fixed threshold.

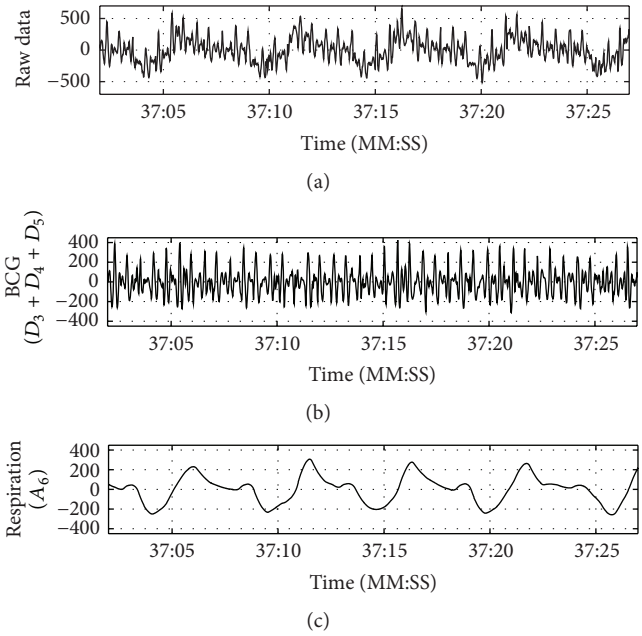

Figure 4: (a) Raw EMFi, (b) BCG, and (c) respiration signals used to obtain vital signs.

Transform (DWT). The DWT filter bank allows decomposing the original signal into n subsignals called details (D_i) and approximations (A_i), where i is the ith decomposition level. The decomposition is done passing the raw data through several low-pass and high-pass filters designed with a specific mother wavelet, selected based on the similarity to the clean BCG waveforms. High frequency information (D_i) and low frequency information (A_i) are contained on the resulting signals; however, to obtain heart and respiratory activity, specific details and approximations must be selected. Raw EMFi data are decomposed into 6 levels using, as mother wavelets, *symlet 5* for $EMFi_B$ and *daubechies 10* for $EMFi_S$. An example of BCG and respiratory reconstruction is shown in Figure 4. Respiration signals are reconstructed using A_6 because it contains frequency components below 0.5 Hz where respiration activity is found. On the other hand, BCG signals are reconstructed adding the details D_3, D_4, and D_5 because they contain frequency components between 1 and 10 Hz where most of the power of the BCG signal is found.

3.5. Respiratory Rate Calculation. An algorithm for RR calculation was implemented using the respiratory signal obtained from raw EMFi data. It works by recognizing inspiration and expiration cycles from respiratory waveform and extracting features such as area, width, and maximum and minimum of each cycle to discriminate valid respiration from artifacts produced by movements. The implemented algorithm was based on [30, 31].

Figure 5 shows a typical respiration waveform where it is possible to observe the features used by the algorithm to detect valid respiration. First of all, the respiratory signal or R_{LOC} is filtered using a 500-sample moving average to obtain

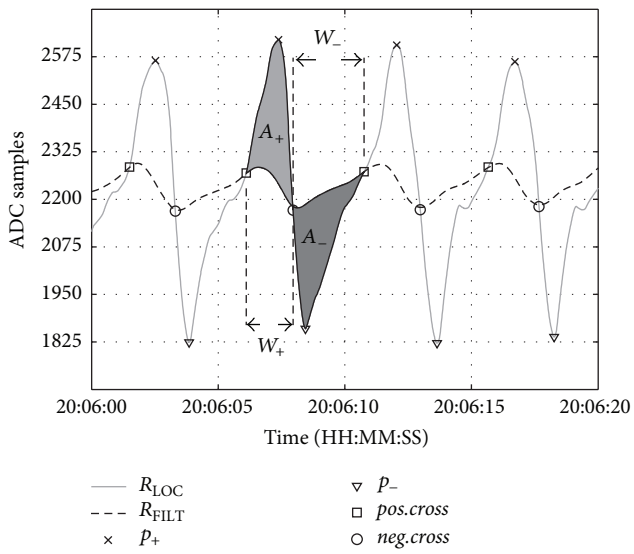

Figure 5: Respiration waveform and the features used by the RR algorithm.

its baseline, hereafter called R_{FILT}. It defines 2 cycles according to the crossings with R_{LOC}: a positive cycle associated with the inspiration, when $R_{LOC} > R_{FILT}$, and a negative cycle associated with the expiration, in the other case. These cycles are characterized by their area, width, and maximum and minimum values. The area for the positive cycle (A_+) and negative cycle (A_-) is defined as $\sum_{i=0}^{N} |R_{LOC}(i) - R_{FILT}(i)|$, where i is the ith sample of R_{LOC} and R_{FILT} from the beginning ($i = 0$) to the end ($i = N$) of the cycle. The width of a positive cycle (W_+) is defined as the number of samples from the first crossing (when $R_{LOC} > R_{FILT}$) to the second crossing (when $R_{LOC} < R_{FILT}$). For a negative cycle (W_-), it is defined as the number of samples from the second cross until the third cross (or the first cross for the next respiration). The maximum value of R_{LOC} during a positive cycle (p_+) and the minimum value of R_{LOC} during a negative cycle (p_-) are measured to calculate the amplitude of R_{LOC} as $|p_+ - p_-|$.

After a complete cycle, new values of A_+, W_+, p_+, A_-, W_-, and p_- are calculated. Then, the algorithm moves to a decision stage to determine whether valid respiration is detected. The decision stage checks three conditions: (1) the ratio of W_+ to W_- is greater than 0.3 and less than 1.3, (2) the ratio of A_+ to A_- is greater than 0.4 and less than 2.5, and (3) the absolute amplitude of the current respiratory cycle is greater than 50% of the amplitude of the previous respiratory cycle.

These thresholds were determined empirically. If all three conditions are met, a valid respiration cycle is detected; otherwise, the cycle is considered noise. To calculate RR, at least two consecutive valid respiration instances must be detected.

3.6. Heart Rate Calculation. An algorithm to calculate HR was also implemented using BCG signals extracted from raw EMFi records. It works by looking for possible beats in zones of BCG signal with high energy.

First of all, the energy of BCG signal is calculated using the following expression:

$$E_{BCG} = \sum_{k=i}^{i+q-1} \left|BCG_k\right|^2, \quad (1)$$

where q is a 30 ms sliding window. Then, a peak detector is applied to the energy signal to detect high energy peaks. When a peak of energy is detected, a window of 700 ms is scanned in the BCG signal to detect potential beats. Consecutives maxima and minima of BCG signal inside the 700 ms window are used to calculate the Euclidean distance and the slope of the straight line generated between these two points. Once the 700 ms window is scanned completely, the segment with the longest distance and the minimum slope is considered a potential beat. Finally, if the time between the maximum and the minimum of the selected segment is less than 0.5 seconds, a valid beat is assumed; otherwise, it is treated as noise. Figures 6 and 7 show the flow diagram and an example of the algorithm.

3.7. Heat Index Calculation. T_{AMB} and RH measured by the SHT15 sensor were used to calculate the dew point and the HI. These parameters are tabulated in ranges of exposure and the possible effects on human body if the exposure is prolonged. The dew point has been described as a possible indicator of the symptoms exacerbation produced by heat in MS patients [32]. High dew point values (usually over 17°C) can increase the probability of the symptoms worsening. On the other hand, the HI provide warnings due to heat-related illness such as sunstroke, heat exhaustion, and fatigue which can affect a diverse group of at-risk people such as children, the elderly, and people with disabilities. Table 1 shows established ranges of exposure for HI and dew point.

3.8. Pilot Study. A pilot study was conducted to evaluate the capabilities of the system [25]. To this end, volunteers were recruited from the Boston Home (TBH), a specialized care residence for people with advanced MS and other neurological diseases. To participate in this study, all participants should be full-time wheelchairs users with severe disability. Also, their wheelchairs should be electric-powered and equipped with at least a tilt-in-space system and an inflatable pressure relief cushion as methods to relieve pressure.

The protocol consists of deploying the prototypes on the wheelchairs at the beginning of the study. Every day, before the volunteers start to use their wheelchairs, the prototypes are checked to avoid technical issues. Then, prototypes collect data continuously during the whole time spent on the wheelchair. This study was approved by the MIT Committee on the Use of Humans as Experimental Subjects.

4. Results

The study was conducted during a period of 2 weeks. Six TBH residents consented to participate in this study: 4 women and 2 men (hereafter called S1 to S6) with a mean age of 56 ± 12 years. All were diagnosed with a progressive form of MS. The

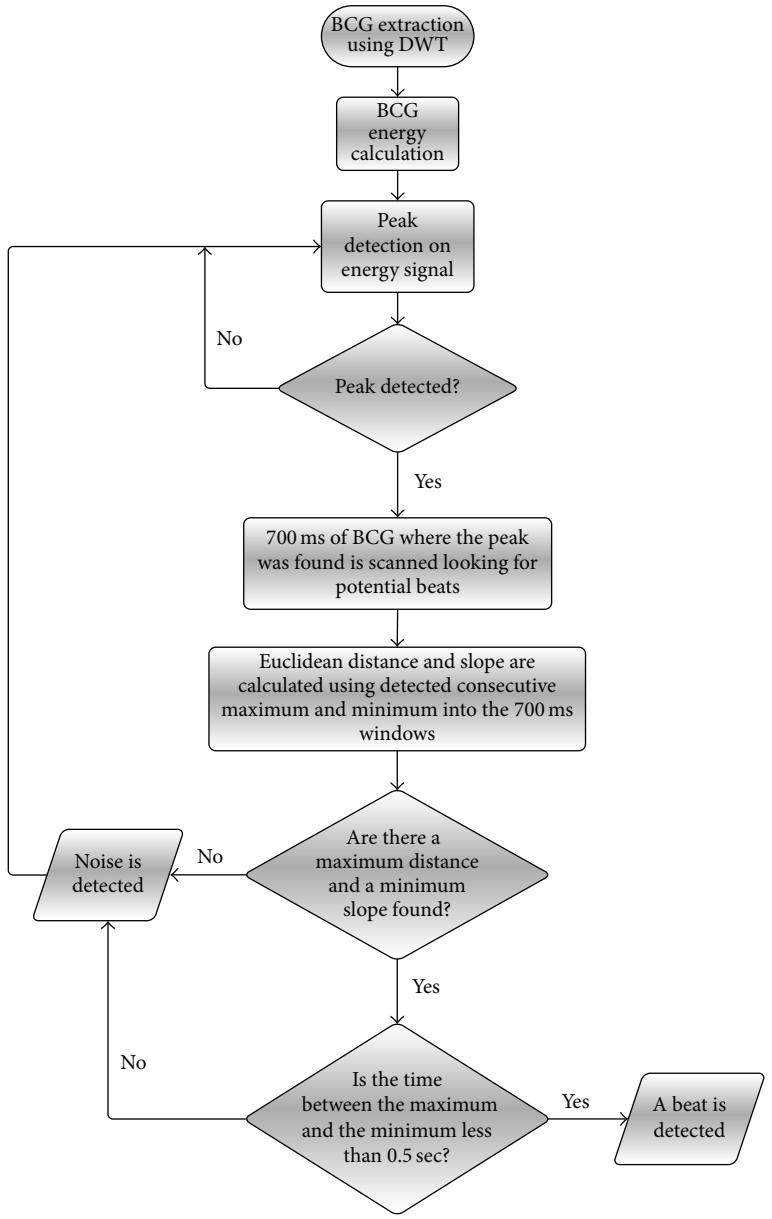

Figure 6: Flow diagram of the peak detection algorithm to calculate HR from BCG.

Table 1: HI effects on people in high risk group and effects of dew point on MS.

Heat index		Dew point	
HI (°C)	General effects	Dew point (°C)	MS symptoms
Above 54	*Highly likely* heat or sunstroke with continued exposure	Above 17	Severe
41–54	*Likely* sunstroke, heat cramps, or heat exhaustion; possible heatstroke with prolonged exposure and/or physical activity	14–17	Moderate
32–40	*Possible* sunstroke, heat cramps, or heat exhaustion with prolonged exposure and/or physical activity	11–15	Slight
26–31	*Possible* fatigue with prolonged exposure and/or physical activity	5–10	Very slight

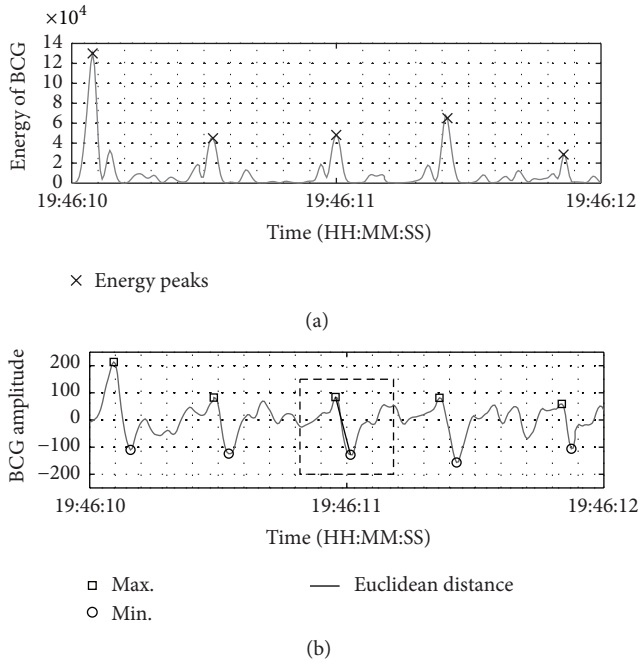

Figure 7: (a) Peak detection over the energy of BCG. (b) Beat detection over BCG signal. The dashed line rectangle indicates the 700 ms window.

mean time after diagnosis was 24 ± 6 years. The Expanded Disability Status Scale [33] varies between 7.5 and 8.5 which indicates a high disability level. All participants use a pressure relief cushion manufactured by ROHO®.

Figure 8 shows the AI and the wheelchair occupancy distribution from all subjects during the period of 39 days of data collection. On average, the participants presented an activity index of 18.6 ± 11.3% with a maximum of 61.1% and minimum of 5%. In most cases (29 days), the subjects showed an AI between 10% and 30%. Only in 2 days (2.2% of time) did they present an AI greater than 30%. Regarding the wheelchair occupancy, the participants spent on their chairs 6.38 ± 1.72 hours per day. The maximum occupancy registered was 10.58 hours and the minimum was 2.17 hours. On most days (17 days), the subjects spent between 4 and 6 hours (44%) on their wheelchairs. Only in 3 days (7.7%) was the wheelchair occupancy less than 4 hours. On the rest of the days, the occupancy time was distributed as follows: 6–8 hrs in 12 days (31%), 8–10 hrs in 6 days (15.4%), and over 10 hrs in 1 day (2.6%). Figure 9 shows a full report of activity and wheelchair occupancy registered for S1. On average, S1 used her chair 7.47 ± 0.92 hours/day. During this time, she showed an AI between 20% and 30%, except for day 3 where the AI reached 48%. The increase in the AI is coincidental to when S1 left the nursing home to go to a shopping mall.

There are several recommendations about the frequency to relieve pressure. Some guidelines recommend relieving pressure every 15 min [34]; other guidelines recommend longer intervals such as every 1 hour or every 2 hours [35]. Only 2.1% of PRT performed by the subjects meet the recommendation if the interval is every 15 min, 25.8% if the interval is every 1 hour, and 57.7% if the interval is every 2 hours. For instance, Figures 10 and 11 show two different cases of pressure relief patterns: a subject who performs several PRT and another who does not. Figure 10 shows a full record from S1 during day 9, where the subject performed 10 PRT during a period of 9.47 hours on the chair. Each tilt lasted 16 min, on average. On the other hand, Figure 11 shows S4 performing only 1 PRT during a period of 10.58 hours spent on the wheelchair. In this case, each tilt lasted 1.25 hours on average. It is also possible to observe that the subject only touches the sensors on the backrest when tilting which can be an indication of bad posture.

Figure 12 shows a histogram that reflects the time intervals spent by the subjects on their chairs without performing a PRT. S1 and S2 achieved shorter intervals. 18.9% of the intervals for S1 and 5.1% for S2 were under 1 hour. For S1, most of the intervals (41.7%) were between 1 and 2 hours. On the other hand, more than 50% of the intervals spent by the rest of the subjects (S2 to S6) were longer than 3 hours, exceeding all recommendations to avoid PU. The maximum was registered by S6, with 93.9% of the intervals over 3 hours. There were days when S2 to S6 did not perform PRT at all. For instance, S3 spent 3.57 hours without tilting the chair during day 6. If this situation is frequent, the subject is prone to develop PU. However, the situation is more risky when the wheelchair occupancy is high. For instance, S6 spent 9.18 hours on the chair without performing a PRT during day 1, four hours more than S3, increasing the probability of developing PU. The average duration in a PRT position is 1.57 hours. However, those who perform frequent PRT spent a shorter time in a tilted position than the subjects who do not. For instance, S1 spent 21 minutes in a tilted position on average. On the other hand, S6 spent around 4.5 hours in this position.

Regarding vital signs calculation, raw EMFi signals were acquired and processed to estimate HR and RR. As data was collected during patient's daily life, signals were severely affected by noise. Situations like wheelchair driving, operation of the tilt-in-space system, wheelchair crashes, subject's movements, and any technical issues that affect signal quality destroy BCG and respiratory cycles, rendering it impossible to estimate vital signs. However, when the subjects stay calm on their wheelchairs during passive activities (e.g., taking a nap, watching TV, and/or resting), it was possible to estimate vital signs. For example, Figure 13 shows over 1 hour of record obtained from S1. During this period, the HR and RR averages were 90.9 ± 6.2 beats/min and 14.7 ± 0.8 breaths/min, respectively. It is possible to observe clean segments of the raw EMFi signal as well as segments that are affected by severe noise (marked with rectangular areas). HR and RR trends were estimated only when clean signals are detected. The algorithms are stopped to reduce false detection in noisy segments. The collected data show that raw EMFi signals are clean between 40% and 50% of the wheelchair occupancy time.

In the study, it was usual to observe the residents resting in their chairs or taking a nap. During this time, the system was able to capture respiratory abnormalities such as apneas. Figure 14 shows a 5 min record captured from S3 where it is possible to observe 4 consecutive apneas lasting more than 15 sec each, a condition that would be very difficult to

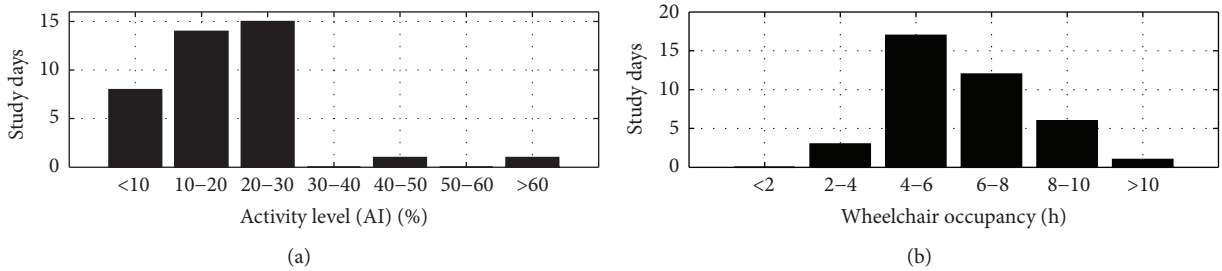

Figure 8: (a) AI and (b) wheelchair occupancy for all subjects during a period of 39 days of data collection.

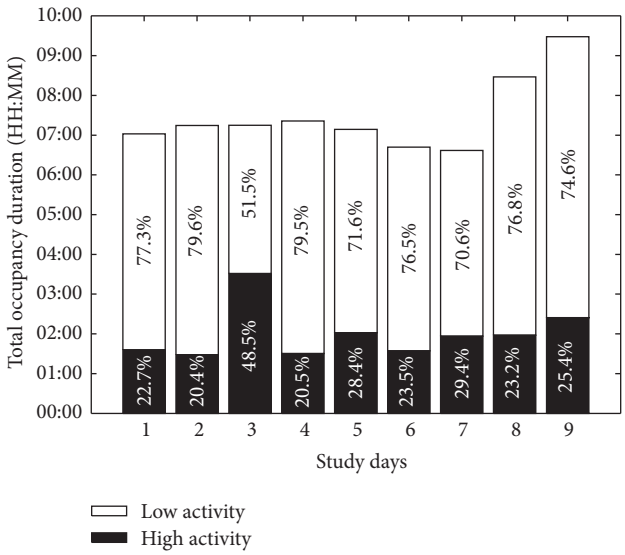

Figure 9: Wheelchair occupancy and AI registered by S1 during a period of 9 days of study.

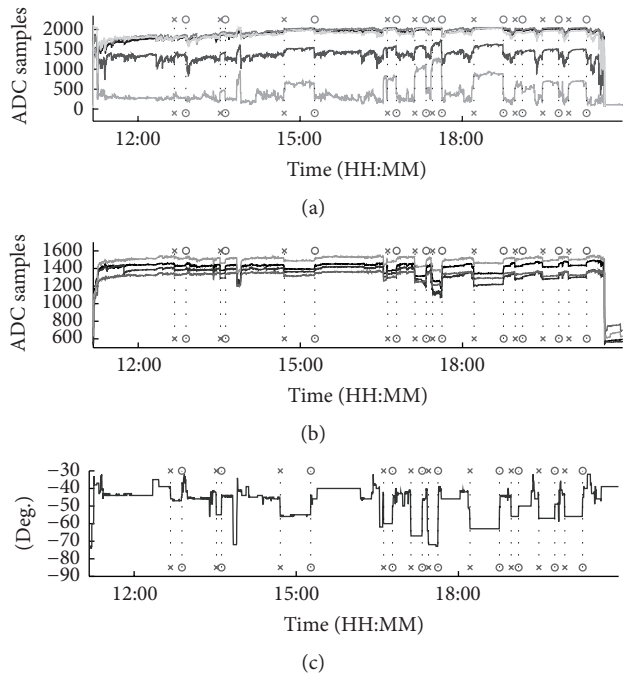

Figure 10: Pressure and angles recorded from S1 wheelchair for 9.47 consecutive hours. (a) FSR_B, (b) FSR_S, and (c) angle data are labeled with the PRT detection. In this case, S1 registered 10 PRT, with an average tilt duration of 16 min.

detect otherwise. Apnea events, usually associated with sleep apnea, affect the cardiovascular system producing progressive damage to the heart [36].

As mentioned before, people with severe mobility impairment are very sensitive to heat, which can produce exacerbation of the symptoms and/or heat-related illness. For this reason, caregivers should be extra careful when patients spend time outside in summer. For example, TBH provides some recommendations for residents and caregiver staff to avoid dangerous heat exposure. The recommendations include checking patient's status every 30 min while they are outside and avoiding exposure to T_{AMB} above 35°C or HI greater than 35°C. However, the protocol relies on human evaluation and is susceptible to failure. Sometimes high workload in nursing homes can lead to forgetting checking on patients as what happened in [2] with fatal consequences. The implemented system allows monitoring ambient conditions continuously, which can be used for a potential alarm system. For example, Figure 15 shows a full-day record of T_{AMB} and RH used to calculate HI and dew point value. It is of note that the wheelchair user went outdoors for almost an hour, a period of time where the temperature rose to 30°C. These values are classified both by the HI and by the dew point as dangerous exposure, implying that the patient should go back inside.

5. Final Hardware

The final system was implemented in a single board computer (SBC) in order to reduce the power consumption and have a self-contained system that does not require external processing. The SBC is a Raspberry Pi 2, Model B running Raspbian Jesse Linux OS. The algorithms and the alarm system were programmed in Python. The main characteristics are shown in Table 2.

5.1. Single Board Computer Setup. The SBC and its main accessories are shown in Figure 16. The MCU acquires data from the 4 sensor types: EMFi, FSR, ADXL335, and SHT15. Then, data is labeled and packaged and sent to the SBC

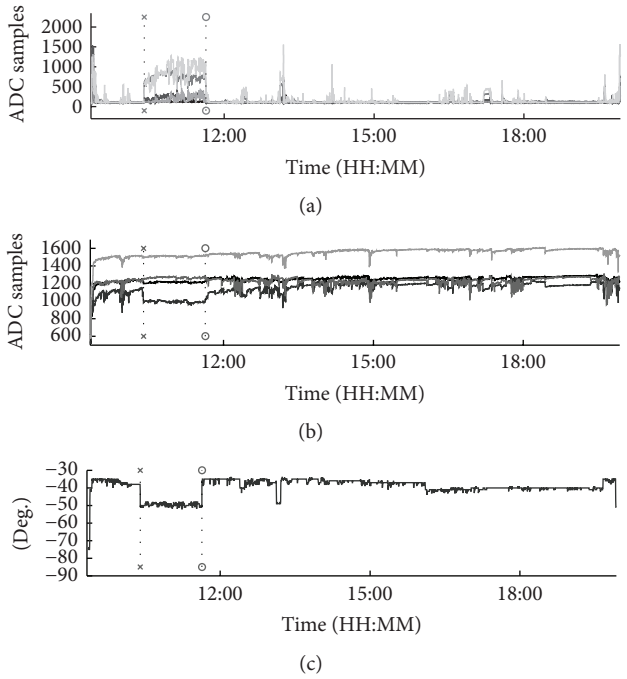

Figure 11: Pressure and angles recorded from S4 wheelchair for 10.58 consecutive hours. (a) FSR_B, (b) FSR_S, and (c) angle data are labeled with the PRT detection. In this case, S4 presents only one PRT lasting 1.25 hours.

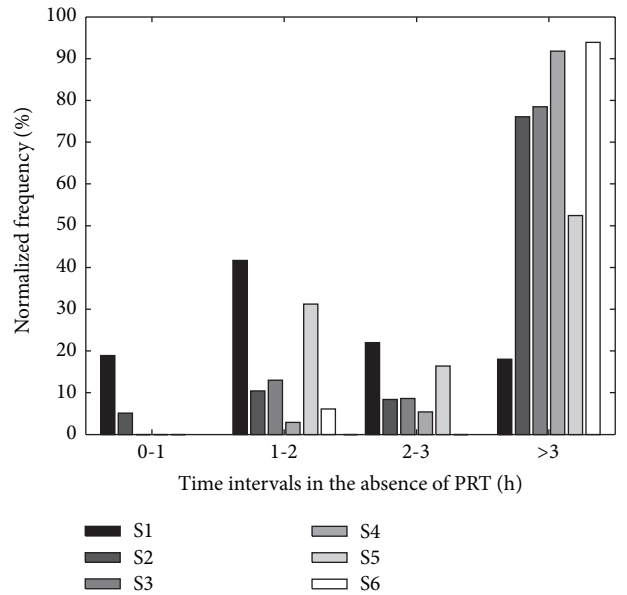

Figure 12: Time intervals in the absence of PRT obtained from all subjects.

through RS-232/USB adapter, at 57.6 kbps. The SBC runs the tilt, activity, HR, RR, apnea detection, and heat index algorithms to process the information from the sensors and issues alarms or recommendations to the user. The notifications are issued using recorded voice messages sent through a standard 3.5 mm jack into a powered speaker. When the system is connected to the Internet via WiFi, an email is also sent to the configured account to alert a caregiver.

Table 2: Technical specifications for Raspberry Pi 2 SBC.

Characteristic	Value
CPU	900 MHz quad-core ARM Cortex-A7
RAM	1 GB
Storage	8 GB SDHC class 10 card
OS	Raspbian Jessie Linux
Audio and video	3.5 mm jack, HDMI
Size	85.6 mm × 53.98 mm
Power consumption	800 mA (4.0 W)
Power supply	5 V through micro USB or GPIO header

5.2. Alerts. The programmed alerts can be divided into 3 groups.

(i) General Information. This group comprises the following:

(i) "The system is on": this indicates the start of the data processing, once a person is detected in the wheelchair.

(ii) "The system is off": this indicates the end of data processing and is issued when the pressure sensors indicate that the person has left the wheelchair.

(ii) Heat Index Alarms. This group comprises the following:

(i) "Please, go to a cooler place": this is issued when the user has been in the 26–31°C range for more than 1 hour or in the 32–40°C range for more than 30 minutes.

(ii) "You must go to a cooler place": this is issued when the user has been in the 41–54°C range for more than 20 minutes.

(iii) "You must go to a cooler place, immediately": this is issued when the user has been in the highest heatstroke level, over 54°C, for more than 5 minutes.

(iii) Tilting. This group comprises the following:

(i) "Please, tilt the chair": a tilt is recommended after one hour without PRT.

5.3. SBC Performance. The performance of the SBC was evaluated in terms of power consumption and processing load. The average power consumption is 0.374 A at 5 V. This is 56% lower than the first version using a netbook. The whole system, considering the MCU and sensors, requires 0.624 A. The average load in 60 s of the SBC is 8.05%. The Python program uses 7%, leaving enough processing power for other tasks.

6. Discussion

The implemented system captures pressure relief habits, activity level, vital signs, and ambient conditions unobtrusively during daily activities. Analyzing the data acquired

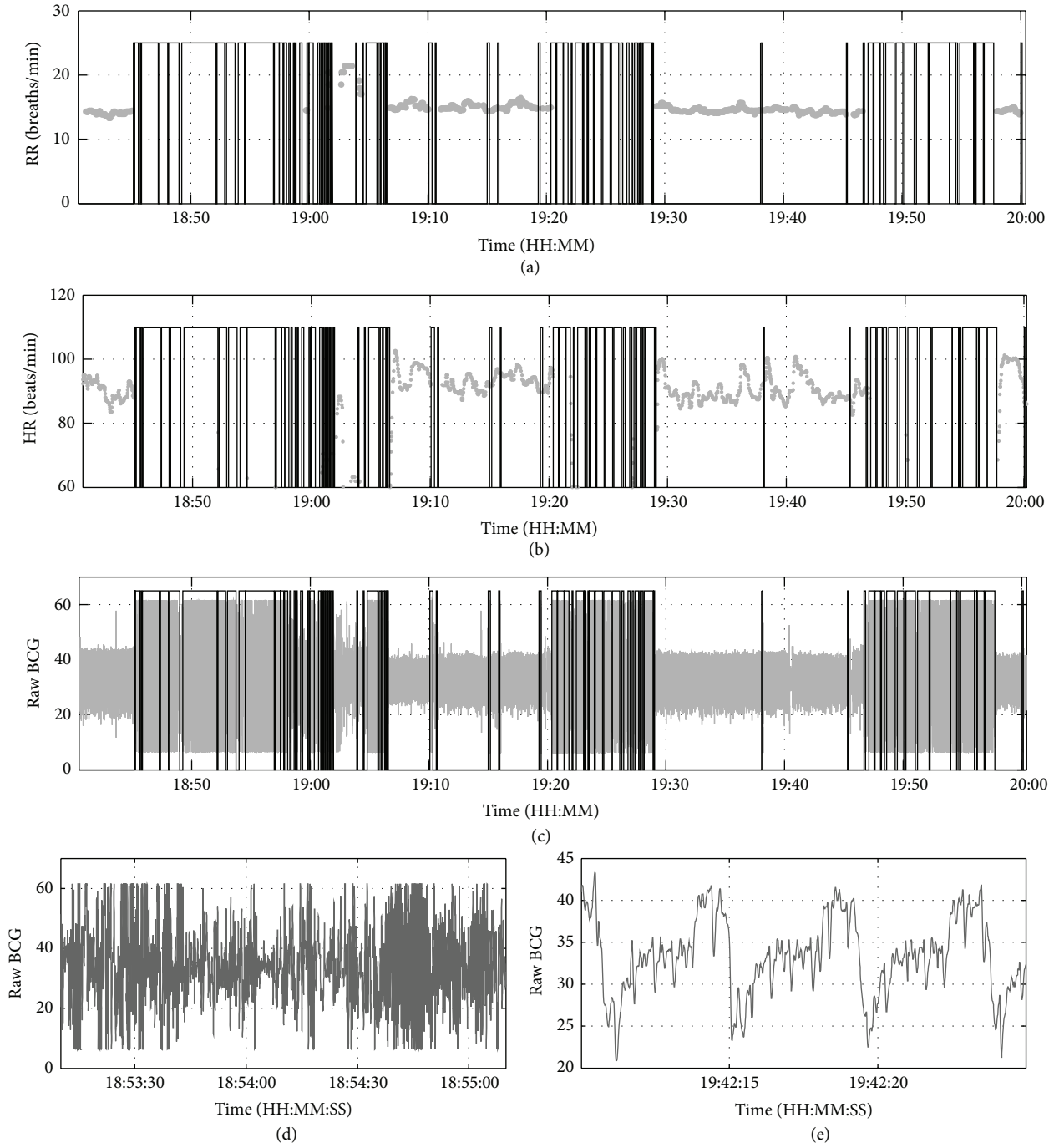

Figure 13: (a) RR and (b) HR series obtained from raw EMFi signals. Rectangular areas mark the zones of (c) BCG signal detected as noise. Vibration during wheelchair driving and subject's movements produces (d) noise signals. When this occurs, the algorithms to calculate HR and RR are stopped. Only during (e) clear BCG signals are vital signs estimated.

from noninvasive sensors, useful parameters are obtained such as wheelchair occupancy, activity level, PRT per day, heart and respiration rate, apneas, and ambient heat index, which are useful to suggest actions that can improve life quality or to provide objective information to clinicians about social engagement and physiological status.

Multiple data sources are combined to determine the status of the subject. During activity periods, as determined by the accelerometer, the HR and RR algorithms are turned off. PRT is validated when both accelerometer and pressure sensors show that pressure relief has been produced. However, advanced methods of data fusion were not included for lack of a better framework to integrate sensor data [37]. For instance, RR is present in both the FSR and the EMFi sensors, but the information is only extracted from EMFi. Also, as proposed in [38], valuable information could be obtained

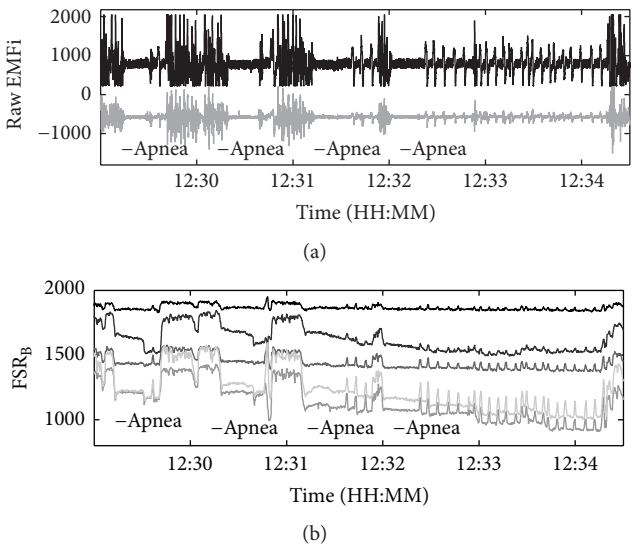

Figure 14: Four consecutive apneas captured by (a) the EMFi and (b) the FSR_B sensors.

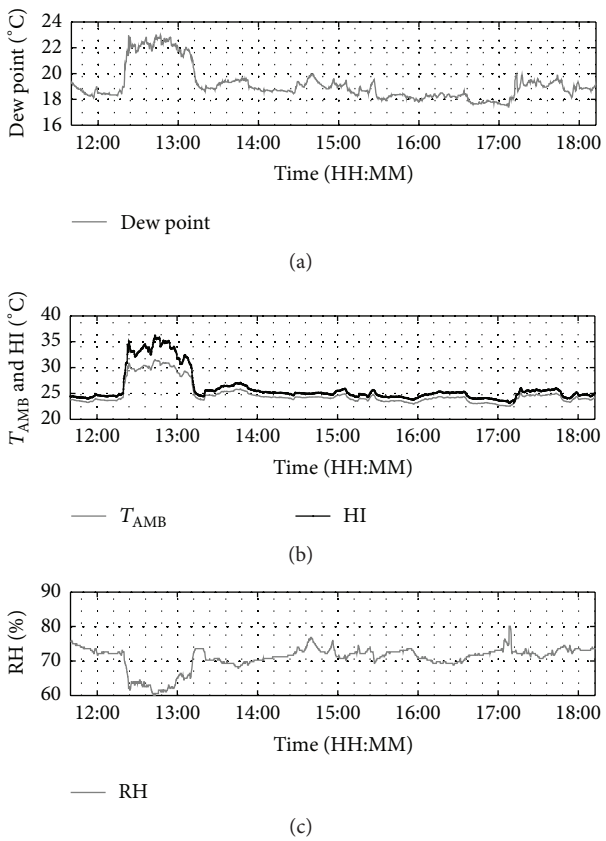

Figure 15: HI and dew point data as a wheelchair user moves outdoors after lunch, in the summer. (a) Calculated dew point, (b) T_{AMB} from the sensor and calculated HI, and (c) RH from the sensor.

from the social interactions between users of the system, as a proxy for mental decline.

The pilot study conducted shows that most of the subjects spent long periods of time on the wheelchair, but they present a low activity level (AI between 10% and 30%) due to their severe disability. However, we also found some participants who spent a short time on it (wheelchair occupancy < 4 hours in 7.7% of the monitored days). This can be explained by the fact that the volunteers recruited for this study are affected by advanced MS, which is characterized by fatigue and/or depression [39]. These symptoms seriously affect the mood and the capacity to perform daily activities which can lead to spending more time in bed. In this case, the usage of this assistive device could be complemented with nursing care and/or assistive devices focused on the time spent in bed.

The results also show that the subjects did not relieve pressure in a proper way using the tilt-in-space system. This result is similar to those presented in [15]. In most cases, the subjects did not comply with the recommendations related to the frequency of pressure relief. They spent long periods (over 3 hours) without performing a PRT. In addition, during the study, there were entire days when the subjects did not perform PRT. If these situations recur frequently and the subjects spend long hours on the chair without relieving pressure, the probability of PU increases.

No pressure changes and tilt absence during long period of time should cause a warning to be sent to caregivers/family member or patient to avoid pressure ulcers. The designed system will allow implementing an alarm system which helps remind the subjects when they should tilt their chair. The collected data shows the feasibility of implementing just-in-time personalized alarms or reminders for PRT with a much better expected outcome than general broadcast reminders or "once in a while" nursing reminders. In this study, the system was deployed for wheelchair users living in a nursing home; however, it can also provide valuable assistance in a home-care environment.

Regarding vital signs, HR and RR were obtained from raw EMFi signals. Although there are periods of time where it is not possible to estimate vital signs due to severe artifacts, the system is able to acquire information that it is not collected normally. Usually caregivers measure vital signs once a day using methods such as taking the pulse on the wrist or counting the patient's breaths. The obtained vital signs are useful to improve patient's care through assessing their vital signs continuously to quickly assist in case of emergency. RR information was also useful for detecting apnea events during the day. This was a particularly interesting finding, because, up to this point, caregivers could only register apnea events through obtrusive and uncomfortable methods such as polysomnography. Also, measuring vital signs allows knowing a patient's normal ranges considering their impaired condition. During the data collection, it was clear that even a simple "noninvasive" pulse oximeter to capture HR can produce discomfort in patients with advanced chronic diseases such as MS. For this reason, it is important to look for alternative ways of measuring vital signs in these patients.

In relation to heat exposure, which is a real concern in assisted living facilities, the collected data show that patients are exposed to high temperatures which can affect their health status. Reminders targeted at the wheelchair user

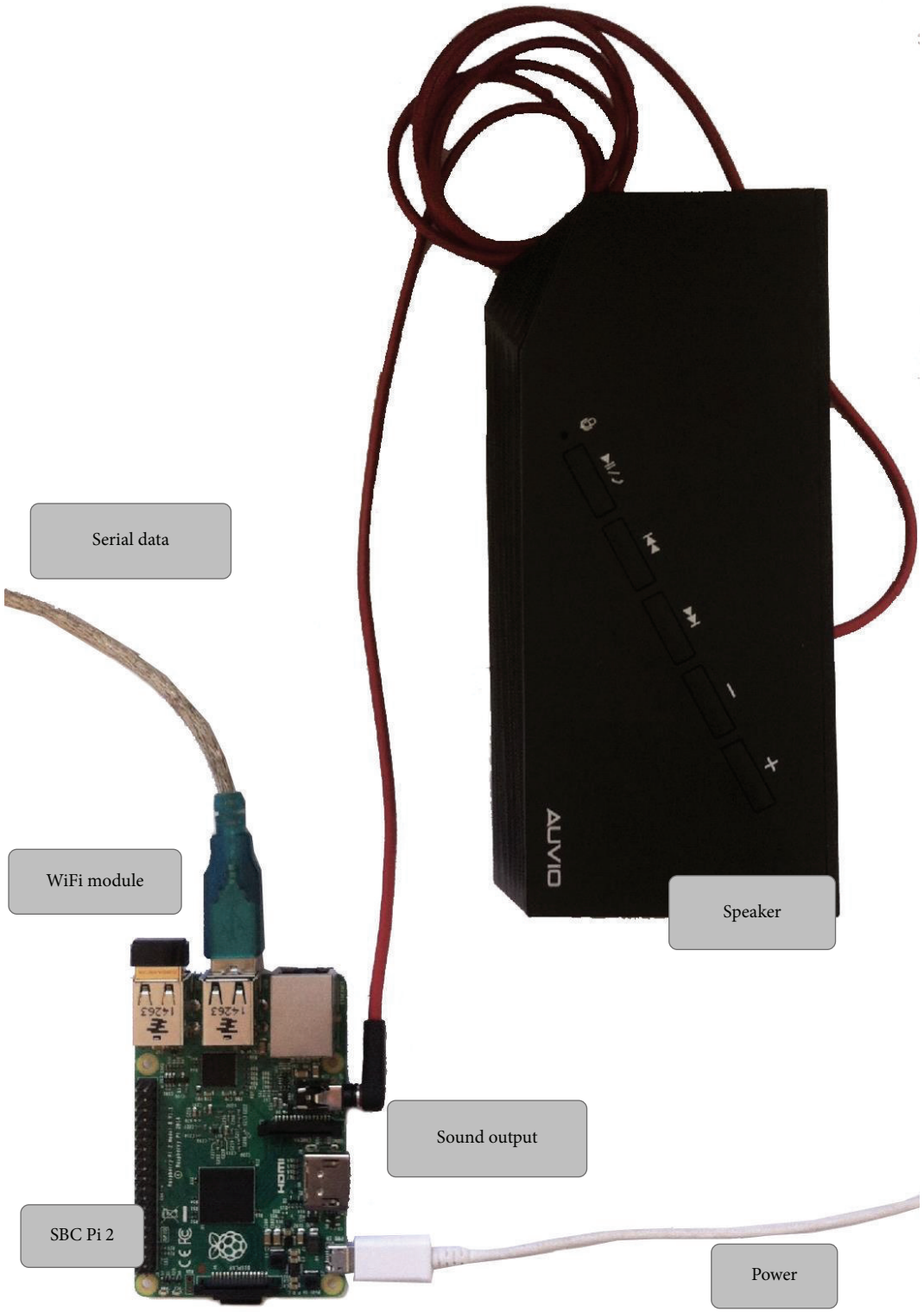

Figure 16: Raspberry Pi 2 board with USB serial data connection, WiFi module, external speaker, and micro USB power source.

and/or caregivers regarding current ambient conditions also contribute to preventing risky exposure and improving care.

All these alarms and reminders were successfully programmed on a Raspberry Pi 2 Model B (900 MHz quad-core ARM Cortex-A7, 1 GB RAM, Raspbian Jessie Linux). This single board computer is powerful enough to replace the netbook used for the original data collection. In the Raspberry Pi 2, a Python program is in control of issuing context-aware recommendations such as "Please, tilt the chair" after a long time in the same position or "You must go

to a cooler place, immediately" when in risk of heatstroke. For medical conditions, such as abnormal heart rate, respiration rate, and apneas, an email is sent to the appropriate caregivers. The system is performing as expected.

7. Conclusion

The proposed system with the selected unobtrusive sensors was able to detect daily activity events in long-term wheelchair users. All sensors were able to provide sufficient ambient and physiological information to provide context-aware recommendations, both to the user and to the caregivers to improve care. The real-time conditions considered to develop a reminder and alarm system from the acquired data are (1) normal condition, (2) pressure relief warning, (3) heatstroke warning, (4) abnormal HR (high or low), and (5) abnormal RR (high or low and apneas).

Conditions (1) and (2) are best communicated directly to the wheelchair user, as voiced recommendations ("Please tilt your wheelchair") or alarms ("Go back to a cooler location") to try to influence or correct behavior. Depending on the situation, they can be escalated as alarms to a caregiver or family member via email notification, SMS messages, or pop-up windows in a nursing station. Medical conditions such as abnormal HR or RR acquired from the BCG data are sent via email to the caregivers as notification in order to avoid unnecessary stress for the patient.

The data collected at the Boston Home show that lack of tilting, adverse ambient conditions, and apnea events do occur; hence, this system would be a useful addition to support daily activities in long-term wheelchair users. In this way, it is expected that the care of these patients will be improved without any discomfort, thus increasing their quality of life.

Competing Interests

The authors declare that there are no competing interests regarding the publication of this paper.

Acknowledgments

Esteban J. Pino would like to thank project Fondecyt Iniciación 11130340 for the financial support. Pablo Aqueveque wants to acknowledge Grant Fondequip EQM150114. The authors also would like to thank Marva Serotkin and Don Fredette from the Boston Home for their continuous support and the former students Dannie Araya, Belén Cavallar, and Javier Chávez for their work on the project.

References

[1] World Health Organization, *Guidelines on the Provision of Manual Wheelchairs in Less Resourced Settings*, World Health Organization, Geneva, Switzerland, 2008.

[2] The CNN Wire Staff, "Possible heat-related deaths reported in 3 states," *The Blade*, 2011.

[3] A. F. Henke, S. D. Cohle, and S. L. Cottingham, "Fatal hyperthermia secondary to sunbathing in a patient with multiple sclerosis," *American Journal of Forensic Medicine and Pathology*, vol. 21, no. 3, pp. 204–206, 2000.

[4] R. E. Kohlmeier, V. J. M. DiMaio, and K. Kagan-Hallet, "Fatal hyperthermia in hot baths in individuals with multiple sclerosis," *American Journal of Forensic Medicine and Pathology*, vol. 21, no. 3, pp. 201–203, 2000.

[5] F. K. Mutluay, H. N. Gürses, and S. Saip, "Effects of multiple sclerosis on respiratory functions," *Clinical Rehabilitation*, vol. 19, no. 4, pp. 426–432, 2005.

[6] J. Myers, M. Lee, and J. Kiratli, "Cardiovascular disease in spinal cord injury: an overview of prevalence, risk, evaluation, and management," *American Journal of Physical Medicine & Rehabilitation*, vol. 86, no. 2, pp. 142–152, 2007.

[7] B. S. Kozniewski and J. L. Cezeaux, "Wheelchair pressure monitoring alert system for the reduction of the occurrence of pressure sores," in *Proceedings of the IEEE 37th Annual Northeast Bioengineering Conference (NEBEC '11)*, pp. 1–2, IEEE, Troy, NY, USA, April 2011.

[8] J. G. Rocha, H. Carvalho, F. M. Duarte, M. A. F. Carvalho, and V. M. Moreira, "System providing discomfort monitoring for people in wheelchairs," in *Proceedings of the IEEE International Symposium on Industrial Electronics*, pp. 961–966, IEEE, Cambridge, Mass, USA, July 2008.

[9] R. Dai, S. E. Sonenblum, and S. Sprigle, "A robust wheelchair pressure relief monitoring system," in *Proceedings of the 34th Annual International Conference of the IEEE Engineering in Medicine and Biology Society (EMBS '12)*, pp. 6107–6110, San Diego, Calif, USA, August 2012.

[10] Y.-S. Yang, G.-L. Chang, M.-J. Hsu, and J.-J. Chang, "Remote monitoring of sitting behaviors for community-dwelling manual wheelchair users with spinal cord injury," *Spinal Cord*, vol. 47, no. 1, pp. 67–71, 2009.

[11] R. P. Rush, "Sensation augmentation to relieve pressure sore formation in wheelchair users," in *Proceedings of the 11th International ACM SIGACCESS Conference on Computers and Accessibility (Assets '09)*, pp. 275–276, ACM, October 2009.

[12] B. E. Dicianno, J. Arva, J. M. Lieberman et al., "RESNA position on the application of tilt, recline, and elevating legrests for wheelchairs," *Assistive Technology: The Official Journal of RESNA*, vol. 21, no. 1, pp. 13–22, 2009.

[13] D. Ding and E. Leister, "Usage of tilt-in-space, recline, and elevation seating functions in natural environment of wheelchair users," *Journal of Rehabilitation Research & Development*, vol. 45, no. 7, pp. 973–983, 2008.

[14] D. Ding, R. A. Cooper, R. Cooper, and A. Kelleher, "Monitoring seat feature usage among wheelchair users," in *Proceedings of the 29th Annual International Conference of the IEEE Engineering in Medicine and Biology Society (EMBC '07)*, pp. 4364–4367, IEEE, Lyon, France, August 2007.

[15] S. E. Sonenblum, S. Sprigle, and C. L. Maurer, "Use of power tilt systems in everyday life," *Disability and Rehabilitation: Assistive Technology*, vol. 4, no. 1, pp. 24–30, 2009.

[16] S. E. Sonenblum and S. Sprigle, "Distinct tilting behaviours with power tilt-in-space systems," *Disability and Rehabilitation: Assistive Technology*, vol. 6, no. 6, pp. 526–535, 2011.

[17] T. D. Yang, S. A. Hutchinson, L. A. Rice, K. L. Watkin, and Y.-K. Jan, "Development of a scalable monitoring system for wheelchair tilt-in-space usage," *International Journal of Physical Medicine & Rehabilitation*, vol. 1, no. 4, article 129, 2013.

[18] D.-K. Han, J.-M. Kim, E.-J. Cha, and T.-S. Lee, "Wheelchair type biomedical system with event-recorder function," in *Proceedings of the 30th Annual International Conference of the IEEE*

Engineering in Medicine and Biology Society (EMBS '08), pp. 1435–1438, IEEE, August 2008.

[19] O. A. Postolache, P. M. B. S. Girao, J. Mendes, E. C. Pinheiro, and G. Postolache, "Physiological parameters measurement based on wheelchair embedded sensors and advanced signal processing," *IEEE Transactions on Instrumentation and Measurement*, vol. 59, no. 10, pp. 2564–2574, 2010.

[20] P. Pancardo, J. A. Pardo, and J. C. Dueñas, "Automatic monitoring for workers healthcare in tropical climates," in *Proceedings of the International Conference on Advanced Information Networking and Applications Workshops (WAINA '09)*, pp. 793–797, Bradford, UK, May 2009.

[21] D. Gun Park, S. Chul Shin, S. Won Kang, and Y. Tae Kim, "Development of flexible self adhesive patch for professional heat stress monitoring service," in *Proceedings of the Annual International Conference of the IEEE Engineering in Medicine and Biology Society*, vol. 4, pp. 3789–3792, 2005.

[22] E. J. Pino, D. E. Arias, P. Aqueveque, P. Melin, and D. W. Curtis, "Wireless pilot monitoring system for extreme race conditions," in *Proceedings of the Annual International Conference of the IEEE Engineering in Medicine and Biology Society*, pp. 5014–5017, San Diego, Calif, USA, August-September 2012.

[23] E. Pino, D. Arias, P. Aqueveque, and D. Curtis, "Assistive devices for healthcare: multiple sclerosis," in *Proceedings of the AMIA Annual Symposium*, p. 1899, Chicago, Ill, USA, November 2012.

[24] E. J. Pino, D. E. Arias, P. Aqueveque, L. Vilugron, D. Hermosilla, and D. W. Curtis, "Monitoring technology for wheelchair users with advanced multiple sclerosis," in *Proceedings of the 35th Annual International Conference of the IEEE Engineering in Medicine and Biology Society (EMBC '13)*, pp. 961–964, Osaka, Japan, July 2013.

[25] D. E. Arias, E. J. Pino, P. Aqueveque, and D. W. Curtis, "Data collection capabilities of a new non-invasive monitoring system for patients with advanced multiple sclerosis," in *Proceedings of the Annual Symposium Proceedings (AMIA '13)*, pp. 61–68, 2013.

[26] D. E. Arias, E. J. Pino, P. Aqueveque, and D. W. Curtis, "Daily activity monitoring for prevention of pressure ulcers in long-term wheelchair users," in *Ambient Intelligence for Health*, pp. 47–58, Springer International, Berlin, Germany, 2015.

[27] D. E. Arias, E. J. Pino, P. Aqueveque, and D. W. Curtis, "Wireless monitoring system for wheelchair users with severe mobility impairment," in *Mobile Health: A Technology Road Map*, vol. 5 of *Springer Series in Bio-/Neuroinformatics*, pp. 195–219, Springer, Berlin, Germany, 2015.

[28] The PostgreSQL Global Development Group, "PostgreSQL database," http://www.postgresql.org.

[29] M. J. Coggrave and L. S. Rose, "A specialist seating assessment clinic: changing pressure relief practice," *Spinal Cord*, vol. 41, no. 12, pp. 692–695, 2003.

[30] L. Chen, T. McKenna, A. Reisner, and J. Reifman, "Algorithms to qualify respiratory data collected during the transport of trauma patients," *Physiological Measurement*, vol. 27, no. 9, pp. 797–816, 2006.

[31] W. Lu, M. M. Nystrom, P. J. Parikh et al., "A semi-automatic method for peak and valley detection in free-breathing respiratory waveforms," *Medical Physics*, vol. 33, no. 10, pp. 3634–3636, 2006.

[32] R. Johnson, "The influence of dew-point temperature on multiple sclerosis symptoms," *Weather*, vol. 60, no. 6, pp. 170–170, 2005.

[33] J. F. Kurtzke, "Rating neurologic impairment in multiple sclerosis: an expanded disability status scale (EDSS)," *Neurology*, vol. 33, no. 11, pp. 1444–1452, 1983.

[34] Consortium for Spinal Cord Medicine, *Pressure Ulcer Prevention and Treatment Following Spinal Cord Injury: A Clinical Practice Guideline for Health-Care Professionals*, Paralyzed Veterans of America, 2000.

[35] R. S. Porter, J. L. Kaplan, and B. P. Homeier, *The Merck Manual Home Health Handbook*, Merck, Rahway, NJ, USA, 2009.

[36] T. Kasai and T. D. Bradley, "Obstructive sleep apnea and heart failure: pathophysiologic and therapeutic implications," *Journal of the American College of Cardiology*, vol. 57, no. 2, pp. 119–127, 2011.

[37] G. Fortino, R. Giannantonio, R. Gravina, P. Kuryloski, and R. Jafari, "Enabling effective programming and flexible management of efficient body sensor network applications," *IEEE Transactions on Human-Machine Systems*, vol. 43, no. 1, pp. 115–133, 2013.

[38] G. Fortino, S. Galzarano, R. Gravina, and W. Li, "A framework for collaborative computing and multi-sensor data fusion in body sensor networks," *Information Fusion*, vol. 22, pp. 50–70, 2015.

[39] V. Janardhan and R. Bakshi, "Quality of life in patients with multiple sclerosis: the impact of fatigue and depression," *Journal of the Neurological Sciences*, vol. 205, no. 1, pp. 51–58, 2002.

Hindawi Publishing Corporation
Mobile Information Systems
Volume 2016, Article ID 2369103, 15 pages
http://dx.doi.org/10.1155/2016/2369103

Research Article

Method for Improving Indoor Positioning Accuracy Using Extended Kalman Filter

Seoung-Hyeon Lee,[1] Il-Kwan Lim,[2] and Jae-Kwang Lee[2]

[1]*Cyber-Physical System Security Research Section, Electronics and Telecommunications Research Institute, 218 Gajeong-ro, Yuseoung-gu, Daejeon 34129, Republic of Korea*
[2]*Department of Computer Engineering, College of Engineering, Hannam University, 70 Hannam-ro, Daedeok-gu, Daejeon 34430, Republic of Korea*

Correspondence should be addressed to Jae-Kwang Lee; jklee@hnu.kr

Received 4 March 2016; Revised 24 May 2016; Accepted 14 June 2016

Academic Editor: Sergio F. Ochoa

Beacons using bluetooth low-energy (BLE) technology have emerged as a new paradigm of indoor positioning service (IPS) because of their advantages such as low power consumption, miniaturization, wide signal range, and low cost. However, the beacon performance is poor in terms of the indoor positioning accuracy because of noise, motion, and fading, all of which are characteristics of a bluetooth signal and depend on the installation location. Therefore, it is necessary to improve the accuracy of beacon-based indoor positioning technology by fusing it with existing indoor positioning technology, which uses Wi-Fi, ZigBee, and so forth. This study proposes a beacon-based indoor positioning method using an extended Kalman filter that recursively processes input data including noise. After defining the movement of a smartphone on a flat two-dimensional surface, it was assumed that the beacon signal is nonlinear. Then, the standard deviation and properties of the beacon signal were analyzed. According to the analysis results, an extended Kalman filter was designed and the accuracy of the smartphone's indoor position was analyzed through simulations and tests. The proposed technique achieved good indoor positioning accuracy, with errors of 0.26 m and 0.28 m from the average x- and y-coordinates, respectively, based solely on the beacon signal.

1. Introduction

Location determination technology in smartphones equipped with global positioning system (GPS) and Wi-Fi has not only triggered a shift in the paradigm of location-based services (LBS) but also contributed significantly toward the further development of such services, including navigation and logistics [1, 2]. IPS are systems that can provide all types of LBS—usually provided outdoors—in an indoor area. It is important for IPS to map a user's indoor positioning information on indoor maps in order to provide the services required by the user. Indoor positioning techniques previously adopted by IPS include the K-nearest neighbor, Bayesian, and triangulation methods, which are based on wireless technologies such as Wi-Fi, radio frequency identification (RFID), and ZigBee [3–6]. Recent studies have focused on an ultrawideband-based indoor positioning technology [7, 8].

In recent years, beacons have not only contributed toward the growth of mobile LBS but also emerged as a new paradigm of IPS. Beacons are BLE-based short-distance communication technologies. Their advantages include low power consumption, miniaturization, wide signal range, and low cost. Moreover, when communicating with devices as far away as 70 m, the accuracy of BLE is sufficiently high for distinguishing each device with a resolution of 5–10 cm [9–11].

In 2013, Apple introduced iBeacon™, and in the following year, iBeacon began to be implemented in areas where various types of information could be provided on the basis of user position, such as information regarding restaurants, airports, art galleries, and other indoor areas. Figure 1 shows an example of a service using iBeacon [12]. An iBeacon transmitter is installed at a specific location within a store; although it does not attempt to guide customers to a specific location, it provides them with an automated

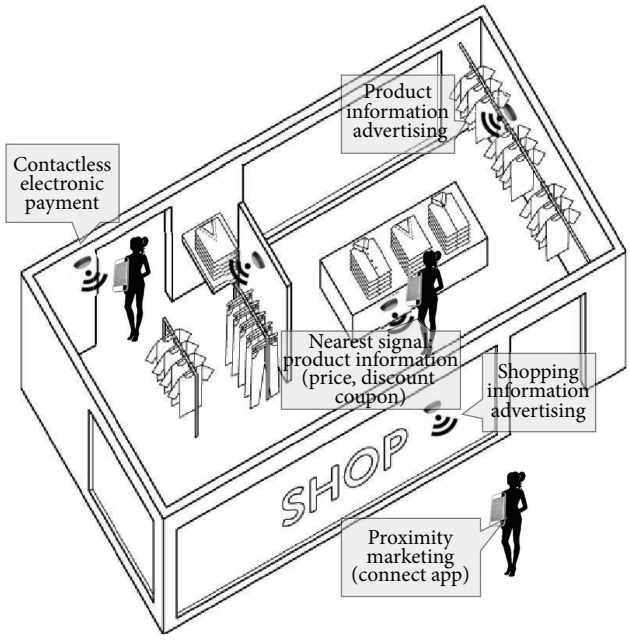

Figure 1: Service case with iBeacon.

shopping service by determining their positions throughout the shopping process. This extends from the moment they enter the store to when they request for information about a product (including price) and eventually pay for the product.

As shown in Figure 1, the iBeacon transmitter periodically broadcasts advertising packets, including the device identification (ID), area ID, and signal strength, and each smartphone that receives this information calculates the distance based on the location at which the iBeacon transmitter is installed and the signal strength. Then, the position of the smartphone is located through either control point positioning or multilateral positioning, thus providing the customer with the necessary service and information.

Although the BLE-based iBeacon has many advantages, its performance is poor in terms of the indoor positioning accuracy of a smartphone, and it is difficult to estimate the distance accurately using only the strength of the signal transmitted from the iBeacon transmitter to the smartphone. These issues are attributable to noise, movement, and fading [13, 14], all of which are characteristic of a bluetooth signal and depend on the installation location. Therefore, although it is possible to achieve indoor positioning depending solely on the iBeacon signal, the indoor positioning accuracy needs to be improved by fusing the iBeacon approach with another indoor positioning approach based on technologies such as Wi-Fi. However, this would require multiple sensors with different models to be installed in an indoor space, which would introduce additional issues such as higher costs associated with initial construction and maintenance.

Accordingly, this study proposes a technique for improving the indoor positioning accuracy of smartphones using only the iBeacon signal. Because the beacon is installed in an open space, the movement of a smartphone indoors is defined as movement on a flat two-dimensional surface. In addition, because the beacon's received signal strength indicator- (RSSI-) based distance measurement and the smartphone's location on the two-dimensional surface have a nonlinear relationship, an extended Kalman filter is used. Once the standard deviation and properties of the beacon signal are analyzed, the extended Kalman filter is designed on the basis of this analysis. Finally, the indoor positioning accuracy of the smartphone is analyzed by performing simulations and tests.

The remainder of this study is organized as follows. Section 2 briefly reviews previous studies on iBeacon and the extended Kalman filter, which are applied to the technique proposed herein. Section 3 explains the design and implementation of the extended Kalman filter, which improves the iBeacon-based indoor positioning accuracy. In addition, the components of the indoor positioning system and the testing environment are described. Section 4 presents and discusses the results of both the iBeacon signal analysis and the indoor positioning test. Finally, Section 5 states our conclusions and briefly explores the scope for future work.

2. Related Work

2.1. iBeacon. Having introduced the BLE-based iBeacon in June 2013, Apple subsequently launched a variety of services that use iBeacon. BLE, which was introduced in June 2010, is equipped with low-energy technology and is commonly referred to as bluetooth smart. BLE minimizes the time spent sending/receiving data by reducing the duty cycle to several milliseconds, and it maximizes the sleep mode to reduce power consumption [10]. Because iBeacon is based on a standard BLE technology, it can be supported by any device. Therefore, it is extendible even to a non-iOS device as long as the device is compliant with the standard specifications [15].

iBeacon periodically broadcasts only a few signals, including the universally unique identifier (UUID), major value, minor value, and transmissions (TX) power, to identify the beacon and calculate the distance, as shown in Figure 2. Thus, all indoor LBS are processed on smartphones and service servers.

In the case of the Estimote Beacon (Estimote Beacons are small wireless sensors based on BLE; they broadcast tiny radio signals that can be received and interpreted by smartphones, thereby facilitating microlocation and contextual awareness; Estimote Beacons are tiny computers, each having a powerful Advanced RISC Machine (ARM) processor, memory, and bluetooth smart module; Estimote Beacons are certified to be compatible with iBeacon), which supports iBeacon, the signal transmission cycle and output can be easily modified using a specialized tool. Changing the signal transmission cycle and output will alter the distance measured between the iBeacon transmitter and the smartphone [16]. However, modifying the signal output does not guarantee improved accuracy of the measured distance. Therefore, the measurement derived from the iBeacon signal has to be interpreted differently depending on the distance, as summarized in Table 1 [15].

Nevertheless, the definitions stated in Table 1 do not mean that the distance cannot be directly measured using iBeacon. In fact, it means that, in the case of distances estimated using

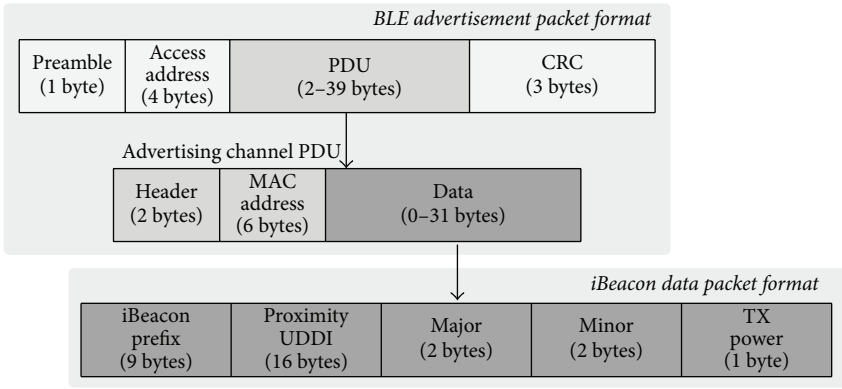

Figure 2: iBeacon packet format.

Table 1: Four proximity states of iBeacon.

Glossary	Description
Accuracy	A distance value in terms of meters
Proximity state (estimates of the distance between the iBeacon transmitter and the smartphone that appears in the CLBeacon class)	(i) *Immediate*: distance between 0 and 1 m; high reliability. (ii) *Near*: distance between 1 and 3 m; trusted distance. (iii) *Far*: distance greater than 3 m. The measured distance is not the actual distance to the iBeacon transmitter. (iv) *Unknown*: iBeacon signal is not received. *Measurement reference value*: the RSSI values (−59 dBm) received at a distance of 1 m.

iBeacon, a relative revision should be considered from the perspective of accuracy.

2.2. Extended Kalman Filter. In 1960, Kalman proposed the Kalman filter as a recursive filter for determining the random values of linear and nonlinear systems containing noise [17]. Using its algorithm to track/predict and thus revise the past, present, and future states, the Kalman filter can plot a system's trajectory, making it suitable for application to model systems such as radars, which anticipate and estimate the next state [18–21].

Figure 3(a) shows the basic algorithm of the Kalman filter, which takes a measurement value (Z_k) as input and outputs a priori state estimate ($\widehat{x}_k$) of the next state. It is a repetition of prediction and correction processes [22].

(i) The prediction process inputs a former a posteriori state estimate ($\widehat{x}_{k-1}$) and a posteriori error covariance (P_{k-1}), calculating a posteriori state estimate and a priori estimate error covariance ($\widehat{x}_{\overline{k}}$, $P_{\overline{k}}$) as the end result. These values are used in the correction process. The system model variables used in the prediction process are the state transition matrix (A) and the process noise covariance (Q).

(ii) The output of the correction process is a posteriori state estimate ($\widehat{x}_k$) and a posteriori estimate error covariance (P_k). The values used for the input are not only the a posteriori state estimate and the a priori estimate error covariance ($\widehat{x}_{\overline{k}}$, $P_{\overline{k}}$) from the prediction process but also the measurement (Z_k). The system model variables used in the correction process are the measurement prediction matrix (H) and the measurement error covariance matrix (R).

The Kalman filter allows accurate forecasting by using the measured value of the current state as well as the value reflecting the prediction from the current state. It is fundamentally based on a linear system. Hence, when it is applied to a nonlinear system, a section of the whole is linearized before the algorithm is applied, rendering it problematic, as a meaningful result can only be drawn from the property of the designated section and not the whole.

An extended Kalman filter allows the nonlinear relationship between the state value and the dynamic model or the measurement model in the Kalman filter to be linearized and used with respect to the nominal point [23, 24]. It is used as a de facto standard in navigation, GPS, and other nonlinear state estimations [25]. The Kalman filter has a measurement model and a dynamic model, whereas the extended Kalman filter shapes either model or both models into a nonlinear model.

Figure 3(b) shows the basic algorithm of the extended Kalman filter, which is a repetition of the prediction and correction processes, as with the Kalman filter. However, it differs from the Kalman filter in that the state value of x_k does not use the coefficient separately but uses the nonlinear dynamic model or measurement model as it is, such as $x_{k+1} = f(x_k) + w_k$ or $z_k = h(x_k) + v_k$ [22].

3. Design and Implementation of Extended Kalman Filter

3.1. Design. This study employs an iBeacon transmitter as a control point for measuring the indoor position of a smartphone. Because the BLE technology applied to iBeacon can only be used in an open space owing to the nature of radio

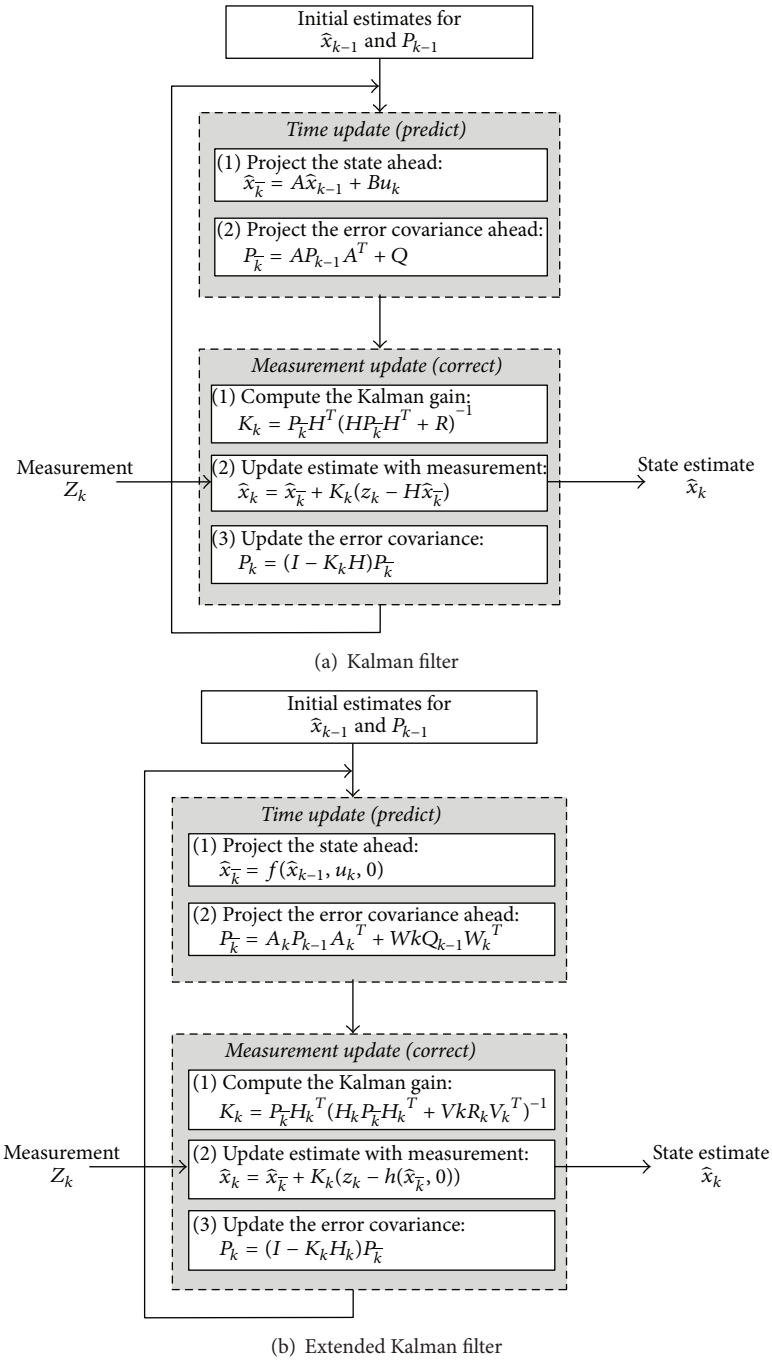

Figure 3: Comparison between Kalman filter and extended Kalman filter (the state transition matrix (A) has the following differences: (a) it is not a Jacobian matrix with a linear property; (b) its value is defined in accordance with a Jacobian matrix having nonlinear properties).

signals, separate iBeacon transmitters have to be installed per floor and per space. Therefore, when setting a space map using the iBeacon transmitters, registration/management has to be performed according to the iBeacon ID value per floor and per space.

As discussed later (Section 4.1), iBeacon signals undergo fading. Therefore, the accuracy is low when measuring the distance using only RSSI measurements. In order to improve the distance measurement accuracy, sampling must be performed to eliminate the iBeacon signal noise. A smartphone requires a sampling time of 20 s.

The Kalman filter processes the input data including noise recursively. Further, it provides higher accuracy because it is based on a series of measurements observed over time rather than a single measurement alone, thereby facilitating statistical prediction of the current state. The Kalman filter can estimate the current state from the previous state using the linear property. However, if the signal is nonlinear, as in

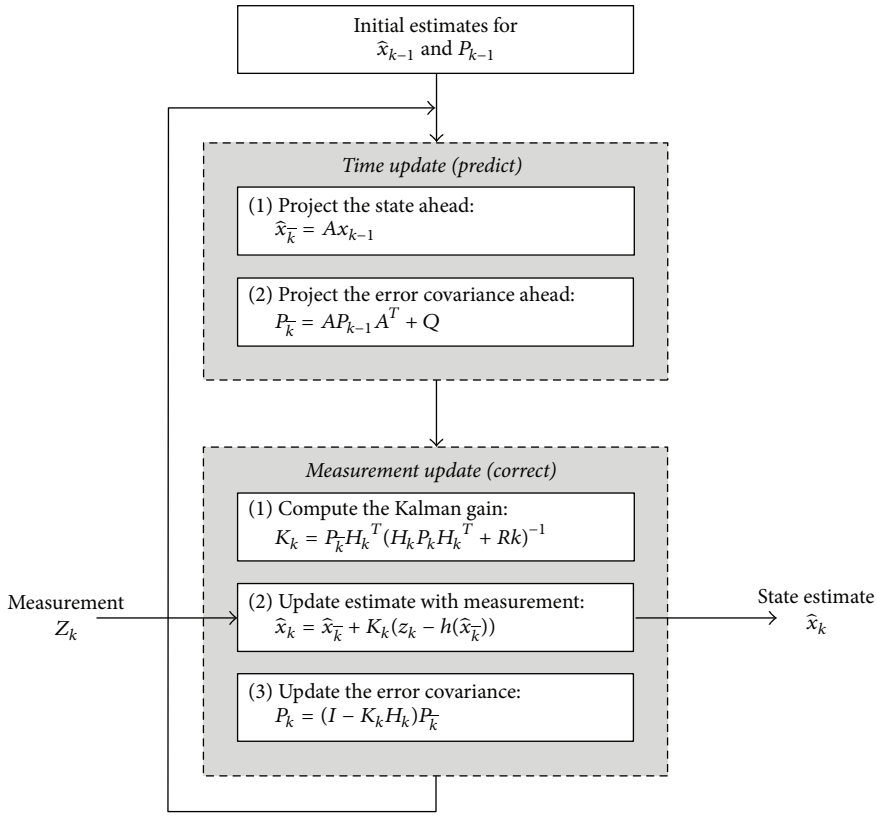

Figure 4: Design of extended Kalman filter.

the case of iBeacon signal analysis, the Kalman filter cannot be applied. In this study, considering the nonlinear property of iBeacon signals, the extended Kalman filter is employed.

In this study, the extended Kalman filter is designed as follows:

(i) In the measurement model, iBeacon's RSSI-based distance measurement shares a nonlinear relationship with the state value of the smartphone position.

(ii) In the dynamic model, movements of the smartphone position have the appearance of a uniform motion-based linear motion model.

In the measurement model, the RSSI value of the iBeacon signal is assumed to be a measurement (Z), and this is used when calculating the distance. When the distance is determined using the RSSI value, the decrease in the reception rate per distance can be inconsistent; hence, the nature of the measurement (Z) is deemed nonlinear. The dynamic model is primarily used when calculating the trajectory of missiles, artificial satellites, and so forth. Factors that cause changes in x_k include the location, velocity, and acceleration, and the resistance it faces varies according to the object's shape and altitude, meaning that there is a quality of dynamic change. The component of the existing algorithm of the Kalman filter that considers the dynamic quality is the weight (W).

The extended Kalman filter designed for this study assumes that smartphones move linearly on a flat surface without changes in height; therefore, the dynamic quality is equivalent to the characteristic of an object moving on a two-dimensional surface.

Figure 4 shows the algorithm of the extended Kalman filter that was newly designed to reflect the characteristics of the iBeacon signal as well as the smartphone's movement described above.

3.2. Implementation. The indoor positioning function of a smartphone using the newly designed extended Kalman filter based on iBeacon (Section 3.1) is shown in Figure 5.

(1) The smartphone calculates the distance between the iBeacon transmitter and itself on the basis of the RSSI of the received iBeacon signal. It sets the RSSI value received from 1 m away as the standard of measurement (−59 dBm).

(2) The data structure containing the identifier of the iBeacon signal and the calculated distance are transmitted to the IPS module via Wi-Fi (or cellular network).

(3) The IPS module extracts the base station (BS) coordinates (x-y) allotted to each iBeacon transmitter and creates an input structure of the extended Kalman filter using the coordinates and distance; "age" is the total number of iBeacon signals found on the smartphone.

(4) The location based on the nonlinear distance is calculated by repeatedly performing the initialization,

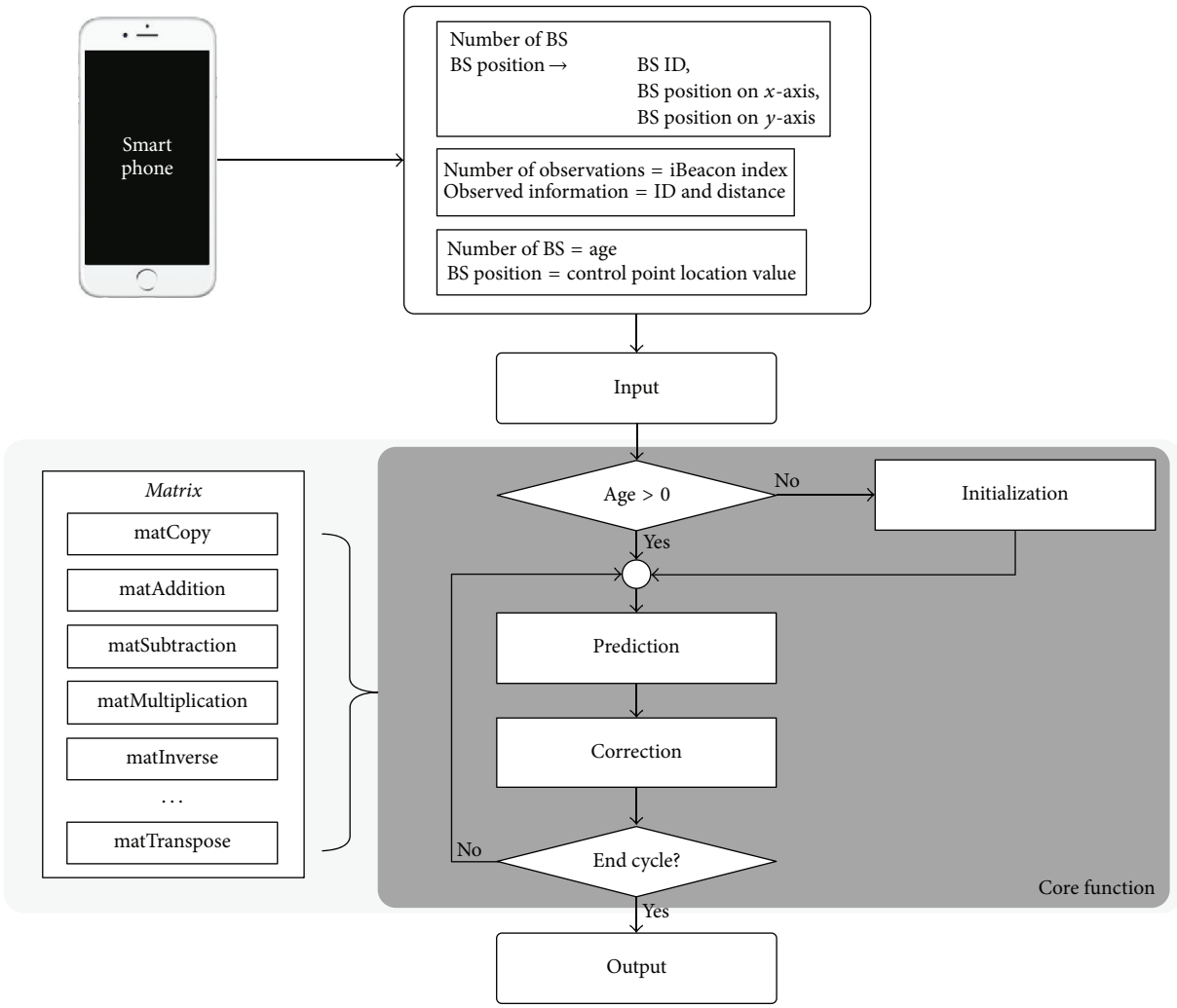

Figure 5: Logic configured for the implementation of the extended Kalman filter.

prediction, and correction processes. The matrix function is a two-dimensional covariance matrix.

Figure 6 shows the detailed flow of the initialization, prediction, and correction processes of the "Core Function" in Figure 5.

(1) *Initialization*. The BS value is received by the smartphone and the "age" is confirmed. The initialization process is conducted when the number of recursions is zero. The initialization process involves calculating the x and y values using the extracted BS value, and it initializes the a priori state estimate value. Once this process is completed, the number of recursions increases and the variable value is delivered for the next process.

(2) *Prediction*. Once the initial value of the initialization process or the a priori state estimate value based on the recursion result of the extended Kalman filter is provided as input, the local value is initialized to estimate the a posteriori state estimate value. In addition, the time and a posteriori state estimate value are computed with a fixed process noise covariance. The state transition matrix is set as noise for the covariance matrix. Then, a posteriori state estimate is extracted by calculating the state error covariance, and it is delivered to the correction process.

(3) *Correction*. The local value is initialized, the BS value is extracted, and the state vector is transmitted. Then, the measurement prediction matrix and residual value are calculated. Subsequently, the Kalman gain is computed and the state vector correction and transmission value are estimated. Next, the correct value and error covariance are calculated, which concludes the correction process, after which the "age" value is increased.

(4) Steps (2) and (3) are repeated until smartphone location tracking is completed.

3.3. Configuration of Base Station and Indoor Positioning System. Figure 7 shows a smartphone location tracking

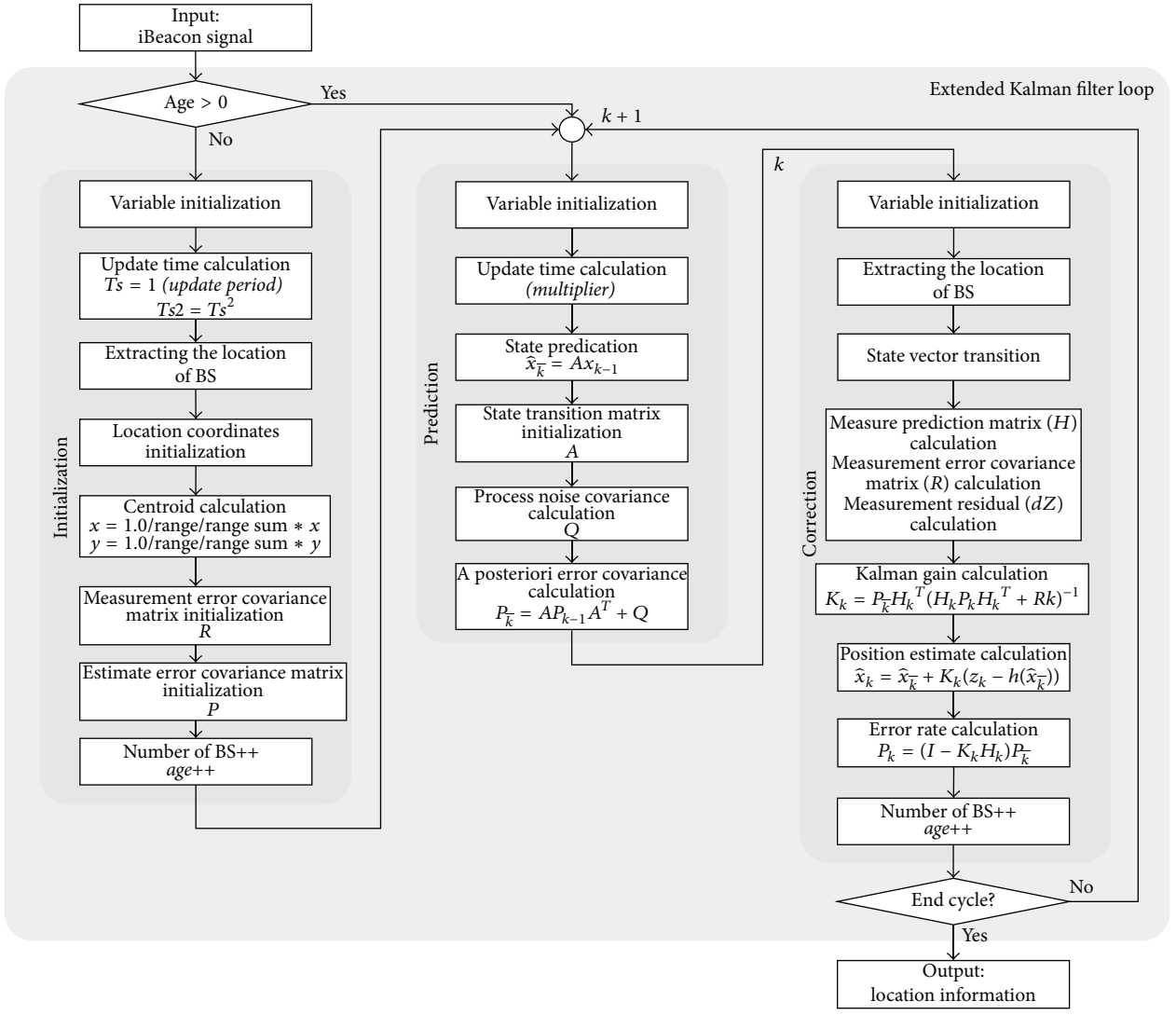

Figure 6: Smartphone positioning process using extended Kalman filter.

system that uses iBeacon. It consists of a smartphone that estimates and transmits the distance between the BS and itself on the basis of the RSSI from the compiled iBeacon signals and a server system that calculates the smartphone's location on the basis of the BS coordinates and estimated distance. This system was developed in an environment described in Table 2.

iBeacon's maximum transmission distance is defined as 90 m and the standard transmission cycle is defined as 100 ms. However, the cycle can be programmed to operate slower, that is, at 900 ms. The Estimote Beacon, which was used in this study, has a transmission cycle of 200 ms and a maximum transmission distance of 70 m. Figure 8 shows the configuration of a BS using Estimote Beacons. Each grid is 0.5 m long and six iBeacons are installed.

The BS was configured on the basis of the signal property (see Section 4.1). The iBeacons were defined to be located within 5 m according to the distance standard deviation of the iBeacon signals received at the smartphone.

4. Analysis

4.1. Signal Property. In this study, we analyzed the signal property of the iBeacon's measured distance, which was used in experiments before we performed the indoor positioning of smartphones using the extended Kalman filter. The distance was estimated using the RSSI value included in the iBeacon signal. The reference points for the measured distance were 1 m, 3 m, and 5 m; each was measured 1,500 times, after which their standard deviation and average were calculated. Allowing for the signal's path loss, the distance measurement using the iBeacon RSSI can be calculated as follows:

$$\mathrm{PL} = P_{\mathrm{TX}} - P_{\mathrm{RX}}, \tag{1}$$

$$\mathrm{PL}(d) = \mathrm{PL}(d_0) + 10 \cdot n \cdot \log_{10}\left(\frac{d}{d_0}\right) + X_g, \tag{2}$$

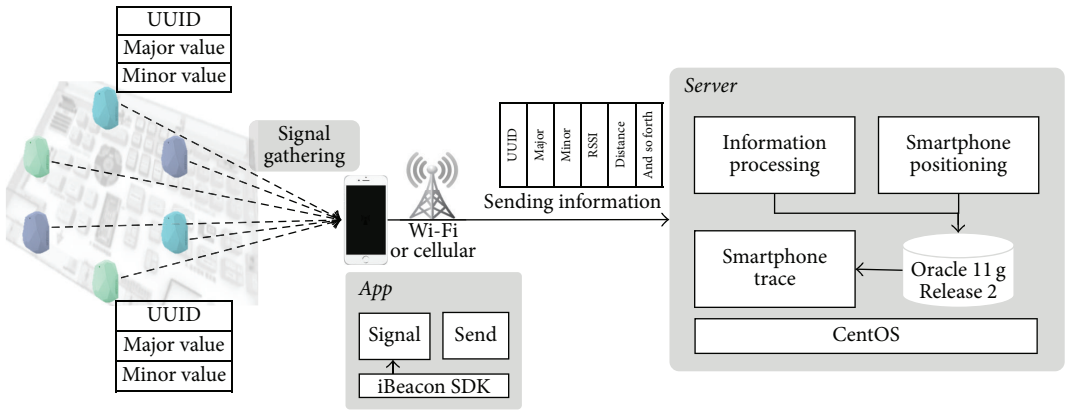

Figure 7: Configuration of smartphone indoor positioning system based on iBeacon.

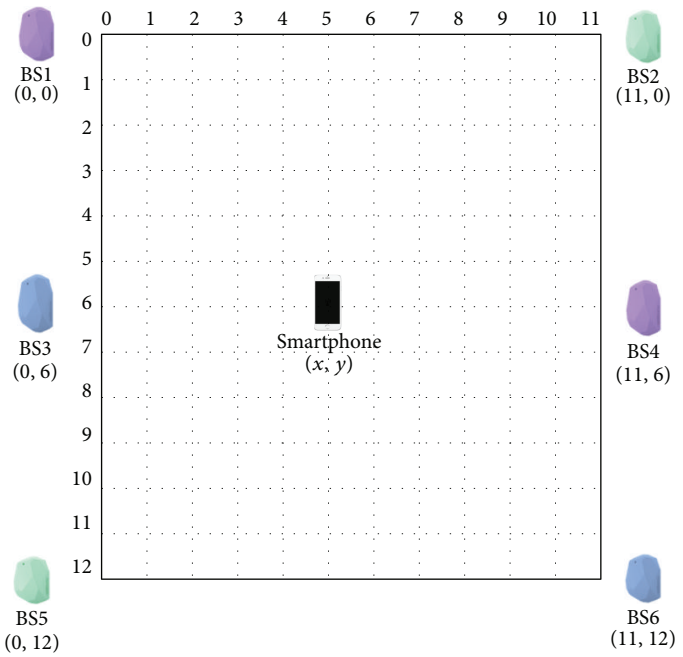

Figure 8: Configuration of BS. iBeacon Specification [26]: (i) Model: Estimote model REV.D3.4 Radio Beacon. (ii) CPU: 32-bit ARM® Cortex-M0. (iii) Frequency range: 2400–2483.5 MHz. (iv) TX-receptions (RX) channel separation: 2 MHz. (v) Sensitivity: −93 dBm. (vi) Range: up to 70 m. (vii) Upgrade: over-the-air firmware and security upgrades.

Table 2: Development environment.

Division	Item	Specifications
iBeacon	Estimote Beacon ×6	ARM Cortex-M0, BLE, motion and temperature sensors
Smartphone	H/W	iPhone 5S
App development platform	OS	OS X version 10.10.5 (Yosemite)
	Tool	Xcode version 7.1.1
	Language	Objective-C
	H/W	MacBook Pro, 3.1 GHz Intel Core i7, 16 GB DDR3 RAM
Server	OS	CentOS release 6.5 (Final)
	Kernel	64 bit
	Language	C, XML
	DB	Oracle Database Express Edition 11g Release 2

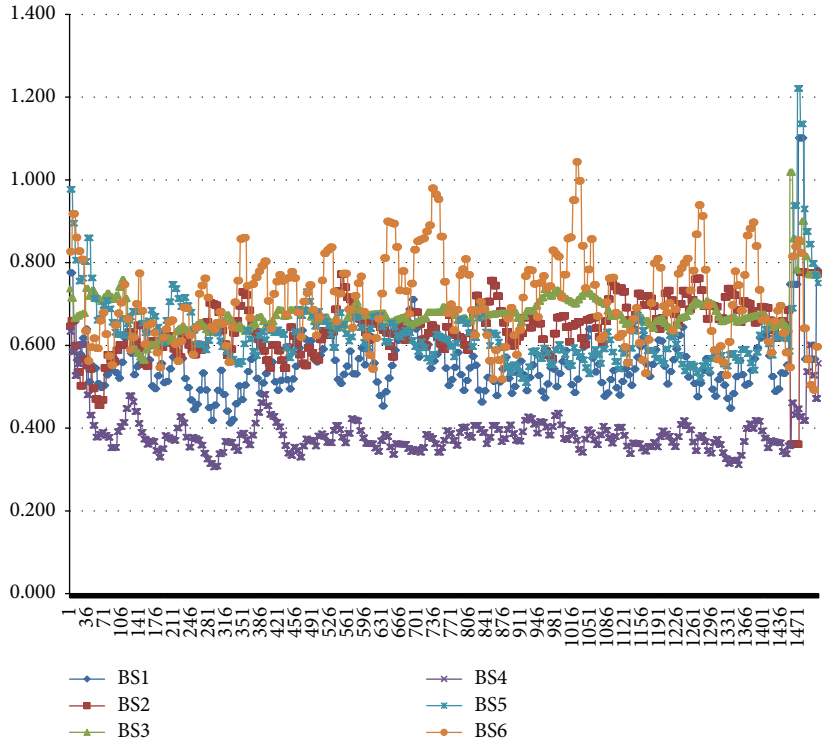

Figure 9: Signal property at 1 m.

$$P_{RX}(d) = P_{RX}(d_0) - 10 \cdot n \cdot \log_{10}\left(\frac{d}{d_0}\right), \quad \text{(derived from (2))}, \tag{3}$$

$$d = d_0 \cdot 10^{(P_{RX}(d_0) - P_{RX}(d))/10n}, \quad \text{(derived from (3))}, \tag{4}$$

where PL is total path loss, P_{TX}/P_{RX} are transmitted and received signal strength, respectively, d is measured distance, d_0 is standard distance (define: 1 m), X_g is standard deviation (define: 0), and n is path loss exponent.

After substituting $P_{RX}(d_0)$ with −59 dBm, the signal strength for the 1 m reference point described in the iBeacon development document, (1), (2), (3), and (4) were used to calculate the relative distance measurement per RSSI signal strength.

Figure 9 shows measurements of the distance to the iBeacon transmitter from a distance of 1 m. The average of the six measurements to the iBeacon transmitter was 0.6 m, which had an error of 0.34 m. Figure 10 shows measurements of the distance to the iBeacon transmitter from a distance of 3 m. The average of the six measurements to the iBeacon transmitter was 1.39 m, which had an error of 1.61 m. Figure 11 shows measurements of the distance to the iBeacon transmitter from a distance of 5 m. The average of the six measurements to the iBeacon transmitter was 2.21 m, which had an error of 2.79 m.

Thus, the distance measurements from the 1 m, 3 m, and 5 m points resulted in errors of 0.34–2.79 m from the real distance. Based on this result, it can be confirmed that while it is possible to measure the distance using only the iBeacon's RSSI value, an error would exist between the real and calculated distances. This is due to a number of factors that cause changes in the received RSSI value, such as the battery life, experiment environment, space configuration, human movement, and smartphone location and direction.

Figure 12 shows the average measurement per unit distance. The average was calculated using the distance measured on the basis of the RSSI value determined from distances of 1 m, 2 m, 3 m, 5 m, and 10 m. Figure 13 shows the standard deviation of the measurements per distance. The distance was measured using 1 m, 2 m, 3 m, 5 m, and 10 m as reference points to verify the accuracy of the "immediate," "near," and "far" distances defined in the iBeacon development document. As can be seen, the deviation was not high when the measurement was taken from distances of 1 m and 2 m, but it increased for distances of 3 m and 5 m and increased further for 10 m.

4.2. Indoor Positioning Using Extended Kalman Filter. From the analysis of the iBeacon's signal property (Section 4.1), we confirmed that there were irregularities and variations in the measurements of the iBeacon RSSI according to the distance and the beacon. Because a single distance measurement using the iBeacon RSSI is not reliable, it is necessary to create a measurement noise model for application to an extended Kalman filter based on the result of the signal property analysis. Table 3 lists the inclination per section of the standard deviation shown in Figure 13.

As can be seen in Table 3, BS6 is not a reliable measurement because of the irregular change in the deviation per

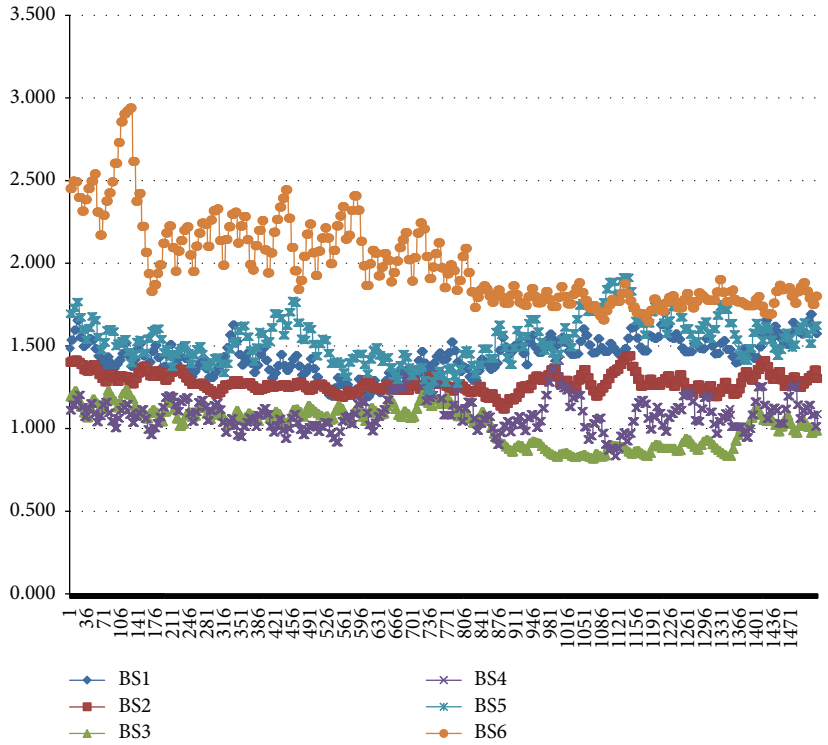

Figure 10: Signal property at 3 m.

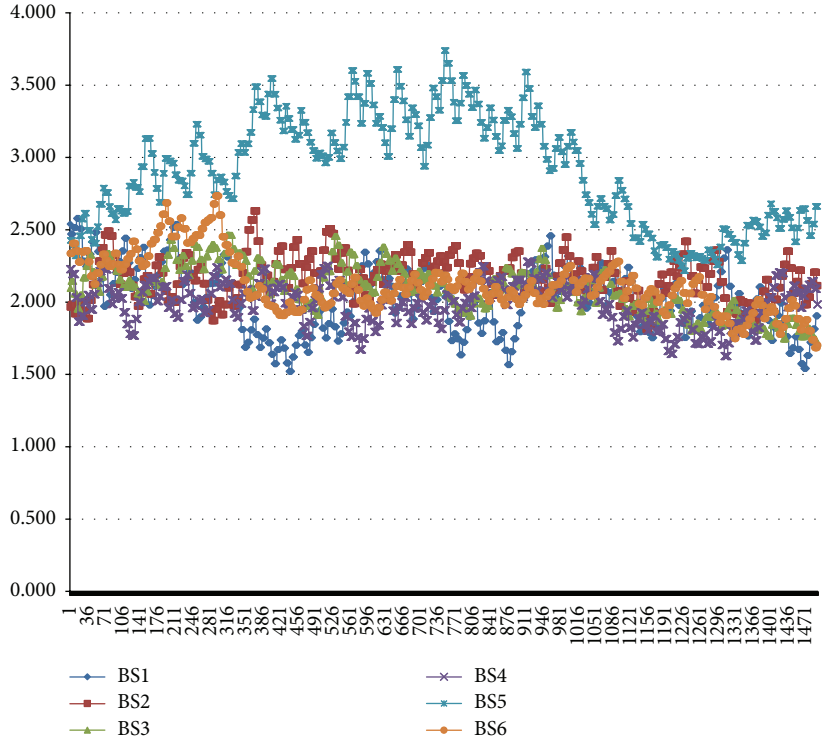

Figure 11: Signal property at 5 m.

Table 3: Distance standard deviation of iBeacon.

Section	BS1	BS2	BS3	BS4	BS5	BS6
1 m-2 m standard deviation	0.02	0.05	0.02	0.1	0.05	−0.05
2 m-3 m standard deviation	0.01	−0.06	0.05	−0.05	0	0.2
3 m–5 m standard deviation	0.12	0.1	0.06	0.04	0.24	−0.07
5 m–10 m standard deviation	0.23	0.36	0.37	0.34	0.01	0.06
Standard deviation	0.09	0.11	0.12	0.11	0.08	0.04
1 m–5 m standard deviation	0.05	0.03	0.04	0.03	0.1	0.03

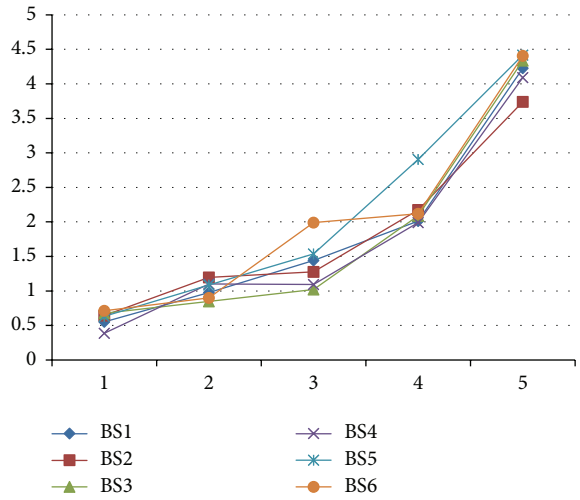

Figure 12: Average measurement chart.

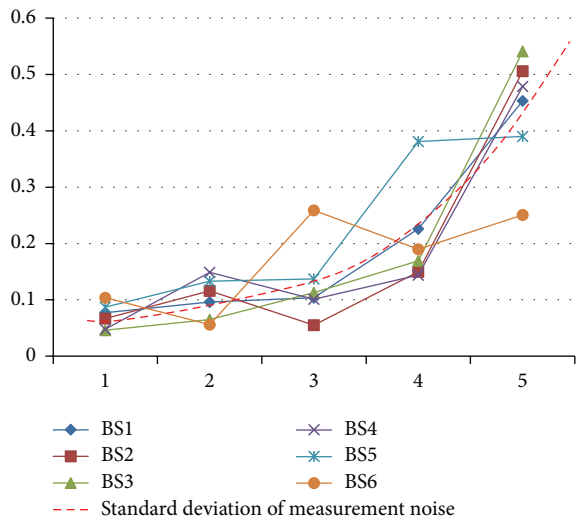

Figure 13: Standard deviation chart.

section. The deviations of the other iBeacon RSSIs besides BS6 increased sharply in the section between 5 m and 10 m. Therefore, in this study, the measurement noise model was defined as follows, by reflecting the property of the iBeacon RSSI to apply the model to the algorithm of the extended Kalman filter:

$$\sigma_d = k^2 d, \quad k = 0.2, \quad \text{(derived from Table 3)}. \tag{5}$$

The system variables of the extended Kalman filter using the results presented above can be defined as follows:

(i) Q Value (standard deviation of process noise): it is standard deviation of the motion model errors. In this study, a scale factor of 1.0 was applied.

Define

$$Q = 1.0. \tag{6}$$

(ii) R Value (standard deviation of measurement noise): it is standard deviation of the measurement model errors. In this study, the value was derived from (5).

Define

$$R = \begin{pmatrix} \sigma_1 & & 0 \\ & \ddots & \\ 0 & & \sigma_m \end{pmatrix} \tag{7}$$

Next, we discuss the analysis result of the smartphone coordinates measured in an experiment environment using the extended Kalman filter, which reflects the analysis of the iBeacon's signal property.

Table 4 lists the values of the iBeacon signal that was measured 1,000 times at the x- and y-coordinates $(2, 5)$. Table 5 and Figure 14 specify the indoor positioning value applied with the extended Kalman filter. The average values of the x- and y-coordinates were 2.05 and 5.3, that is, errors of 0.05 and 0.3 from the actual coordinates, and the standard deviations were 0.16 and 0.13, respectively. Because of the nature of the extended Kalman filter, where the accuracy improves as the number of recursions increases, the average x- and y-coordinates were 2.13 and 5.3, respectively, when the number of recursions ranged from 1 to 20. Moreover, the average coordinates became 2.1 and 5.3 when the number of recursions varied from 81 to 100, indicating an error reduction of up to 0.03 and 0.04, respectively.

Table 6 lists the values of the iBeacon signal that was measured 1,000 times at the x- and y-coordinates $(6, 7)$. Table 7 and Figure 15 specify the indoor positioning value applied with the extended Kalman filter. The average values

Table 4: Gathering signals from (2, 5).

Number	BS ID	BS x-coordinates	BS y-coordinates	RSSI	Distance
1	BS1	0	0	−70	3.57
2	BS2	11	0	−63	1.56
3	BS3	0	6	−76	4.97
4	BS4	11	6	−74	7.73
5	BS5	0	12	−70	4.81
6	BS6	11	12	−74	5.69
7	BS1	0	0	−68	3.50
8	BS2	11	0	−62	1.53
9	BS3	0	6	−76	5.09
10	BS4	11	6	−74	7.73
⋮	⋮	⋮	⋮	⋮	⋮
991	BS1	0	0	−70	3.83
992	BS2	11	0	−63	1.44
993	BS3	0	6	−69	4.5
994	BS4	11	6	−74	7.22
995	BS5	0	12	−88	5.55
996	BS6	11	12	−74	6.08
997	BS1	0	0	−68	3.73
998	BS2	11	0	−64	1.46
999	BS3	0	6	−69	4.39
1000	BS4	11	6	−76	7.2421

Table 5: Positioning result from (2, 5).

Age	x	y
1	3.38	5.57
2	2.62	5.38
3	2.09	4.97
4	2.16	5.3
5	2.11	5.38
6	2.07	5.28
7	2.14	5.35
8	2.16	5.19
9	2.18	5.54
10	2.05	5.24
⋯	⋯	⋯
91	2.13	5.24
92	2.11	5.4
93	2.07	5.39
94	2.04	5.25
95	2.06	5.27
96	2.16	5.29
97	2.08	5.23
98	2.08	5.28
99	2.03	5.19
100	2.07	5.39

of the x- and y-coordinates were 5.24 and 8.2, that is, errors of −0.76 and 1.2 from the actual coordinates, and the standard

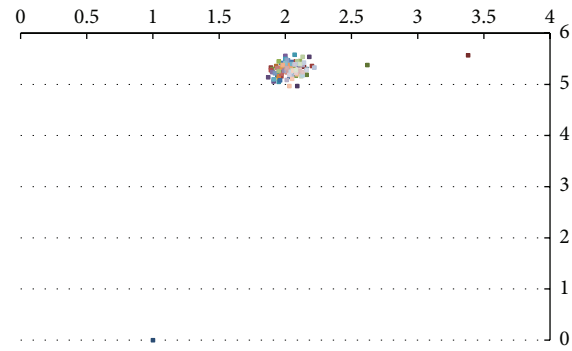

Figure 14: Positioning result chart (2, 5).

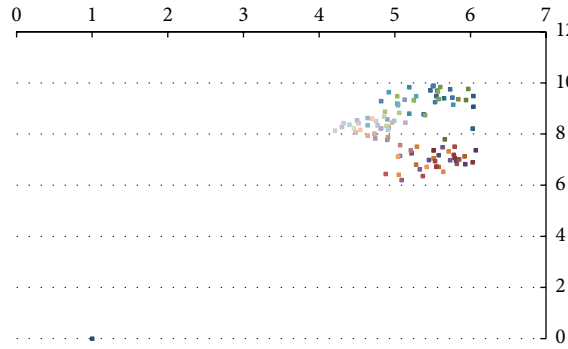

Figure 15: Positioning result chart (6, 7).

deviations were 0.48 and 1.03, respectively. The errors derived from the average coordinates were accumulated, and when the number of recursions ranged from 81 to 100, the errors in the average x- and y-coordinates became 1.14 and 0.1, respectively, as listed in Table 7. The coordinates with the largest error exhibited a higher standard deviation compared to the other coordinates; thus, it could be concluded that the iBeacon RSSI value was influenced most significantly by the external environment.

Table 8 lists the values of the iBeacon signal that was measured 1,000 times at the x- and y-coordinates (9, 8). Table 9 and Figure 16 specify the indoor positioning value applied with the extended Kalman filter. The average values of the x- and y-coordinates were 9.43 and 7.81, that is, errors of 0.43 and −0.19 from the actual coordinates, and the standard deviations were 0.48 and 1.03, respectively. As specified in Table 9, the errors in the x- and y-coordinates increased by 0.35 and 0.2, respectively, when the number of recursions ranged from 81 to 100.

By combining all the measurements for each coordinate, it could be confirmed that the errors in the average coordinates reflecting the total number of recursions were 0.53 and 0.56 for the x- and y-coordinates, respectively. This is due to the nature of the extended Kalman filter, where the error margin decreases as the number of recursions increases. The average errors for 1 to 20 recursions were 0.33 and 0.53, respectively, while the errors reduced to 0.17 and 0.48, respectively, when the number of recursions ranged from 80 to 100. Considering that each grid was 0.5 m long,

Table 6: Gathering signals from (6, 7).

Number	BS ID	BS x-coordinates	BS y-coordinates	RSSI	Distance
1	BS1	0	0	−87	6.53
2	BS2	11	0	−62	1.69
3	BS3	0	6	−73	5.53
4	BS4	11	6	−65	2.15
5	BS5	0	12	−67	2.94
6	BS6	11	12	−65	2.12
7	BS1	0	0	−75	6.56
8	BS2	11	0	−66	1.74
9	BS3	0	6	−73	5.5
10	BS4	11	6	−75	2.4
⋮	⋮	⋮	⋮	⋮	⋮
991	BS1	0	0	−79	6.61
992	BS2	11	0	−62	2.1
993	BS3	0	6	−74	5.89
994	BS4	11	6	−71	2.76
995	BS5	0	12	−66	2.54
996	BS6	11	12	−68	2.82
997	BS1	0	0	−75	6.62
998	BS2	11	0	−62	1.99
999	BS3	0	6	−76	5.97
1000	BS4	11	6	−67	2.73

Table 7: Positioning result from (6, 7).

Age	x	y
1	5.51	7.36
2	5.66	7.79
3	6.07	7.37
4	6.03	8.22
5	5.82	6.84
6	6.04	9.07
7	5.79	7.07
8	5.94	9.33
9	5.93	6.82
10	5.65	9.4
⋯	⋯	⋯
91	4.48	8.06
92	4.21	8.14
93	4.3	8.28
94	4.4	8.37
95	4.7	8.61
96	4.75	8.51
97	4.52	8.42
98	4.46	8.23
99	4.32	8.43
100	4.61	8.44

Table 8: Gathering signals from (9, 8).

Number	BS ID	BS x-coordinates	BS y-coordinates	RSSI	Distance
1	BS1	0	0	−80	3.8
2	BS2	11	0	−66	4.42
3	BS3	0	6	−70	4.35
4	BS4	11	6	−60	0.99
5	BS5	0	12	−74	6.96
6	BS6	11	12	−64	1.33
7	BS1	0	0	−91	4.44
8	BS2	11	0	−66	4.09
9	BS3	0	6	−69	4.23
10	BS4	11	6	−72	1.29
⋮	⋮	⋮	⋮	⋮	⋮
991	BS1	0	0	−87	3.4898
992	BS2	11	0	−66	3.99
993	BS3	0	6	−69	4.34
994	BS4	11	6	−71	1.37
995	BS5	0	12	−76	6.63
996	BS6	11	12	−66	1.36
997	BS1	0	0	−80	3.67
998	BS2	11	0	−65	3.73
999	BS3	0	6	−68	4.19
1000	BS4	11	6	−72	1.49

Table 9: Positioning result from (9, 8).

Age	x	y
1	8.11	7.05
2	9.43	7.89
3	9.32	8.1
4	9.27	8.23
5	10.02	7.99
6	8.68	8.12
7	10.12	7.98
8	9.14	8.02
9	9.8	8.19
10	9.1	8.01
⋯	⋯	⋯
91	9.95	8.13
92	9.85	8.15
93	9.87	7.94
94	9.73	7.66
95	10.55	8.34
96	7.92	7.96
97	10.06	7.55
98	9.06	7.86
99	9.7	7.57
100	9.58	7.5

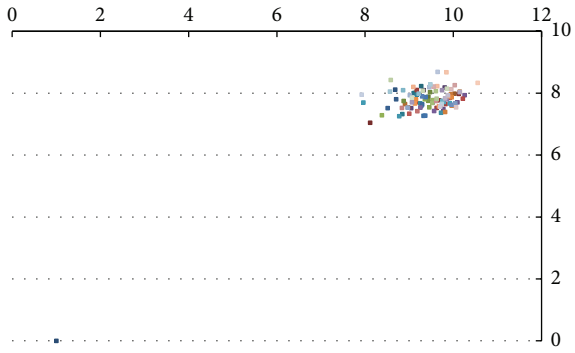

Figure 16: Positioning result chart (9, 8).

the smartphone's indoor positioning accuracy had errors of 0.26 m and 0.28 m for the x- and y-coordinates, respectively.

5. Conclusion

Although LBS have been diversified and enhanced through the use of bluetooth, Wi-Fi, GPS, and sensor technologies in smartphones, most such services are still used outdoors. With the proliferation of construction techniques and information and communications technologies, there is a growing need to provide LBS indoors in the same way as they have been previously provided outdoors. Facilitating the provision of LBS in an indoor area requires technologies that can plot indoor maps, identify the positions of users accurately, and analyze routes efficiently. BLE-based beacons periodically broadcast signals containing ID and RSSI, thus playing the role of reference points for locations, as with indoor GPS. Following the launch of iBeacon, Apple applied it to a mobile payment service that replaced near field communication and to a service that provides information on matches held at the stadiums of the Boston Red Sox, LA Dodgers, and so forth. The key technology of IPS involves the identification of a smartphone location. The existing beacon-based indoor positioning technology has low performance accuracy because of the characteristics of bluetooth signals; hence, it is necessary to enhance the indoor positioning accuracy by combining the existing approach with a location determination approach, which uses wireless technologies such as Wi-Fi and ZigBee. However, this increases the burden of the installation cost for a number of sensors having different models and leads to an increase in the development and maintenance costs because of the fusion of multilateral positioning technology.

To overcome the abovementioned issues, this study proposed a technique for enhancing the indoor positioning accuracy in a two-dimensional indoor area using only a beacon signal. Once it was assumed that the RSSI signal has a nonlinear property, the iBeacon measurement was analyzed and the standard deviation was used to define the measurement noise model (R) that reflected the signal properties by iBeacon and by distance. The defined R model was applied to the extended Kalman filter that was improved on the basis of the bluetooth signal property, which resulted in a relatively accurate calculation of the smartphone's indoor position. In this study, we were able to achieve improved accuracy compared to beacon-based trilateration. However, a limitation of this study is its inability to sufficiently reflect the smartphone's movement and the beacon's signal property. Based on this study, the next step is to conduct a detailed analysis of the smartphone's movement and the bluetooth signal deviation to generate a weighted value model for each beacon signal and its standard deviation model, which will then be applied to the extended Kalman filter. Furthermore, in the future, we aim to develop a model for restricted area access control using indoor positioning accuracy enhancements.

Competing Interests

The authors declare that they have no competing interests.

Acknowledgments

This work was supported by the Human Resource Training Program for Regional Innovation and Creativity through the Ministry of Education and National Research Foundation of Korea (NRF-2014H1C1A1073140).

References

[1] S. J. Vaughan-Nichols, "Will mobile computing's future be location, location, location?" *Computer*, vol. 42, no. 2, pp. 14–17, 2009.

[2] P. Bellavista, A. Küpper, and S. Helal, "Location-based services: back to the future," *IEEE Pervasive Computing*, vol. 7, no. 2, pp. 85–89, 2008.

[3] Y. Gu, A. Lo, and I. Niemegeers, "A survey of indoor positioning systems for wireless personal networks," *IEEE Communications Surveys and Tutorials*, vol. 11, no. 1, pp. 13–32, 2009.

[4] D. Madigan, E. Einahrawy, R. P. Martin, W.-H. Ju, P. Krishnan, and A. S. Krishnakumar, "Bayesian indoor positioning systems," in *Proceedings of the 24th Annual Joint Conference of the IEEE Computer and Communications Societies*, pp. 1217–1227, IEEE, March 2005.

[5] B. Shin, J. H. Lee, T. Lee, and H. S. Kim, "Enhanced weighted K-nearest neighbor algorithm for indoor Wi-Fi positioning systems," in *Proceedings of the 8th International Conference on Computing Technology and Information Management (ICCM '12)*, pp. 574–577, IEEE, Seoul, South Korea, April 2012.

[6] R. Mautz, *Indoor positioning technologies [Ph.D. thesis]*, Habilitationsschrift ETH Zürich, 2012.

[7] S. Y. Cho, J. Y. Kim, and M. Enkhtur, "P2P ranging-based cooperative localization method for a cluster of mobile nodes containing IR-UWB PHY," *ETRI Journal*, vol. 35, no. 6, pp. 1084–1093, 2013.

[8] S. Y. Cho, "Hybrid linear closed-form solution in wireless localization," *ETRI Journal*, vol. 37, no. 3, pp. 533–540, 2015.

[9] C. Gomez, J. Oller, and J. Paradells, "Overview and evaluation of bluetooth low energy: an emerging low-power wireless technology," *Sensors*, vol. 12, no. 9, pp. 11734–11753, 2012.

[10] Bluetooth Special Interest Group, *Bluetooth Specification Version 4.1*, Bluetooth Special Interest Group, Kirkland, Wash, USA, 2013.

[11] P. Martin, B.-J. Ho, N. Grupen, S. Muñoz, and M. Srivastava, "An ibeacon primer for indoor localization: demo abstract," in

Proceedings of the 1st ACM Conference on Embedded Systems for Energy-Efficient Buildings (BuildSys '14), pp. 190–191, Memphis, Tenn, USA, November 2014.

[12] D. Namiot, "On indoor positioning," *International Journal of Open Information Technologies*, vol. 3, no. 3, pp. 23–26, 2015.

[13] R. Faragher and R. Harle, "An analysis of the accuracy of bluetooth low energy for indoor positioning applications," in *Proceedings of the 27th International Technical Meeting of the Satellite Division of the Institute of Navigation (ION GNSS+ '14)*, pp. 201–210, Tampa, Fla, USA, September 2014.

[14] L. Pei, R. Chen, J. Liu, H. Kuusniemi, T. Tenhunen, and Y. Chen, "Using inquiry-based Bluetooth RSSI probability distributions for indoor positioning," *Journal of Global Positioning Systems*, vol. 9, no. 2, pp. 122–130, 2010.

[15] Apple, *Getting Started with iBeacon Version 1.0*, 2014.

[16] Estimote Developer Docs, http://developer.estimote.com/.

[17] R. E. Kalman, "A new approach to linear filtering and prediction problems," *Journal of Basic Engineering*, vol. 82, no. 1, pp. 35–45, 1960.

[18] O. Frank, *Multiple target tracking [Ph.D. thesis]*, University of Sydney, Sydney, Australia, 2003.

[19] S.-T. Park and J. G. Lee, "Improved Kalman filter design for three-dimensional radar tracking," *IEEE Transactions on Aerospace and Electronic Systems*, vol. 37, no. 2, pp. 727–739, 2001.

[20] Y. Bar-Shalom, X. Rong Li, and T. Kirubarajan, *Estimation with Applications to Tracking and Navigation: Theory Algorithms and Software*, John Wiley & Sons, New York, NY, USA, 2004.

[21] E. Brookner, *Kalman Filter. Tracking and Kalman Filtering Made Easy*, Wiley-Interscience, 1998.

[22] G. Welch and G. Bishop, "Course 8—An introduction to the Kalman filter. SIGGRAPH 2001 course," in *Computer Graphics, Annual Conference on Computer Graphics & Interactive Techniques*, 2001.

[23] L. Ljung, "Asymptotic behavior of the extended Kalman filter as a parameter estimator for linear systems," *IEEE Transactions on Automatic Control*, vol. 24, no. 1, pp. 36–50, 1979.

[24] S. J. Julier and J. K. Uhlmann, "Unscented filtering and nonlinear estimation," *Proceedings of the IEEE*, vol. 92, no. 3, pp. 401–422, 2004.

[25] E. Wan, "Sigma-point filters: an overview with applications to integrated navigation and vision assisted control," in *Proceedings of the Nonlinear Statistical Signal Processing Workshop*, pp. 201–202, IEEE, Cambridge, UK, September 2006.

[26] Technical specification of Estimore Beacons and Stickers, https://community.estimote.com/hc/en-us/articles/204092986-Technical-specification-of-Estimote-Beacons-and-Stickers.

Hindawi Publishing Corporation
Mobile Information Systems
Volume 2016, Article ID 2097158, 14 pages
http://dx.doi.org/10.1155/2016/2097158

Research Article

Improving Healthcare Team Collaboration in Hospital Transfers through Cloud-Based Mobile Systems

Andres Neyem,[1] Marie J. Carrillo,[2,3] Claudio Jerez,[2,3] Guillermo Valenzuela,[1] Nicolas Risso,[1] Jose I. Benedetto,[1] and Juan S. Rojas-Riethmuller[1]

[1]*Computer Science Department, Pontificia Universidad Católica de Chile, Vicuña Mackenna 4860, Santiago, Chile*
[2]*Nursing School, Pontificia Universidad Católica de Chile, Vicuña Mackenna 4860, Santiago, Chile*
[3]*Servicio de Atención Médica de Urgencia (SAMU), Santiago, Chile*

Correspondence should be addressed to Andres Neyem; aneyem@ing.puc.cl

Received 4 February 2016; Accepted 29 May 2016

Academic Editor: Giancarlo Fortino

It is a clinical fact that better patient flow management in and between hospitals improves quality of care, resource utilization, and cost efficiency. As the number of patients in hospitals constantly grows, the need for hospital transfers is directly affected. Interhospital transfers can be required for several reasons but they are most commonly made when the diagnostic and therapeutic facilities required for a patient are not available locally. Transferring a critical patient between hospitals is commonly associated with risk of death and complications. This raises the question: How can we improve healthcare team collaboration in hospital transfers through the use of emerging information technology and communication services? This paper presents a cloud-based mobile system for supporting team collaboration and decision-making in the transportation of patients in critical condition. The Rapid Emergency Medicine Score (REMS) scale was used as an outcome variable, being a useful scale to assess the risk profile of critical patients requiring transfers between hospitals. This helps medical staff to adopt proper risk-prevention measures when handling a transfer and to react on time if any complications arise in transit.

1. Introduction

Interhospital transfers (IHTs) of patients, also known as interfacility or secondary transfers, are an integral part of healthcare services delivery. There are a variety of reasons why patients may require IHTs [1]. Patients may require transfers due to the lack of critical care facilities or beds in the referring hospital. Others may be in need of more specialized treatment and equipment available only in more sophisticated facilities. A commonly used classification for transfers is as follows: (a) *primary transfers*, moving the patient from the prehospital setting to the receiving hospital; (b) *secondary transfers*, hospital to hospital transfers, including to tertiary centers; (c) *tertiary transfers*, moving from secondary or tertiary hospitals to a national center of expertise; and (d) *quaternary transfers*, international transfers.

This situation leads to healthcare and transportation services often needing assistance with logistics and decision-making. Specifically, IHTs are needed when the diagnostic and therapeutic facilities required for a patient are not available locally [2]. Unfortunately, it is common for complications to arise during transportation. The decision of transporting a patient must be done after balancing the potential benefits of transportation and the risks involved. Although meticulous pretransfer checks can be made to assess the risks, patients' vital signs may be subject to major variations while traveling [3].

Chile's current emergency medical transport system is managed by SAMU (Emergency Medical Care Services). It provides a central hub for first response vehicles and ambulances with or without a physician on board. However, most ambulances are not properly equipped to be able to remotely monitor the patient's vital signs while being transported. SAMU has had many problems with equipment on board their ambulances. The devices they use are very large and are not suited for emergency transports: some are very fragile while very few are capable of transmitting data to

a server. Often sudden accelerations, stops, and the constant vibration inherent of an IHT can significantly alter the measurements of the sensors and even break the equipment, resulting in huge monetary losses. SAMU also manages communications between vehicles and hospitals through radio channels, which puts the responsibility of analyzing the patient's condition entirely on the personnel on board and creates coordination difficulties for simultaneous transfers. Despite an increased interest in embedded devices, mobile applications, and cloud platforms, there is still a gap between current vital sensor design used by SAMU and the actual requirements of the physicians and doctors monitoring the patient being transported.

This project tries to fill that gap by providing a low-power embedded solution capable of capturing some of the patient's vital signs, such as heart rate and oxygen saturation, and sending them to a smartphone using wireless connectivity. Patients' vital signs are monitored by embedded devices fitted with vital sensors. Outfitting patients with such devices enables the capturing and transmission of real-time vital sign data. This in turn allows for the construction of remote monitoring platforms and intelligent mobile applications in order to improve the healthcare team collaboration in IHTs. By centralizing this information in the cloud through the smartphones' cellular radio, offsite physicians can support paramedics in their decision-making process while simultaneously monitoring the patient's vital functions. This project aims to establish a risk assessment platform to be used to determine whether or not to transport a patient through SAMU, trigger early responses to in-transit complications, and overcome many of the current monitoring system's shortcomings.

Section 2 describes the current state of the art in mHealth technologies with a focus on mobile telemedicine. Section 3 describes emerging trends in information technology for healthcare services. Section 4 describes the Rapid Emergency Medicine Score (REMS) research carried out in Chile. Section 5 presents the proposed system and Section 6 presents discussion, conclusions, and future work.

2. Related Work

Mobile telemedicine is the science of providing healthcare services to distant patients through the use of information and communication technologies. It has been the subject of study for several decades as the early provision of prehospital attention to critical patients can mean the difference between life and death, yet mobile telemedicine solutions have always been limited to inherent mobility-related constraints such as limited throughput and connection unreliability. One of the first documented mobile telemedicine initiatives is the AMBULANCE telemedicine system [4] proposed in the early 1990s. It featured a biosignal monitor hooked up to a notebook computer with a GSM modem. It allowed the transmission of 320 × 240 JEPG images and real-time biosignals of the patient (ECG, heart rate, blood pressure, and oxygen saturation) to a medical team monitoring the situation at long distances. The architecture followed a client-server model where the client would be responsible for establishing communications, sending the data, and requesting a patient's medical record if needed. The system used the TCP/IP protocol over GSM and was capped at a maximum speed of 9.6 kbit/s due to the limitations of 2G technologies at the time.

Later, advancements in mobile networks saw many new mobile telemedicine initiatives taking advantage of them to develop new applications. The WAP telemedicine system [5] introduced mHealth applications to devices available to consumers: in this particular case, a WAP-enabled phone. It allowed for the storage and relay of ECG signals, patient history, hospital messages, and the physician's advice. In 2004, a system that would allow for the transmission of still images, videos, and vehicle control and management was proposed [6]. This saw the addition of GPS and wireless camera equipment to the ambulances to provide richer information. Reliability was still an issue in the less developed rural areas where mobile network availability was less abundant. To tackle this challenge, the authors in [7] proposed a system that would cycle through multiple wireless communication standards in order to send the information through the most reliable channel.

Moving on to 3G networks, the platform proposed in [8] introduced a cost-effective portable system implemented through a laptop or tablet that would collect and relay ECG signals, medical images, and real-time video. These would then be sent through 3G to a hospital unit implemented in a desktop computer. Such features were only made possible by the increased data transmission rates of the new networks. A similar device is presented in [9], where an ultramobile PC with a camera and a microphone/earphone was hooked up to a WIBRO modem for wireless connectivity. This solution would exploit the increased QoS, area coverage, and bit rate transmission of WiMax to successfully enable teleconferencing between paramedics and the medical staff in the hospital. However, testing in practical conditions showed that the device only met basic performance parameters, mostly due to connection reliability issues.

Mobile telemedicine systems in ambulances exploiting 4G LTE-advanced are less common in literature due to their relative novelty, but they are still fairly abundant in the areas of remote patient monitoring and self-care. These technologies are fairly predominant in the context of body sensor networks. BSNs are a subset of wireless sensor networks in which sensors are explicitly used to monitor an individual. However, effective implementation of BSNs is very challenging because of the large amount of data streams being generated concurrently. They need to be collected, processed, and analyzed in order to generate information of use to the patient or medical staff. Other operational challenges include privacy, security, and the seamless integration of heterogeneous devices. Efforts into streamlining this process have led to the creation of BSN frameworks such as BodyCloud, a cloud computing system architecture for the management and monitoring of body sensor data streams [10], and C-SPINE, a framework for collaborative BSNs enabling sensor discovery, activation, execution, intercommunication, and data fusion [11]. Bourouis et al. present an example of a specific BSN implementation in which they make use of

a mobile device to collect kinematic and physiological parameters of elderly patients via Bluetooth. This data is analyzed and sent to a server upon any relevant perceived change [12]. A similar architecture is presented in [13], although the collected information is further enriched by the patients' own status logging and social network messaging information. The data is later referred to a server via a SOAP API.

A thorough survey of mobile telemedicine solutions for moving vehicle scenarios is available at [14]. Batistatos et al. [15] also analyze the same kind of technologies but their research is more focused in their requirements, characteristics, benefits, and limitations. They conclude the biggest challenge of telemedicine in mobile scenarios is the continuously changing operational environment. Therefore, solutions should either support adaptive networking to adapt to whatever infrastructure is currently available or be fully functional in situations where network availability is poor or nonexistent.

Our system is designed to take advantage of the latest APIs and mobile devices available to consumers to create a low-cost solution for vital sign monitoring in the specific environments of patient pickup and IHT. We do not delve into resource intensive multimedia interactions as communication reliability has been shown in several of these studies to be a very important issue. Instead, we focus on the set of parameters that is most likely to affect patient survivability during emergency transfers. We make those available to the local paramedic team and use them to calculate a global score. This information is then shared to the medical staff at the hospital as long as a network connection is available; however, the primary function of the system is not impeded by lack of connectivity and paramedics may still yield some benefits from the solution in such scenarios.

While many remote patient monitoring initiatives exist, these are mostly meant for static contexts and do not consider the constraints introduced by mobility. Others limit themselves to simple monitoring of vital signs and do not perform any historical data analysis to proactively alert physicians of any irregularity, or they may be dependent on a high quality wireless network being available, often not the case in less developed areas. Our solution was specifically designed with these goals in mind.

Section 3 describes emerging trends in information technology in healthcare services that have been considered in our cloud-based mobile system proposal.

3. Mobile Cloud Computing and Healthcare Services

Cloud computing is a model for enabling on-demand network access to a configurable set of cloud resources with minimum amount of developer effort. These resources can be rapidly allocated or released depending on the current server demand either automatically (e.g., Amazon EC2) or manually. Cloud computing has been used in mobile healthcare services for several years now and it has been effectively demonstrated to ease development of health-related architectures [16]. Nevertheless, integrating these services with mobile platforms is far from trivial and that constitutes a different challenge altogether. Effective mobile telemedicine solutions are required to support pervasive and ubiquitous access to data and to properly process it with limited hardware resources and without excessive battery usage. Ideally they should also support at least partial offline functionality and automatic database syncing.

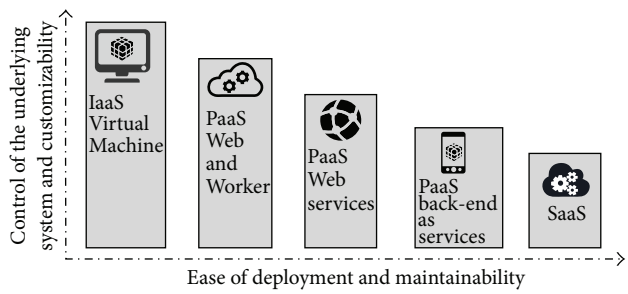

Figure 1: Tradeoff between different layers of cloud computing.

Infrastructures that allow mobile platforms to harness the resources of the cloud and support the aforementioned features belong in the category of mobile cloud computing (MCC). A MCC architecture consists of a mobile and cloud component connected by the Internet through a mobile network. Cloud services are deployed on a cluster of servers usually managed by a cloud service provider (e.g., Google Cloud Platform, Microsoft Azure, and Amazon Web Services). Cloud services can then be classified based on the amount of customizability and control of the underlying system available to the developer versus deployment speed and ease of maintenance (see Figure 1). In this paradigm, we recognize three major categories: infrastructure as a service (IaaS), platform as a service (PaaS), and software as a service (SaaS) [17].

IaaS is highly customizable because developers are responsible for everything from setting up the operating system to deploying the application and configuring its runtime environment. General PaaS solutions like Web and Worker do a little more of the heavy lifting for developers because the service comes with an OS and certain middleware applications already configured. A subset of PaaS solutions targeted towards particular applications, such as Web, media, or mobile, could supply even more of the glue code the application needs. Finally, SaaS allows for little to no customization and supports only a specific software distribution. As such, SaaS solutions are tailored towards a very particular set of requirements.

In order to ease the integration of cloud services and mobile clients, there has been a recent surge of Mobile Back-End as a Service (MBaaS) providers that allow developers to establish complex mobile cloud interactions with very little configuration. These solutions provide programmers with two major features: on the client side, we have custom libraries for mobile clients made specifically for each relevant mobile operating system; on the server side, we have control panels that make extensive configuration possible in a matter of minutes. MBaaS not only enables the connectivity and

Table 1: Scoring system for calculating the REMS score.

	Low abnormal range				Normal range		High abnormal range				
	+4	+3	+2	+1	0	+1	+2	+3	+4	+5	+6
MAP	<50	—	50–69	—	70–109	—	110–129	130–159	>159	—	—
HR	<39	40–54	55–69	—	70–109	—	110–139	140–179	>179	—	—
RR	<5	—	6–9	10-11	12–24	25–34	—	35–49	>49	—	—
SpO2	<75	75–85	—	86–89	>89	—	—	—	—	—	—
GCS	<5	5–7	8–10	11–13	>13	—	—	—	—	—	—
Age (years)	—	—	—	—	<45	—	45–54	55–64	—	65–74	>74

MAP: mean arterial pressure.
HR: heart rate.
RR: respiratory rate.
SpO2: peripheral oxygen saturation.
GCS: Glasgow coma scale.

scalability that come with all cloud-based services but also supplies solutions for common mobile development challenges like user authentication, push notifications, data storage, social media integration, geospatial queries, offline sync, analytics, and more. This provides a consistent way to manage mobile back-end requirements as services and removes the need for having to develop custom ad hoc solutions that more often than not suffer from serious performance and security issues.

As can be seen in [18], the usage of MBaaS is not foreign to healthcare applications, where it is used to greatly facilitate data routing, security, authentication, authorization, offline functionality, and service orchestration.

In the previous paragraphs we explained how mobile and cloud computing represents a drastically different approach to IT solution delivery and how this technology could be one of the foundations of the next generation of computing. The next section describes the importance of REMS in IHTs and the relevance of IT solutions for improving healthcare team collaboration in IHTs.

4. Understanding the Importance of REMS as a Risk Assessment Tool for Interhospital Transfers of Critical Patients

The Rapid Emergency Medicine Score (REMS) is an in-hospital mortality predictor for critically ill emergency department patients. It was first mentioned in literature by Olsson and Lind in 2003 and it has been proven to be superior to similar mortality predictors such as RAPS [19] and MEWS [20]. The REMS varies between 0 and 26 where a higher score signifies a greater mortality risk. It considers six variables: mean arterial pressure, heart rate, respiratory rate, peripheral oxygen saturation, Glasgow coma scale, and age. Each of them may contribute up to 4 points to the final score, with the exception of age, which may contribute up to 6 points. Table 1 summarizes in detail how to calculate the score. One of the main advantages of the REMS is its noninvasive nature and ease to determine. All of these variables can be either estimated by trained physicians or measured by common healthcare monitors. Despite its simplicity, it is a very powerful tool for assisting clinical decision-making.

Since its inception, there have been several initiatives to evaluate its applications to areas other than in-hospital mortality for ICU patients. In [21], a study conducted amongst traumatically injured patients found a similar correlation between REMS and in-hospital mortality (AUC of 0.91). For our case in particular, REMS has also been proven to perform relatively well when assessing mortality risk in interhospital transfers. In [20], researchers conducted a retrospective study amongst critically ill patients who underwent transfers to an ICU and found that REMS behaved reasonably well as a predictor of mortality (AUC of 0.72). They further emphasize that the REMS incorporated into electronic decision support tools can "assist clinicians in balancing resource, risk, and logistic options in complex patient transfer scenarios."

In order to verify these results and assess the applicability of REMS to SAMU transfers, we conducted our own study to verify its effectiveness in evaluating the clinical state of patients undergoing secondary transfers between hospitals. We performed a retrospective analysis of all interhospital transfers made by SAMU in Santiago, Chile, between October 2014 and May 2015. In total, 3629 patients (61.9% male, 38.1% female) were included in the analysis. We considered the REMS at the beginning of the IHT as well as other relevant variables. This data is summarized in Table 2. By analyzing the relation between the initial REMS and patient mortality, our results showed an AUC of 0.72, thereby confirming the previously published results. Additional studies are available at [1, 22].

With this in mind, the REMS can be used as an early warning system to assess the seriousness of a patient's condition. As such, patients are classified in one of three categories: low risk (REMS < 6), medium risk ($6 \leqslant$ REMS $\leqslant 13$), and high risk (REMS > 13). Depending on the classification, additional precautions may be taken to secure a patient's wellbeing during a transfer. In transfer, sudden REMS spikes are indicative of an increased mortality risk and may trigger early therapeutic actions from the paramedics with collaboration from the on-hospital medical staff that may save a patient's life. These may include the use of vasoactive drugs, reevaluating the use of assisted oxygenation and ventilation, or rerouting the transfer to a nearer clinic. As a result, paramedics can take the appropriate measure at an early stage

Table 2: Average characteristics of IHT patients between October 2014 and May 2015 handled by SAMU in Santiago, Chile.

	Mortality	
	Yes	No
	$n = 163$	$n = 3466$
Relevant variables		
Age	58.3	56.9
Initial body temperature (°C)	36.2	36.1
Length of IHT (minutes)	52.7	53.2
Distance of IHT (Km)	20.4	17.2
REMS related variables		
Initial REMS	*11*	*6.9*
Initial SpO2	92.15	97.17
Initial GCM	8.19	11.68
Initial HR	96.02	87.36
Initial RR	10.39	14.86
Initial MAP	113.53	123.3

to avoid the patient's physiopathological deterioration. Thus, we can prevent riskier and more aggressive interventions, lower the usage of clinical resources, and avoid prolonged hospital stays. Therefore, when initiating transfer of a patient with an intermediate or high REMS, constant evaluation must be maintained in order to identify potentially risky situations in time [3].

5. The Proposed Cloud-Based Mobile System

5.1. Applying Lean Startup as a Viable Methodology for Addressing Healthcare Research Projects with Multidisciplinary Teams. The lean startup movement made its first official attempt to break into the healthcare sector when Steve Blank launched The Lean LaunchPad for Life Sciences and Healthcare: the right way to redesign healthcare [23]. The goal was to teach researchers and clinicians how to move their technology from an academic lab or clinic into the commercial world. The life sciences class gathered together drug developers, software engineers, and medical device inventors and encouraged them to test their ideas before launching them as a business.

The lean startup principles are in many ways analogous to applying the scientific method to startups [24, 25]. That is, treat your assumptions as hypotheses, and then go out and test them starting with the most critical and cheapest tests first to turn your assumptions around the business model into data. Using lean startup principles allows multidisciplinary teams to present personal project or research ideas to be voted on by the broader team [24].

The core of the lean startup model is the Build-Measure-Learn feedback loop (Figure 2), employing a team of people with professional training that focuses on one element of this feedback loop [26]. Due to this, using lean startup principles allows this research to easily properly integrate multidisciplinary perspectives to propose a solution for healthcare research projects. The formation of an interdisciplinary team is particularly relevant as healthcare professionals have

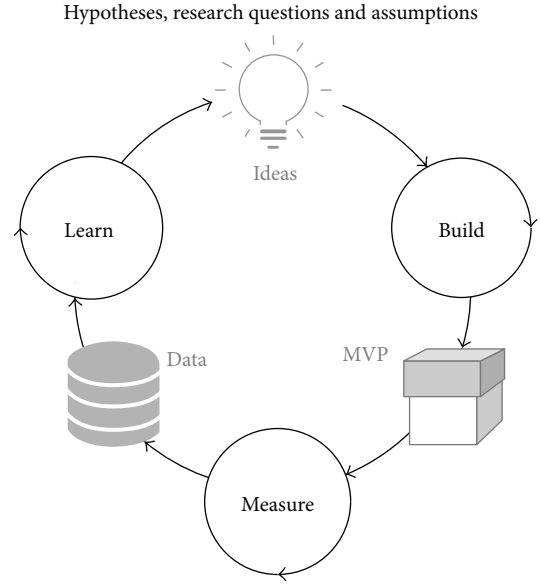

Figure 2: The lean startup methodology.

a greater insight of the needs of the healthcare sector, while computer scientists are more familiar with the key factors of the success of mobile services: identifying actual and potential open research issues, investigating how mobile services are influenced and how they behave (i.e., users' behavior), and revealing what they really expect (i.e., needs and preferences).

This research used data exposed in Section 4, regarding the REMS scale as an entry point. During this initial learning phase, we identified the REMS as a useful predictor of the risk and severity of a patient's condition during an IHT; however, it was not being actively used as a decision-making tool. Thus, we envisioned a platform that can compute, among other data, the REMS in real time and support decision-making for IHTs.

In the first cycle of this methodology, we focused on providing a set of tools to help in-hospital clinical staff and paramedics on board ambulances. Initial mockups were built as our first product and tested with real users. We used semistructured interviews to measure our first approach, identifying several key aspects regarding usability and architecture, thus informing us of which features added more value to the end users. Finally, in the learning phase, those comments and feedback were analyzed and consolidated, resulting in the improvement and validation of the proposed mockups and core features.

With the feedback gathered from the first cycle, our team moved on to focus on building and obtaining the initial Minimum Viable Product (MVP) that would incorporate the core features we determined. We divided our platform into 3 main components: a back-end, a mobile application, and a set of embedded devices. Each component tackles a core feature we identified: the back-end provides scalability and data centralization, the mobile application provides the monitoring interfaces, and the embedded devices were used

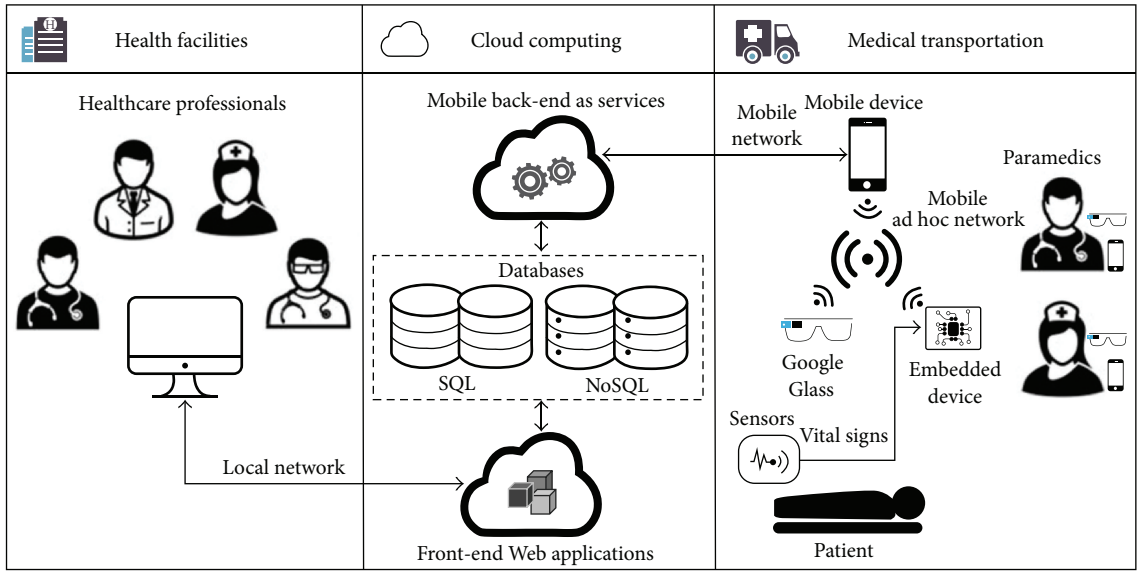

Figure 3: General architecture of the proposed cloud-based mobile system.

for data extraction. We tested this first version of the platform with mock data to simulate real IHTs and used the same approach as the first cycle to gather feedback. The core features were well received, but the usability of our mobile application was identified as paramount to the platform's success.

Finally, we fixed the problems identified in previous cycles and we built a stable release of the platform. The system was tested with a simulated transfer using our embedded sensors within a real ambulance. We gave access to healthcare professionals, undergraduate civil computing students, and nursing students to test the platform. Successful communication was established between the remote medical transfer team and the professionals on-board, and everyone was able to follow the REMS variation in real time.

5.2. The Architecture of the Cloud-Based Mobile System. Cloud-based mobile applications that provide constant monitoring features and guidelines for healthcare, such as our solution, can be classified under the field of collaborative systems. These software applications can be particularly challenging to implement due to mobility-related limitations in both the front-end and back-end [27]. Mobile front-end requirements are related to the intrinsic limitations of interacting with the device and are constant for most applications. On the other hand, requirements related to the application back-end are very varied and unique to monitoring and collaborative platforms. These include environmental (interoperability, heterogeneity, scalability, and availability), security (reliability and privacy), and performance (battery life, storage, and bandwidth) requirements.

In order to deal with these limitations, our solution augments the capabilities of mobile devices by incorporating mobile cloud computing principles. MCC architectures seek to leverage the capabilities of external resource-rich nodes to improve performance and battery life [28]. As such, our solution uses a smartphone simply as a hub and display for wirelessly transmitted data of a variety of sensors; it later relays them to a server in charge of all the computer-intensive processing whenever a network connection is available. This enables the server to process and analyze incoming data in real time in order to obtain statistics and contextual information without straining the battery of the mobile device [29].

Figure 3 shows the general architecture of the proposed system, separating functionality into three basic applications: (a) cloud-based back-end services for computational and data storage purposes, (b) mobile and Web applications that enhance collaboration and analysis between SAMU and medical teams, and (c) embedded and mobile applications that aid vital sign monitoring and improve communication within medical services.

Relying on this general architecture, the proposed platform works as follows. Before initiating a transfer, an in-office healthcare professional assigns the transfer to an ambulance by using the Web system. The paramedics of the designated ambulance are notified by the mobile system. Once the patient is ready and the sensors are connected to him, the transfer starts. During the transfer, the embedded sensors measure some vital signs and send the measurements to the mobile system. The mobile system calculates the REMS and displays the information graphically while sending the data to the cloud. Then, in-office healthcare professionals are able to observe all the information regarding the state of the patient in real time, which enhances the collaboration between different members of SAMU staff during the transfer. Figure 4 shows a sequence diagram of the process described.

5.3. Mobile Back-End as a Service. Back-end services enable convenient, on-demand network access to a shared pool

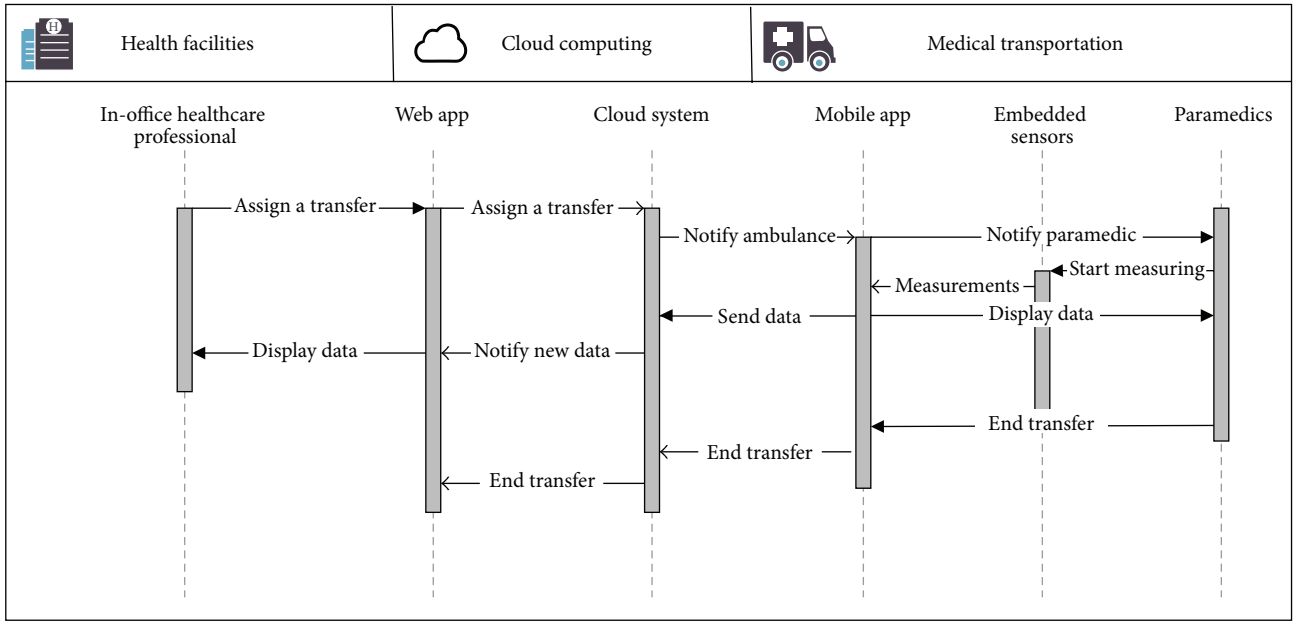

Figure 4: Sequence diagram showing flow of communication between the different components of the architecture.

of computing resources or services that can be rapidly distributed with minimal management effort. These cloud-based back-end services were used to gather data from multiple sensors and for providing access to this information to different users. Among the advantages of using the cloud to power mobile services are the following:

(i) On-demand self-service: the resources can be used and accessed at any time.

(ii) Broad network access: the resources can be accessed over a network from multiple kinds of devices.

(iii) Scalability: users can quickly acquire more resources from the cloud by scaling out.

(iv) Processing power: it permits reducing the computational time of complex tasks compared to devices with limited resources.

(v) Security and privacy: authentication and authorization can be centralized.

The service platform is built with the Ruby on Rails (RoR) framework. It exposes a REST Web service through which it receives data and defines the protocols used by paramedics in case of emergency. Only authenticated users are allowed to interact with our Web services, therefore ensuring the patient's medical data remains secure. For storage purposes, our cloud service uses SQL and NoSQL databases. The MongoDB NoSQL database was selected over a relational database due to its higher scalability and better performance when handling large loads of concurrent write operations [30]. This paradigm fits very well with the intrinsically write-intensive characteristic of sensor data collection applications.

The RoR services and database instances are hosted on Heroku's cloud platform using one dyno, which is a lightweight Linux container that runs a single user-specified command. Namely, the components use the Platform as a Service solution, which allows us to manage the applications while avoiding the complexity of the infrastructure.

The back-end service needs to share and distribute data to several users and several devices and platforms. To achieve this, two technologies were adopted. The first is Google Cloud Messaging, which was used to send nonsensitive information from the cloud service to the mobile devices. The second is PubNub, which was used to provide real-time interaction with Web users as the data arrives into the cloud.

5.4. Front-End Web Applications. The primary goal of the Web application is to provide remote real-time tracking of patients being transferred. It is mainly targeted to medical regulators that can give remote assistance to paramedics in case of emergency. With this information readily available, they are able to promptly order a retransfer should the situation require it.

Medical data is provided graphically by charts that show the tendency of the clinical state of the patient (REMS and its parameters) for each active transfer. The technologies behind the application include RoR, AngularJS, and common Web technologies (HTML, CSS, and JavaScript). We used the Model-View-Controller design pattern for the back-end services and the Web application front-end.

The main layout of the Web application is shown in Figure 5. On the left side, there is a list of current transfers. When a transfer is selected, the tendency of the REMS and its parameters is displayed in charts on the right side. When the parameter being observed is in its normal range, the data is shown in green, but when it reaches dangerous values, it is displayed in red. Alerts generated by the mobile application

Figure 5: Remote Web application.

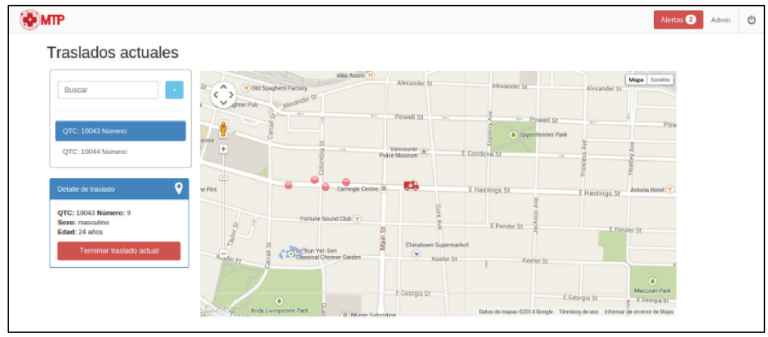

Figure 6: Remote Web application showing map with location of an ambulance.

are displayed at the top of this interface. They are removed when a paramedic attends to it or when the condition of the patient returns to a normal state.

Given that a deterioration in the condition of the patient could lead to serious situations, it is important to be able to provide correct directions to paramedics. One important decision is the change of the target hospital when the state of the patient requires it. In order to support this kind of decision, the Web application is capable of displaying a map that shows the location of the ambulance in real time (see Figure 6).

Finally, as transfers are completed, information disappears from the screen and is visible only to medical administrators. These health professionals have access to historical information on IHTs (see Figure 7).

5.5. Mobile Application. Monitoring systems provide a tool by which paramedics on board ambulances and medical regulators in SAMU offices can track the state of patients in transfer. It is achieved with the use of a mobile application and a Web application. Both of them interact with the back-end services to send and receive data in real time. The main components of the mobile application are listed below:

(i) Communication: the mobile application manages the reception of data from sensors and the sending of processed data to the cloud.

(ii) Transfer: it is in charge of performing updates of the user interface as new data is received.

(iii) Storage: it manages access to different files that are stored locally.

(iv) Location: it manages all the procedures related to determining the location of the ambulance.

(v) Calculator: it performs the calculations needed for determining the patient's REMS and breathing rate.

(vi) Persistence: it is in charge of saving data when the mobile network is unavailable.

The mobile application was built natively on the Android Platform and requires a device running Android 4.1 or higher. It provides a simple graphical user interface that enables paramedics to monitor the patient's vital signs over time through dynamic charts. These charts allow the paramedic to observe the tendency of the patient's REMS and its parameters, while a panel displays the current values of those parameters. The application also includes a list of protocols and guidelines to be applied when specific situations occur during the transfer.

The mobile application receives data from the sensors by the use of a local Wi-Fi network. It then processes the data, calculates the REMS, and updates the corresponding graphs. At the same time, the information is sent to the cloud service by the use of the mobile network. If the mobile network is unavailable, the data is stored locally until a connection is reestablished. When this occurs, the data is sent on a last-come-first-serve basis.

Figure 8 shows the mobile application user interface. Its layout is divided as follows: on the left side there is a list

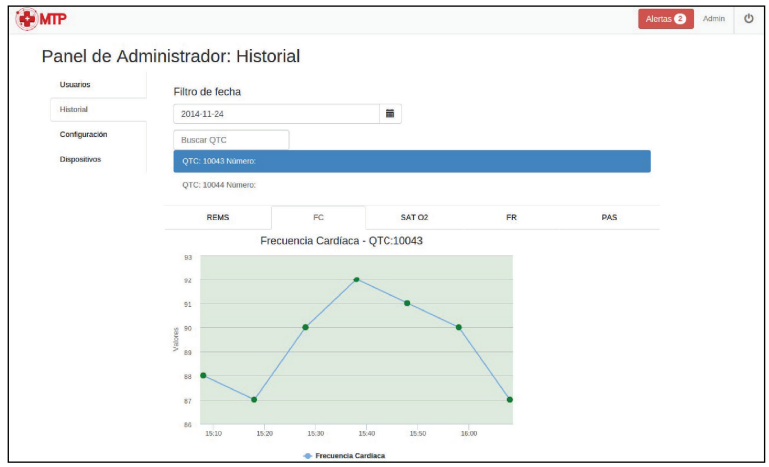

Figure 7: Historical information of IHTs.

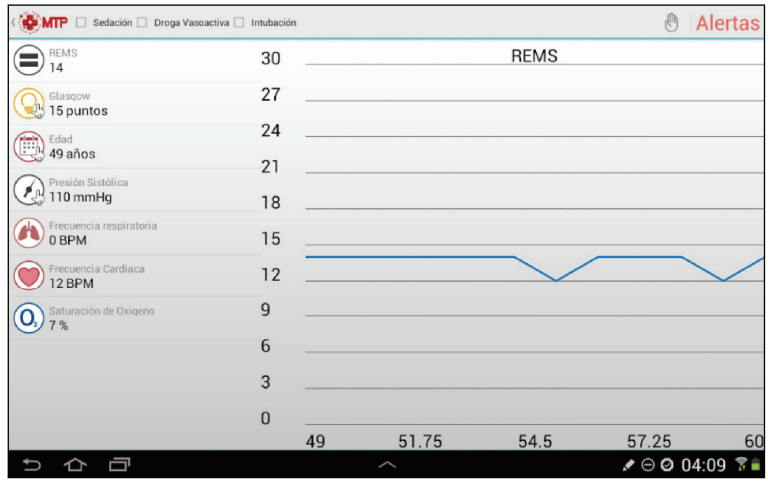

Figure 8: Ambulance mobile application.

displaying the current values of the REMS and its parameters. On the right side, there is a chart showing the tendency over time for the REMS. Selecting a specific parameter on the left in order to observe its own tendency in the chart is possible. At the top, there is a list of checkboxes that allows the paramedics to select special conditions that a patient could have. Finally, at the top right, one can observe alerts that are generated when potential risky situations are detected.

In addition, this application supports an optional Google Glass peripheral. The main advantage of Google Glass over other user interfaces such as smartphones is the ability to interact with it without the use of one's hands. For instance, during an emergency, the paramedics' attention must be centered on the patient and should have their hands free to attend to him. The paramedic would be able to take a picture of a medical case using the camera mounted on the Google Glass peripheral (see Figure 9). Google Glass sends the image to doctors in health facilities in order to receive indications of what procedure to follow. Thus, with Google Glass, paramedics can focus their full attention on the patient while the relevant information is delivered directly in front of their eyes.

5.6. Embedded Devices. The embedded application is designed to enhance the process of collecting data from wearable vital sign sensor devices. The sensor platform is composed of two components, the sensor device itself and a mobile application focused on vital sign monitoring and communication with the cloud platform.

Figure 10 shows the configuration of the different shields used by the platform. An Arduino Uno and an e-Health Sensor Shield v2.0 were used to support the retrieval of data from the corresponding sensors. In particular, an SpO2 sensor (see Figure 11(a)) was used for reading pulse and blood oxygen levels, while an airflow sensor (see Figure 11(b)) was used for calculating breathing rate. The SpO2 sensor is mounted on a finger of the patient. The airflow sensor is mounted on the head of the patient, with the sensor itself in the nose. These sensors were connected to the e-Health Shield through a wired connection. The e-Health Shield was

(a) (b)

Figure 9: (a) Paramedics using Google Glass while attending to the patient in the ambulance; (b) information displayed on Google Glass.

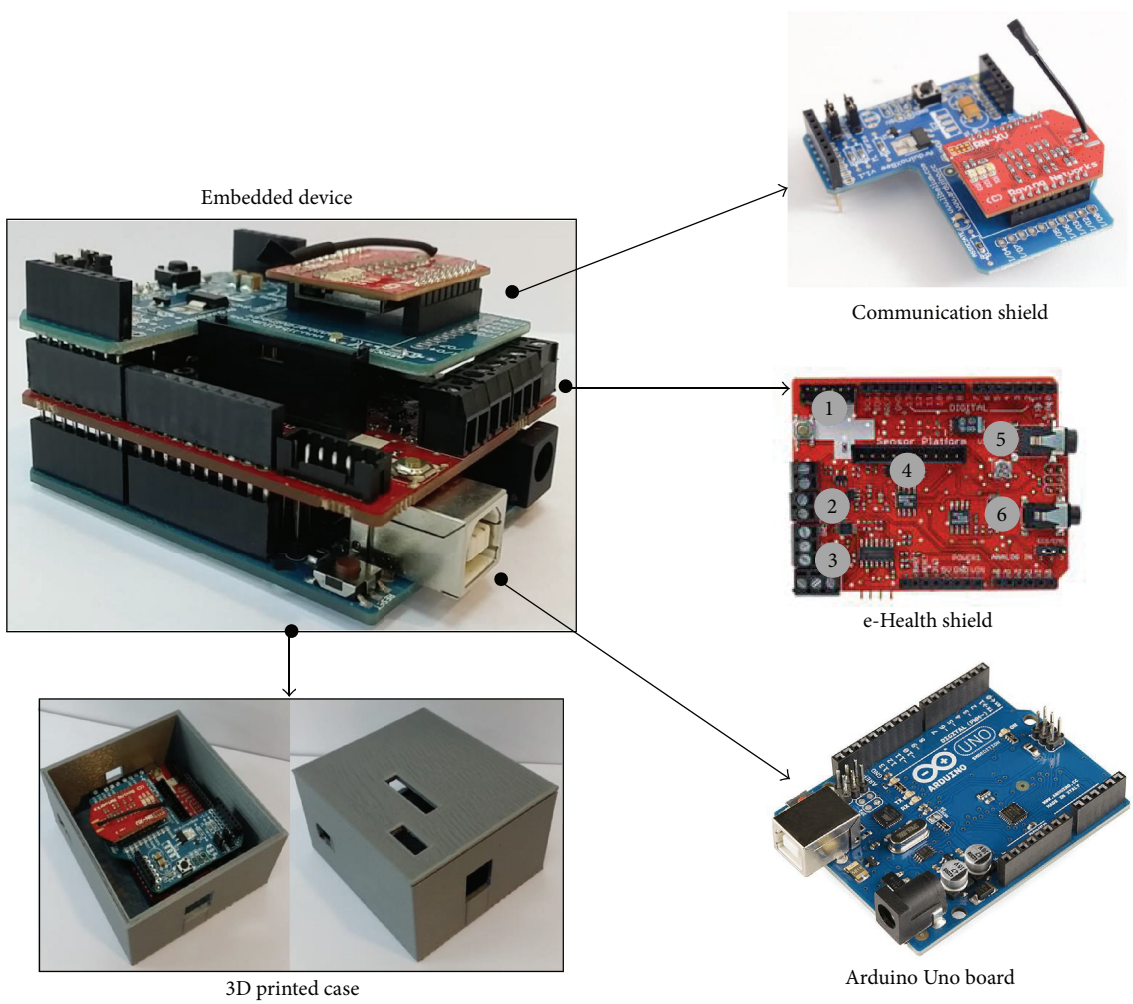

(1) Body position connector
(2) Airflow connector
(3) 3-channel ECG connector
(4) Pulse oximeter connector
(5) Blood pressure connector
(6) Temperature connector

Figure 10: Configuration of the shields. From bottom to top: Arduino Uno, e-Health Sensor Shield, xBee Shield, and RN-XV WiFly module.

(a) (b)

Figure 11: (a) SpO2 sensor and (b) airflow sensor.

(a) (b)

Figure 12: Testing the proposed cloud-based mobile system: (a) SAMU ambulance and paramedics; (b) sensors and the mobile device in the SAMU ambulance.

mounted on the Arduino Uno, which was programmed to receive data and send it through Wi-Fi and the UDP protocol to the mobile device, using an xBee Shield and the RN-XV WiFly module.

The main advantage of the proposed setup versus the current equipment used by medical services is the low cost. Not only is every component of the arrangement available at very low prices, but each one of them is independent from the other. Therefore, eventual malfunctions that affect individual modules will not compromise the rest and the embedded device can continue to function while the defective module is replaced.

Two important constraints were present with regard to the sensors. The first was the fact that no blood pressure sensor that could send data wirelessly was available at the time the prototype was built. For this reason, this data had to be collected using the standard equipment available at the ambulance and entered manually into the mobile application. Nevertheless, it is possible to create automated blood pressure cuffs compatible with Arduino using very basic electronic components; we did not include one due to time concerns. The second constraint was that currently no respiratory rate sensor exists for Arduino. We managed to circumvent this limitation by adapting the readings of an airflow sensor. Our system takes airflow measurements every 50 milliseconds and infers whether it corresponds to the patient inhaling or exhaling. With enough measurements over time, it is easy to estimate breathing rate.

5.7. Results of Testing the Cloud-Based Mobile System. In order to test the system in a real environment, we performed a transfer of a simulated patient in an actual ambulance used for secondary transfers. Three paramedics were on board, while the rest of health professionals stayed at the office monitoring the transfer through the Web application (see Figure 12(a)). Continuous communication was established in order to compare the information in the mobile device to the information in the Web application. Figure 12(b) shows pictures of the sensors and the mobile device in use during a simulated transfer. The Arduino is in the gray box shown in the first image, while the mobile device is in the hands of a paramedic shown in the second picture. The second picture also shows the current equipment available in ambulances for monitoring the patient's health state.

The ambulance's path was approximately 6 km long, at points going behind hills in order to test the signal strength. The simulation called for an unconscious patient; therefore, Glasgow was assigned a score of 4 on the REMS. The simulated patient was also under respiratory assistance, giving a score of 4 for respiration rate. Thus, the initial REMS was 8, assuming that all the other parameters were evaluated with a score of 0.

The sensors were connected to the patient during the journey. Blood pressure readings were taken every five minutes and were updated manually in the mobile device. With the data, it was possible to observe how the REMS

changed due to variations in heart rate as well as changes in blood pressure.

In terms of the usability and performance of the system, the sensor platform performed favorably compared to the sensors available on the ambulance. In fact, the readings were almost the same throughout the journey. One negative aspect was the fact that the heart rate sensor occasionally lost connection due to the vibrations that occur during ambulance transfers. The connection was interrupted for about 5 seconds and was therefore not critical. According to paramedics, these disconnections also occur with the sensor platform currently available on ambulances.

On the other hand, the mobile application gave constant feedback on the state of the patient in REMS terms via charts. The information was successfully sent to the cloud in real time around 98% of the time. The rest of the data was delivered with some delay due to the nature of mobile network signal. Nevertheless, since the downtime of the network was insignificant compared to its uptime, this was not considered an issue.

Another important aspect is the fact that the mobile application was capable of detecting disconnected sensors. When this occurred, the system assigned the worst possible score to REMS parameters, which was reflected as peaks in the REMS chart. The system also generated corresponding alerts, which prompted paramedics to check the devices. The Web application allowed the observation and analysis of information about the transfer in real time without issues. The tendency of the parameters was displayed in charts, as well as the generated alerts.

6. Discussion and Conclusions

This paper presents a novel low-cost cloud-based mobile system for assisting clinical decision-making in high-risk patients undergoing interhospital transfers. It has proven to be reliable enough to promote communication and collaboration between paramedics and in-hospital medical staff when mobile networks are available and to provide a valuable indicator of a patient's status when they are not. The usage of Google Glass has also shown promising results, despite the hardware's lack of maturity, and we expect to refine these solutions with future iterations of the Glass device. While battery life in this case was deemed to be impractical, paramedics have shown a favorable attitude towards the practical applications of Google Glass should this issue be resolved.

In terms of performance, the sensor platform was able to accurately read the required parameters with a low disconnection rate and rapid recovery when such disconnection errors occurred. The mobile application was able to receive the data at a fast rate, perform calculations, and send the data to the cloud without major problems. It was able to provide the data to the cloud in real time during approximately 98% of the transfer.

The Web application was able to show the information sent by the mobile device and update it in real time, allowing the paramedic to track the state of the patient efficiently while the transfer was made. Requirements for this component included the upkeep of several simultaneous ambulance transfers, each one sending data at a high transfer rate. Using a NoSQL database increased the performance of the application significantly.

In terms of usability, both the mobile and Web applications provided the information in a way that was easy to read for paramedics, and they are expected to be useful for conducting future studies. With regard to the sensor platform, it was found that the sensor wires were rather short and that extending them can improve usability.

Our current prototype fulfills all the requirements to stand on its own as an MVP. Unfortunately, we have so far been unable to move forward towards real applications due to the lack of medical certification of our embedded sensors. Due to this, we have been unable to proceed with practical tests as there are ethical and legal concerns amongst hospital administrators. However, it must be stressed that our tests have shown very little variation between our equipment and that used by SAMU's ambulances. In theory, they should produce similar results.

In the future, we hope to integrate approved medical equipment in order to make this final step. Additionally, we expect to include more wireless sensors in the system in order to broaden the benefits of the platform. 12-channel ECG, for example, is widely used by paramedics and doctors to help diagnose a patient. By using the available hardware in today's smartphones, we should also be able to add real-time conferencing functionalities whenever possible. With additional work, we can expect to make this system affordable and robust enough to be included in any ambulance and flexible enough to be connected to several emergency systems. One in particular we are currently studying is the interregional transfer system. It is often the case in southern Chile that there is no road access to some of the more remote locations. In dire situations (natural catastrophes, industrial accidents), ambulances become unavailable due to the collapse of SAMU in the face of a large influx of patients. For instance, on September 16, 2015, an 8.4 magnitude earthquake hit northern Chile. Urban emergency transportation vehicles were insufficient to attend to all the injured and airplanes had to be used as a last resort to carry the wounded (see Figure 13). The use of air and sea transportation vehicles in these kinds of scenarios is not uncommon, yet obviously there is no Internet access through conventional mobile networks in such situations. As a possible solution, we are looking into satellite networks in order to circumvent this constraint and incorporate this platform in airplanes and ships.

In summary, we believe that the evidence obtained from research data generated within real transfers can increase the quality, effectiveness, and efficiency of decisions in patient care. Based on epidemiological needs and prevalence, we identify a need to create risk profiles of patients treated in the health system, which would allow us to characterize risk groups and develop strategies aimed at preventing health problems and complications during transfers. A cloud service information database built on top of predictive analysis

Figure 13: Interhospital transfers performed by airplane.

solutions will quickly identify the groups most at risk, such as patients in extreme old age, generating new severity scales for such groups.

Disclosure

The present paper is an extended and revised version of a paper presented at the 9th International Conference on Ubiquitous Computing and Ambient Intelligence (UCAmI 2015) [31].

Competing Interests

The authors declare that there is no conflict of interests regarding the publication of this paper.

Acknowledgments

This work was partially supported by VRI-PUC Interdisciplinary Grant no. 03/2013, FONIS 2014 SA 12I2045 CONICYT, and SAMU. Finally, we would like to thank all students from the Department of Computer Science and Nursing School at Pontificia Universidad Católica de Chile who were involved in this research project.

References

[1] M. J. Carrillo Barrera, C. Jerez, A. Cortéz et al., "Traslado interhospitalario samu área metropolitana: En búsqueda de una mejor calidad de atención," FONIS SA12I2045, 2014.

[2] D. Sethi and S. Subramanian, "When place and time matter: how to conduct safe inter-hospital transfer of patients," *Saudi Journal of Anaesthesia*, vol. 8, no. 1, pp. 104–113, 2014.

[3] B. M. J. Carrillo and S. M. T. Urrutia, "Perfil de riesgo de pacientes adultos sometidos a traslado secundario por móviles avanzados del sistema de atención médica de urgencia del Área metropolitana," *Revista Médica de Chile*, vol. 140, no. 10, pp. 1297–1303, 2012.

[4] S. Pavlopoulos, E. Kyriacou, A. Berler, S. Dembeyiotis, and D. Koutsouris, "A novel emergency telemedicine system based on wireless communication technology—AMBULANCE," *IEEE Transactions on Information Technology in Biomedicine*, vol. 2, no. 4, pp. 261–267, 1998.

[5] K. Hung and Y.-T. Zhang, "Implementation of a WAP-based telemedicine system for patient monitoring," *IEEE Transactions on Information Technology in Biomedicine*, vol. 7, no. 2, pp. 101–107, 2003.

[6] G. Mandellos, D. Lymperopoulos, M. Koukias, A. Tzes, N. Lazarou, and C. Vagianos, "A novel mobile telemedicine system for ambulance transport. Design and evaluation," in *Proceedings of the IEEE 26th Annual International Conference of the IEEE EMBS*, vol. 2, pp. 3080–3083, San Francisco, Calif, USA, 2004.

[7] E. Sutjiredjeki, S. Soegijoko, T. L. R. Mengko, and S. Tjondronegoro, "Development of a mobile telemedicine system with multi communication links for urban and rural areas in Indonesia," in *3rd Kuala Lumpur International Conference on Biomedical Engineering 2006: Biomed 2006, 11–14 December 2006 Kuala Lumpur, Malaysia*, vol. 15 of *IFMBE Proceedings*, pp. 660–663, Springer, Berlin, Germany, 2007.

[8] Y. Chu and A. Ganz, "A mobile teletrauma system using 3G networks," *IEEE Transactions on Information Technology in Biomedicine*, vol. 8, no. 4, pp. 456–462, 2004.

[9] M. J. Kwak, J. M. Kim, I. H. Shin et al., "Real-time medical control using a wireless audio-video transmission device in a prehospital emergency service in Korea," *Journal of Telemedicine and Telecare*, vol. 15, no. 8, pp. 404–408, 2009.

[10] G. Fortino, D. Parisi, V. Pirrone, and G. Di Fatta, "BodyCloud: a SaaS approach for community body sensor networks," *Future Generation Computer Systems*, vol. 35, pp. 62–79, 2014.

[11] G. Fortino, S. Galzarano, R. Gravina, and W. Li, "A framework for collaborative computing and multi-sensor data fusion in body sensor networks," *Information Fusion*, vol. 22, pp. 50–70, 2015.

[12] A. Bourouis, M. Feham, and A. Bouchachia, "Ubiquitous mobile health monitoring system for the elderly (UMHMSE),"

International Journal of Computer Science and Information Technology, vol. 3, no. 3, pp. 74–82, 2011.

[13] A. K. Triantafyllidis, V. G. Koutkias, I. Chouvarda, and N. Maglaveras, "A pervasive health system integrating patient monitoring, status logging, and social sharing," *IEEE Journal of Biomedical and Health Informatics*, vol. 17, no. 1, pp. 30–37, 2013.

[14] C.-F. Lin, "Mobile telemedicine: a survey study," *Journal of Medical Systems*, vol. 36, no. 2, pp. 511–520, 2012.

[15] M. C. Batistatos, G. V. Tsoulos, and G. E. Athanasiadou, "Mobile telemedicine for moving vehicle scenarios: wireless technology options and challenges," *Journal of Network and Computer Applications*, vol. 35, no. 3, pp. 1140–1150, 2012.

[16] C. Doukas, T. Pliakas, and I. Maglogiannis, "Mobile healthcare information management utilizing cloud computing and android OS," in *Proceedings of the 32nd Annual International Conference of the IEEE Engineering in Medicine and Biology Society (EMBC '10)*, pp. 1037–1040, Buenos Aires, Argentina, September 2010.

[17] H. T. Dinh, C. Lee, D. Niyato, and P. Wang, "A survey of mobile cloud computing: architecture, applications, and approaches," *Wireless Communications and Mobile Computing*, vol. 13, no. 18, pp. 1587–1611, 2013.

[18] H.-K. Kim, "U-healthcare enterprise frameworks for mobile applications," *International Journal of Bio-Science and Bio-Technology*, vol. 7, no. 1, pp. 207–218, 2015.

[19] T. Olsson and L. Lind, "Comparison of the rapid emergency medicine score and APACHE II in nonsurgical emergency department patients," *Academic Emergency Medicine*, vol. 10, no. 10, pp. 1040–1048, 2003.

[20] M. Bulut, H. Cebicci, D. Sigirli et al., "The comparison of modified early warning score with rapid emergency medicine score: a prospective multicentre observational cohort study on medical and surgical patients presenting to emergency department," *Emergency Medicine Journal*, vol. 31, no. 6, pp. 476–481, 2014.

[21] B. F. Imhoff, N. J. Thompson, M. A. Hastings, N. Nazir, M. Moncure, and C. M. Cannon, "Rapid Emergency Medicine Score (REMS) in the trauma population: a retrospective study," *BMJ Open*, vol. 4, no. 5, Article ID e004738, 2014.

[22] B. M. J. Carrillo, *Deterioro fisiopatológico y mortalidad, de los pacientes adultos sometidos a traslado interhospitalario a Unidades de Paciente Crítico por móviles del Servicio de Atención Médica de Urgencia del área Metropolitana, Santiago de Chile [Ph.D. thesis]*, Universidad de Sao Pablo, 2015.

[23] A. Weintraub, "Lean startup lessons for healthcare businesses," February 2014, http://www.entrepreneur.com/article/230862.

[24] K. Juréen, *The lean healthcare entrepreneur: is the lean startup methodology applicable when facing a healthcare challenge? [M.S. thesis]*, School of Industrial Engineering and Management, Stockholm, Sweden, 2014.

[25] S. E. P. Silva, R. D. Calado, M. B. Silva, and M. A. Nascimento, "Lean startup applied in healthcare: a viable methodology for continuous improvement in the development of new products and services," in *Proceedings of the 6th IFAC/ACM Conference on Management and Control of Production and Logistics (MCPL '13)*, pp. 295–299, Fortaleza, Brazil, September 2013.

[26] E. Ries, *The Lean Startup*, Crown Business, 2011.

[27] A. Neyem, S. F. Ochoa, J. A. Pino, and R. D. Franco, "A reusable structural design for mobile collaborative applications," *Journal of Systems and Software*, vol. 85, no. 3, pp. 511–524, 2012.

[28] M. R. Rahimi, J. Ren, C. H. Liu, A. V. Vasilakos, and N. Venkatasubramanian, "Mobile cloud computing: a survey, state of art and future directions," *Mobile Networks and Applications*, vol. 19, no. 2, pp. 133–143, 2014.

[29] P. Bahl, R. Y. Han, L. E. Li, and M. Satyanarayanan, "Advancing the state of mobile cloud computing," in *Proceedings of the 3rd ACM Workshop on Mobile Cloud Computing and Services (MCS '12)*, pp. 21–27, ACM, Lake District, United Kingdom, June 2012.

[30] J. S. van der Veen, B. van der Waaij, and R. J. Meijer, "Sensor data storage performance: SQL or NoSQL, physical or virtual," in *Proceedings of the IEEE 5th International Conference on Cloud Computing (CLOUD '12)*, pp. 431–438, IEEE, Honolulu, Hawaii, USA, June 2012.

[31] A. Neyem, G. Valenzuela, N. Risso, J. S. Rojas-Riethmuller, J. I. Benedetto, and M. J. Carrillo, "A cloud-based mobile system for improving vital signs monitoring during hospital transfers," in *Ubiquitous Computing and Ambient Intelligence. Sensing, Processing, and Using Environmental Information*, vol. 9454 of *Lecture Notes in Computer Science*, pp. 467–479, Springer, 2015.

Hindawi Publishing Corporation
Mobile Information Systems
Volume 2016, Article ID 3592581, 10 pages
http://dx.doi.org/10.1155/2016/3592581

Research Article

Power Control in Wireless Sensor Networks with Variable Interference

Michele Chincoli,[1] Aly Aamer Syed,[2] Georgios Exarchakos,[1] and Antonio Liotta[1]

[1]*Electrical Engineering Department, Eindhoven University of Technology, De Zaale, 5612 AJ Eindhoven, Netherlands*
[2]*NXP Semiconductors, High Tech Campus 60, 5656 AG Eindhoven, Netherlands*

Correspondence should be addressed to Michele Chincoli; m.chincoli@tue.nl

Received 17 March 2016; Revised 20 May 2016; Accepted 8 June 2016

Academic Editor: Sergio F. Ochoa

Adaptive transmission power control schemes have been introduced in wireless sensor networks to adjust energy consumption under different network conditions. This is a crucial goal, given the constraints under which sensor communications operate. Power reduction may however have counterproductive effects to network performance. Yet, indiscriminate power boosting may detrimentally affect interference. We are interested in understanding the conditions under which coordinated power reduction may lead to better spectrum efficiency and interference mitigation and, thus, have beneficial effects on network performance. Through simulations, we analyze the performance of sensor nodes in an environment with variable interference. Then we study the relation between transmission power and communication efficiency, particularly in the context of Adaptive and Robust Topology (ART) control, showing how appropriate power reduction can benefit both energy and spectrum efficiency. We also identify critical limitations in ART, discussing the potential of more cooperative power control approaches.

1. Introduction

Wireless sensor networks (WSNs) are gaining significant attention from institutions, entrepreneurs, and researchers alike, due to the promising and innovative applications in the context of Internet of Things (IoT) and due to the lowering cost of the components, which enables a widespread deployment. Practical scenarios can be categorized in three main groups: rural, urban, and indoor. In rural environments, the sensor nodes are spread discontinuously in vast areas such as battlefields, natural sites, and farmlands, for the purpose of monitoring, surveying, and management. WSN deployments in urban scenarios denote the increasing demand for more efficient cities, which are increasingly expected to provide high-tech services to the citizens (commonly referred to as Smart City). Last category comprehends indoor scenarios and embraces wireless network installations in buildings (e.g., home, office, and shopping mall) [1]. Such areas may be smaller than in the previous cases, but, on the other hand, the density of the sensor nodes may be much higher. As for Smart Cities, also here it is very important to accurately monitor energy consumption, which helps both the consumers (to be aware of the expenses in real time) and the service provider (to estimate and predict the quantity of resources to provide, e.g., Smart Grids [2]). Home and Building Automation (HABA), as described in [3], will impact the current home architecture and design and even change people's habits. The skeleton of future buildings will see many wires replaced by wireless devices. Electrical household appliances can be collectively managed either by one remote control or by a smart phone. Blinds, heaters, and coolers can adapt autonomously to physical metrics (e.g., temperature, light level, and humidity) and predictable human presence for intelligent future applications [4].

Zigbee is one of the instances that are trying to standardise indoor connected, cooperative systems. Other examples are the WiFi HaLow, WirelessHART, and 6LoWPAN, to mention but a few. Sensor nodes are constrained devices, having low transmission power, battery, memory, and computational capacity [5, 6]. WSNs can comprise a large and growing number of devices, becoming in some cases highly dense in HABA scenarios. The nodes can assume the role of routers,

aggregators, and coordinators. Moreover, in the urban and indoor domains, the sensor nodes are typically combined with actuators, objects that react with specific actions when triggered [7]. The focus of our research lies on the study of indoor scenarios including HABA applications that are based on ZigBee specifications.

WSNs inherit typical problems of other wireless technologies while also having their own complications. The wireless channel is unreliable and variable over space, time, and frequency, providing nondeterministic signal strength [8, 9]. Sensor nodes, within the HABA context, are in the majority of cases static or, at most, barely moved to different positions. Currently, indoor environments contain many WiFi networks, whose power is much higher than the power used by 802.15.4 devices and Bluetooth communications.

Besides the influence of external interference, since sensor nodes may operate in very dense networks, the internal interference is also an important factor. When devices transmit at their highest transmission power, contention can heavily affect the performance of the whole network, in terms of QoS and energy consumption [10]. Simultaneous nearby communications at significant transmission power provoke packet collisions; then retransmissions and Clear Channel Assessment (CCA) fail, with increasing number of access attempts and backoff time [11]. Hence, the transceivers are overused, which causes further battery depletion, packet delay, and packet losses. It is the area where power control can play a crucial role.

The work presented hereafter builds on the preliminary findings introduced in [12]. We have significantly extended our analysis, studying a broader range of cases and the effects of node density and of a fine-grained transmission power variation. Situations with low, intermediate, and high interference have been studied in combination with small, medium, and strong transmission power levels. We show that increasing transmission power toward the maximum is not always a wise solution. At the same time, decreasing the transmission power down to the minimum is not a right solution either. Depending on the network condition, an intermediate transmission power should balance the communication quality of each link. We compare the performance of homogeneous transmission power control (TPC) with Adaptive and Robust Topology (ART) control, as introduced in [13] and further evaluated in [14], under the same conditions. We find that ART reduces the contention, while respecting the Packet Reception Ratio (PRR) constraint. However, our analysis unveils that, in its current formulation and due to lack of collaboration among nodes, ART still fails to meet the combined requirements of power efficiency and spectrum efficiency. Because of the large number of nodes and the complexity of WSNs, a flexible, distributed, and collaborative approach should be preferable, as we previously hinted in [15, 16].

2. Transmission Power Control Protocols

For many years, researchers have been targeting TPC protocols to solve the energy problem relating to good link quality [13, 14, 17–26]. The author of [10] considers a collection of works divided in homogeneous and heterogeneous transmission power configuration of the network components, highlighting why it is important that nodes transmit at different power levels, depending on specific criteria and circumstances. Yet, multihop communications allow signals to travel on a sequence of short distances, employing lower transmission power than direct communications. This contributes to lowering the total energy consumption and the overall contention in the network. Below, we present an overview of some of the most significant methods and elaborate on ART, which is used in our study.

Power Control with Blacklisting (PCBL) requires an initial beaconing phase where all the nodes broadcast a sequence of messages at every transmission power level, while their neighbors record the PRR [18]. Power levels are chosen depending on the required PRR for each link. Unreliable links, those which cannot achieve the required PRR at any transmission power, are blacklisted and are not subsequently used for communication.

In adaptive transmission power control (ATPC) the authors use a linear regression model to obtain the coefficients of the linear relationship and predict the appropriate transmission power, based on the desired Received Signal Strength Indicator (RSSI) threshold [17]. Their goal is to obtain the minimum distinguished transmission power per neighbor bases, while maintaining good link quality. Eventually, a routing table, containing the proper transmission power per link, is built.

On-Demand TPC (ODTPC) is designed to eliminate the bootstrapping phase required by algorithms like PCBL and ATPC, while reducing energy consumption and providing good link quality [19]. ODTPC is based on the assumption that there is a threshold in RSSI that separates good links from intermediate or bad links [27].

Adaptive On-Demand Transmission Power Control (AODTPC) [20] is an attempt to improve the performance of ODTPC under channel fading. While ODTPC reacts to changes in signal strength, AODTPC uses a Kalman filter to estimate future values of RSSI based on past measurements. The advantage of the Kalman filter over other prediction techniques is its lower amount of memory and computation required to store and process the variation of the analyzed variable. The authors show by simulations how the algorithm improves energy savings and node lifetime in comparison to ODTPC.

Hackmann et al. propose ART to reduce power consumption and channel contention in WSNs [13]. The authors choose to rely on packet reception rate (PRR) as link quality estimator, since both RSSI and the Link Quality Indicator (LQI) are demonstrated to be too sensitive to the environment. The study also provides a case in favor of TPC on a per-link basis as a way to reduce network contention in dense networks, demonstrating that lowering the transmission power under high contention can reduce interference and thus increase the average PRR.

In [21], two distributed local algorithms, LMA and LMN, are discussed. The transmission power is chosen based on the "life acknowledge messages," as defined in [21] that are received from the neighbors, which is compared with two

thresholds. The goal is to improve the lifetime of WSNs while keeping the nodes connected.

Another algorithm to enhance the lifetime of the network is described in [22]. In this case, a technique to build a geographical topology is used. Links in Non-Line-of-Sight are excluded and the transmission power is calculated based on the Signal-to-Interference-and-Noise Ratio (SINR) and Received Signal Strength (RSS) targets.

Similarly, in [23] the transmission power is controlled by measuring RSSI to ensure good link quality based on the estimated and reference SINR values. Moreover the authors determine an adaptive Golden Receive Power Range (GRPR) to preserve the performance from the fading variations. Again, comparing RSSI with two thresholds (low and high) set in GRPR, the transmission power is either increased or decreased accordingly.

Energy efficiency is addressed also in [24] where the techniques Hybrid and AEWMA are proposed specifically for WSNs. The first, through a closed control loop that iterates on the available transmission powers, and the second, through calculations using the transmission power, received power and average noise, determine the transmission power level to use for a communication. The results show enhancements in energy savings of up to 57% compared to the case using a fixed power level.

The impact, in terms of energy consumption, of one node on the whole network is studied in [25], where it is suggested that the energy consumed by the whole network is of greater importance than the energy that a node itself consumes.

Authors in [26] introduce a TPC algorithm based on PRR in order to reduce the transmission power and provide sufficient data packet delivery, at the expense of frequent overhead injected in the network. The work is concluded emphasizing the importance of periodic updates of PRR estimation for PRR-based algorithms, although they require higher energy consumption proportional to the frequency of the updates.

A classification is performed instead in [28], in which transmission power control algorithms used for energy efficiency are divided into active and passive techniques. The former consider protocols that may be identified in one among the MAC, Network, or Transport layers. Each protocol aims to improve the energy consumption by adjusting the transmission power. Passive techniques manipulate hardware components (i.e., the radio transceiver) while a sensor node is supposed to either transmit, receive, or stay idle [29]. The authors emphasize the importance of QoS of real applications in TPC algorithms.

Compared to earlier work, our main contribution is to investigate the applicability of TPC in WSNs to mitigate interference, which results in communication improvements and, consequently, also in energy reduction. We change transmission power over time, aiming for the minimum whenever possible, by taking into account PRR requirements.

3. ART Description

Among the above discussed works, we chose to analyze ART for different reasons. Firstly, as it is asserted in [13, 30, 31], RSSI is a good indicator only when PRR is very high. Otherwise, RSSI alone cannot provide reliable information. For this reason, we prefer to use PRR (as ART does) as direct link quality estimator (LQE). Secondly, ART considers contention reduction along with energy efficiency, although only PRR is analyzed as performance indicator in the network. Ultimately, the overhead of extra control messages is avoided calculating PRR at the transmitter side, exploiting Acknowledgements (ACKs) reception.

ART is a PRR-based TPC algorithm implemented at the transmitter side and can be used to reduce energy consumption and contention. It works on a per-link basis. Considering node pairs, one transmitter and one receiver, a stream of data is transmitted. The packets have fixed size and are generated periodically at an interarrival time μ. The transmission power, P_{tx}, can assume different values distributed in discrete levels provided in the radio transceiver. When a packet is correctly received, an ACK is sent back for confirmation. PRR is calculated as the ratio of the number of received packets over transmitted packets, within a window W of N transmitted packets. In this case, the number of received packets is considered equal to the number of received ACKs. Then, PRR is compared with two thresholds, η_l and η_h, chosen in order to keep it in the specified range of values. η_l in [13] is calculated as the product of the window size and PRR target p ($\eta_l = N * p$). Similarly $\eta_h = N * p'$, where p' represents PRR upper bound as the maximum acceptable performance by the system. Tuning P_{tx} to the lowest power, the failures should be kept under the threshold $1 - \eta_l$. Following the experiments of the authors in [13], because of the bimodal relationship between PRR and P_{tx}, decreasing the power may lead to a PRR lower than p. For this reason, the authors have introduced a trial state, following a reduction of power level, to evaluate the effects on the PRR. In this case, if the number of failures in W is higher than $(1 - \eta_h) \cdot N$, the calculation of PRR is stopped, the previous P_{tx} is restored, and W is flushed. Otherwise, if the trial is successful, the new power is confirmed. Moreover, ART protocol provides a gradient-based mechanism to monitor the contention on a link, which is enabled when PRR is lower than η_l. Thus, if the contention is low, P_{tx} is increased; otherwise P_{tx} is decreased. In our implementation, we have disabled this mechanism, in order to analyze the outcome in preferring high transmission powers. Figure 1 shows the Finite State Machine (FSM) of our examined ART version. If PRR is greater than η_h, P_{tx} is decreased by one level; otherwise, if PRR is lower than η_l, P_{tx} is raised by one level. In any other case, P_{tx} stays constant. After the comparison, W is flushed and the calculation starts again. Algorithm 1 provides a pseudocode specification of ART.

4. Evaluation

4.1. Experimental Setup. Simulations are used to investigate a broad range of scenarios to achieve statistical significance and repeatability while having more control over the networks' behavior. In our setup, we monitor the performance of a pair of sensor nodes (used as probes) placed in the center of a variable grid of other sensor nodes, used as interferers (Figure 2). Every cell of the grid contains a point-to-point

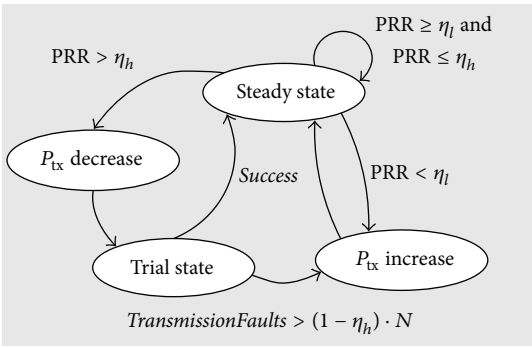

Figure 1: Finite State Machine of the protocol ART.

```
    Generate W with size N
    i = 1
(3) while Packet is generated do
      if Packet loss then
        W[i] ← 0
(6)   else
        W[i] ← 1
      end if
(9)   i ← i + 1
      if i == N + 1 then
        PRR ← Σ_{i=1}^{N} W[i]/N
(12)    if PRR > η_h then
          P_tx ← P_tx − 1
          Enter in Trial State
(15)      if TransmissionFaults > (1 − η_h) · N then
            P_tx ← P_tx + 1
          end if
(18)    else if PRR < η_l then
          P_tx ← P_tx + 1
        end if
(21)    Flush W and start new PRR calculation
        i ← 1
      end if
(24) end while
```

Algorithm 1: ART pseudocode specification.

communication between one transmitter and one receiver. The relative distances between adjacent transmitters are indicated as Δx and Δy, respectively. The relative distance within transmitter-receiver pairs, d, is set to five meters, which provides a good overall experimental tradeoff. The experiment (simulation) parameters and settings are summarized in Table 1.

We modeled transceivers with a sensitivity S of −95 dBm and 22 different transmission power levels ($P_{tx}^{(lev)}$) comprised between −35 dBm and 10 dBm. The default transmission power is 0 dBm. The transmission of the ACK packets is not involved in the TPC process, so their transmission power is set to the value specified at that instant. The PHY and MAC are based on the IEEE 802.15.4 standard and the radio transceiver operates at the 2.45 GHz frequency, employing Direct Sequence Spread Spectrum (DSSS) and

Table 1: Experimental setup for simulations.

Parameter	Symbol	Value
Sensitivity	S	−95 dBm
Packet interarrival time	μ	100 ms
Packet size	s	50 bytes
Transmission power levels	$P_{tx}^{(lev)}$	22
Number of retransmissions		3
Number of CCA attempts		4
Transmitter buffer size		∞
Grid horizontal gap	Δx	5–300 m
Grid vertical gap	Δy	5–300 m
Distance within transmitter-receiver pairs	d	5 m
PRR window	W	100
PRR moving factor	W^{mov}	100
Minimum transmission power	MinPow	−35 dBm
Intermediate transmission power	InterPow	−18.42 dBm
Default transmission power	DefPow	0 dBm
Maximum transmission power	MaxPow	10 dBm
Network interferer density	LowDense	2 pairs
	MidDense	16 pairs
	HighDense	36 pairs
ART		
Low threshold	η_l	95%
High threshold	η_h	99%
Transmission power scale		3.18 dBm
Initial transmission power		0 dBm

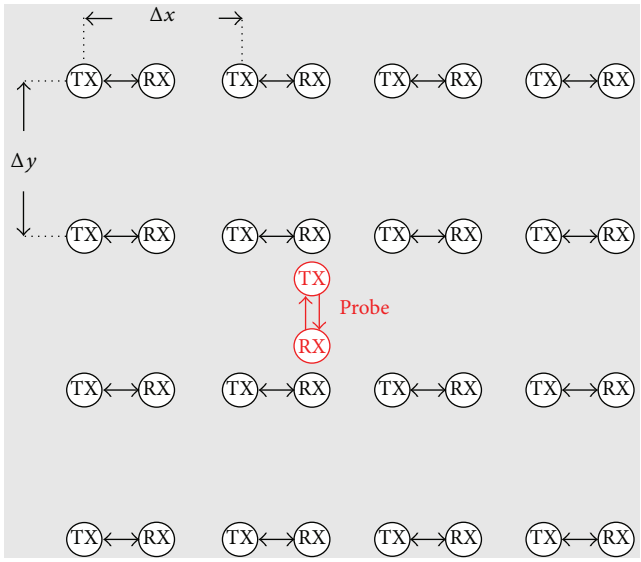

Figure 2: Simulation scenario including two sets of node pairs: one probe (in the middle) and sixteen interferers.

O-QPSK modulation. The simulations are carried out using the NS3 simulator: an open source, scalable, modular, and event-driven simulator, using the module Low Rate-Wireless Personal Area Network (LR-WPAN) from the release ns-3.23. Having a fully implemented reliable model for WSNs, several models for multiple aspects (i.e., path loss, fading, WiFi

interference, and energy), and an active community, among the other features described above, NS3 simulator has been our favorite choice. In this study we have used exclusively the 802.15.4 module, which follows the 2006 version of the standard [11]. We adopted the site-general ITU-R P.1238-7 model in an office environment for large-scale path loss and the Nakagami model for small-scale fading [32]. The antennas were assumed to be ideally isotropic. We considered the unslotted Carrier Sense Multiple Access/Collision Avoidance (CSMA/CA) channel access technique and CCA mode 1, that is, energy above threshold. The maximum number of retries and CCA attempts is set to the default indicated by the standard 802.15.4, equal to three and four, respectively. The transmitter buffer size of the generated packets was set to infinite in order to capture only the packet loss incurred by the CCA fails and collisions.

We consider two sets of simulations. In the first set, we explore three different scenarios: LowDense, MidDense, and HighDense, whereby the number of pairs in the grid is equal to 2, 16, and 36, respectively. Counting also the monitored couple, the network contains a total of 6, 34, and 74 nodes, correspondingly (an exemplary grid with 16 couples is shown in Figure 2). For each scenario, only one homogeneous transmission power is used in the network: the minimum (MinPow), the intermediate (IntPow, −18.42 dBm), and the default transmission power (DefPow). In the second set of simulations, the number of pairs is fixed to 16 and two cases are compared: when ART is enabled and when the constant default transmission power is used. In the former case, the initial transmission power is equal to 0 dBm. All transmitters generate traffic following a Poisson distribution with an average interarrival time μ of 100 ms and a payload size s of 50 bytes. Δx and Δy are varied from 5 to 300 meters; thus the grid can be either stretched or shrunk. In this set of simulations, the intensity of interference is modified by changing the transmission power and the distance of the transmitters in the grid from the probe pair.

The generation and independence of streams of pseudorandom numbers in NS3 can be done in two different ways, either through seed or through number of runs. In the first case, 1.8×10^{19} independent streams can be generated, whereas, in the second one, 2.3×10^{15} independent substreams can be extracted using the same seed. We use substreams to get random independent input to test each individual scenario. In this case, the period of the simulations must be shorter than 7.6×10^{22} random numbers, the period of a pseudorandom subsequence. In each scenario, an amount of around 10,000 packets is generated. The randomness is given by the Nakagami fading model [32], which provides an additive channel loss to the signal and the packet generation. Since the sequence of random numbers is lower than the subsequence period, we use the number of runs as variable. For a specific scenario, we collect the results from 10 simulations with different number of runs and average them for statistical significance.

Assuming the absence of any external interference, we analyze the PRR, latency, number of CCA attempts, and retransmissions of the probe pair. PRR is computed as the number of received ACK messages divided by the number of transmitted packets and the latency as the time interval between the transmission of a message and reception of the related ACK. Latency is only computed for successful transmissions, as it only makes sense when a message is delivered. PRR is calculated in a window of 100 packets.

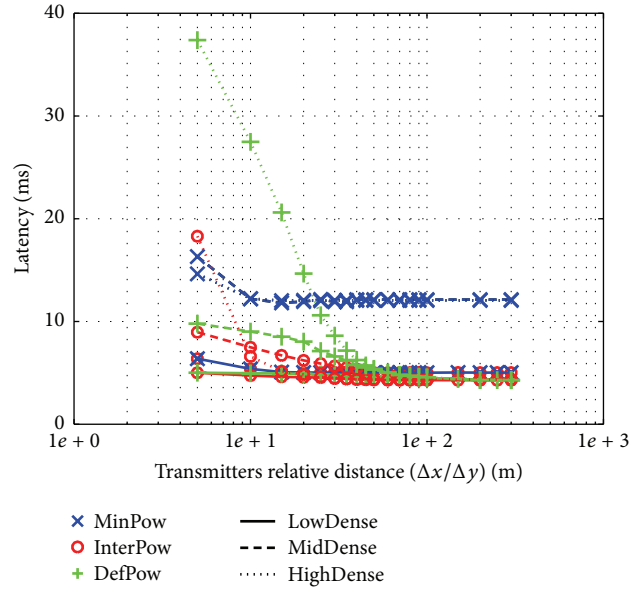

Figure 3: Average latency of the probe pair's traffic using MinPow, InterPow, and DefPow in LowDense, MidDense, and HighDense scenarios.

4.2. Results Using Homogeneous Transmission Power. Here we discuss the effect of varying the transmission power levels and number of nodes in the network. We use the probe pair to measure this effect as described above. The transmission power is kept constant during each simulation scenario and is the same for all the nodes. We compare the performance of the reference couple for the scenarios LowDense, MidDense, and HighDense, described above, in the three cases of different transmission power MinPow, InterPow, and DefPow, while varying Δx and Δy (the distance between the transmitters in the grid).

In Figures 3–6 we present the results, whereby each point is a combination of some of the variable parameters mentioned before. Thus, the level of interference is variable too. For example, we have the lowest interference possible combining LowDense, MinPow, and long distance for Δx and Δy, while we have the highest interference when HighDense and DefPow are used with small Δx and Δy. The interference is referred to the probe pair placed in the middle of the grid. The main idea is to assess the effect of the transmission power in the three different scenarios at different distances. For instance, using very low transmission power, the interference may be detrimental to the monitored nodes. Indeed in Figure 6 the number of CCA attempts is very low in the case of MinPow, below 0.5 and equal to 0 starting from 15 meters, regardless of the node density. At the same time, the number

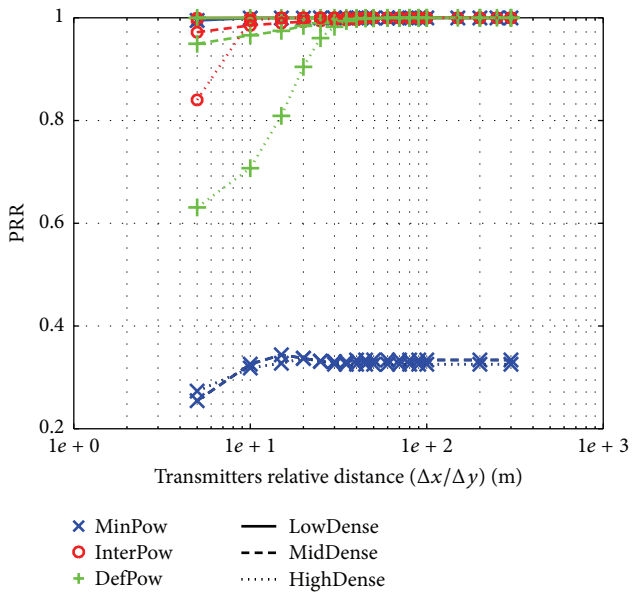

Figure 4: Average packet reception rate of the probe pair's traffic using MinPow, InterPow, and DefPow in LowDense, MidDense, and HighDense scenarios.

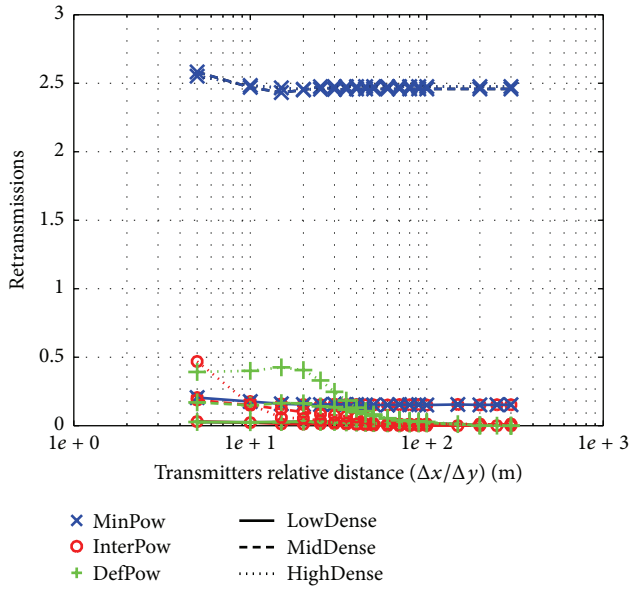

Figure 5: Average number of retransmissions of the probe pair's traffic using MinPow, InterPow, and DefPow in LowDense, MidDense, and HighDense scenarios.

of retransmissions in Figure 5 is very high, around 2.5, with MidDense and HighDense, and low in the case of LowDense. The effect is that, in the former situation, PRR is significantly low around 30% from 10 meters and beyond, and the latency is high, close to 12 ms. While, in the second situation, the latency is 6.5 ms at 5 m of distance flattening to 5 ms and PRR is over 99.5%. Thus, MinPow is a good choice when the interference is weak; otherwise the communications suffer massively the contention.

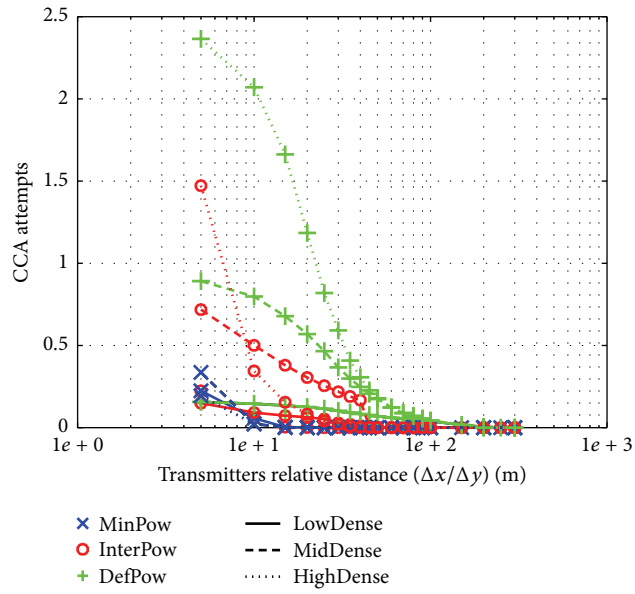

Figure 6: Average number of CCA attempts of the probe pair's transmitter using MinPow, InterPow, and DefPow in LowDense, MidDense, and HighDense scenarios.

The case of DefPow (i.e., P_{tx} = 0 dBm) is different. The worst case scenario happens when many nodes transmit in a dense network (HighDense) where the number of CCA attempts (Figure 6) is as high as 2.3 when Δx and Δy are equal to the minimum, decreasing asymptotically until reaching no contention at 200 meters. Instead when the grid is less populated with nodes, the number of CCA attempts, when the grid is shrunk, is smaller than in the previous case more than one unit in MidDense and more than two units in LowDense. All the three curves meet in zero CCA attempts from 200-meter distance. As expected, the number of retransmissions is highest in HighDense but lower than 0.5. Instead, looking at one value of the distance for Δx and Δy in Figure 5 the number of retransmissions diminishes as less nodes are in the grid. The performance shown in Figures 3 and 4 provides the answer to our claim in this paper. The latency is at its maximum value at 37.5 ms in the case of HighDense, which is reduced to 10 and 5 ms for the other two scenarios MidDense and LowDense. As the distance between the couple goes up, the latency decays consequently. Similarly the PRR is 63.1%, 94.94%, and 99.98% for HighDense, MidDense, and LowDense, respectively, while Δx and Δy are equal to the minimum, increasing up to 100% at 100 meters for all the curves.

Lastly, using the intermediate transmission power, we obtain better results than in the previous cases. Compared to DefPow, the latency and the number of retransmissions and CCA attempts are lower and the PRR is higher, starting with a difference of 20% and 25% in the HighDense scenario at a distance of 5 and 10 meters. While compared in MidDense, PRR is higher, as much as 2% at the beginning, until the values in the two scenarios are the same when Δx is equal to 80 meters. In Figure 3, it is possible to notice the big

difference between the two curves, InterPow and DefPow, especially in HighDense, where the latency differs by about 19 ms, increasing to 21 ms, and finally reduces following the x-axis to the right. Then, although the difference between the two curves in LowDense and MidDense is smaller, InterPow outperformes DefPow in all the scenarios.

Looking at Figures 4 and 3, InterPow is also better than (i.e., MidDense and HighDense) or at least comparable (i.e., LowDense) to MinPow.

The key point of our results is that neither increasing nor decreasing too much the transmission power can provide good performance in the network. But instead, the network should adaptively find its best intermediate P_{tx} in order to reach a global optimum. Moreover we show that increasing the number of nodes, so increasing the amount of traffic in the network, produces more interference and, in turn, the performance of the network worsens. Some solutions are needed to provide reliability to a network in terms of connectivity and Quality of Service (QoS) guarantees. Next, we analyze the behavior of ART in one of the scenarios depicted above.

4.3. Results Using ART. The ART protocol is tested in a network composed of a grid of 16 interfere couples (Figure 2) and one probe pair in the middle. Each node runs ART starting at a transmission power P_{tx} set to 0 dBm. The results are compared with the ones obtained using a homogeneous transmission power as in DefPow. The thresholds are equal to 95% and 99% for the low and high threshold, respectively. The step size to switch from a level of transmission power to another is equal to 20.

In Figure 7 we can see the average transmission power used during the simulations as outcome of ART. In the two closest positions (i.e., 5 and 10 meters) ART pushes the transmitter to use the maximum transmission power equal to 10 dBm. This happens because PRR, using the initial transmission power, does not satisfy the requirements to settle between the thresholds. Following ART policy, P_{tx} is increased. Intuitively, we see that the initial transmission power is an important factor for this purpose. Based on our previous results, the intermediate power level performs better than high P_{tx}. So, setting the initial transmission power to a low value may result in a longer transition time before reaching the right power but, at the same time, may perform better using lower power levels. When Δx and Δy are lowered to 15 meters, we start obtaining benefits in terms of power savings, as the average transmission power is equal to about −24 dBm. It finally stabilizes to −29 dBm as the couples of nodes are moved apart. Therefore the number of CCA attempts is lower than in DefPow (Figure 11) but the number of retransmissions is higher (Figure 10).

In view of the fact that ART's target is to keep PRR between the thresholds, we can notice in Figure 9 that indeed PRR is around 98% from a distance of 15 meters, while it was not at the shortest distance (94.2%). Although PRR values in ART are lower than DefPow, they have been forced by the algorithm to be in the range η_l-η_h and so evaluated acceptable for our setup, gaining transmission power reduction. On

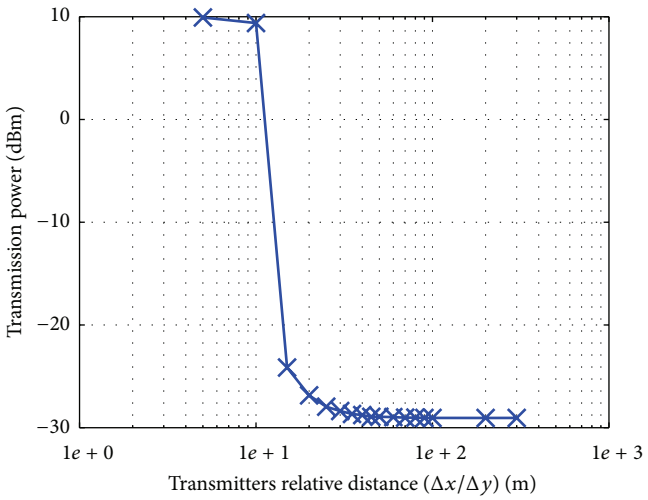

Figure 7: Average transmission power of the probe pair's transmitter using ART.

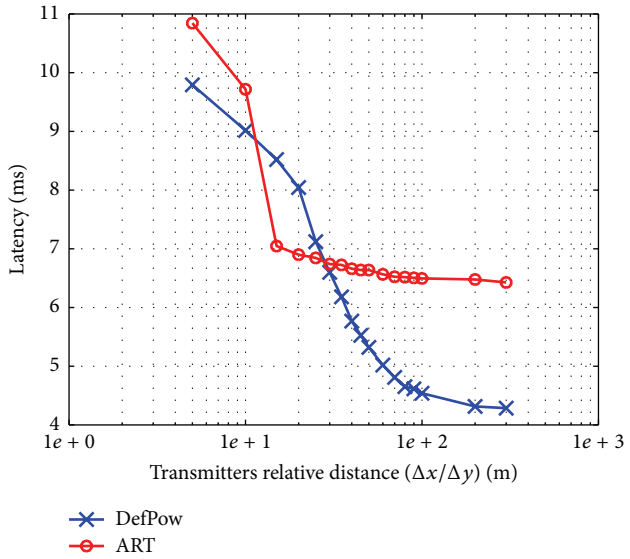

Figure 8: Average latency of the probe pair's traffic using ART and the default transmission power.

the contrary, the latency, which does not have any protocol constraints, is influenced indirectly by the PRR trend. In Figure 8 there are some points in which ART operates better than DefPow (i.e., from 15 to 25 meters). Instead, for instance, from 35 meters of distance, the latency in ART is higher and decreases more slowly than DefPow, reaching around 6.4 ms (against the 4.2 ms in DefPow) at the maximum distance.

5. Conclusions

Through simulations, we have verified our assumptions on the beneficial effects of transmission power reduction on network performance. Firstly, we showed that varying level of interference, represented by the load of nodes and traffic in the network, an arbitrary intermediate power level

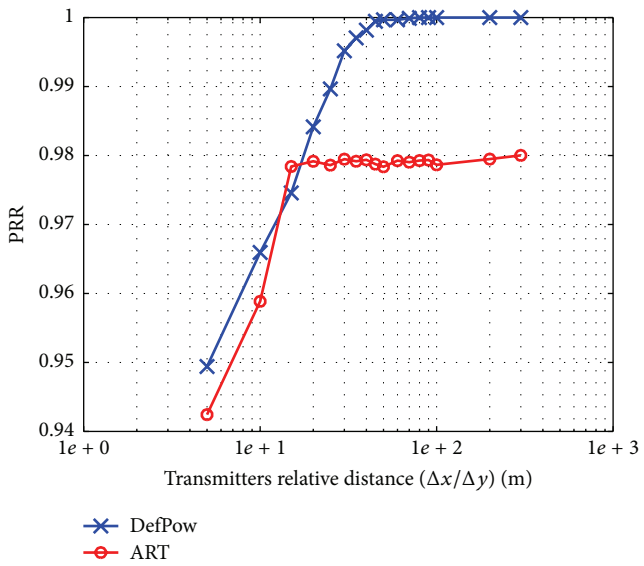

Figure 9: Average packet reception rate of the probe pair's traffic using ART and the default transmission power.

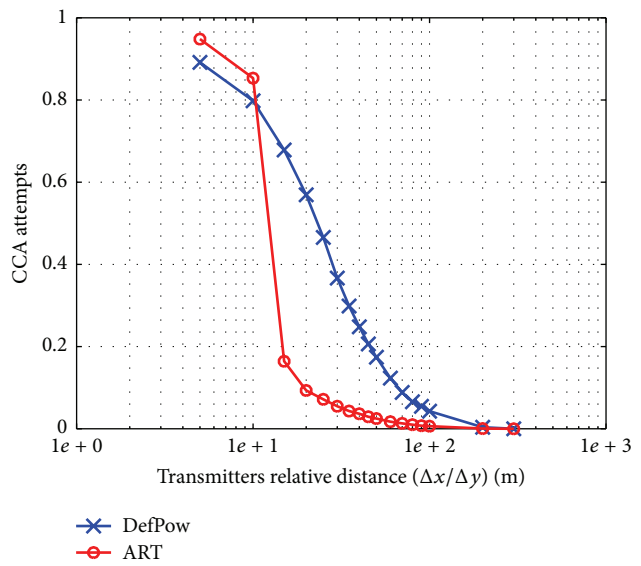

Figure 11: Average number of CCA attempts of the probe pair's transmitter using ART and the default transmission power.

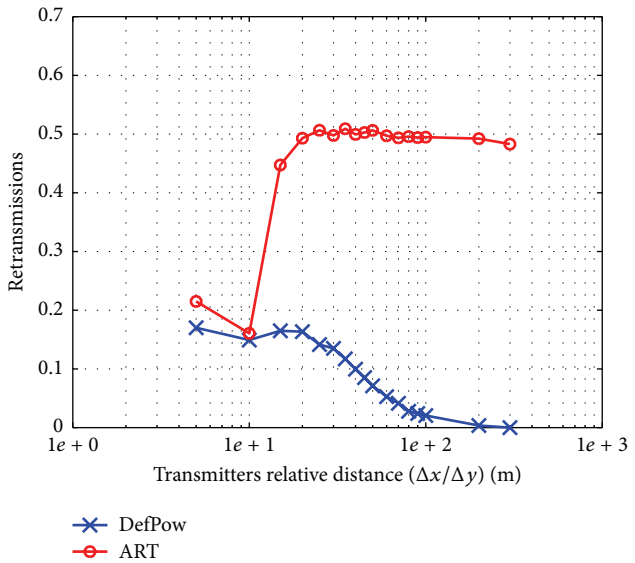

Figure 10: Average number of retransmissions of the probe pair's traffic using ART and the default transmission power.

outperforms the lowest and close to the highest transmission powers. This verifies that, under certain conditions, increasing transmission power does not necessarily lead to better performance. In fact, by lowering transmission power it is possible to reach an intermediate level that maximizes the overall network performance.

Intuitively, one would want a control protocol that keeps the nodes at minimum power to simultaneously pursue energy and spectrum efficiency. However, finding the bottom-line power which avoids loosing connectivity is not straightforward. That is why we believe that a promising research direction is to look at protocols that are smart [16] rather than deterministic [9].

We also observed that, compared to the situation in which the transmission power was always set to the default 0 dBm, ART achieved lower transmission power and maintained PRR in the required range. On the other hand, there are still many aspects to take into consideration to improve the algorithm. For example, ART does not consider latency requirements, nor does it fulfill them; thus it cannot guarantee QoS. The initial transmission power is relevant to the transition time used to research the right power. Plus, when PRR is not guaranteed, a lower transmission power may be more beneficial than just increasing by one or more levels as indeed is taken into account in the original version of ART through a flag related to the level of contention [13].

Moreover, the step size of transmission power levels is another variable to examine. On the one hand, a small gap provides more power levels options, which may help finding the best tradeoffs between energy and spectrum efficiency. On the other hand, greater granularity may lead to slow transients. Instability is another issue linked with power changes.

A major limitation of current adaptive protocols such as ART is their lack of collaboration among nodes. ART operates only on a per-link basis and the transmission power is set considering only the information gathered from the associated receiver. Collaborative, smart protocols have the potential to lead to the most significant breakthroughs and this is the direction we are going to explore next.

A promising direction is to explore self-learning methods and algorithms that may be implemented directly in the nodes, with the aim of allowing the sensor network to gradually determine the actions that lead to any given goal. Particularly, distributed, collaborative methods have the potential to use localized, in-node information towards global goals. Our first move will be to verify performance, convergence, and stability of learning-based methods and implement a pilot prototype.

Competing Interests

The authors declare that there is no conflict of interests regarding the publication of this paper.

Acknowledgments

This work was jointly supported by NXP Semiconductors and Eindhoven University of Technology within the IMPULS program and by the EU INTER-IoT project (Grant 687283).

References

[1] G. Fortino, A. Guerrieri, G. M. P. O'Hare, and A. Ruzzelli, "A flexible building management framework based on wireless sensor and actuator networks," *Journal of Network and Computer Applications*, vol. 35, no. 6, pp. 1934–1952, 2012.

[2] A. Liotta, D. Geelen, G. van Kempen, and F. van Hoogstraten, "A survey on networks for smart-metering systems," *International Journal of Pervasive Computing and Communications*, vol. 8, no. 1, pp. 23–52, 2012.

[3] C. Gomez and J. Paradells, "Wireless home automation networks: a survey of architectures and technologies," *IEEE Communications Magazine*, vol. 48, no. 6, pp. 92–101, 2010.

[4] D. C. Mocanu, H. Bou Ammar, D. Lowet et al., "Factored four way conditional restricted Boltzmann machines for activity recognition," *Pattern Recognition Letters*, vol. 66, pp. 100–108, 2015.

[5] I. F. Akyildiz, W. Su, Y. Sankarasubramaniam, and E. Cayirci, "Wireless sensor networks: a survey," *Computer Networks*, vol. 38, no. 4, pp. 393–422, 2002.

[6] J. Yick, B. Mukherjee, and D. Ghosal, "Wireless sensor network survey," *Computer Networks*, vol. 52, no. 12, pp. 2292–2330, 2008.

[7] I. F. Akyildiz and I. H. Kasimoglu, "Wireless sensor and actor networks: research challenges," *Ad Hoc Networks*, vol. 2, no. 4, pp. 351–367, 2004.

[8] T. S. Rappaport, *Wireless Communications: Principles and Practice*, Prentice Hall, New York, NY, USA, 2002.

[9] A. Liotta, "Farewell to deterministic networks," in *Proceedings of the 19th IEEE Symposium on Communications and Vehicular Technology in the Benelux (SCVT '12)*, pp. 1–4, IEEE, Eindhoven, The Netherlands, November 2012.

[10] P. Santi, "Topology control in wireless ad hoc and sensor networks," *ACM Computing Surveys (CSUR)*, vol. 37, no. 2, pp. 164–194, 2005.

[11] IEEE Computer Society, LAN/MAN Standards Committee, Institute of Electrical and Electronics Engineers, and IEEE-SA Standards Board, *IEEE Standard for Information Technology Telecommunications and Information Exchange between Systems—Local and Metropolitan Area Networks—Specific Requirements. Part 15.4, Part 15.4*, Institute of Electrical and Electronics Engineers, New York, NY, USA, 2006.

[12] M. Chincoli, C. Bacchiani, A. A. Syed, G. Exarchakos, and A. Liotta, "Interference mitigation through adaptive power control in wireless sensor networks," in *Proceedings of the IEEE International Conference on Systems, Man, and Cybernetics (SMC '15)*, pp. 1303–1308, IEEE, Hong Kong, October 2015.

[13] G. Hackmann, O. Chipara, and C. Lu, "Robust topology control for indoor wireless sensor networks," in *Proceedings of the 6th ACM Conference on Embedded Network Sensor Systems (SenSys '08)*, pp. 57–70, ACM, November 2008.

[14] Y. Fu, M. Sha, G. Hackmann, and C. Lu, "Practical control of transmission power for wireless sensor networks," in *Proceedings of the 20th IEEE International Conference on Network Protocols (ICNP '12)*, pp. 1–10, IEEE, Austin, Tex, USA, November 2012.

[15] S. Galzarano, C. Savaglio, A. Liotta, and G. Fortino, "Gossiping-based AODV for wireless sensor networks," in *Proceedings of the IEEE International Conference on Systems, Man, and Cybernetics (SMC '13)*, pp. 26–31, IEEE, Manchester, UK, October 2013.

[16] A. Liotta, "The cognitive NET is coming," *IEEE Spectrum*, vol. 50, no. 8, pp. 26–31, 2013.

[17] S. Lin, J. Zhang, G. Zhou, L. Gu, J. A. Stankovic, and T. He, "ATPC: adaptive transmission power control for wireless sensor networks," in *Proceedings of the 4th International Conference on Embedded Networked Sensor Systems (SenSys '06)*, pp. 223–236, ACM, November 2006.

[18] D. Son, B. Krishnamachari, and J. Heidemann, "Experimental study of the effects of transmission power control and blacklisting in wireless sensor networks," in *Proceedings of the 1st Annual IEEE Communications Society Conference on Sensor and Ad Hoc Communications and Networks (SECON '04)*, pp. 289–298, IEEE, Santa Clara, Calif, USA, October 2004.

[19] J. Kim, S. Chang, and Y. Kwon, "ODTPC: on-demand transmission power control for wireless sensor networks," in *Proceedings of the International Conference on Information Networking (ICOIN '08)*, pp. 1–5, IEEE, Busan, South Korea, January 2008.

[20] M. M. Y. Masood, G. Ahmed, and N. M. Khan, "A Kalman filter based adaptive on demand transmission power control (AODTPC) algorithm for wireless sensor networks," in *Proceedings of the International Conference on Emerging Technologies (ICET '12)*, pp. 1–6, IEEE, Islamabad, Pakistan, October 2012.

[21] M. Kubisch, H. Karl, A. Wolisz, L. C. Zhong, and J. Rabaey, "Distributed algorithms for transmission power control in wireless sensor networks," in *Proceedings of the Wireless Communications and Networking (WCNC '03)*, pp. 558–563, IEEE, New Orleans, La, USA, March 2003.

[22] J.-H. You, J.-H. Jeon, T.-H. Lee, and Y.-G. Kwon, "Transmission power controlled localization with topology building for NLOS environments," *International Journal of Distributed Sensor Networks*, vol. 2014, Article ID 250692, 6 pages, 2014.

[23] W. Ikram, S. Petersen, P. Orten, and N. F. Thornhill, "Adaptive multi-channel transmission power control for industrial wireless instrumentation," *IEEE Transactions on Industrial Informatics*, vol. 10, no. 2, pp. 978–990, 2014.

[24] L. H. A. Correia, D. F. Macedo, A. L. dos Santos, A. A. F. Loureiro, and J. M. S. Nogueira, "Transmission power control techniques for wireless sensor networks," *Computer Networks*, vol. 51, no. 17, pp. 4765–4779, 2007.

[25] L. Xu, D. T. Delaney, G. M. P. Ohare, and R. Collier, "The impact of transmission power control in wireless sensor networks," in *Proceedings of the 12th IEEE International Symposium on Network Computing and Applications (NCA '13)*, pp. 255–258, IEEE, Cambridge, Mass, USA, August 2013.

[26] M. Nikodem, M. Słabicki, T. Surmacz, and B. Wojciechowski, "Transmission power control based on packet reception rate," in *Proceedings of the 6th IEEE International Conference on New Technologies, Mobility and Security (NTMS '14)*, pp. 1–4, Dubai, UAE, April 2014.

[27] M. Zuniga, I. Irzynska, J.-H. Hauer, T. Voigt, C. A. Boano, and K. Roemer, "Link quality ranking: getting the best out of unreliable links," in *Proceedings of the 7th IEEE International Conference on*

Distributed Computing in Sensor Systems (DCOSS '11), pp. 1–8, IEEE, Barcelona, Spain, June 2011.

[28] N. A. Pantazis and D. D. Vergados, "A survey on power control issues in wireless sensor networks," *IEEE Communications Surveys and Tutorials*, vol. 9, no. 4, pp. 86–107, 2007.

[29] S. Galzarano, A. Liotta, and G. Fortino, "QL-MAC: a Q-learning based MAC for wireless sensor networks," in *Algorithms and Architectures for Parallel Processing*, R. Aversa, J. Kołodziej, J. Zhang, F. Amato, and G. Fortino, Eds., vol. 8286 of *Lecture Notes in Computer Science*, pp. 267–275, Springer, Berlin, Germany, 2013.

[30] N. Baccour, A. Koubaa, L. Mottola et al., "Radio link quality estimation in wireless sensor networks: a survey," *ACM Transactions on Sensor Networks (TOSN)*, vol. 8, no. 4, article 34, 2012.

[31] K. Srinivasan, P. Dutta, A. Tavakoli, and P. Levis, "Understanding the causes of packet delivery success and failure in dense wireless sensor networks," in *Proceedings of the 4th International Conference on Embedded Networked Sensor Systems (SenSys '06)*, pp. 419–420, ACM, Boulder, Colo, USA, November 2006.

[32] M. Nakagami, "The m-distribution—a general formula of intensity distribution of rapid fading," in *Statistical Method of Radio Propagation*, Pergamon, Oxford, UK, 1960.

Hindawi Publishing Corporation
Mobile Information Systems
Volume 2016, Article ID 4102163, 11 pages
http://dx.doi.org/10.1155/2016/4102163

Research Article

Design and Implementation of a Vehicle Social Enabler Based on Social Internet of Things

Taehwan Shin[1] and Jinsung Byun[2]

[1]*School of Electrical and Electronics Engineering, Chung-Ang University, 84 Heukseok-ro, Dongjak-gu, Seoul 06974, Republic of Korea*
[2]*Division of Computer Engineering, Dongseo University, 47 Jurye-ro, Sasang-gu, Busan 47011, Republic of Korea*

Correspondence should be addressed to Jinsung Byun; jsbyun@dongseo.ac.kr

Received 23 February 2016; Accepted 3 May 2016

Academic Editor: Sergio F. Ochoa

In recent years, the combination of novel context-aware systems with the Internet of Things (IoT) has received great attention with the advances in network and context-awareness technologies. Various context-aware consumer electronics based on IoT for intelligent and personalized user-centric services have been introduced. However, although the paradigm of the IoT has evolved from smart objects into social objects, the existing context-aware systems have not reflected the changes in these paradigms well. Therefore, this paper proposes a social enabler (S-Enabler) in order to overcome this limitation. The S-Enabler plays an important role in converting the existing objects into social objects. This paper presents the middleware architecture and cooperation processes for a social IoT-based smart system. In this paper, the S-Enabler is designed to be applied to a vehicle and an energy saving service is introduced by using the S-Enabler. The proposed energy saving service can reduce energy consumption and fuel consumption based on social behaviors such as sharing or competition. The performance of the S-Enabler is discussed through a simple vehicle service scenario. The experimental results show that the S-Enabler reduced fuel consumption by up to 31.7%.

1. Introduction

With the development of context-awareness technology, various spaces, such as the home or the office, are becoming smart spaces [1–3]. In smart spaces, for example, various sensors gather the environmental and situational context, and smart systems recognize the user's situations or preferences, and various service providers then serve personalized services to users. Recently, such context-aware systems have been combined with the Internet of Things (IoT).

The IoT is a new ICT (information and communications technology) paradigm, and this paradigm shift is attributed to the advanced connectivity of various things, such as systems, devices, and services. That is, things are able to communicate with each other and provide smart services autonomously. Various IoT-based applications and services have begun to emerge in various areas such as home automation, healthcare, vehicle management, and energy management [4–9]. In the latest consumer product exhibition, various consumer electronics based on IoT that have been newly released also reflect this technical trend.

IoT is evolving continuously, as shown in Figure 1. The early IoT focused on improved interoperability and connectivity of objects (things). These objects are connected objects. In this stage, the standard of communication between objects, network convergence, and the address management of various objects were important issues. The current IoT is focused on interactivity with the surrounding context. In other words, various objects provide intelligent services to users through the interaction with the surrounding context. These objects are smart objects. Recently released smart consumer electronics are types of smart objects with the ability to cooperate with other smart devices and recognize surrounding environments in order to provide smart services. The next step of the IoT is the object socialization. In this stage, the objects can configure their social network themselves and provide more advanced services through the social behavior, such as competition, collaboration, and sharing. These objects are social objects. This paper focuses on a social object and proposes the IoT-based LED car enabler, named a social enabler (S-Enabler), to use connected objects or smart objects as social objects in vehicle environments.

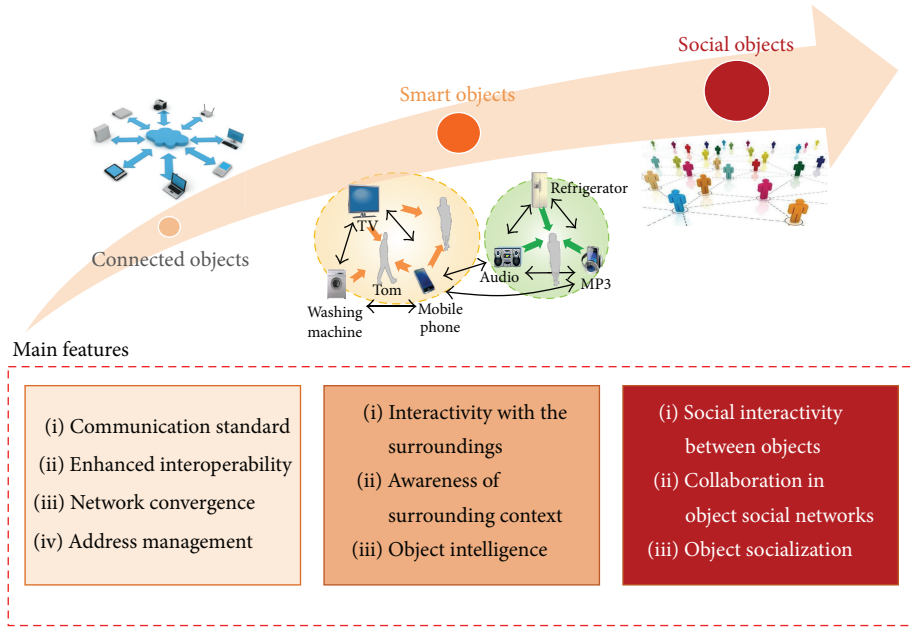

Figure 1: Paradigm of the Internet of Things.

Environmental issues, such as climate change, are threatening humanity. Fossil fuels are being depleted because of a sharp increase in energy consumption. Some environmental experts expect that fossil fuels will be exhausted completely in the not-too-distant future. For this reason, Green ICT has become increasingly essential in recent years. Therefore, this paper presents an energy saving scheme using the S-Enabler. In other words, the proposed energy saving scheme reduces the fuel consumption of a car through social behavior, such as competition, collaboration, and sharing. The S-Enabler has the following features:

(i) *Smart Service Provision Based on Social Behavior in the Social IoT.* In recent years, various consumer devices have been equipped with microprocessors and network transceivers. These devices are part of the IoT and can interact with other devices and provide services to users autonomously, which is called the smart IoT. Furthermore, as described above, the paradigm of the IoT has changed from smart IoT to social IoT. Therefore, the S-Enabler is designed to cooperate with networked devices and utilizes a short-range wireless communication technology, particularly Bluetooth, for establishing the social IoT. This paper also introduces an energy saving service using the S-Enabler based on the social IoT.

(ii) *Management of Multiobjects and Multiroles.* There were many changes in the role of the objects in the IoT. In the past, the object mainly had one-role. This paper calls it one-object one-role (O2OR). For example, a mobile phone was used for communication between people and a sensor was used for gathering environmental information. In recent years, the object has evolved into a multirole-object. That is, the object has various roles. This paper calls it one-object multirole (O2MR). For example, a modern smartphone has various functions, such as communications, social network service (SNS), camera, messenger, and sensor. In the future, the object will have various roles. Furthermore, the object will be able to create various functions by cooperating with other objects. This paper calls it multiobject multirole (MOMR). Therefore, this paper considers this new paradigm of IoT.

(iii) *Dynamic Configuration of a User-Centric Service Domain.* An important feature of the smart space is to configure a service domain around the users. Currently, most spaces have a particular purpose. A user enters into the space in order to receive the particular service. For example, a user exercises in a gym, drives in a car, and works in an office. However, in the future, the convergence of services and spaces will further accelerate. For example, it is possible to receive healthcare services in a car. It is also possible to process work at home. Therefore, the S-Enabler is utilized for configuring the user-centric service domain through the fusion of services and spaces.

The rest of this paper is organized as follows: Section 2 will describe related works of the IoT. This section will describe various technologies related to the IoT and smart services based on IoT. Section 3 will present the background and paradigm of the IoT. Section 4 will present the system architecture and core technologies. Section 5 will present the implementation of the proposed system with the hardware architecture and smartphone application. Section 6 discusses service scenarios and presents some experiments on energy saving. Finally, the conclusion will be given in Section 7.

2. Related Works

2.1. Enabling Technologies for IoT. Recently, enabling technologies for IoT have been widely studied around the world. Cirani et al. [10] proposed a scalable and self-configuring architecture for the IoT. This architecture aimed to provide automated service and resource discovery mechanisms with no human intervention for configuration. Perumal et al. [11] proposed an interoperability framework for the implementation of a smart home based on heterogeneous home networks. This framework utilized the simple object access protocol (SOAP) technology for providing platform-independent interoperation among heterogeneous systems. Wu and Fu [12] proposed a framework in order to improve interactivity between humans and systems. Özçelebi et al. [1] suggested a lightweight system architecture for discovery, monitoring, and management of the objects that form the smart space, such as nodes, services, and resources. In particular, this system architecture was utilized for the limited environment in which the objects had low resource capacity.

2.2. Applications and Services Based on IoT. The topic of development of applications and services based on IoT has been widely studied. Islam et al. [4] reviewed IoT-based healthcare technologies, including network architectures, platforms, and applications, and also presented industrial trends in IoT-based healthcare solutions. Kelly et al. [5] discussed effective implementation for IoT used for environmental condition monitoring in homes based on a low-cost ubiquitous sensing system. Li et al. [6] presented an IoT application in the form of a smart community with cooperating objects (Neighborhood Watch and Pervasive Healthcare). Li and Yu [7] presented the design of a smart home system based on IoT and service component technologies. Chong et al. [8] analyzed the characteristics of a smart home system and designed and implemented a smart home system based on the IoT for the flexible and convenient control of a home system.

2.3. Social IoT. Recently, there have been a lot of research activities integrating social networking concepts into the IoT. Atzori et al. [13] presented the concept, architecture, and network characterization of the social IoT. Their paper proposed the policies for the establishment and the management of social relationships between objects. A possible architecture for the social IoT was also proposed. Mendes [14] presented social-driven Internet of connected objects. The paper discussed the technology for ensuring an efficient interaction among the physical, virtual, and social world. Nitti et al. [15] proposed a subjective model for trustworthiness evaluation based on the social Internet of Things. This model was used for computing the trustworthiness of its neighbors. Guo et al. [16] proposed the opportunistic IoT, which improved the harmonious interaction among humans, society, and smart objects. Their paper presented the innovative application areas and discussed the challenges caused by this new computing paradigm.

As described above, the IoT has been extensively studied. However, the study in this current paper differs in two aspects from the previous works. First, this study applies the new ICT paradigm to design and implement the proposed system. Second, this study presents various smart services in a car through cooperation in the vehicle social network.

3. Paradigm of the Internet of Things

The IoT is a new networking paradigm in which a variety of things (e.g., networked devices, sensors, and actuators) become an integral part of the Internet. In other words, the various things become "smart things" that are equipped with microprocessors and network transceivers, which enable them to communicate with each other and provide smart services autonomously. Various products and service applications of the IoT have started to be released in various areas, such as home automation, energy management, healthcare, and vehicle management. The important features of an IoT-based smart system can be summarized as follows:

(i) First, it improves the capability of collaboration: the IoT-based smart systems can create/provide information and services through collaboration with other smart systems. This is possible owing to intense interactions among smart systems. The IoT-based systems consist of different and heterogeneous objects that can communicate with each other transparently and seamlessly.

(ii) Second, improved situation awareness ability is also an important characteristic: IoT-based smart systems often aim at enhanced recognition of the surrounding environments compared to the existing context-aware systems. With the changes in network paradigms to IoT, the capability of situation awareness can be greatly improved.

(iii) Lastly, it can provide enhanced service quality, such as guaranteeing the quality of experience (QoE): information collected from various objects in the IoT forms big data and it is possible to provide user-centric services by utilizing this big data. It is impossible to communicate with each other and create/provide intelligent services for users autonomously unless the components of the IoT are smart objects. These objects can perform various functions to create/provide intelligent services through the interaction with various objects. The IoT has the important ability to support novel applications and services based on cooperation between objects in more effective and efficient ways.

The proposed system in this paper, S-Enabler, is designed and implemented by applying IoT-enabling and IoT application technologies. This paper also introduces a social IoT application, an energy saving vehicle (ESV) that reduces the fuel consumption through cooperation between smart devices.

4. System Architecture

4.1. Overview of System Architecture. The suggested system, S-Enabler, is designed reflecting on the novel IoT paradigm.

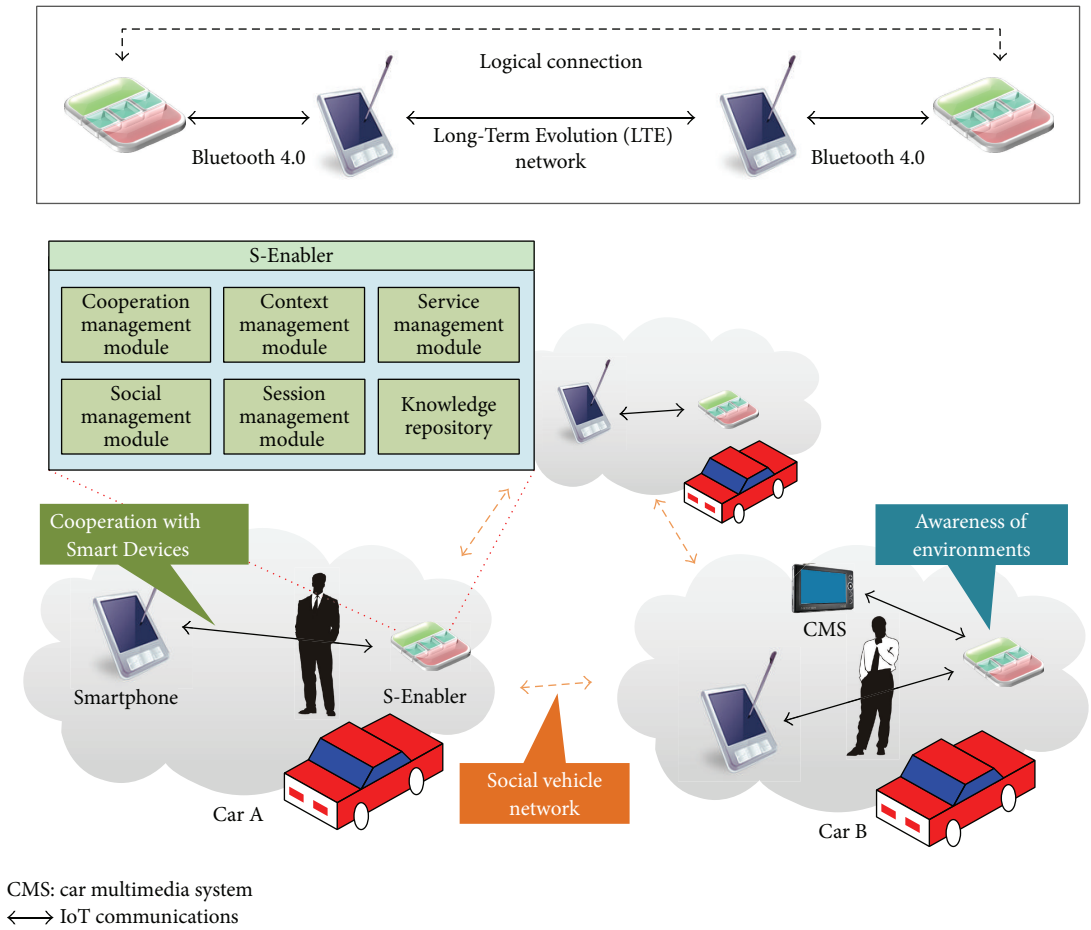

Figure 2: Overview of the social enabler (S-Enabler).

The S-Enabler was designed to implement social service domains. Figure 2 illustrates an overview of the S-Enabler and roughly describes how the S-Enabler provides social vehicle services to users. The S-Enabler aims to convert a normal space into a smart social space through intervehicular communications between the S-Enabler and a user's smartphone. The S-Enabler communicates with the user's smartphone via a wireless personal area network (WPAN) based on the Bluetooth technology. In addition, the S-Enabler communicates with other S-Enablers by cooperation with user's smartphone with the Long-Term Evolution (LTE) network. The S-Enabler has three important functions. First, it has mutual cooperation functionality with smart devices. The mutual cooperation with smart devices is implemented through a personal area network (PAN). This study uses Bluetooth technology for mutual cooperation. Because most modern smart devices have Bluetooth capability, this paper uses Bluetooth technology for PAN among various PAN standards. The S-Enabler not only receives information through cooperation with smart devices but also recognizes the user. It is necessary to implement user-centric service domains. Second, it has the function of awareness of surrounding environments. This function enables smart devices to provide intelligent services such as context-aware services. Accurate recognition of the surrounding environment has the important role of increasing service satisfaction. Third, it has the function of configuration of social vehicle networks. The user in a car configures a social network between vehicles through the S-Enabler. The smart device can create various smart services through cooperation between vehicles based on this social vehicle network. This study will also introduce a social IoT application, an ESV that reduces fuel consumption by using this function.

4.2. Middleware Architecture of the S-Enabler. In this paper, the middleware architecture for the S-Enabler is designed in order to implement the function explained above. Figure 3 shows the middleware architecture for the proposed system. The middleware architecture consists of six types of management modules according to the functions of the S-Enabler. The six types of management modules are the context management module for recognizing the surrounding environment, the cooperation management module for collaboration between the smart devices, the social management module for establishment of a safe and reliable vehicle social network (e.g., discovering the objects and assessing object reputations), the session management module for configuring a seamless service domain, the service management

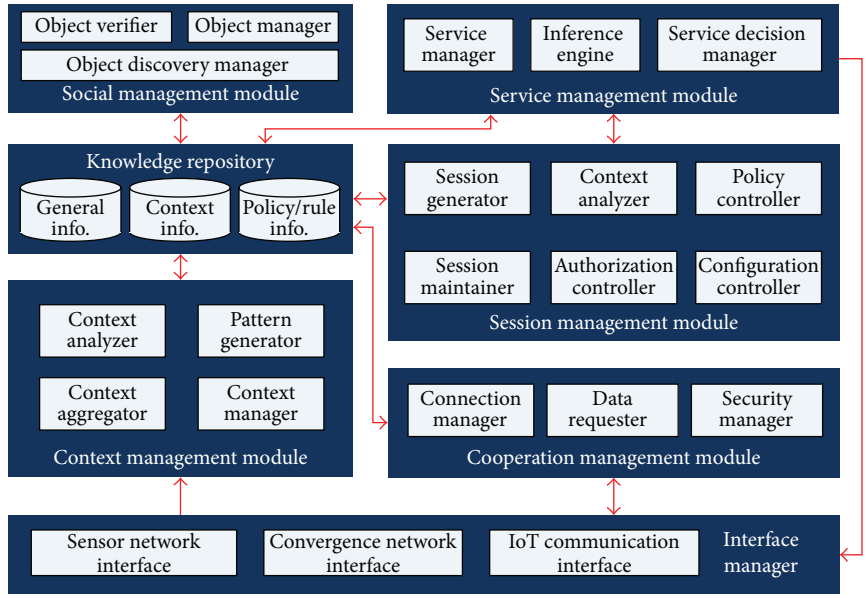

Figure 3: Middleware architecture of the S-Enabler.

module for service creation and decisions, and the knowledge repository for storing various pieces of information required for operating as a social object. The detailed description of the middleware architecture is as follows.

4.2.1. Cooperation Management Module (CooM) . The CooM performs the role of enabling autonomous collaboration between various smart devices. The CooM consists of the connection manager, data requester, and security manager. The connection manager manages the connection between a variety of smart devices and the data requester performs the role of periodically requesting information from smart devices upon the occurrence of a specific event. Lastly, the security manager performs the role of enabling a safe and reliable connection between the smart devices and the S-Enabler. To achieve this, the CooM performs the role of security capability and requirement management, key management, and the authentication and authorization of smart devices.

4.2.2. Context Management Module (ConM). The ConM manages the collected information and performs the role of recognizing the surrounding environment. In addition, this module plays an important role of generating patterns through analyzing the collected information. The ConM is composed of a context analyzer, the context manager, and the pattern generator. Various data entering the ConM are utilized as information for recognizing the surrounding environment in the context analyzer. Particularly in this paper, recognition of the current status of users will be introduced. Collected information performs the role of either updating the stored information in the knowledge repository (KR) by the context manager, storing it in the KR, or discarding. Lastly, the pattern generator performs the role of generating patterns by analyzing the collected situational information. Such patterns can be utilized for providing the prediction-based services.

4.2.3. Social Management Module (SocM). The SocM performs the role of establishing the social networks. The role includes object discovery and object reliability verification in order to implement a safe and reliable vehicle social network. The SocM consists of an object discovery manager, object verifier, and object manager. The object discovery manager performs the role of searching for the objects that will have a meaningful relationship with itself. The object verifier inspects whether the found social object is trustworthy and performs a reputation assessment to improve the quality of the social service. The object manager performs the role of registering, authenticating, and authorizing the objects.

4.2.4. Session Management Module (SesM). The SesM is required to provide a user-centered service. The SesM has two major functions. The first is to provide a user-centric service and the second is to provide a seamless service. The SesM uses the session ID and user ID to provide the above two services. For example, when the service is interrupted, the SesM stores the session ID and user ID with all the related contexts, such as location, service information, and content information. By using the session ID and user ID, the S-Enabler can restart the service at the interrupted point. The policy controller manages various policies and rules. The policies and rules are decided according to the situation. For example, when more than two users enter the same service domain, the priority of the service provision is determined according to predefined policies. In addition, when the user moves into different service domains, the policy controller requests the cloud server to send the relevant policies and rules. The configuration controller organizes a new service environment according to the changes in the situation.

4.2.5. Service Management Module (SerM). The SerM performs the role of inferring the service based on the context. Through this inference, the SerM configures and manages the service. The SerM is composed of an inference engine, decision manager, and service manager. The inference engine performs the role of inferring the service candidates from a variety of service applications. Then, the most appropriate service is determined by the decision manager. The decision manager correlates the current situation with the service candidates. The service manager performs the role of registering, deleting, and managing the services, also known as convergence.

4.2.6. Knowledge Repository (KR). The KR manages the use of a database. The KR is a set of components that manages the context, rules and policies, and patterns. The KR also controls the information ontology, service-pattern-look-up table, context, and rules and policies. The KR autonomously updates the database when a new situational event occurs. Furthermore, The KR autonomously modifies the policies and rules to improve the service maintenance and the pattern management efficiency.

4.3. Social Cooperation Diagram for Smart Service Provision. The S-Enabler can configure vehicle social networks to provide the user with smart services based on social behavior. In this paper, the social networks refer to the networks that consist of social objects. More specifically, we refer to the social networks as the social interaction among the S-Enablers. We proposed a new vehicle social network based on the smartphone application for smart social services. The S-Enabler can create a variety of useful smart services by utilizing the user's social behaviors based on the vehicle social network. The S-Enabler plays the role of enabling the application, recognizing the user and social context, learning the pattern, and creating the service. In other words, the S-Enabler has the role of implementing smart service domains based on social behavior. For this, the S-Enabler has three main social cooperation processes (initial connection process, social cooperation process, and service creation process). The ultimate goal of the S-Enabler is to voluntarily cooperate with surrounding smart devices in order to socialize the smart devices. As explained above, the paradigm of the IoT is changing from smart objects to social objects. Thus, the goal of the S-Enabler is to change the smart devices (objects) into social devices (objects). Therefore, the S-Enabler supports the wireless technology to cooperate with surrounding smart devices. This paper uses Bluetooth technology for wireless communications. An advantage of Bluetooth is that it has very low power consumption and recent smart devices, such as smartphones and smart wearable devices, have a Bluetooth transceiver module for wireless communications by default.

4.3.1. Initial Connection Process with a Smart Device. Figure 4 shows the initial connection processes between the S-Enabler and a smart device. Initially, when the car starts, the S-Enabler periodically broadcasts an advertising packet. If the advertising packet is received, the smart device sends an initiation request packet. If the initiation request packet is received, the S-Enabler sends an initiation response packet after the authentication process. Then, the S-Enabler initially connects with the smart device. Managing energy consumption is a very important issue because the periodical signal transmission consumes a lot of energy and smart devices, such as smartphones and smart watches, commonly operate by battery. In this study, two options are offered to reduce the energy consumption used in an initiation process. First, the user can make the Bluetooth interface enabled manually. Second, the smart device with our smartphone application utilizes the schedule patterns of the user to decide whether to enable or disable the Bluetooth interface. From the user's schedule pattern, the smart device derives the probability that the user is riding in a vehicle. Then, the smart device determines the enabling/disabling cycle of the Bluetooth interface on the basis of the derived probability.

4.3.2. Social Cooperation Process. Humans take on various roles according to the situation. A man, for example, has various roles such as a father, a son, an employee of a company, or a member of an interest group. These relations sometimes have a hierarchal structure and sometimes have an egalitarian structure. This study focuses on these characteristics of the human relations and the S-Enabler is designed and implemented considering these social features. Figure 5 illustrates the sequence of the social cooperation process and the service creation process.

(i) *Situation Recognition.* First, the S-Enabler periodically broadcasts signals to recognize surrounding smart devices and creates logical connections. Then, the S-Enabler receives a schedule of the user from the management server and environmental information, such as time, location, and temperature/humidity, from the smart devices. The ConM (context management module) of the S-Enabler aggregates/analyzes this context, generates the patterns, and stores the context and pattern in the KR.

(ii) *Social Cooperation.* The SocM of the S-Enabler searches for objects (or smart service domains) that have similarity to the local objects. These similarities include the user's characteristics and schedules, the types of smart devices, and environmental information. After being verified by the SocM, the object becomes a member of the vehicle social network. The S-Enabler uses the information that is collected via the configured vehicle social network for decision and creation of the social IoT-based smart services.

(iii) *Role Decision.* The SerM (service management module) of the S-Enabler assigns a role to each device in the social service domain by evaluating schedule and environmental information (time, location, temp/humidity, etc.). If the role overlaps, the SerM adjusts each role to enable the efficient operation.

4.3.3. Service Creation Process Based on Social Behavior. Because dynamic role decisions can cause a large amount of resource and energy consumption, the S-Enabler assigns the

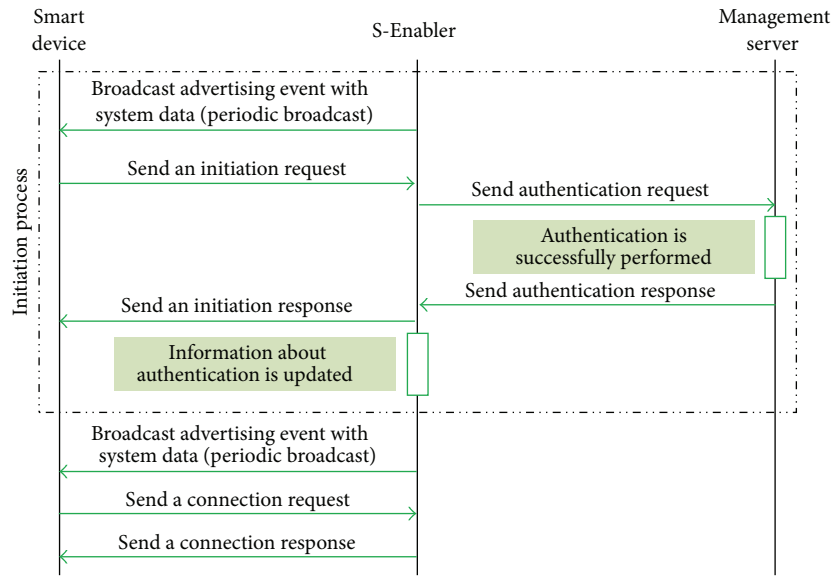

Figure 4: Sequence diagram of the initial connection process.

role to each device according to resource sharing in order to reduce energy consumption. The S-Enabler has the role of managing resources of smart devices in the social service domains and periodically updates the shared resource profile. The S-Enabler infers the context and creates service rules based on social behaviors.

4.4. Energy Saving Algorithm Based on Social Behavior. This subsection will introduce an energy saving algorithm based on social behaviors such as competition and sharing. Figure 6 shows the energy saving application based on vehicle social networks.

Step 1. The user first enters the fuel cost that he desires to use for a month (threshold value) and the average fuel consumption per 100 km for the vehicle. Then, the total distance to drive for a month is calculated by using the fuel cost, the fuel consumption per 100 km, and the average price of the gas stations.

Step 2. The recommended driving distance by unit hour can be calculated by $D_h = D_m/(N_i \times 24)$, where D_h, D_m, and N_i refer to the total distance to be able to drive for a month and days in the ith month.

Step 3. The recommended driving distance is compared with the actual driving distance, and the S-Enabler shows the energy saving level through LED lighting. This information can be checked in detail through the user's smartphone application. The actual driving distance of the user used here is calculated through autonomous cooperation between the S-Enabler and the user's smartphone. Bluetooth is used for the establishment of PANs. It is possible to save energy by sharing the driving information, such as driving distance, with other vehicles that have a similarity to the user.

Step 4. The shortcoming of this method is that it does not consider geography, vehicle year, and user's driving style. Therefore, actual fuel costs and driving distance can be used for correcting this error. If there is a credit card that is mainly used for refueling, the fuel cost can be easily collected by the smartphone by using the short message service (SMS) upon making payment. Then, it is possible to obtain more accurate average fuel consumption per 100 km through comparing the actual driving distance and fuel costs. This method cannot be used if a credit card is not used for paying for fuel and in this case the S-Enabler resolves this by establishing vehicle social networks. The S-Enabler corrects the error through comparing the driver's vehicle with other vehicles that have a similarity in the vehicle social network.

By utilizing social behavior, it is possible to resolve the problems in the IoT environments and to create a novel smart service that has high energy efficiency and high user satisfaction, that is, to guarantee the QoE.

5. Implementation

This study implemented the proposed system, S-Enabler. In this section, technical realization of the S-Enabler is addressed based on the hardware architecture and the feasible smartphone application. Figure 7 illustrates the main features of the prototype of the S-Enabler.

5.1. Hardware Architecture. Figure 8 shows the hardware architecture and prototype of the proposed system. The hardware architecture functionally consists of four parts: the main processor, the network and communication part, the LED and LED driving unit part, and the power management part. This paper utilizes an 8-bit microcontroller as the main CPU. The main processor part has the main

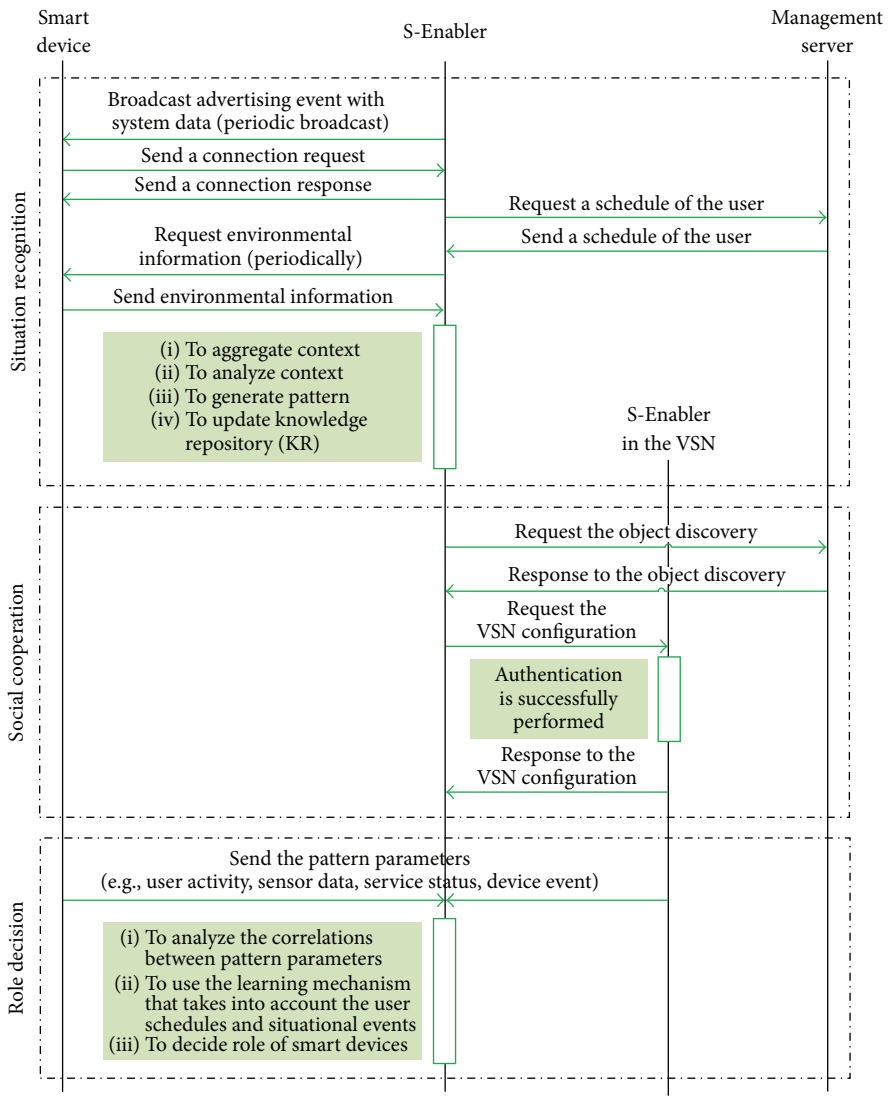

*VSN: vehicle social network

Figure 5: Sequence diagram of the social cooperation process.

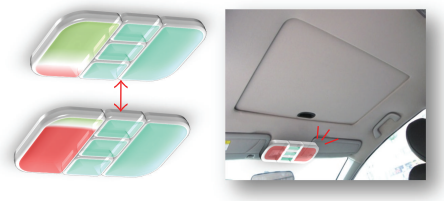

Figure 6: Energy saving application based on vehicle social networks.

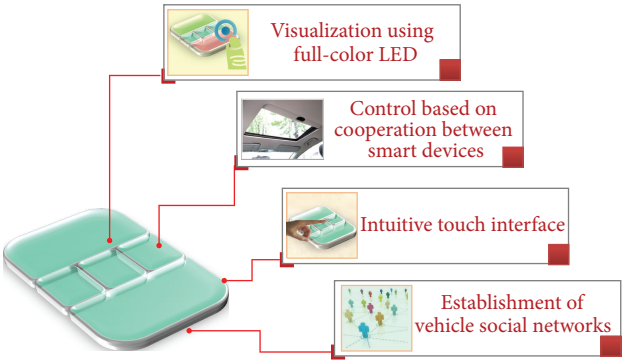

Figure 7: Features of the prototype of the S-Enabler.

role of running and storing the middleware, processing events, analyzing contexts, and generating and managing patterns. The network and communication part is composed of a Bluetooth transceiver module. In this paper, we use the Bluetooth standard for intervehicular communications. Particularly, we used Bluetooth 4.0 with Bluetooth low energy (BLE) technology. The BLE technology provides considerably

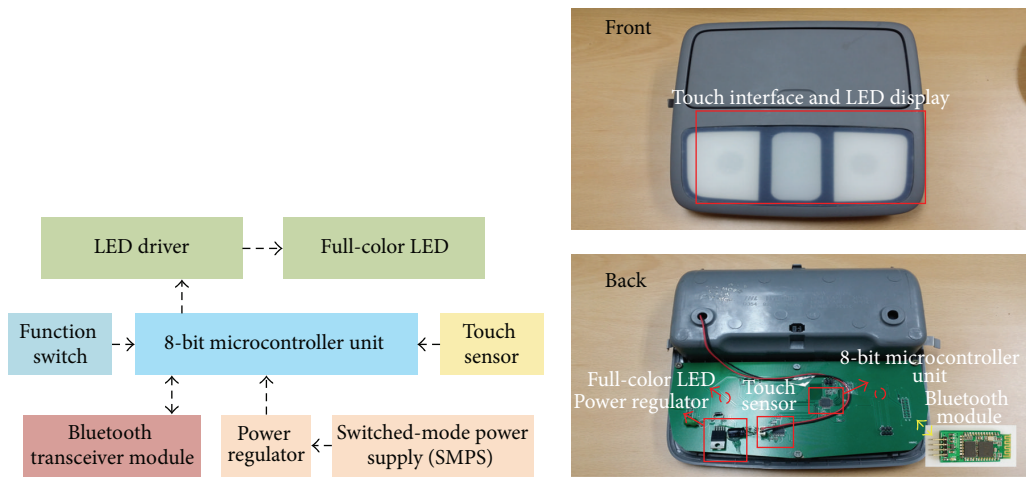

Figure 8: System implementation; (a) hardware block diagram; and (b) prototype of the S-Enabler.

reduced energy consumption and cost compared to the previous version of Bluetooth. In addition, currently, the BLE is widely used as a WPAN by various smart devices such as smartphones and wearable devices due to these advantages. Thus, systems that want to cooperate with various smart devices should use the BLE. For these reasons, we used Bluetooth 4.0 with BLE for building a WPAN.

Bluetooth technology is designed to establish WPANs with low-cost and low power characteristics. Thus, it is widely used in modern smart devices. For this reason, this paper uses a Bluetooth transceiver module for implementing the system. The LED and LED driving unit part consists of a full-color LED and the LED driving circuit. The power management part consists of a power regulator and a switched-mode power supply (SMPS).

5.2. Smartphone Application. This study developed a smartphone application to increase the convenience for the users. We proposed a new vehicle social network based on the smartphone application for smart social services. The S-Enabler can create a variety of useful smart services by utilizing the user's social behaviors based on the vehicle social network. Figure 9 shows the social IoT-based smartphone application for fuel saving. It is possible to monitor the driving distance like the LED of the S-Enabler. If the user touches the "my car" menu, it highlights in detail the actual distance the user drove, the threshold distance the user entered, the number of days remaining, and the recommended daily driving distance, which enables the user to check in detail his driving history. If the user touches the "friends" menu, there is a ranking in order of the driving status of friends. The amount of cost saving is calculated using the average fuel consumption, the current gas price, and the distance traveled on foot. This plays the role of helping to save fuel further through competition. Finally, if the user touches the "car sharing" menu, it lists the friends who can carpool with the user. This menu analyzes the driving information, such as the collected driving destination of each

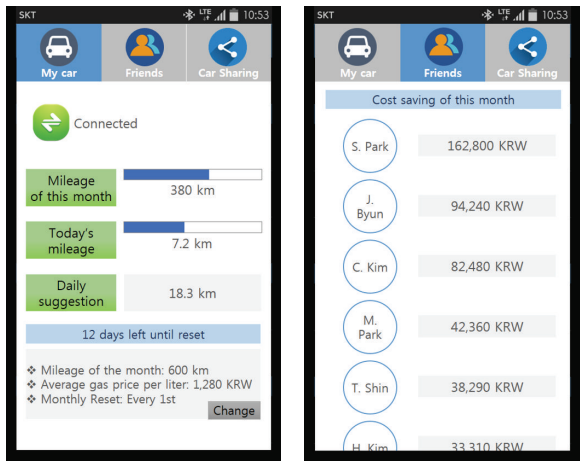

Figure 9: Social IoT-based smartphone application for fuel saving through interaction with the S-Enabler.

user and average driving time, to show the list of friends that can carpool. Therefore, the user can send a message to his friend to share a car. In this way, fuel costs can be dramatically reduced. This application enables the user to save energy through competition and sharing, which is a social relationship between people through the S-Enabler.

6. Experiment and Discussion

It is not easy to measure the average energy savings from the energy management method suggested in this study. This is because the energy management method based on social behavior, such as competition or sharing, reflects user intentions related to energy reduction, which can result in a diverse energy reduction range according to the user. In addition, the energy savings can be perceived as small as time passes owing to psychological factors. Thus, there needs to be a large control group to accurately measure the amount of

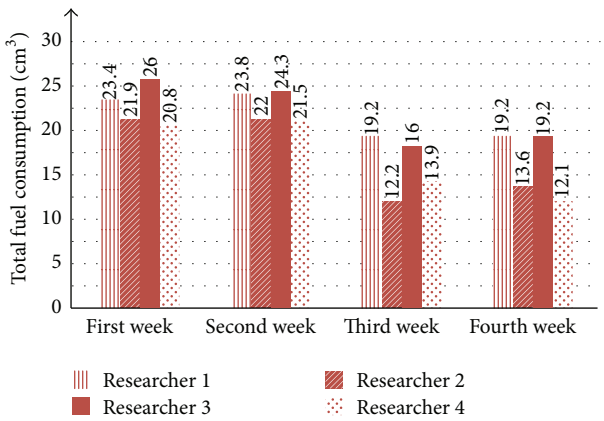

Figure 10: Results of the energy saving experiment.

average energy savings and it is determined that meaningful energy saving results will be derived when the experiment is done over a long-term period (over one year). Therefore, this study first draws its conclusion by discussing the significance of the proposed research with a simple experiment rather than a large-scale experiment.

In the experiment, the energy savings experiment was done over four weeks on five researchers that commute by car. On the first and second weeks, fuel consumption was measured while commuting by car as usual and, on the third and fourth weeks, fuel consumption was measured after installing the suggested system. Since two of the researchers knew that they lived in the same area, they could share a car. These two researchers commuted by car sharing on the third and fourth weeks. To emphasize the social behavior called competition, on the third and fourth weeks 50,000 KRW (about 42 USD) worth of gift cards was given to the user with the highest fuel savings and 30,000 KRW (about 25 USD) worth of gift cards was given to the user with the second highest fuel savings. The threshold fuel amount was decided by the users themselves. The results of the experiment over the four weeks are presented in Figure 10. There was an average saving of 31.7% in the third and fourth weeks. In the results, users 2 and 4 engaged in car sharing and agreed to divide the payment of fuel 50-50. With more car sharing, bigger savings effect will be seen. Although the performed experiment has a limitation, the results are significant and meaningful.

7. Conclusion

This paper proposed the S-Enabler based on vehicle social networks considering the new paradigm of IoT. The paradigm of IoT has changed from the smart IoT to the social IoT. Therefore, the S-Enabler is designed to cooperate with smart devices based on social behavior and utilize wireless technology, particularly Bluetooth, for establishing the social IoT. This paper presented the middleware architecture and cooperation processes for a social IoT-based smart system and also introduced an energy saving algorithm based on social behavior, such as competition and sharing. This paper designed and implemented the proposed system and performed an experiment to evaluate the performance of energy savings. The S-Enabler reduced total fuel consumption by 31.7%. It is expected that this work will contribute to providing guidance on the design and development of a social IoT-based smart system.

Competing Interests

The authors declare that there is no conflict of interests regarding the publication of this paper.

Acknowledgments

This research was supported by Basic Science Research Program through the National Research Foundation (NRF) of Korea funded by the Ministry of Science, ICT and Future Planning (NRF-2015R1C1A1A01054828) and by the Chung-Ang University Graduate Research Scholarship in 2015.

References

[1] T. Özçelebi, J. Lukkien, R. Bosman, and Ö. Uzun, "Discovery, monitoring and management in smart spaces composed of low capacity nodes," *IEEE Transactions on Consumer Electronics*, vol. 56, no. 2, pp. 570–578, 2010.

[2] N. Dimakis, J. K. Soldatos, L. Polymenakos, P. Fleury, J. Cuřín, and J. Kleindienst, "Integrated development of context-aware applications in smart spaces," *IEEE Pervasive Computing*, vol. 7, no. 4, pp. 71–79, 2008.

[3] H.-N. Lee, S.-H. Lim, and J.-H. Kim, "UMONS: ubiquitous monitoring system in smart space," *IEEE Transactions on Consumer Electronics*, vol. 55, no. 3, pp. 1056–1064, 2009.

[4] S. M. R. Islam, D. Kwak, M. H. Kabir, M. Hossain, and K.-S. Kwak, "The internet of things for health care: a comprehensive survey," *IEEE Access*, vol. 3, pp. 678–708, 2015.

[5] S. D. T. Kelly, N. K. Suryadevara, and S. C. Mukhopadhyay, "Towards the implementation of IoT for environmental condition monitoring in homes," *IEEE Sensors Journal*, vol. 13, no. 10, pp. 3846–3853, 2013.

[6] X. Li, R. Lu, X. Liang, X. Shen, J. Chen, and X. Lin, "Smart community: an internet of things application," *IEEE Communications Magazine*, vol. 49, no. 11, pp. 68–75, 2011.

[7] B. Li and J. Yu, "Research and application on the smart home based on component technologies and internet of things," *Procedia Engineering*, vol. 15, pp. 2087–2092, 2011.

[8] G. Chong, L. Zhihao, and Y. Yifeng, "The research and implement of smart home system based on Internet of Things," in *Proceedings of the International Conference on Electronics, Communications and Control (ICECC '11)*, pp. 2944–2947, IEEE, Zhejiang, China, September 2011.

[9] L. Atzori, A. Iera, and G. Morabito, "The Internet of Things: a survey," *Computer Networks*, vol. 54, no. 15, pp. 2787–2805, 2010.

[10] S. Cirani, L. Davoli, G. Ferrari et al., "A scalable and self-configuring architecture for service discovery in the internet of things," *IEEE Internet of Things Journal*, vol. 1, no. 5, pp. 508–521, 2014.

[11] T. Perumal, A. R. Ramli, and C. Y. Leong, "Interoperability framework for smart home systems," *IEEE Transactions on Consumer Electronics*, vol. 57, no. 4, pp. 1607–1611, 2011.

[12] C.-L. Wu and L.-C. Fu, "Design and realization of a framework for human-system interaction in smart homes," *IEEE Transactions on Systems, Man, and Cybernetics: Systems*, vol. 42, no. 1, pp. 15–31, 2012.

[13] L. Atzori, A. Iera, G. Morabito, and M. Nitti, "The social internet of things (SIoT)—when social networks meet the internet of things: concept, architecture and network characterization," *Computer Networks*, vol. 56, no. 16, pp. 3594–3608, 2012.

[14] P. Mendes, "Social-driven internet of connected objects," in *Proceedings of the Interconnecting Smart Objects with the Internet Workshop*, Prague, Czech Republic, March 2011.

[15] M. Nitti, R. Girau, and L. Atzori, "Trustworthiness management in the social internet of things," *IEEE Transactions on Knowledge and Data Engineering*, vol. 26, no. 5, pp. 1253–1266, 2014.

[16] B. Guo, Z. Yu, X. Zhou, and D. Zhang, "Opportunistic IoT: exploring the social side of the internet of things," in *Proceedings of the IEEE 16th International Conference on Computer Supported Cooperative Work in Design (CSCWD '12)*, pp. 925–929, Wuhan, China, May 2012.